Marine thorium and protactinium distributions: Tools for past and present chemical flux

Christopher Tyler Hayes

Submitted in partial fulfillment of the
requirements for the degree
of Doctor of Philosophy
in the Graduate School of Arts and Sciences

COLUMBIA UNIVERSITY

2013

ABSTRACT

Marine thorium and protactinium distributions: Tools for past and present chemical flux

Christopher Tyler Hayes

Adsorption to sinking particulate matter, known as scavenging, is an important yet elusive term in the budgets of many bioactive and contaminant trace metals in the ocean. Scavenging is also involved in the cycling of other trace metals used in ocean sediments to learn about ocean processes, such as circulation rates or biological productivity, of the geologic past. This dissertation is an oceanographic exploration of the naturally-occurring radionuclides ^{230}Th, ^{232}Th and ^{231}Pa aimed to better understand how their scavenging behavior can be utilized to trace chemical flux in the modern and the past ocean.

Measurements ^{230}Th and ^{231}Pa in the water column of the North Pacific (Chapter 1), and in surface sediments throughout the Pacific (Chapter 3) demonstrate gyre-scale contrasts in scavenging intensity for both elements, linked to the chemical composition of particles produced by distinct biogeographic communities. Pacific surface sediment ^{231}Pa/^{230}Th distributions are largely consistent with biogeographic variations and may offer a way to reconstruct gyre boundaries through time which is of interest in terms of both biogeochemistry and physical circulation.

While ^{230}Th and ^{231}Pa are produced by the radioactive decay of uranium dissolved in seawater, ^{232}Th is added to the ocean via the input of continental material. Removal of Th by scavenging should be equivalent for both Th isotopes based on chemical principles. I use measured ^{232}Th inventories from the North Pacific water column and apply a removal rate based on ^{234}U:^{230}Th disequilibria to estimate the flux of dissolved trace elements, such as the micro-nutrient Fe, to the ocean through the deposition of mineral dust (Chapter 2). Results from this

study also raise the possibility of differing chemical behavior of the two Th isotopes in shallow water (<500 m depth) related to size-partitioning between truly dissolved and colloidal phases.

Finally, results from the U.S. GEOTRACES North Atlantic Transect are used to investigate the relationship between ^{231}Pa and ^{230}Th in the water column and several of their proposed paleoceanographic purposes. The accuracy of ^{230}Th as a proxy for constant sediment flux can be directly quantified to 40±10% with observations of boundary scavenging near the coast of Northwest Africa (Chapter 4). The ^{231}Pa/^{230}Th ratio in the water column is not clearly controlled by either ocean ventilation (Chapter 4) or particle composition (Chapter 5) alone. Near-bottom enhanced scavenging of both isotopes is also occurring over large regions, in benthic layers of resuspended sediments and in a hydrothermal plume emanating from the mid-Atlantic ridge. These novel observations must be reconciled in a new conceptual model, likely requiring future numerical modeling work, in order to clarify the use of the ^{231}Pa/^{230}Th ratio as a proxy for the Atlantic meridional overturning circulation.

Table of Contents

List of Figures

Chapter 1

Chapter 2

Chapter 3

Chapter 4

Chapter 5

List of Tables

Chapter 1

Chapter 2

Chapter 3

Chapter 5

Acknowledgements

My residence at Lamont has been one of the most intellectually stimulating periods of my life. At the same time, with experiences working at sea, taking on ambitious laboratory projects, and preparing manuscripts, I have also learned the discipline required of a scientist. I owe to my community the inspiration for pursuing fruitful scientific goals while developing the logistical prowess to make things happen.

I want to thank my advisor Bob Anderson especially for encouraging my own self-promotion and relating the benefits of scientific collaboration. Martin Fleisher has been a stalwart role model of a careful and productive analyst. Jerry McManus, Samar Khatiwala, Tim Kenna, Leo Pena and Wally Broecker, have all mentored me in some way, if they knew it or not, providing encouragement and advice for pursuing a career in science. It was really a pleasure to come to work because of many of my peers, not exclusively including Kat Allen, Rafael Almeida, Jason Jweda, Alex Lloyd, Jordan Landers and all the Lamont soccer players. Finally I want to thank my family and my fiancé Kirsten for their unconditional moral support that I am lucky to have.

Preface

An over-arching motivation of this dissertation is to learn where and how fast marine trace metals, of biogeochemical and paleoclimatological interest, are being added to or removed from the ocean. To do this, I have joined an endeavor to map the marine distributions of the naturally-occurring radioactive elements thorium and protactinium. Three isotopes in particular, ^{230}Th, ^{232}Th, and ^{231}Pa, have seen more than 50 years of application in quantifying the rates of a variety of processes, from biological productivity to ocean circulation, largely on the basis of their distribution in ocean sediments. Recent advances in mass spectrometry and clean sampling techniques have allowed us to observe these three isotopes in modern seawater itself, at much higher spatial resolution than was previously possible. Therefore, a new set of scientific questions has become amenable to data-based hypothesis testing. Here I give a brief and selective historical account to set the stage for the questions addressed in this thesis about marine thorium and protactinium and their implications for improved understanding of chemical fluxes in the ocean.

The isotopes ^{232}Th (half-life 14.1 x 10^9 yrs; Holden, 1990), ^{230}Th (75.58 x 10^3 yrs; Cheng et al., 2013) and ^{231}Pa (32.76 x 10^3 yrs; Robert et al., 1969), first found favor in marine science as tools for dating deep-sea sediment records (Ku, 1976; and references therein) because of their long half-lives and certain aspects of their chemical behavior in seawater. Th-230 and ^{231}Pa are produced in seawater by the uniformly distributed decay of dissolved ^{234}U and ^{235}U, respectively. Th and Pa, unlike their parent U, are highly insoluble in seawater. Th and Pa are thus rapidly (<40 and <200 yrs, respectively) removed from solution and transported to the seafloor by adsorption to sinking particles (Anderson et al., 1983b), a process called scavenging (Goldberg,

1954). The major isotope of Th, ^{232}Th, is not produced by radioactive decay but is added to the ocean via the addition of continental material, such as desert dust or riverine clays.

By assuming that ^{232}Th is removed by scavenging in a similar way as ^{230}Th and given a known initial input of ^{230}Th (since its production by U is well-known), the ratio of ^{230}Th/^{232}Th in sediments was proposed as a way to date age horizons in ocean sediments up to ~10^5 yrs in the past based on the amount of ^{230}Th decay having occurred (Picciotto and Wilgain, 1954). Subsequent work proposed, instead, using the ratio ^{230}Th/^{231}Pa for dating sediment records. Once buried, this ratio also evolves with age following known half-lives. In contrast to ^{230}Th and ^{232}Th, however, ^{230}Th and ^{231}Pa have the same uniform source (U decay) in addition to being removed by the same scavenging process (Rosholt et al., 1961; Sackett, 1960).

The application of either the ^{230}Th/^{232}Th ratio or the ^{230}Th/^{231}Pa ratio as methods of dating sediments was eventually abandoned because it became clear in the following decades that both ratios had substantial geographic variation in surface sediments (reviewed by Ku, 1976). Thus, assumptions about the initially buried ratios could not be made *a priori*. Nonetheless, marine chemists took this finding in stride and realized that in observing geographic variations in these radionuclide ratios, one could learn about the ocean processes responsible for them.

Early research was able to infer many aspects of the water column behavior of Th and ^{231}Pa. For instance, from simple laboratory adsorption experiments, Holland and Kulp (1954) concluded that ^{230}Th was removed from seawater by an equilibrium adsorption reaction with sinking particles. The first direct measurements of ^{230}Th (Koczy et al., 1957; Sackett et al., 1958) and ^{231}Pa (Sackett, 1960) in seawater were able to establish upper limits on their concentration. These measurements had large uncertainties, owing to the difficulties of handling insoluble elements and their low concentrations in seawater (~10^{-15} g per kg seawater). Nonetheless, early

seawater analyses supported the claims of the sediment-dating techniques, that nearly all (99.95% for ^{230}Th, 99.8% for ^{231}Pa) of the production of these isotopes due to U decay in seawater is removed to the seafloor on timescales less than 50-100 yrs (Moore and Sackett, 1964).

Although 50-100 yrs is instantaneous in comparison to many geologic phenomena, this is ample time for seawater ^{230}Th and ^{231}Pa to be redistributed by ocean circulation. Additionally, the scavenging process is not necessarily spatially uniform. It is precisely the interplay between circulation and variations in scavenging intensity that leads to the major questions explored in this thesis.

A concept termed boundary scavenging was developed (Bacon, 1988; Spencer et al., 1981) to explain observations (Anderson et al., 1983a; Anderson et al., 1983b; Yang et al., 1986) that ^{231}Pa/^{230}Th ratios in sediments increased from ocean interior to continental margins. It was hypothesized that since ^{231}Pa is removed to the seafloor by scavenging more slowly than ^{230}Th, it can be transported to a greater extent by ocean currents and mixing to be preferentially buried at sites of high scavenging intensity. One expects high scavenging intensity in places like continental margins where there are elevated fluxes of lithogenic and biogenic particulate matter. In addition to total particle flux, a change in particle chemistry associated with certain ocean regions could also enhance the removal of ^{231}Pa (Anderson et al., 1983a; DeMaster, 1979; Taguchi et al., 1989). Boundary scavenging has important implications for understanding the removal of many insoluble elements with sufficiently long ocean residence times (>100 yrs) such as the micro-nutrient Fe, and contaminant elements, such as Pb and Pu. Documenting boundary scavenging in seawater itself, however, was difficult prior to the high-throughput, high-precision methods now available.

In the Pacific, I attempt to map where and how the enhanced removal of ^{231}Pa is occurring in the water column (Chapter 1) and use a new perspective on boundary scavenging to outline a basin-scale redistribution of ^{231}Pa (Chapter 3). In the Atlantic, the actual amount of ^{230}Th and ^{231}Pa which are boundary scavenged off the coast of West Africa can be quantified (Chapter 4) and found to be much less significant for the basin-wide budget.

Boundary scavenging is thus not well-expressed in the Atlantic, confirming previous work (Walter et al., 1999; Yu et al., 1996). Variations in the sediment ^{231}Pa/^{230}Th ratios in this basin have been hypothesized to reflect the large-scale southward flux of deep water which forms part of the climatically-important Atlantic meridional overturning circulation (McManus et al., 2004; Yu et al., 1996). The ^{231}Pa/^{230}Th ratio is also potentially sensitive to variations in particle composition (Chase et al., 2002; Keigwin and Boyle, 2008; Walter et al., 1999), insofar as different particle types scavenge the two elements with differing efficiencies. As was the case for boundary scavenging, the influences of both overturning circulation and particle composition are largely inferred from radionuclide distributions in sediments and have not been adequately ground-truthed in the water column.

In a transect across the North Atlantic, I document the relationships between seawater ^{231}Pa/^{230}Th distributions, ocean ventilation (Chapter 4), particle concentration (Chapter 4) and particle composition (Chapter 5). Unable to demonstrate simple relationships between these parameters, the results presented here, instead, provide an excellent basis for ocean modeling efforts to refine the proxy interpretation of Atlantic ^{231}Pa/^{230}Th ratios.

Finally, it has long been recognized that variations in sediment ^{232}Th/^{230}Th ratios reflect geographic variation in the input of continental material (Goldberg and Koide, 1962; Ku, 1966). Indeed, sediment records of ^{232}Th/^{230}Th have been used to reconstruct the flux of mineral dust to

the open ocean over the late Pleistocene (e.g., Adkins et al., 2006; Anderson et al., 2006; Marcantonio et al., 2001). Based on similar principles, the $^{232}Th/^{230}Th$ ratio in seawater (rather than in sediments) had been proposed decades previously as a proxy for the flux of dust or other lithogenic inputs into the modern ocean (Hirose and Sugimura, 1987; Huh et al., 1989). Dust dissolution as a source of elements to the ocean is of particular relevance to the cycle of Fe, a micronutrient whose abundance can limit marine biological productivity. In vast regions of the remote ocean, the only significant source of Fe is eolian dust (Jickells et al., 2005; Mahowald et al., 2009).

Despite this method's potential, seawater data on $^{232}Th/^{230}Th$ of sufficient quality has only recently become available. Hsieh et al. (2011) have reported dust deposition fluxes using seawater $^{232}Th/^{230}Th$ in the Atlantic. In Chapter 2, I demonstrate in the North Pacific an estimation of dust deposition and the associated supply of trace elements due to dust dissolution using dissolved $^{232}Th/^{230}Th$.

Each chapter in this dissertation is designed to stand alone. Therefore each is given an abstract and introduction of its own in greater detail than presented here. Specific acknowledgements and references are also given as an unnumbered section at the end of each chapter. I list my intended co-authors for peer-reviewed publications at the beginning of each chapter. While their intellectual and logistical contributions have been invaluable, I take full responsibility (for better or for worse) for the writing of this thesis.

References

Adkins, J., deMenocal, P., Eshel, G., 2006. The "African humid period" and the record of marine upwelling from excess ^{230}Th in Ocean Drilling Program Hole 658C. Paleoceanography 21, PA4203.

Anderson, R.F., Bacon, M.P., Brewer, P.G., 1983a. Removal of ^{230}Th and ^{231}Pa at ocean margins. Earth Planet. Sci. Lett. 66, 73-90.

Anderson, R.F., Bacon, M.P., Brewer, P.G., 1983b. Removal of ^{230}Th and ^{231}Pa from the open ocean. Earth Planet. Sci. Lett. 62, 7-23.

Anderson, R.F., Fleisher, M.Q., Lao, Y., 2006. Glacial–interglacial variability in the delivery of dust to the central equatorial Pacific Ocean. Earth Planet. Sci. Lett. 242, 406-414.

Bacon, M.P., 1988. Tracers of chemical scavenging in the ocean: boundary effects and large-scale chemical fractionation. Philos. Trans. R. Soc. London, Ser. A 325, 147-160.

Chase, Z., Anderson, R.F., Fleisher, M.Q., Kubik, P.W., 2002. The influence of particle composition and particle flux on scavenging of Th, Pa and Be in the ocean. Earth Planet. Sci. Lett. 204, 215-229.

Cheng, H., Edwards, R.L., Shen, C.-C., Polyak, V.J., Asmerom, Y., Woodhead, J., Hellstrom, J., Wang, Y., Kong, X., Spötl, C., Wang, X., Calvin Alexander Jr, E., 2013. Improvements in ^{230}Th dating, ^{230}Th and ^{234}U half-life values, and U–Th isotopic measurements by multi-collector inductively coupled plasma mass spectrometry. Earth Planet. Sci. Lett. 371–372, 82-91.

DeMaster, D.J., 1979. The marine budgets of silica and ^{32}Si, PhD Dissert. Yale University, New Haven, CT.

Goldberg, E.D., 1954. Marine geochemistry 1. chemical scavengers of the sea. J. Geol. 62, 249-265.

Goldberg, E.D., Koide, M., 1962. Geochronological studies of deep sea sediments by the ionium/thorium method. Geochim. Cosmochim. Acta 26, 417-450.

Hirose, K., Sugimura, Y., 1987. Thorium isotopes in the surface air of the Western North Pacific Ocean. J. Environ. Radioactiv. 5, 459-475.

Holden, N.E., 1990. Total half-lives for selected nuclides. Pure & Appl. Chem. 62, 941-958.

Holland, H.D., Kulp, J.L., 1954. The mechanism of removal of ionium and radium from the oceans. Geochim. Cosmochim. Acta 5, 214-224.

Hsieh, Y.-T., Henderson, G.M., Thomas, A.L., 2011. Combining seawater ^{232}Th and ^{230}Th concentrations to determine dust fluxes to the surface ocean. Earth Planet. Sci. Lett. 312, 280-290.

Huh, C.-A., Moore, W.S., David C, K., 1989. Oceanic ^{232}Th: A reconnaissance and implications of global distribution from manganese nodules. Geochim. Cosmochim. Acta 53, 1357-1366.

Jickells, T.D., An, Z.S., Andersen, K.K., Baker, A.R., Bergametti, G., Brooks, N., Cao, J.J., Boyd, P.W., Duce, R.A., Hunter, K.A., Kawahata, H., Kubilay, N., laRoche, J., Liss, P.S., Mahowald, N., Prospero, J.M., Ridgwell, A.J., Tegen, I., Torres, R., 2005. Global iron connections between desert dust, ocean biogeochemistry, and climate. Science 308, 67-71.

Keigwin, L.D., Boyle, E.A., 2008. Did North Atlantic overturning halt 17,000 years ago? Paleoceanography 23, PA1101.

Koczy, F.F., Picciotto, E., Poulaert, G., Wilgain, S., 1957. Mesure des isotopes du thorium dans l'eau de mer. Geochim. Cosmochim. Acta 11, 103-129.

Ku, T.-L., 1966. Uranium series disequilibrium in deep sea sediments, PhD Dissert. Columbia University, New York, NY.

Ku, T.L., 1976. The Uranium-Series Methods of Age Determination. Ann. Rev. Earth Planet. Sci. 4, 347-379.

Mahowald, N.M., Engelstaedter, S., Luo, C., Sealy, A., Artaxo, P., Benitez-Nelson, C., Bonnet, S., Chen, Y., Chuang, P.Y., Cohen, D.D., 2009. Atmospheric Iron Deposition: Global Distribution, Variability, and Human Perturbations. Ann. Rev. Mar. Sci. 1, 245-278.

Marcantonio, F., Anderson, R.F., Higgins, S., Fleisher, M.Q., Stute, M., Schlosser, P., 2001. Abrupt intensification of the SW Indian Ocean monsoon during the last deglaciation: constraints from Th, Pa, and He isotopes. Earth Planet. Sci. Lett. 184, 505-514.

McManus, J.F., Francois, R., Gherardi, J.M., Keigwin, L.D., Brown-Leger, S., 2004. Collapse and rapid resumption of Atlantic meridional circulation linked to deglacial climate changes. Nature 428, 834-837.

Moore, W.S., Sackett, W.M., 1964. Uranium and thorium series inequilibrium in sea water. J. Geophys. Res. 69, 5401-5405.

Picciotto, E., Wilgain, S., 1954. Thorium Determination in Deep-Sea Sediments. Nature 173, 632-633.

Robert, J., Miranda, C.F., Muxart, R., 1969. Mesure de la periode du protactinium-231 par microcalorimetrie. Radiochim. Acta 11, 104-108.

Rosholt, J.N., Emiliani, C., Geiss, J., Koczy, F.F., Wangersky, P.J., 1961. Absolute dating of deep-sea cores by the Pa^{231}/Th^{230} method. J. Geol. 69, 162-185.

Sackett, W.M., 1960. Protactinium-231 content of ocean water and sediments. Science 132, 1761-1762.

Sackett, W.M., Potratz, H.A., Goldberg, E.D., 1958. Thorium Content of Ocean Water. Science 128, 204-205.

Spencer, D.W., Bacon, M.P., Brewer, P.G., 1981. Models of the distribution of ^{210}Pb in a section across the North Equatorial Atlantic Ocean. J. Mar. Res. 39, 119-138.

Taguchi, K., Harada, K., Tsunogai, S., 1989. Particulate removal of ^{230}Th and ^{231}Pa in the biologically productive northern North Pacific. Earth Planet. Sci. Lett. 93, 223-232.

Walter, H.-J., Rutgers v. d. Loeff, M.M., Francois, R., 1999. Reliability of the $^{231}Pa/^{230}Th$ Activity Ratio as a Tracer for Bioproductivity of the Ocean, in: Fischer, W., Wefer, G. (Eds.), Use of Proxies in Paleoceanography: Examples for the South Atlantic. Springer-Verlag, Berlin, pp. 393-408.

Yang, H.-S., Nozaki, Y., Sakai, H., Masuda, A., 1986. The distribution of ^{230}Th and ^{231}Pa in the deep-sea surface sediments of the Pacific Ocean. Geochim. Cosmochim. Acta 50, 81-89.

Yu, E.-F., Francois, R., Bacon, M.P., 1996. Similar rates of modern and last-glacial ocean thermohaline circulation inferred from radiochemical data. Nature 379, 689-694.

Chapter 1. A new perspective on boundary scavenging in the North Pacific Ocean

Christopher T. Hayes[a,b], Robert F. Anderson[a,b], Samuel L. Jaccard[c], Roger François[d], Martin Q. Fleisher[a], Maureen Soon[d], Rainer Gersonde[e]

[a]Lamont-Doherty Earth Observatory of Columbia University, Palisades, NY, USA

[b]Department of Earth and Environmental Sciences, Columbia University, New York, NY, USA

[c]Geological Institute, Department of Earth Sciences, ETH Zürich, Switzerland

[d]Department of Earth and Ocean Sciences, University of British Columbia, Vancouver, BC, Canada

[e]Alfred Wegener Institute for Polar and Marine Research, Bremerhaven, Germany

Published in Earth and Planetary Science Letters 369-370 (2013), 86-97

Abstract

Boundary scavenging, or the enhanced removal of adsorption-prone elements from the ocean in areas of high particle flux, is an often cited, though not well-quantified, concept used to understand the oceanic distribution of many trace metals. Because ^{230}Th and ^{231}Pa are produced uniformly from uranium decay and removed differentially by scavenging, the process of boundary scavenging can be elucidated by a more detailed knowledge of their water column distributions. To this end, filtered seawater was collected across the gradients in particle flux which span the subarctic Pacific: in the west during the Innovative North Pacific Experiment (INOPEX) and in the east along Line P. Lateral concentration gradients of dissolved ^{230}Th are small throughout the subarctic Pacific at 12 sites of variable particle flux. This contradicts the prediction of the traditional boundary scavenging model. A compilation of water column data from throughout the North Pacific reveals much larger lateral concentration gradients for ^{230}Th between the subarctic North Pacific and subtropical gyre, over lateral gradients in scavenging intensity similar to those found within the subarctic. This reflects a biogeochemical-province aspect to scavenging. Upper water column distributions of ^{231}Pa and ^{231}Pa/^{230}Th ratio are consistent with the influence of scavenging by biogenic opal, while deep waters (> 2.5 km) reveal an additional ^{231}Pa sink possibly related to manganese oxides produced at continental margins or ridge crests.

1. Introduction

Boundary scavenging (Bacon et al., 1976; Spencer et al., 1981) is a classic mechanism used to understand the cycling of chemical elements having the tendency to adsorb onto sinking particles, or to be scavenged. Scavenging (Goldberg, 1954) affects the cycling of many trace elements from micronutrients, such as Fe (Boyd and Ellwood, 2010) or Co (Bown et al., 2011), to tracers of dust deposition, such as Al (Measures and Vink, 2000) or Th (Hsieh et al., 2011). It is therefore valuable to better understand the nature of the boundary scavenging process.

The boundary scavenging mechanism predicts that those elements whose residence times are long enough to allow basin-wide isopycnal diffusion (>100 yrs), such as Pa, will be transported away from areas of low scavenging intensity to be removed in areas of high scavenging intensity (often associated with ocean boundaries) (Bacon, 1988). This lateral transfer reduces the concentration difference between ocean margin and ocean interior imposed by differential scavenging intensities. An element like Th, on the other hand, whose residence time (<50 yrs) is short enough to limit isopycnal transport, should therefore display concentrations which scale inversely with scavenging intensity. More detailed accounts of the development of boundary scavenging are given elsewhere (Anderson et al., 1990; François, 2007; Roy-Barman, 2009; Rutgers v. d. Loeff and Geibert, 2008), but few historical data exist to elucidate it in the dissolved phase of the water column. The prime objectives of this study are to relay new measurements of dissolved ^{230}Th and ^{231}Pa throughout the North Pacific and offer a new perspective on the traditional boundary scavenging concept.

The North Pacific Ocean lacks active deep water formation, which is known to influence ^{231}Pa/^{230}Th distributions in the Atlantic where surface waters of low radionuclide concentration

are injected to depth (Luo et al., 2010; Moran et al., 2002). We cannot, however, discount quantitatively the influence of the Pacific Meridional Overturning Circulation (PMOC) on dissolved $^{231}Pa/^{230}Th$ in the North Pacific, namely the northward inflow of Lower Circumpolar Deep Water (LCDW) and upwelling to form southward flowing North Pacific Deep Water (NPDW). We defer to modeling studies for a more complete treatment of PMOC (Luo et al., 2012) but signify in our work where the influence of overturning may be important. Aside from overturning, we expect ^{231}Pa and ^{230}Th distributions to be determined by the balance between production due to U decay, removal by scavenging, and redistribution by mixing. Below we elaborate on how we approach each of these terms.

The uniform distribution of ^{235}U and ^{234}U (Andersen et al., 2010; Delanghe et al., 2002; Robinson et al., 2004; Weyer et al., 2008) amounts to a constant and uniform production for ^{231}Pa and ^{230}Th, respectively, throughout the ocean. The production term, P, depends on the seawater concentration of U, which as a conservative element, varies with salinity (Chen et al., 1986).

Our basis for understanding scavenging is the one-dimensional reversible-scavenging model (Bacon and Anderson, 1982). Neglecting lateral inputs, this model predicts a linear increase with depth (z) for the concentration of dissolved (C_d) and particulate (C_p) phases for *in-situ*-produced scavenged elements. Given a group of small particles, which assumedly carry most of the scavenged element and sink at a constant speed, S, the concentrations are:

$$C_d \cong \frac{Pz}{SK}; \qquad C_p = \frac{Pz}{S}; \qquad \text{Equations (1); (2)}$$

C_d and C_p are expressed in units per volume of seawater. K is the distribution coefficient between particulate and dissolved phases $\left(\frac{C_p}{C_d}\right)$, which may vary as a function of particle

concentration or particle composition. If lateral effects can be neglected, distributions of C_d, the primary subject of study here, are expected to respond inversely to scavenging intensity, parameterized by SK.

When spatial concentration gradients exist, mixing by eddy diffusion will transport radionuclides from areas of high concentration to areas of low concentration. However, for the case of scavenged elements, one must consider the timescale (Δt) required for mixing to take place over a certain length scale (Δx) against the residence time (τ) of the element or isotope in question. Spatial concentration gradients will be undisturbed if $\Delta t >> \tau$. On the other hand, imposed gradients could be mixed away if $\Delta t << \tau$. In one-dimension, as presented by Roy-Barman (2009), the root-mean-square displacement ($\sqrt{(\Delta x)^2}$, given here for simplicity as Δx) of a randomly walking water parcel is:

$$\Delta x = \sqrt{2K_{mix}\Delta t} \qquad \text{Equation (3)}$$

where K_{mix} is the coefficient of eddy diffusion. Following Okubo et al. (2012), when substituting Δt by τ, Δx then represents the maximum length scale over which mixing influences spatial concentration gradients. Typical values in the North Pacific of isopycnal (lateral), K_H, and diapycnal (vertical), $K\rho$, eddy diffusivity are 10^3 m^2 s^{-1} and 10^{-4} m^2 s^{-1}, respectively (Kawabe, 2008).

The mixing length-scale argument calls for an appropriate definition of τ. Assuming steady-state, neglecting advective or diffusive inputs, the residence time of dissolved ^{230}Th (^{231}Pa) at any point is given by its concentration divided by the sum of its *in situ* sources: production via uranium decay and desorption, the latter of which unfortunately cannot be characterized with measurements of only C_d. Alternatively, the inventory of C_d from the surface

to some depth divided by the depth-integrated P results in the average time a dissolved nuclide resides in the integrated water column before being removed to deeper water by scavenging, irrespective of desorption within that depth zone. We find this integrated residence time to be most appropriate when considering the influence of mixing on dissolved nuclide distributions in the absence of constraints on desorption. Nonetheless, this residence time is not independent of advective or diffusive inputs where they exist. The integrated residence time will be an overestimate at locations which receive ^{230}Th (^{231}Pa) by circulation and an underestimate at locations where ^{230}Th (^{231}Pa) is removed by circulation.

2. Materials and Methods

2.1 Dissolved Th (Pa) sampling and analysis

The new data presented here were produced by groups at the Lamont-Doherty Earth Observatory (L-DEO) and the University of British Columbia (UBC). Seven profiles of dissolved ^{230}Th, ^{231}Pa, and ^{232}Th from the SO202-INOPEX cruise of July-August 2009 (Gersonde, 2012) (SO202- stations in Fig. 1) were produced at L-DEO. Five profiles of dissolved ^{230}Th from the eastern subarctic Pacific collected in summer 2006 (P and Z stations in Fig. 1, referred to collectively as Line P in the text) were produced at UBC. Additionally we draw from reported profiles of dissolved ^{230}Th and ^{231}Pa from the Hawaii Ocean Time-series collected in 2002 (ALOHA station in Fig. 1) produced by the UBC group (François, 2007) and the 2009 “baseline” profile of dissolved ^{230}Th, ^{231}Pa, and ^{232}Th from the U. S. GEOTRACES Intercalibration (SAFe station in Fig. 1) produced at L-DEO (Anderson et al., 2012). Hydrographic data for the newly reported sample locations are included in the Supplementary

Material. INOPEX data are available through PANGAEA (pangaea.de) and the BCO-DMO data repository (bcodmo.org). SAFe data are available at BCO-DMO.

Both the INOPEX and Line P cruises used similar methods for sampling for dissolved (<0.45 μm) radionuclides. The INOPEX cruise is considered GEOTRACES compliant (see geotraces.org). Detailed sampling procedures are described by Anderson et al. (2012). Logistics for both cruises did not permit the collection of sufficient particulate material for radionuclide analysis.

Radionuclide concentrations were determined by isotope dilution Inductively Coupled Plasma Mass Spectrometry at L-DEO (^{230}Th, ^{232}Th, and ^{231}Pa) and UBC (^{230}Th). Th and Pa were pre-concentrated along with ^{229}Th and ^{233}Pa by co-precipitation with 15-50 mg of added Fe. After HNO_3-$HClO_4$-HF digestion of the precipitate, Th and Pa were isolated and purified using anion exchange chromatography (Bio-rad resin AG1-X8). Full details on L-DEO procedures are reported by Anderson et al. (2012) and UBC procedures are reported by Choi et al. (2001).

For samples stored for more than a few months prior to Th/Pa purification, a small correction must be made for the ingrowth of ^{230}Th or ^{231}Pa by uranium decay during the time period between sample collection and U-Th/Pa separation (~0.03 dpm m^{-3} ^{230}Th and 0.002 dpm m^{-3} ^{231}Pa are ingrown annually). U concentrations in the samples were estimated using the bottle salinity measured from the CTD. For a full description of this correction, see the metadata associated with the INOPEX data at BCO-DMO.

A correction was also made for the ^{230}Th and ^{231}Pa added to the dissolved pool through the partial dissolution of lithogenic minerals, assuming an average lithogenic U/Th ratio, secular equilibrium within the lithogenic material and congruent dissolution, based on measured

dissolved ^{232}Th. We used ^{230}Th/^{232}Th = 4.0 x 10^{-6} mol/mol (Roy-Barman et al., 2009) and ^{231}Pa/^{232}Th = 8.8 x 10^{-8} mol/mol (Taylor and McLennan, 1985) as representative of detrital Th and Pa, respectively. This correction was possible for the INOPEX and SAFe data but not for the Line P or ALOHA data, where ^{232}Th was not measured. Detrital ^{230}Th was found to be a significant fraction (>10 %) of the dissolved ^{230}Th only in surface waters (< 200 m) proximal to mineral dust sources. Detrital ^{231}Pa was 1% of the dissolved ^{231}Pa in the INOPEX samples at its highest and <0.5% below 200 m. Dissolved ^{230}Th from ALOHA is likely less than 1% detrital below surface waters based on historical ^{232}Th measurements there (Roy-Barman et al., 1996) and detrital ^{231}Pa even less. The Line P stations are outside of the influence of Asian dust deposition, but detrital ^{230}Th advected from margin sediments is possible.

2.2 Use of total ^{230}Th and ^{231}Pa data

We draw upon previously reported profiles of total (dissolved + particulate) ^{230}Th (Nozaki et al., 1981; Nozaki and Nakanishi, 1985; Nozaki et al., 1987; Okubo et al., 2012) and of total ^{231}Pa (Nozaki and Nakanishi, 1985; Nozaki et al., 1998) (see Fig. 1). We converted total ^{230}Th (^{231}Pa) to dissolved ^{230}Th (^{231}Pa), as an attempt to remove the influence of particulate ^{230}Th (^{231}Pa), using the equation: dissolved = total*(1–K). We used average values from the most geographically relevant measurements of K, from ALOHA, K = 0.18±0.09 for ^{230}Th (Roy-Barman et al., 1996), and from AN-1, K = 0.04±0.01 for ^{231}Pa (Nozaki et al., 1998). The uncertainty in K was propagated in our dissolved estimates, but K at a specific location may be outside the cited ranges. Total radionuclides are not corrected for detrital contributions. All radionuclide concentrations have been converted into volumetric radioactivity units (dpm m^{-3}), assuming constant seawater density (1026 kg m^{-3}).

2.3 Hydrographic considerations

We use the term subarctic somewhat loosely to distinguish the INOPEX and Line P stations from the (sub)tropical sites in Figure 1. While stations SO202-36, -39, -41, and -44 are a few degrees south of the Subarctic Front defined by the 4°C isotherm at 100 m depth, they are nearly on the Subarctic Boundary defined by the surface salinity front of S = 34 (Yasuda, 2003). The Subarctic Boundary roughly corresponds to the southern and northern limits, respectively, of the cyclonic subarctic gyre and the anticyclonic subtropical gyre which are the major expressions of surface circulation in the North Pacific. There is also a relatively weak shallow overturning cell with a net northward transport of subtropical water balanced by a southward interior flow, in the form of North Pacific Intermediate Water (NPIW) (Macdonald et al., 2009).

In terms of deep circulation, Kawabe and Fujio (2010) have mapped observed flows of LCDW entering the western North Pacific at approximately 4.5 km depth, which travel north and east throughout the basin. LCDW along with the overlaying Upper Circumpolar Deep Water (UCDW) eventually upwell at various locations to become southerly flowing NPDW across the basin between ~1.5-3 km depth (Macdonald et al., 2009). This represents the schematic pattern of deep overturning in the North Pacific, but advective features may not be the dominant circulation of the basin. Circuitous, random-walk circulation generated by eddies in the deep North Pacific apparently dominate inter-basin water flux pathways (Holzer and Primeau, 2006, 2008). In the ensuing analysis, we refrain from adhering to an "advective-ocean" circulation framework and consider the influence of eddy diffusion more generally.

2.4 Indicators of expected scavenging intensity

Satellite-derived estimates of net primary productivity (NPP) are not directly related to scavenging intensity, but more biological productivity at the surface likely results in a greater sinking flux of scavenging particles. In lieu of detailed observations of the particulate matter and its scavenging characteristics at our study sites (surface area, chemical composition, aggregation tendency, etc.) and due to the long-term nature and excellent geographical coverage of satellite records, we appeal to NPP as a qualitative indicator for spatial variability in scavenging intensity. Monthly SeaWiFS-NPP data (1997-2009, 1/6°-resolution) were time-weighted averaged, ignoring missing values (Fig. S1) (http://www.science.oregonstate.edu/ocean.productivity) (Behrenfeld and Falkowski, 1997).

Export production (EP), an alternative qualitative indicator of scavenging intensity (Coale and Bruland, 1987), is defined as the sinking flux of particulate organic carbon from the euphotic zone to the ocean interior (Eppley and Peterson, 1979). The ratio of EP to NPP is termed the ef-ratio and can be estimated as a function of sea surface temperature (SST) and NPP itself (Laws et al., 2000). Export production estimates were derived by calculating the ef-ratio (Laws et al., 2000) and multiplying by the aforementioned long-term average NPP. SSTs for the ef-ratio algorithm were from the World Ocean Atlas 2009 (Locarnini et al., 2010). One reason that EP may more accurately reflect variations in scavenging intensity than does NPP is that higher EP can be associated with a greater flux of ballasting minerals (biogenic opal, $CaCO_3$, and aluminosilicates) (Boyd and Trull, 2007; Bradtmiller et al., 2010; Honda and Watanabe, 2010) which also contribute to scavenging.

3. Results and Discussion

3.1. Distribution of ^{230}Th in the subarctic Pacific

3.1.1. Uniformity of INOPEX and Line P ^{230}Th profiles

The depth profiles of dissolved ^{230}Th from the INOPEX (Fig. 2) and Line P (Fig. 3) locations are all nearly linear and quite similar to each other. Linear profiles are consistent with reversible scavenging (which neglects lateral transport) (Bacon and Anderson, 1982). We note, however, that relatively linear ^{230}Th profiles are not inconsistent with some lateral ^{230}Th transport (discussed further below) (Roy-Barman, 2009; Venchiarutti et al., 2008).

The ^{230}Th data fall within the linear depth profiles described by: [^{230}Th] = (0.05 ± 0.05) dpm m^{-3} + (0.2 ± 0.05) dpm m^{-3} km^{-1} * z, except at SO202-32 below 4.4 km. In other words, ^{230}Th concentrations at a given depth vary spatially by no more than about 25%. Our indicators for scavenging intensity, on the other hand, range from 156-436 g C m^{-2} yr^{-1} (a factor of 2.8) in NPP and 84-268 g C m^{-2} yr^{-1} (a factor of 3.2) in EP among the stations (see Table 1). A section across the North Pacific (Fig. 4) displays the uniformity of [^{230}Th] on a given isopycnal throughout the bulk of the water column. Positive (SO202-32) and negative (SO202-39, SO202-41) concentration anomalies near the seafloor are exceptions to this uniformity (section 3.1.2).

The spatial homogeneity of ^{230}Th is surprising in light of the strong gradients in expected scavenging intensity in this region, especially near the continental margins. The INOPEX stations near 40°N (SO202-36, -39, -41, and -44) are situated on an east-west NPP and EP gradient of 23 and 13 mg C m^{-2} yr^{-1} km^{-1}, respectively. Gradients are calculated by the difference in NPP (EP) over the distance between stations (SO202-36 to SO202-44 in this case). The ^{230}Th profiles from these 4 stations are consistent within error with the margin profile of dissolved

^{230}Th (converted from total) at station AN-4 (Nozaki et al., 1998), revealing little lateral gradients over even a larger transect and gradient in scavenging intensity (lateral NPP and EP gradients of 38 and 25 mg C m^{-2} yr^{-1} km^{-1}, respectively). The true gradient in scavenging intensity is most likely greater than based solely on NPP or EP because we also expect a positive east-west gradient in the flux of aerosol dust (Mahowald et al., 2005) and biogenic opal (Honjo et al., 2008; Shibamoto and Harada, 2010) on the western margin. On the eastern margin (Line P), we estimate even larger lateral gradients in scavenging intensity (NPP and EP gradients of 203 and 118 mg C m^{-2} yr^{-1} km^{-1}, respectively).

Lateral concentration gradients imposed by variable scavenging intensity could be overcome by horizontal homogenization by mixing along isopycnals, and this must be addressed in light of the observed lack of lateral gradient in [^{230}Th] in the subarctic. Using station SO202-44 as representative of the region, the integrated residence time of dissolved ^{230}Th is 11 yrs in the upper 2.5 km and is 22 yrs in the full water column (5.5 km). Using Eq. 3 ($K_H = 10^3$ m^2 s^{-1}), a timescale of 11 and 22 yrs allows diffusion to propagate to a radius of about 830 km and 1200 km, respectively. The east-west transects IN36-44 and Line P are 2100 km and 1300 km in distance, respectively. Therefore, lateral mixing does not influence ^{230}Th distributions in the upper 2.5 km of the water column. However, we cannot rule out some ^{230}Th redistribution back across lateral gradients in scavenging intensity in the deepest depths of the subarctic Pacific, as the deep mixing lengths are comparable to the section distances. If, however, SO202-44 were receiving a small input of ^{230}Th by lateral mixing, as might be expected at the "high-scavenging"-end of the 40°N transect, the cited residence times would be an overestimate and the corresponding mixing lengths would be smaller. Advection across concentration gradients

will also contribute to a redistribution of ^{230}Th (Roy-Barman, 2009), and strong deep boundary currents have been observed in the Northwest Pacific (Owens and Warren, 2001). However, given that these currents are generally non-continuous and often change direction we cannot quantify the advective contribution. Nonetheless, lateral mixing cannot explain the "missing" depletion of ^{230}Th at high scavenging intensity sites. Either our indicators of scavenging intensity or mixing rate are inadequate or ^{230}Th is displaying an unexpected insensitivity to variable scavenging intensities in the subarctic Pacific.

3.1.2. Subarctic North Pacific ^{230}Th anomalies

Station SO202-32 revealed much larger ^{230}Th concentrations (1.26-1.37 dpm m^{-3}) between 4484 m depth and the bottom (5301 m) than would be expected by extrapolating to greater depth the linear part of the profile (between 0-3.5 km depth). The neutral density horizon of this concentration anomaly (γ^n = 28.10) also shows a positive concentration anomaly in dissolved Si in the area encompassing SO202-32 (~45-50°N and 150-170°W). Talley and Joyce (1992) linked this deep Si maximum to extreme age of the bottom water which allows a greater accumulation of dissolved Si from opal dissolution at the seafloor. Perhaps this water mass accumulates dissolved ^{230}Th due to its long isolation in a low-particle flux environment. Deep waters further south also have much higher ^{230}Th concentrations (Roy-Barman et al., 1996), but we consider the possibility of advective inflow of ^{230}Th unlikely as only weak, if any, northward currents propagate towards SO202-32 (Kawabe and Fujio, 2010).

The profiles from stations SO202-5, -24, -39, and -41 have negative deviations from linearity for the bottommost sample, taken within the benthic mixed layer, as defined by the well-mixed layer of potential temperature at the bottom of the CTD profile (Richards, 1990).

Although we lack additional information about scavenging intensity in these benthic mixed layers, such as particle concentration, we suggest that the negative deviations in the [^{230}Th] profiles are the result of enhanced scavenging near the seafloor. Bottom scavenging of ^{230}Th has been found to influence many sites in the central North Pacific (Okubo et al., 2012). Sediments resuspended by deep currents, or more generally, by eddies and tidal mixing, could cause a scavenging environment with a larger K than the overlaying water column. We observe, however, that bottom scavenging does not always occur. At stations SO202-32, SO202-36, and the SAFe site (see below), 6-7 samples were taken equally spaced within 200 m of the seafloor and no significant vertical concentration gradients were observed. We infer from the spatial heterogeneity of bottom scavenging that local conditions, involving the interaction of eddies and tides with seafloor topography, influence the intensity of scavenging near the seabed.

The ^{230}Th depth profiles from Line P, SO202-5 and SO202-24 display some curvature (concave down) in the upper km. We interpret this not as reduced scavenging in upper waters but due to shoaling of the shallower isopycnals, associated with NPIW, from 45°N to 50°N (Macdonald et al., 2009). Isopycnal mixing probably supports some transfer of ^{230}Th from the south, where the isopycnal is deeper and [^{230}Th] higher, to shallower depths in the north, of course at a spatial scale concordant with the Th residence time. This situation is analogous to the ^{230}Th distributions in the Southern Ocean, where upward sloping isopycnals result in shoaling isolines of [^{230}Th] south of the polar front (Chase et al., 2003; Rutgers v. d. Loeff and Berger, 1993; Venchiarutti et al., 2011).

3.2. Response of ^{230}Th throughout the North Pacific and the nature of scavenging regimes

In contrast to the relatively homogeneous ^{230}Th profiles across the subarctic North Pacific, significant concentration gradients exist between our subarctic profiles and those reported for the subtropical gyre (Fig. 5a) (Anderson et al., 2012; François, 2007; Nozaki and Nakanishi, 1985; Nozaki and Yang, 1987; Okubo et al., 2012). Abyssal (>4 km depth), waters reach [^{230}Th] of 2 dpm m^{-3} at SAFe and at several (sub)tropical sites reported by Okubo et al. (2012). While only considering the dissolved phase in our analysis, the observed subtropical-subarctic [^{230}Th] difference is larger (≥1 dpm m^{-3}) than can be accounted for by variable contributions of particulate matter (i.e. we expect a similar concentration difference in total ^{230}Th). Additionally, while the GEOTRACES intercalibration of seawater Th analyses revealed potential for inaccuracy between labs (Anderson et al., 2012), the subarctic-subtropical ^{230}Th contrast from INOPEX to SAFe (Fig. 5a) was produced by a single lab. The similar [^{230}Th] contrast between Line P and ALOHA is corroborative evidence against laboratory offsets here.

The contrast in abyssal ^{230}Th concentrations is relatively acute along the north-south transect between SO202-36 and BO-6, spanning the subtropics, nearly to the subarctic boundary (see Fig. 1). The lateral NPP and EP gradients between these stations are 66 and 34 mg C m^{-2} yr^{-1} km^{-1}, respectively, which are similar to or smaller than those found within the subarctic (section 3.1.1). However, while the lateral [^{230}Th] gradient in the subarctic was small (d[^{230}Th]/dx < 1x10^{-4} dpm m^{-3} km^{-1}), between SO202-36 and BO-6, at 2.5 km, the lateral gradient is 2.3x10^{-4} dpm m^{-3} km^{-1}. The true lateral gradient may be larger than this, but it cannot be constrained without greater station density. There is no reason to expect smaller rates of lateral mixing in the north-south direction. Consequently, there must be a larger lateral gradient in scavenging

intensity across the gyres than within the subarctic to explain the larger lateral concentration gradient in ^{230}Th.

To understand why ^{230}Th appears to respond to a scavenging gradient in one area (across gyres) and not another (within a gyre) we compare water column ^{230}Th inventories to a depth of 2.5 km for all locations in Fig. 1, except P4 where water depth is only 1323 m. At each included site, the seafloor is >800 m below 2.5 km, to avoid the influence of bottom scavenging. As well, at 2.5 km depth, neutral density does not vary greatly over the North Pacific (γ^n = 27.98-28.01). This inventory reflects a bulk average of scavenging intensity within the depth zone integrated.

Thorium-230 inventories from INOPEX, Line P, and AN-4 are within 25% of each other (Fig. 6a, Table 1). Yet NPP and EP range between 156-300 and 84-155 g C m^{-2} yr^{-1}, respectively (factors of 1.9 and 1.8). Two of the sites for which the dissolved inventory is estimated from total ^{230}Th in this NPP/EP range show relatively high inventories compared with the INOPEX and Line P locations. These sites (BO-1 and CY-5) are proximal to the INOPEX stations near 40° N, so it is unlikely that an advective influence is responsible for the discrepancy. The true value of K at BO-1 and CY-5 may be larger than 0.18±0.09, the value assumed when converting total ^{230}Th to dissolved ^{230}Th (see section 2.2). These sites would need, however, K=0.5 to bring the inventories into better agreement. A value that high has typically only been found at very productive near-margin sites, for instance K=0.46 in the Guatamala Basin (Bacon and Anderson, 1982) and K=0.52 in the Japan Sea (Nozaki et al., 1987). Thus we cannot fully explain the high ^{230}Th inventories at BO-1 and CY-5.

Thorium-230 inventories rise substantially as NPP and EP decline below 125 and 50 g C m^{-2} yr^{-1}, respectively (Fig. 6). Inventories at the two subtropical sites (ALOHA and SAFe) from

which dissolved data are available rise to nearly twice the average of the subarctic sites. Dissolved inventories based on total ^{230}Th in the lower NPP/EP range are more variable but all are >1000 dpm m^{-2}. Variable contributions of detrital ^{230}Th or unaccounted variations in K across the (sub)tropical sites are unlikely to be large enough to explain this variability.

The observation that ^{230}Th inventories become much larger only below a certain NPP/EP level signifies an apparent threshold behavior for Th removal. Okubo et al. (2012) noted that [^{230}Th] roughly scaled inversely with bio-productivity among sites BO-4, HY-3, HY-2, and HY-1, as expected for a simple relationship between bioproductivity and scavenging intensity. Inclusion of sites from all across the North Pacific here, however, questions the robustness of such a simple relation. A step function of ^{230}Th inventory between high and low scavenging regimes may be more reflective of the data.

This step in Th inventories occurs across a specific threshold of NPP/EP, but the sites on either side of that threshold are geographically distinct. Sites with high and low ^{230}Th inventories largely coincide, respectively, with the subarctic and subtropical gyres, representing very different biomes (Longhurst, 1998). Large phytoplankton and diatoms are more prevalent in the subarctic while picoplankton dominate the subtropics (Alvain et al., 2008; Hashioka and Yamanaka, 2007). We hypothesize that disparate biogeographic communities produce particulate material with sufficiently contrasting physicochemical characteristics (such as surface area, chemical affinity of sorption sties, density, aggregation efficiency, etc.) to produce the threshold between scavenging regimes. This is not inconsistent with our present understanding of boundary scavenging but adds to our knowledge of its geographic scale. “Boundaries” may be more akin to particular biogeographic provinces rather than simply areas of enhanced particle

flux. Future studies of marine particulate matter should seek to constrain which of the relevant particle characteristics vary most strongly across the Th scavenging regimes.

3.3 Scavenging regimes for ^{231}Pa

3.3.1 INOPEX and (sub)tropical ^{231}Pa profiles

The dissolved ^{231}Pa data from the INOPEX sites (Fig. 7), like those of ^{230}Th, are similar to each other when compared in depth profile. The upper (<2.5 km) and full water column residence times of dissolved ^{231}Pa at SO202-44 are 49 and 103 yrs (vs. 11 and 22 yrs for ^{230}Th), respectively. Isopycnal mixing for these timescales would cover a radius of ~1800 km in the upper water column, comparable to the IN36-44 transect, and 2550 km in the full water column, nearly encompassing the entire subarctic. Therefore within the subarctic, the concentration gradients imposed by variable scavenging intensity could be masked by the redistribution of ^{231}Pa by isopycnal mixing.

At station SO202-36, a sample at 996 m depth is outlying as anomalously high compared to the rest of the relatively smooth profile. The ^{230}Th and ^{232}Th analyses of this sample had no profile anomaly and the Pa mass spectrometry was repeated with the same result. We therefore attribute the anomalous ^{231}Pa data point to some other analytical error, perhaps sample-to-sample contamination after Pa had been separated from Th, and do not include it in our analysis.

Unlike the ^{230}Th results, the INOPEX ^{231}Pa profiles are in general non-linear, manifested primarily by a decrease or uniformity with depth of [^{231}Pa] at depths >3500 m (Fig. 7). Stations SO202-5 and SO202-36 do not fully resolve this feature, which the deeper INOPEX stations show consistently. Whatever factor is responsible for the anomalously high [^{230}Th] in the deepest samples of SO202-32 does not affect [^{231}Pa].

Concentrations of ^{231}Pa from the ALOHA and SAFe stations are generally larger than at the subarctic sites, at least between 1 and 3 km (Fig. 5b). Both subtropical profiles are non-linear, with [^{231}Pa] slightly decreasing at depths >2 km (compared with 3.5 km in the subarctic). Non-linear depth profiles of total ^{231}Pa have been reported (Nozaki and Nakanishi, 1985; Nozaki et al., 1998) for the (sub)tropical Pacific (CE-8, CE-13, and AN-1 in Fig. 1) which are generally in agreement with both ALOHA and SAFe.

3.3.2 The upper water column (sub)tropical to subarctic contrast in ^{231}Pa

Inventories down to 2.5 km (Fig. 8, Table 1) show a greater disparity between subarctic and subtropical sites (factor of 3) for ^{231}Pa than for ^{230}Th (factor of 2). In light of the five-fold greater residence time of dissolved Pa, which allows for more lateral homogenization by lateral mixing than for Th, this larger fractional difference in the upper water column inventory informs us that the difference in scavenging intensity between subarctic and subtropical regimes is far greater for Pa than for Th. This is actually captured in the modeling of dissolved ^{231}Pa in the North Pacific by Roy-Barman (2009), imposed by a larger relative difference in K from ocean margin to ocean interior for ^{231}Pa than for ^{230}Th. What is surprising from the INOPEX observations is that “the margin” appears not to be the thin zone of high productivity near the continents but the entire subarctic gyre. The (sub)tropical-subarctic contrast in the upper water column ^{231}Pa distribution also suggests a threshold type behavior related to the biological community contrast between the gyres.

The tendency of Pa to adsorb onto biogenic opal with greater affinity than other prevalent marine particulate phases (Chase et al., 2002; Geibert and Usbeck, 2004; Guo et al., 2002; Kretschmer et al., 2011; Scholten et al., 2005; Yu et al., 2001) is a natural way to link the

chemical property of scavenging intensity to the biogeographic property of community structure. Opal concentration and flux is much larger in the subarctic than in the subtropical North Pacific (Bishop et al., 1999; Bishop and Wood, 2008; Karl et al., 2012; Lam et al., 2011; Scharek et al., 1999; Shibamoto and Harada, 2010). Greater fluxes of opal with high K values likely draw down [^{231}Pa] in the upper waters of the subarctic (Taguchi et al., 1989), so much so that a large lateral subtropical-subarctic concentration gradient is supported despite the influence of lateral mixing. Future paired measurements of particulate ^{231}Pa and opal in North Pacific GEOTRACES sections will test this hypothesis.

3.3.3 Deepwater ^{231}Pa distributions and a proposed deep sink

Negative deviations in [^{231}Pa] from linear profiles are observed in both the subarctic and subtropical regimes (Fig. 5b). The relative depletion of [^{231}Pa], as estimated by extending the linear profile in the upper 2 km downwards and subtracting the observed profile, is larger for the subtropical sites than for that of the INOPEX sites. Whatever process is responsible for these depletions, the result is a relatively uniform distribution of [^{231}Pa] at great depth (3500-5500 m) across the North Pacific ([^{231}Pa] = 0.35-0.5 dpm m^{-3}).

Four possible explanations for deepwater depletions in North Pacific [^{231}Pa] can be suggested: (1) advective inflow of water with lower [^{231}Pa] from the south; (2) upwelling of LCDW into NPDW; (3) intense local scavenging by sediments at the seafloor and/or by resuspended sediments in nepheloid layers (McCave, 1986) (bottom scavenging); or (4) removal by lateral mixing to sites of higher scavenging intensity. We consider each explanation below.

The inflow of LCDW from the Southern Ocean to the subarctic along the western edge of the North Pacific could influence the INOPEX, ALOHA and SAFe profiles. Profiles of total

^{231}Pa from CE-8, CE-13 and AN-1 which are "upstream" of the INOPEX stations, however, show that [^{231}Pa] in LCDW is roughly 0.4-0.5 dpm m^{-3}, higher than or similar to that observed at the INOPEX stations. This is inconsistent with an advective input lowering deepwater [^{231}Pa] at the INOPEX sites. For the subtropical sites, advection is more difficult to discount because "upstream" ^{231}Pa data in the South Pacific are extremely limited. The one site with upstream water column ^{231}Pa data, M1 of the JGOFS-AESOPS program (53°S, 174.7°W), is situated at the beginning of the northward path of LCDW into the Pacific, and has [^{231}Pa] at this density horizon of similar magnitude to that seen in the (sub)tropics (~0.4 dpm m^{-3}) (Chase et al., 2003). However, given that the ageing of deep water between M1 and ALOHA is roughly 500 yrs (Khatiwala et al., 2012; Matsumoto, 2007), one expects in-growth toward a linear profile to increase [^{231}Pa] along this route, as in North Atlantic Deep Water (Moran et al., 2002). Some other process, aside from lateral advection, must be removing ^{231}Pa from the deep North Pacific.

In terms of upwelling, explanation (2), and PMOC in general, the existing distribution of dissolved ^{231}Pa data is too sparse to evaluate the importance of this process. Another scavenged element with an ocean residence time on the order of or longer than that of Pa is Nd (Goldstein and Hemming, 2003). The isotopic composition of Nd (ϵ_{Nd}) does not show the non-radiogenic signature expected from southern-sourced water at BO-1, in the subarctic (Amakawa et al., 2009). Seawater profiles of ϵ_{Nd} from sites across the subtropical North Pacific (Amakawa et al., 2004; Amakawa et al., 2009; Piepgras and Jacobsen, 1988), including SAFe (Pahnke et al., 2012), indicate a characteristic presence of southern-sourced bottom water in the western but not the central or eastern subtropical Pacific. These observations argue against a basin-wide influence of bottom water inflow and subsequent upwelling on scavenged elements; however,

because data on ϵ_{Nd} in the Pacific is also sparse, uncertainties exist as to whether it can be used to trace water masses as it is in the Atlantic (Jones et al., 2008).

Bottom scavenging, explanation (3), as the sole deep Pa-removal process, would require an unreasonably large vertical extension in the subtropics but it may be a factor for subarctic Pa. The full water column residence time of ^{231}Pa at SO202-44 and ALOHA is 103 and 173 yrs, respectively. The resulting extent of vertical mixing influence in the subarctic is therefore 0.8-1.6 km, using Eq. 3 and K_ρ=1-4x10^{-4} m^2 s^{-1}, which is comparable to the depth zone of subarctic ^{231}Pa depletion. The respective mixing scale at ALOHA is 1-2 km which is smaller than the subtropical depletion zone, 2.5-3 km above the bottom. Additionally, there is no measurable bottom depletion of ^{230}Th at the SAFe station, which would be expected if bottom scavenging of ^{231}Pa were occurring in the subtropics.

Removal by lateral mixing, explanation (4), is therefore the lead hypothesis for deep Pa depletions in the North Pacific, while bottom scavenging may be equally likely in the subarctic. Removal by lateral mixing implies some deep (>2.5 km) ^{231}Pa sink somewhere in the Pacific, but our results do not reveal its location(s). Future studies, such as the GEOTRACES program, should seek to identify these deep Pa sinks as well as the processes involved. High scavenging intensity at the site of Pa removal could be manifested by a high vertical flux of particles in addition to a change in the chemical composition of particles. In particular, MnO_2, like biogenic opal, is known to have a strong affinity for Pa (Anderson et al., 1983). We hypothesize that authigenic Mn (oxy)hydroxide particles or coatings associated with reducing sediment conditions (Spencer et al., 1981) or hydrothermal vents and plumes (Anderson et al., 1990; Shimmield and

Price, 1988) act as a predominant ^{231}Pa sink near continental margins and ridge crests, respectively.

In summary, Fig. 5c highlights the differences between subarctic and subtropical profiles of the dissolved ^{231}Pa/^{230}Th ratio. Uncertainties in the ratio are too large above 500 m to differentiate between the subarctic and subtropics. Within 0.5-2.5 km depth, however, the INOPEX profiles clearly have a lower ^{231}Pa/^{230}Th ratio, consistent with ^{231}Pa being more intensely scavenged in the subarctic because of greater opal abundance and with the conclusion that lateral mixing is not fast enough to overcome this imposed gradient. Below 2.5 km, the situation reverses, with lower ^{231}Pa/^{230}Th ratio in the subtropical profiles. This would be consistent with the classical concept of boundary scavenging, where a larger depletion of ^{230}Th (compared to that for ^{231}Pa) in the subarctic drives the increase in the ^{231}Pa/^{230}Th ratio. However, it appears the deep water ^{231}Pa/^{230}Th distribution is not strictly related to contrasting vertical particle flux but involves proximity to a deep ^{231}Pa sink to which ^{231}Pa is removed by lateral mixing to a greater extent in the subtropics.

4. Conclusions

Based on the available data, dissolved ^{230}Th and ^{231}Pa are uniformly distributed throughout the subarctic Pacific despite large spatial gradients in particle flux. Enhanced removal and corresponding depletion from the water column of ^{230}Th toward the margin, expected because of its short residence time, was absent in both the eastern and western subarctic regions. Large lateral [^{230}Th] gradients do exist between the subarctic and subtropical Pacific gyres and the relative contrast is even larger for [^{231}Pa] in the upper 2.5 km, despite its greater residence time. This indicates a much larger relative difference in scavenging intensity between the two

regimes than within either regime, and the effect is greater for Pa than for Th. We suggest a threshold-like behavior between gyres in scavenging removal, tied to the distinct ecosystems that inhabit each gyre, with the larger response of ^{231}Pa linked to scavenging by opal in the subarctic. We conclude that the boundary scavenging concept applies to different spatial scales than originally proposed: gyre to gyre contrast rather than margin (or small zone of high scavenging intensity) to open ocean contrast, at least in the North Pacific.

In deepwater, the contrast in concentration between the subtropics and subarctic is smaller for ^{231}Pa than ^{230}Th, as expected from their respective residence times and the timescale for isopycnal mixing. We hypothesize that ^{231}Pa is strongly scavenged by a putative sedimentary Mn oxide sink primarily at depths >2.5 km throughout the North Pacific. The influence of PMOC on ^{231}Pa/^{230}Th distributions (Luo et al., 2012) cannot be ruled out quantitatively based on our data, although we have focused our interpretations primarily on the biogeographic nature of scavenging regimes.

Acknowledgements

We acknowledge the German Ministry of Education and Research (BmBF) for financially supporting the SO202-INOPEX cruise, the U.S. National Science Foundation for funding the work at L-DEO (award 1029211), and the Swiss National Science Foundation for the postdoctoral fellowship (request no. PBEZ2-111588) that funded the work of SLJ at UBC. The R/V *Sonne* crew, all INOPEX participants, especially Jian Ren and Oliver Esper, are greatly acknowledged for help sampling on SO202. Discussions with Jerry McManus, Samar Khatiwala and Yiming Luo were helpful. We thank Gideon Henderson, Walter Geibert, Mathieu Roy-

Barman, and an anonymous reviewer for constructive reviews. Figures 1 and 4 were produced with Ocean Data View (R. Schlitzer, http://odv.awi.de, 2011). This is L-DEO Contribution 7678.

References

Alvain, S., Moulin, C., Dandonneau, Y., Loisel, H., 2008. Seasonal distribution and succession of dominant phytoplankton groups in the global ocean: A satellite view. Global Biogeochem. Cycles 22, GB3001.

Amakawa, H., Nozaki, Y., Alibo, D.S., Zhang, J., Fukugawa, K., Nagai, H., 2004. Neodymium isotopic variations in Northwest Pacific waters. Geochim. Cosmochim. Acta 68, 715-727.

Amakawa, H., Sasaki, K., Ebihara, M., 2009. Nd isotopic composition in the central North Pacific. Geochim. Cosmochim. Acta 73, 4705-4719.

Andersen, M.B., Stirling, C.H., Zimmermann, B., Halliday, A.N., 2010. Precise determination of the open ocean $^{234}U/^{238}U$ composition. Geochem. Geophys. Geosyst. 11, Q12003.

Anderson, R.F., Bacon, M.P., Brewer, P.G., 1983. Removal of ^{230}Th and ^{231}Pa at ocean margins. Earth Planet. Sci. Lett. 66, 73-90.

Anderson, R.F., Fleisher, M.Q., Robinson, L.F., Edwards, R.L., Hoff, J., Moran, S.B., Rutgers van der Loeff, M.M., Thomas, A.L., Roy-Barman, M., François, R., 2012. GEOTRACES intercalibration of ^{230}Th, ^{232}Th, ^{231}Pa, and prospects for ^{10}Be. Limnol. Oceanogr. Methods 10, 179-213.

Anderson, R.F., Lao, Y., Broecker, W.S., Trumbore, S.E., Hofmann, H.J., Wolfli, W., 1990. Boundary scavenging in the Pacific Ocean: a comparison of ^{10}Be and ^{231}Pa. Earth Planet. Sci. Lett. 96, 287-304.

Bacon, M.P., 1988. Tracers of chemical scavenging in the ocean: boundary effects and large-scale chemical fractionation. Philos. Trans. R. Soc. London, Ser. A 325, 147-160.

Bacon, M.P., Anderson, R.F., 1982. Distribution of thorium isotopes between dissolved and particulate forms in the deep sea. J. Geophys. Res. 87, 2045-2056.

Bacon, M.P., Spencer, D.W., Brewer, P.G., 1976. $^{210}Pb/^{226}Ra$ and $^{210}Po/^{210}Pb$ disequilibria in seawater and suspended particulate matter. Earth Planet. Sci. Lett. 32, 277-296.

Behrenfeld, M.J., Falkowski, P.G., 1997. Photosynthetic Rates Derived from Satellite-Based Chlorophyll Concentration. Limnol. Oceanogr. 42, 1-20.

Bishop, J.K.B., E. Calvert, S., Soon, M.Y.S., 1999. Spatial and temporal variability of POC in the northeast Subarctic Pacific. Deep Sea Res. Part II 46, 2699-2733.

Bishop, J.K.B., Wood, T.J., 2008. Particulate matter chemistry and dynamics in the twilight zone at VERTIGO, ALOHA and K2 sites. Deep Sea Res. Part I 55, 1684-1706.

Bown, J., Boye, M., Baker, A., Duvieilbourg, E., Lacan, F., Le Moigne, F., Planchon, F., Speich, S., Nelson, D.M., 2011. The biogeochemical cycle of dissolved cobalt in the Atlantic and the Southern Ocean south off the coast of South Africa. Mar. Chem. 126, 193-206.

Boyd, P.W., Ellwood, M.J., 2010. The biogeochemical cycle of iron in the ocean. Nat. Geosci. 3, 675-682.

Boyd, P.W., Trull, T.W., 2007. Understanding the export of biogenic particles in oceanic waters: Is there consensus? Prog. Oceanogr. 72, 276-312.

Bradtmiller, L.I., Anderson, R.F., Sachs, J.P., Fleisher, M.Q., 2010. A deeper respired carbon pool in the glacial equatorial Pacific Ocean. Earth Planet. Sci. Lett. 299, 417-425.

Chase, Z., Anderson, R.F., Fleisher, M.Q., Kubik, P.W., 2002. The influence of particle composition and particle flux on scavenging of Th, Pa and Be in the ocean. Earth Planet. Sci. Lett. 204, 215-229.

Chase, Z., Anderson, R.F., Fleisher, M.Q., Kubik, P.W., 2003. Scavenging of ^{230}Th, ^{231}Pa and ^{10}Be in the Southern Ocean (SW Pacific sector): the importance of particle flux, particle composition and advection. Deep Sea Res. Part II 50, 739-768.

Chen, J.H., Lawrence Edwards, R., Wasserburg, G.J., 1986. ^{238}U, ^{234}U and ^{232}Th in seawater. Earth Planet. Sci. Lett. 80, 241-251.

Choi, M.S., Francois, R., Sims, K., Bacon, M.P., Brown-Leger, S., Fleer, A.P., Ball, L., Schneider, D., Pichat, S., 2001. Rapid determination of 230Th and 231Pa in seawater by desolvated micro-nebulization Inductively Coupled Plasma magnetic sector mass spectrometry. Marine Chemistry 76, 99-112.

Coale, K.H., Bruland, K.W., 1987. Oceanic stratified euphotic zone as elucidated by ^{234}Th:^{238}U disequilibria. Limnol. Oceanogr. 32, 189-200.

Delanghe, D., Bard, E., Hamelin, B., 2002. New TIMS constraints on the uranium-238 and uranium-234 in seawaters from the main ocean basins and the Mediterranean Sea. Mar. Chem. 80, 79-93.

Eppley, R.W., Peterson, B.J., 1979. Particulate organic matter flux and planktonic new production in the deep ocean. Nature 282, 677.

François, R., 2007. Paleoflux and Paleocirculation from Sediment ^{230}Th and ^{231}Pa/^{230}Th, in: Claude, H.M., Anne De, V. (Eds.), Developments in Marine Geology. Elsevier, pp. 681-716.

Geibert, W., Usbeck, R., 2004. Adsorption of thorium and protactinium onto different particle types: experimental findings. Geochim. Cosmochim. Acta 68, 1489-1501.

Gersonde, R., 2012. The expedition of the research vessel "Sonne" to the subpolar North Pacific and the Bering Sea in 2009 (SO202-INOPEX). Reports on Polar and Marine Research 643, 323.

Goldberg, E.D., 1954. Marine geochemistry 1. chemical scavengers of the sea. J. Geol. 62, 249-265.

Goldstein, S., Hemming, S., 2003. Long-lived Isotopic Tracers in Oceanography, Paleoceanography, and Ice-sheet Dynamics. Treatise on Geochemistry 6, 453-489.

Guo, L., Chen, M., Gueguen, C., 2002. Control of Pa/Th ratio by particulate chemical composition in the ocean. Geophys. Res. Lett. 29, 1961.

Harrison, P., Whitney, F., Tsuda, A., Saito, H., Tadokoro, K., 2004. Nutrient and Plankton Dynamics in the NE and NW Gyres of the Subarctic Pacific Ocean. J. Oceanogr. 60, 93-117.

Hashioka, T., Yamanaka, Y., 2007. Seasonal and regional variations of phytoplankton groups by top–down and bottom–up controls obtained by a 3D ecosystem model. Ecol. Model. 202, 68-80.

Holzer, M., Primeau, F.W., 2006. The diffusive ocean conveyor. Geophysical Research Letters 33, L14618.

Holzer, M., Primeau, F.W., 2008. The path-density distribution of oceanic surface-to-surface transport. Journal of Geophysical Research: Oceans 113, C01018.

Honda, M.C., Watanabe, S., 2010. Importance of biogenic opal as ballast of particulate organic carbon (POC) transport and existence of mineral ballast-associated and residual POC in the Western Pacific Subarctic Gyre. Geophys. Res. Lett. 37, L02605.

Honjo, S., Manganini, S.J., Krishfield, R.A., Francois, R., 2008. Particulate organic carbon fluxes to the ocean interior and factors controlling the biological pump: A synthesis of global sediment trap programs since 1983. Prog. Oceanogr. 76, 217-285.

Hsieh, Y.-T., Henderson, G.M., Thomas, A.L., 2011. Combining seawater ^{232}Th and ^{230}Th concentrations to determine dust fluxes to the surface ocean. Earth Planet. Sci. Lett. 312, 280-290.

Jones, K.M., Khatiwala, S.P., Goldstein, S.L., Hemming, S.R., van de Flierdt, T., 2008. Modeling the distribution of Nd isotopes in the oceans using an ocean general circulation model. Earth Planet. Sci. Lett. 272, 610-619.

Karl, D.M., Church, M.J., Dore, J.E., Letelier, R.M., Mahaffey, C., 2012. Predictable and efficient carbon sequestration in the North Pacific Ocean supported by symbiotic nitrogen fixation. Proc. Natl. Acad. Sci. U. S. A.

Kawabe, M., 2008. Vertical and horizontal eddy diffusivities and oxygen dissipation rate in the subtropical Northwest Pacific. Deep Sea Res. Part I 55, 247-260.

Kawabe, M., Fujio, S., 2010. Pacific ocean circulation based on observation. J. Oceanogr. 66, 389-403.

Khatiwala, S., Primeau, F., Holzer, M., 2012. Ventilation of the deep ocean constrained with tracer observations and implications for radiocarbon estimates of ideal mean age. Earth Planet. Sci. Lett. 325–326, 116-125.

Kretschmer, S., Geibert, W., Rutgers van der Loeff, M.M., Schnabel, C., Xu, S., Mollenhauer, G., 2011. Fractionation of 230Th, 231Pa, and 10Be induced by particle size and composition within an opal-rich sediment of the Atlantic Southern Ocean. Geochim. Cosmochim. Acta 75, 6971-6987.

Lam, P.J., Doney, S.C., Bishop, J.K.B., 2011. The dynamic ocean biological pump: Insights from a global compilation of particulate organic carbon, $CaCO_3$, and opal concentration profiles from the mesopelagic. Global Biogeochem. Cycles 25, GB3009.

Laws, E.A., Falkowski, P.G., Smith, W.O., Jr., Ducklow, H., McCarthy, J.J., 2000. Temperature effects on export production in the open ocean. Global Biogeochem. Cycles 14, 1231-1246.

Locarnini, R.A., Mishonov, A.V., Antonov, J.I., Boyer, T.P., Garcia, H.E., Baranova, O.K., Zweng, M.M., Johnson, D.R., 2010. World Ocean Atlas 2009, Volume 1: Temperature. U. S. Government Printing Office, Washington, D. C.

Longhurst, A., 1998. Ecological Geography of the Sea. Academic Press, San Diego.

Luo, Y., Francois, R., Allen, S.E., 2010. Sediment $^{231}Pa/^{230}Th$ as a recorder of the rate of the Atlantic meridional overturning circulation: insights from a 2-D model. Ocean Sciences 6, 381-400.

Luo, Y., Francois, R., Allen, S.E., 2012. The influence of deep water circulation on the distribution of ^{231}Pa and ^{230}Th in the water column and sediments of the Pacific Ocean. Mineralogical Magazine 75, 2042.

Macdonald, A.M., Mecking, S., Robbins, P.E., Toole, J.M., Johnson, G.C., Talley, L., Cook, M., Wijffels, S.E., 2009. The WOCE-era 3-D Pacific Ocean circulation and heat budget. Prog. Oceanogr. 82, 281-325.

Mahowald, N.M., Baker, A.R., Bergametti, G., Brooks, N., Duce, R.A., Jickells, T.D., Kubilay, N., Prospero, J.M., Tegen, I., 2005. Atmospheric global dust cycle and iron inputs to the ocean. Global Biogeochem. Cycles 19, GB4025.

Matsumoto, K., 2007. Radiocarbon-based circulation age of the world oceans. J. Geophys. Res. 112, C09004.

McCave, I.N., 1986. Local and global aspects of the bottom nepheloid layers in the world ocean. Netherlands Journal of Sea Research 20, 167-181.

Measures, C.I., Vink, S., 2000. On the use of dissolved aluminum in surface waters to estimate dust deposition to the ocean. Global Biogeochem. Cycles 14, 317-327.

Moran, S.B., Shen, C.C., Edmonds, H.N., Weinstein, S.E., Smith, J.N., Edwards, R.L., 2002. Dissolved and particulate ^{231}Pa and ^{230}Th in the Atlantic Ocean: constraints on intermediate/deep water age, boundary scavenging, and ^{231}Pa/^{230}Th fractionation. Earth Planet. Sci. Lett. 203, 999-1014.

Nozaki, Y., Horibe, Y., Tsubota, H., 1981. The water column distributions of thorium isotopes in the western North Pacific. Earth Planet. Sci. Lett. 54, 203-216.

Nozaki, Y., Nakanishi, T., 1985. ^{231}Pa and ^{230}Th profiles in the open ocean water column. Deep Sea Res. Part A 32, 1209-1220.

Nozaki, Y., Yamada, M., Nakanishi, T., Nagaya, Y., Nakamura, K., Shitashima, K., Tsubota, H., 1998. The distribution of radionuclides and some trace metals in the water columns of the Japan and Bonin trenches. Oceanologica Acta 21, 469-484.

Nozaki, Y., Yang, H.-S., 1987. Th and Pa isotopes in the waters of the western margin of the pacific near Japan: Evidence for release of ^{228}Ra and ^{227}Ac from slope sediments. Journal of Oceanography 43, 217-227.

Nozaki, Y., Yang, H.-S., Yamada, M., 1987. Scavenging of Thorium in the Ocean. J. Geophys. Res. 92, 772-778.

Okubo, A., Obata, H., Gamo, T., Yamada, M., 2012. 230Th and 232Th distributions in mid-latitudes of the North Pacific Ocean: Effect of bottom scavenging. Earth Planet. Sci. Lett. 339–340, 139-150.

Owens, W.B., Warren, B.A., 2001. Deep circulation in the northwest corner of the Pacific Ocean. Deep Sea Research Part I: Oceanographic Research Papers 48, 959-993.

Pahnke, K., van de Flierdt, T., Jones, K.M., Lambelet, M., Hemming, S.R., Goldstein, S.L., 2012. GEOTRACES intercalibration of neodymium isotopes and rare earth element concentrations in seawater and suspended particles. Part 2: Systematic tests and baseline profiles. Limnol. Oceanogr. Methods 10, 252-269.

Piepgras, D.J., Jacobsen, S.B., 1988. The isotopic composition of neodymium in the North Pacific. Geochim. Cosmochim. Acta 52, 1373-1381.

Richards, K.J., 1990. Physical processes in the benthic boundary layer. Philos. Trans. R. Soc. London, Ser. A 331, 3-13.

Robinson, L.F., Belshaw, N.S., Henderson, G.M., 2004. U and Th concentrations and isotope ratios in modern carbonates and waters from the Bahamas. Geochim. Cosmochim. Acta 68, 1777-1789.

Roy-Barman, M., 2009. Modelling the effect of boundary scavenging on thorium and protactinium profiles in the ocean. Biogeosciences 6, 3091-3197.

Roy-Barman, M., Chen, J.H., Wasserburg, G.J., 1996. ^{230}Th-^{232}Th systematics in the central Pacific Ocean: The sources and the fates of thorium. Earth Planet. Sci. Lett. 139, 351-363.

Roy-Barman, M., Lemaître, C., Ayrault, S., Jeandel, C., Souhaut, M., Miquel, J.C., 2009. The influence of particle composition on thorium scavenging in the Mediterranean Sea. Earth Planet. Sci. Lett. 286, 526-534.

Rutgers v. d. Loeff, M., Berger, G.W., 1993. Scavenging of ^{230}Th and ^{231}Pa near the antarctic polar front in the South Atlantic. Deep Sea Res. Part I 40, 339-357.

Rutgers v. d. Loeff, M., Geibert, W., 2008. U- and Th-Series Nuclides as Tracers of Particle Dynamics, Scavenging and Biogeochemical Cycles in the Oceans, in: Krishnaswami, S., Cochran, J.K. (Eds.), Radioactivity in the Environment. Elsevier, pp. 227-268.

Scharek, R., Tupas, L.M., Karl, D.M., 1999. Diatom fluxes to the deep sea in the oligotrophic North Pacific gyre at Station ALOHA. Mar. Ecol. Prog. Ser. 182, 55-67.

Scholten, J.C., Fietzke, J., Mangini, A., Stoffers, P., Rixen, T., Gaye-Haake, B., Blanz, T., Ramaswamy, V., Sirocko, F., Schulz, H., Ittekkot, V., 2005. Radionuclide fluxes in the Arabian Sea: the role of particle composition. Earth Planet. Sci. Lett. 230, 319-337.

Shibamoto, Y., Harada, K., 2010. Silicon flux and distribution of biogenic silica in deep-sea sediments in the western North Pacific Ocean. Deep Sea Res. Pt. I 57, 163-174.

Shimmield, G.B., Price, N.B., 1988. The scavenging of U, ^{230}Th and ^{231}Pa during pulsed hydrothermal activity at 20°S, East Pacific Rise. Geochim. Cosmochim. Acta 52, 669-677.

Spencer, D.W., Bacon, M.P., Brewer, P.G., 1981. Models of the distribution of ^{210}Pb in a section across the North Equatorial Atlantic Ocean. J. Mar. Res. 39, 119-138.

Taguchi, K., Harada, K., Tsunogai, S., 1989. Particulate removal of ^{230}Th and ^{231}Pa in the biologically productive northern North Pacific. Earth Planet. Sci. Lett. 93, 223-232.

Talley, L.D., Joyce, T.M., 1992. The double silica maximum in the North Pacific. J. Geophys. Res. 97, 5465-5480.

Taylor, S.R., McLennan, S.M., 1985. The Continental Crust: Its Composition and Evolution. Blackwell, Oxford.

Venchiarutti, C., Jeandel, C., Roy-Barman, M., 2008. Particle dynamics study in the wake of Kerguelen Island using thorium isotopes. Deep Sea Research Pt. I: Oceanographic Research Papers 55, 1343-1363.

Venchiarutti, C., van der Loeff, M.R., Stimac, I., 2011. Scavenging of ^{231}Pa and thorium isotopes based on dissolved and size-fractionated particulate distributions at Drake Passage (ANTXXIV-3). Deep Sea Res. Pt. II 58, 2767-2784.

Weyer, S., Anbar, A.D., Gerdes, A., Gordon, G.W., Algeo, T.J., Boyle, E.A., 2008. Natural fractionation of ^{238}U/^{235}U. Geochim. Cosmochim. Acta 72, 345-359.

Yasuda, I., 2003. Hydrographic structure and variability in the Kuroshio-Oyashio Transition Area. J. Oceanogr. 59, 389-402.

Yu, E.F., Francois, R., Bacon, M.P., Fleer, A.P., 2001. Fluxes of ^{230}Th and ^{231}Pa to the deep sea: implications for the interpretation of excess ^{230}Th and ^{231}Pa/^{230}Th profiles in sediments. Earth Planet. Sci. Lett. 191, 219-230.

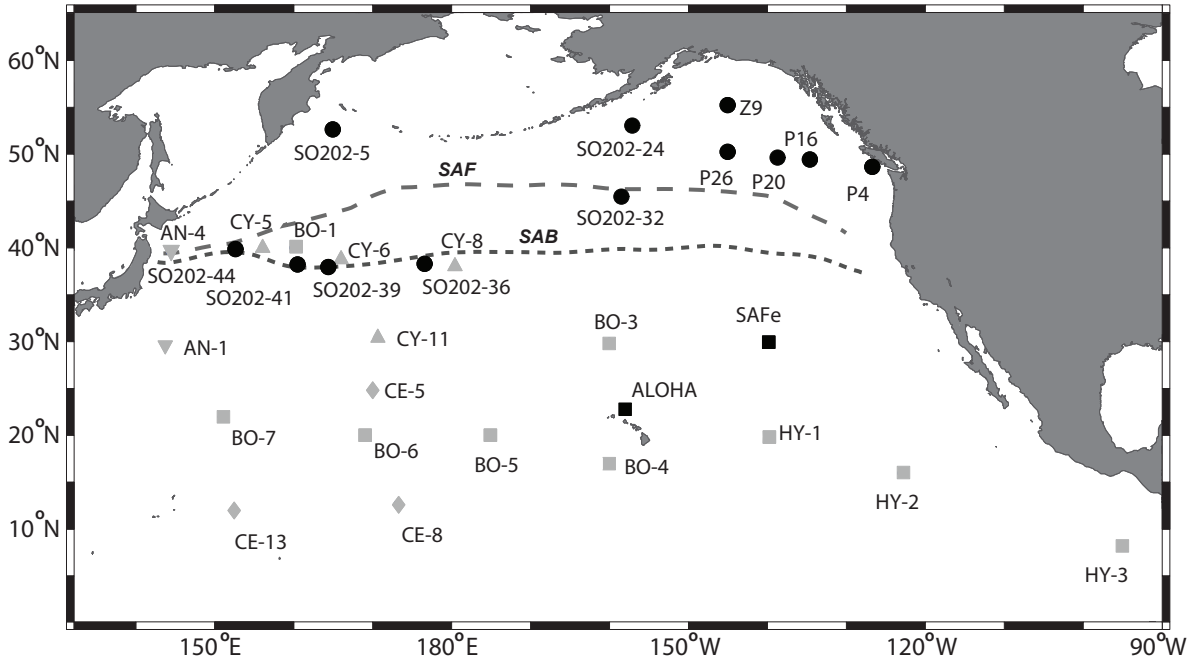

Figure 1. Map of station locations for dissolved radionuclide data presented in the paper (black circles) and those for which total radionuclide data has been reported: gray triangles (Nozaki et al., 1981), graydiamonds (Nozaki and Nakanishi, 1985), gray inverted triangles (Nozaki et al., 1998), and gray squares (Okubo et al., 2012). Dotted lines approximate the subarctic front (SAF) and subarctic boundary (SAB), as drawn by Harrison et al. (2004). SO202- refers to the INOPEX cruise; P and Z stations refer to the Line P cruise (see section 2.1).

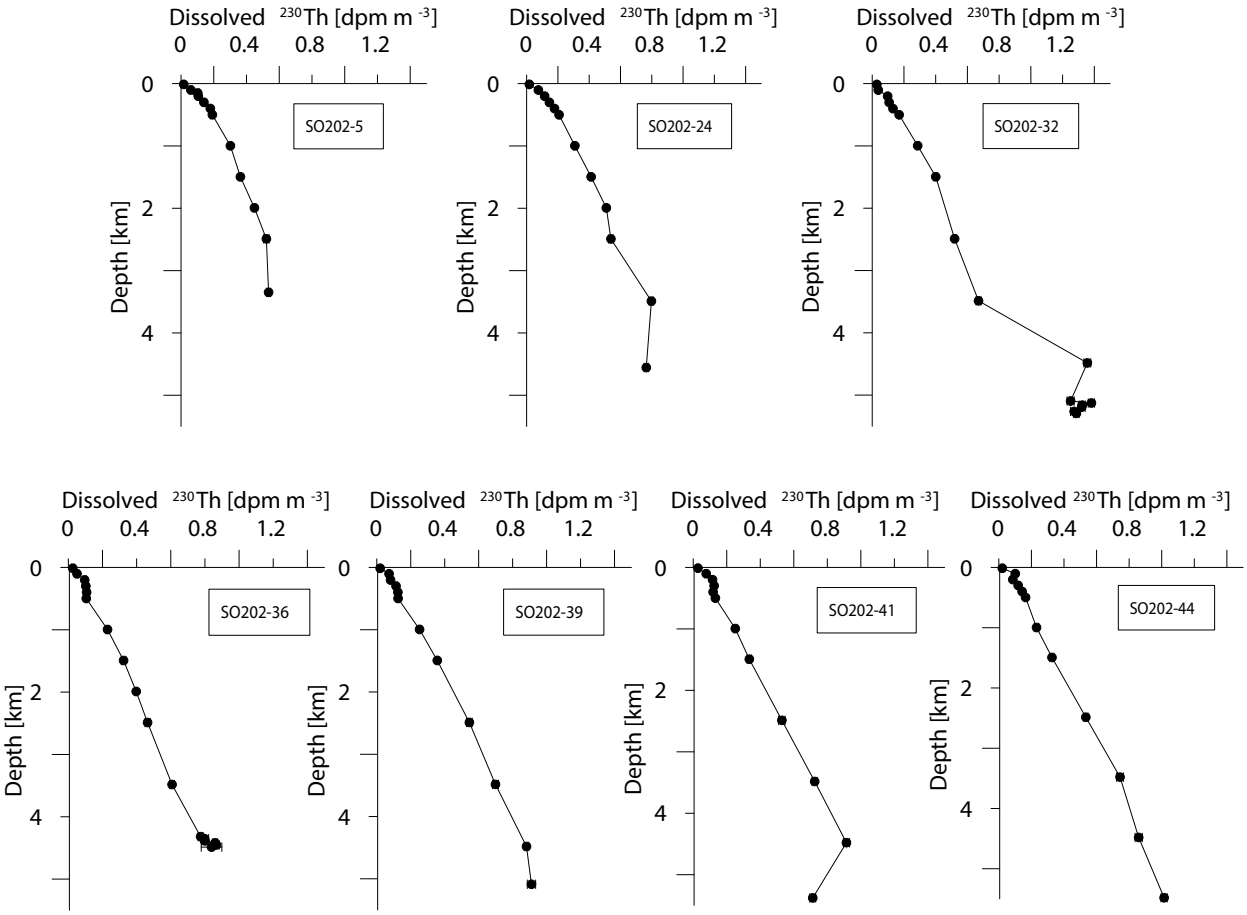

Figure 3. Depth profiles of dissolved ^{230}Th from the INOPEX locations (SO202- in Fig.1). These data have been corrected for the detrital ^{230}Th based on measured dissolved ^{232}Th (see section 2.2). The deepest sample in each profile is 5-15 m above the seafloor. Where error bars are not visible they are smaller than the symbol size.

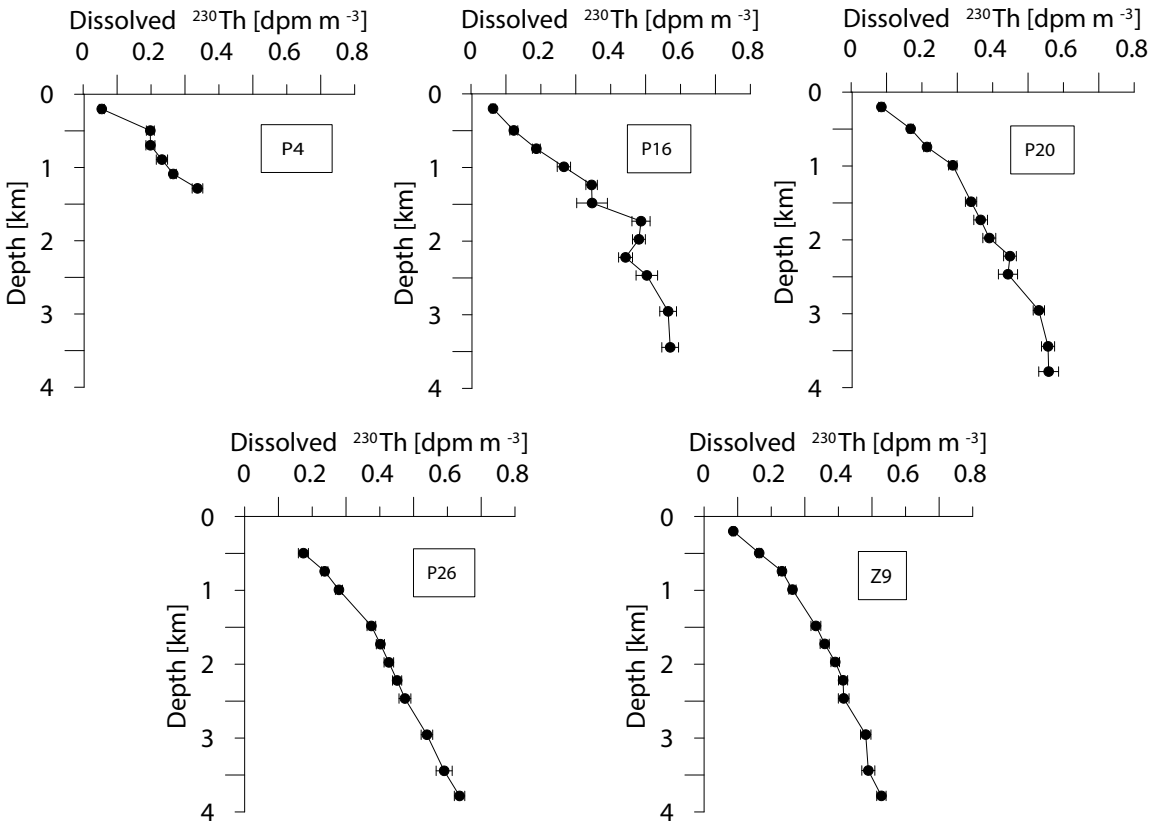

Figure 3. Depth profiles of dissolved ^{230}Th from Line P (P and Z stations in Fig. 1). These data have not been corrected for detrital ^{230}Th (see section 2.2). The deepest sample in each profile is between 38 and 537 m above the seafloor (see Table 1). Where error bars are not visible they are smaller than the symbol size.

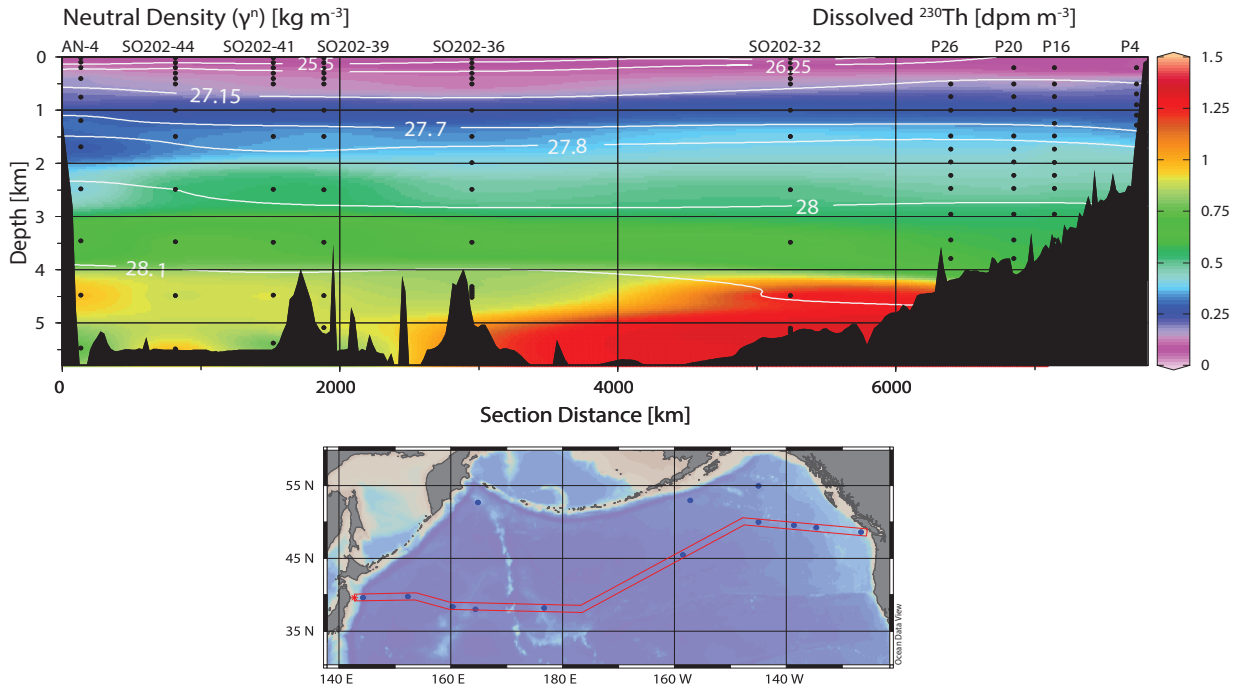

Figure 4. North Pacific section of dissolved ^{230}Th (colormapping). White contours are isopycnals (neutral density). For comparison, none of the data in this figure have been corrected for detrital sources of ^{230}Th. Note that the high concentrations below 4500 m depth around 4000 km section distance are largely unconstrained by the data (shown as black dots).

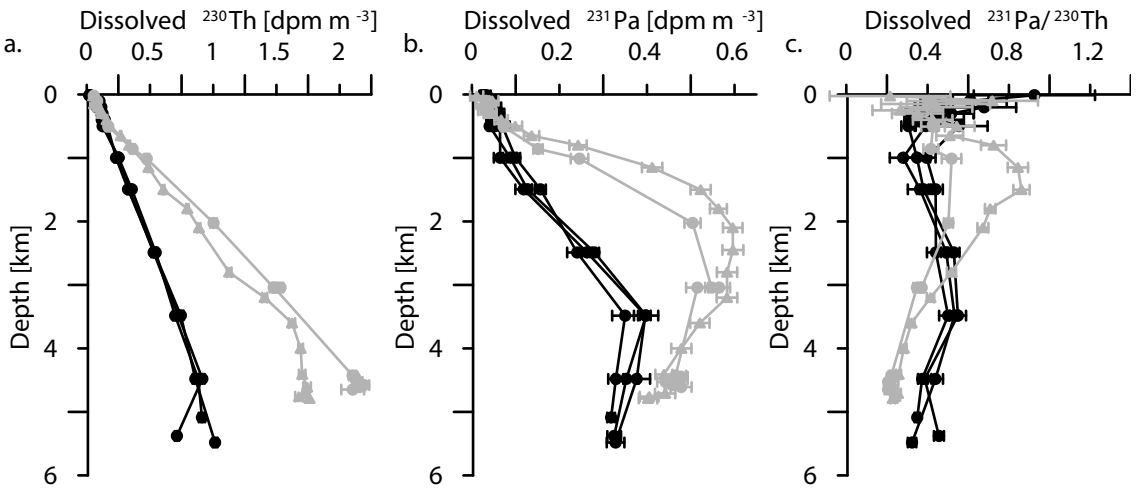

Figure 5. Depth profiles of dissolved ^{230}Th (a.), ^{231}Pa (b.) and the ^{231}Pa/^{230}Th activity ratio (c.) from SO202-39, -41, -44 in black compared with those from SAFe (gray circles) and ALOHA (gray triangles). Where error bars are not visible they are smaller than the symbol size. In (c.), for clarity, ratios whose uncertainty is greater than ± 0.5 activity ratio units are not plotted.

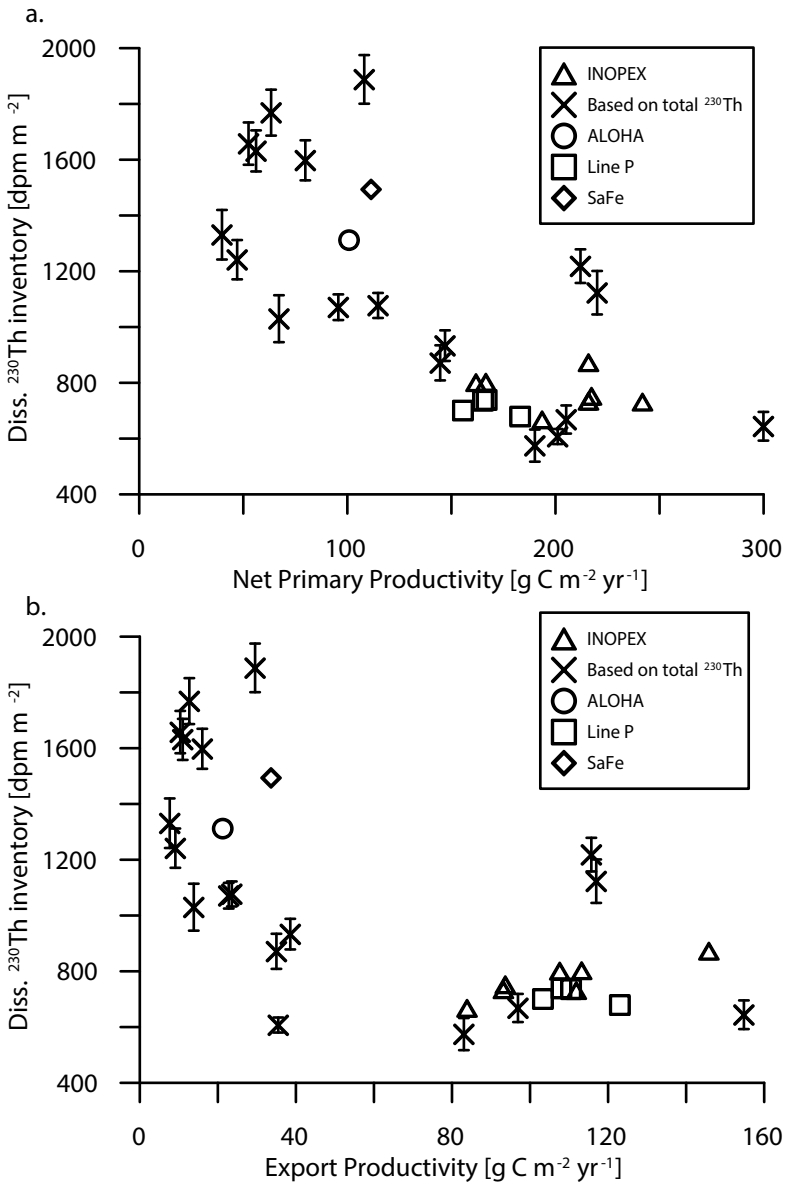

Figure 6. Inventory of dissolved ^{230}Th from 0-2.5 km depth versus (a.) Net Primary Productivity (NPP) and (b.) Export Productivity (EP) for the INOPEX (triangles), Line P (squares), ALOHA (circles), and SAFE (diamond) stations and the sites for which total ^{230}Th data is available in the literature (x's). Error bars on the points estimated from total ^{230}Th include the uncertainty in the distribution coefficient. Error bars based on dissolved data are roughly the size of the symbols and are omitted for clarity.

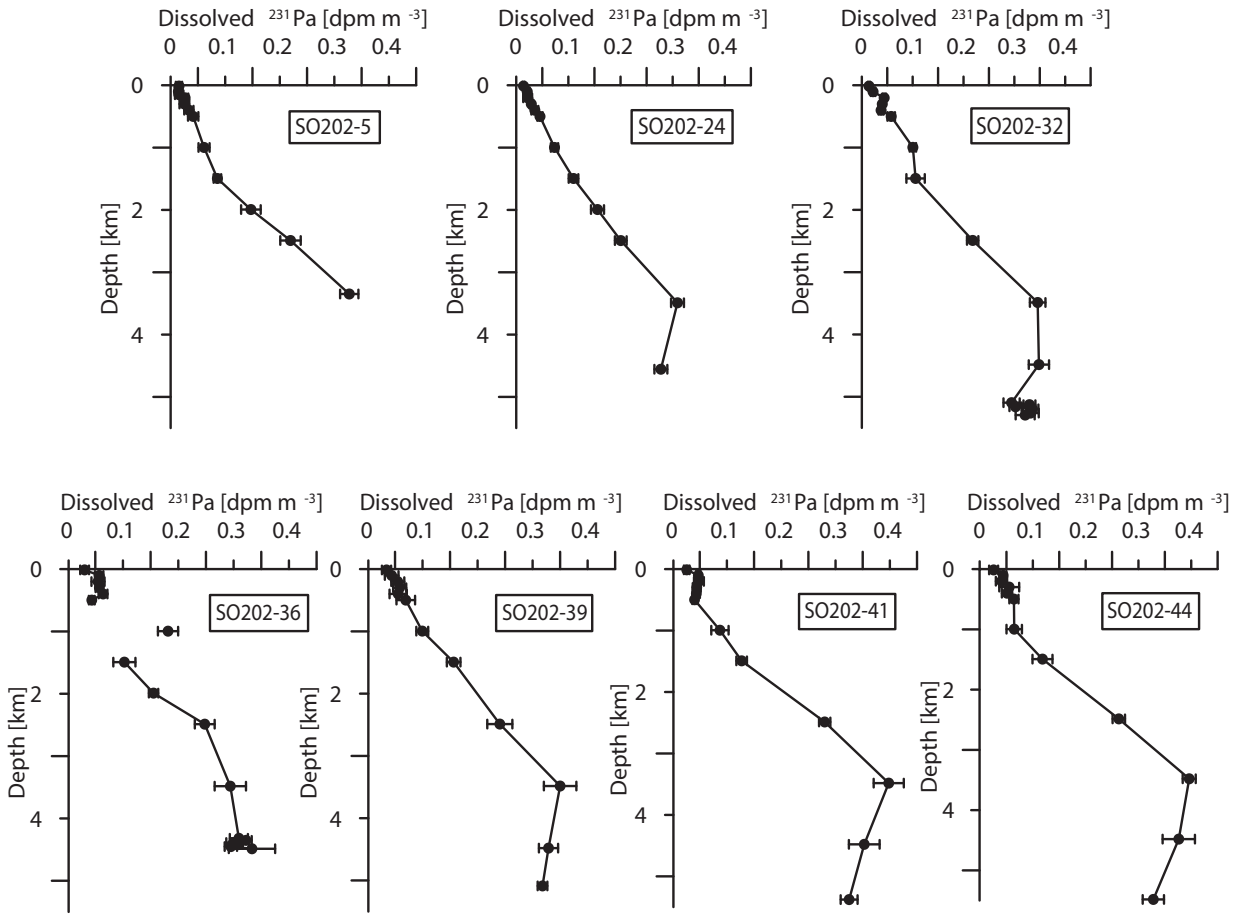

Figure 7. Depth profiles of dissolved ^{231}Pa from the INOPEX locations (Fig.1). These data have been corrected for the detrital ^{231}Pa based on measured dissolved ^{232}Th (see section 2.2). The deepest sample in each profile is 5-15 m above the seafloor. Where error bars are not visible they are smaller than the symbol size.

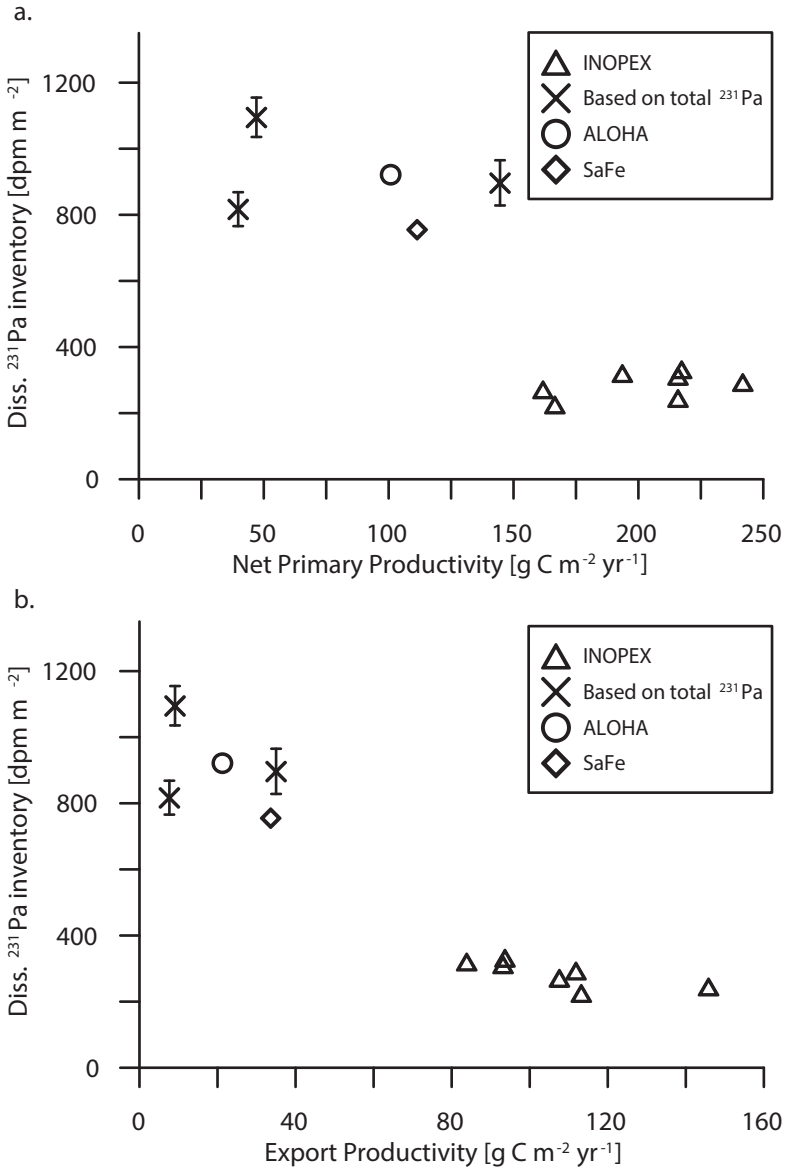

Figure 8. Inventory of dissolved ^{231}Pa from 0-2.5 km depth versus (a.) NPP and (b.) EP for the INOPEX (triangles), Line P (squares), ALOHA (circles), and SAFE (diamond) stations and the sites for which total ^{231}Pa data is available in the literature (x's). Error bars on the points estimated from total ^{231}Pa include the uncertainty in the distribution coefficient used in calculating the inventory. Error bars based on dissolved data are roughly the size of the symbols and are omitted for clarity.

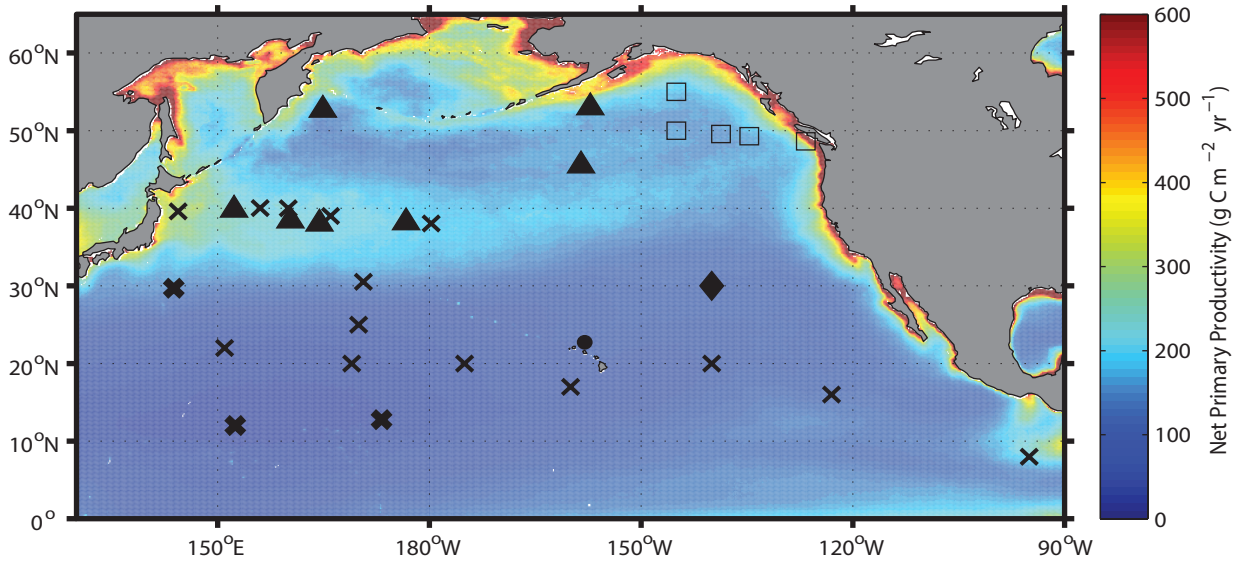

Figure S1. Annually averaged Net Primary Productivity (1997-2009) based on monthly SeaWifs-NPP data (http://www.science.oregonstate.edu/ocean.productivity) (Behrenfeld and Falkowski, 1997). See section 2.4 for more information. Station location symbols are equivalent to those found in Figures 6 and 8. Bold indicates ^{231}Pa data are available in addition to ^{230}Th data.

Table 1. Sea surface temperature (SST), Net Primary Productivity (NPP), ef-ratio, Export Productivity (EP) and dissolved inventories of ^{230}Th and ^{231}Pa in the upper 2.5 km of the water column for station locations used in this study. See Fig. S1 for a high resolution map of NPP in relation to station locations.

Station	Latitude	Longitude	Water	SST	NPP	ef-ratio	EP	Diss. ^{230}Th inventory (2.5km)	±	Diss. ^{2310}Pa inventory (2.5km)	±	Reference
	(°N)	(°E)	Depth (m)	(°C)	g C m^{-2} yr^{-1}		g C m^{-2} yr^{-1}	dpm m^{-2}	dpm m^{-2}	dpm m^{-2}	dpm m^{-2}	
BO-1	40	160	5588	12.9	212	0.55	116	1218	60			a
BO-3	30	-160	5774	21.6	108	0.27	30	1888	87			a
BO-4	17	-160	5591	25.8	80	0.20	16	1598	72			a
BO-5	20	-175	5307	26.2	63	0.20	13	1769	82			a
BO-6	20	169	5372	26.9	53	0.20	10	1658	76			a
BO-7	22	151	5623	26.9	56	0.20	11	1632	74			a
HY-1	20	-140	5287	23.4	96	0.24	23	1071	46			a
HY-2	16	-123	4229	25.1	115	0.21	24	1077	45			a
HY-3	8	-95	3656	27.6	201	0.18	35	607	27			a
CY-5	40.017	156.033	5523	13.3	220	0.53	117	1123	78			b
CY-6	39.017	166	5576	14.7	205	0.47	97	668	50			b
CY-8	38.05	180.267	5553	15.7	190	0.44	83	575	58			b
CY-11	30.533	170.65	5523	22.2	147	0.26	39	933	55			b
CE-5	25	169.983	5960	25.4	67	0.21	14	1030	84			c
CE-8	12.75	173.233	5686	27.7	47	0.19	9	1242	70	1095	60	c
CE-13	12	152.5	5883	28.3	40	0.19	8	1331	89	817	51	c
AN-1	29.7	143.8	9750	23.2	145	0.24	35	872	63	897	68	d
AN-4	39.6	144.4	7585	13.7	300	0.52	155	644	51			d
SO202-5	52.696	164.919	3364	5.0	167	0.68	113	795	7	226	11	e
SO202-24	53.002	-157.193	4567	6.8	216	0.68	146	865	7	245	8	e
SO202-32	45.5	-158.5	5301	9.5	162	0.67	108	794	9	272	12	e
SO202-36	38.19	176.696	4524	15.9	194	0.43	84	662	8	321	13	e
SO202-39	38.011	164.445	5098	15.9	217	0.43	94	745	10	332	20	e
SO202-41	38.413	160.335	5392	15.9	216	0.43	93	728	13	312	16	e
SO202-44	39.801	152.351	5505	14.9	242	0.46	112	725	11	294	12	e
ALOHA	22.75	-158	4800	24.8	101	0.21	21	1313	6	922	12	f
SAFE	30	-140	4750	20.2	111	0.30	34	1494	20	756	16	g
P16	49.283	-134.667	3550	10.4	167	0.65	108	739	12			e
P20	49.567	-138.667	4020	9.7	156	0.66	103	701	9			e
P26	50	-145	4320	8.3	165	0.67	111	737	8			e
Z9	55	-145	4025	7.6	183	0.67	123	680	7			e
P4	48.633	-126.65	1323	11.3	436	0.62	268					e

a Okubo et al. 2012 (Based on total ^{230}Th)
b Nozaki et al. 1981 (Based on total ^{230}Th)
c Nozaki and Nakanishi 1985 (Based on total ^{230}Th and ^{231}Pa)
d Nozaki et al. 1998 (Based on total ^{230}Th and ^{231}Pa)
e Present Work
f François 2007
g Anderson et al. 2012

Chapter 2. Quantifying lithogenic inputs to the North Pacific Ocean using the long-lived thorium isotopes

Christopher T. Hayes[a,b], Robert F. Anderson[a,b], Martin Q. Fleisher[a], Sascha Serno[a,c], Gisela Winckler[a,b], Rainer Gersonde[d]

[a]Lamont-Doherty Earth Observatory of Columbia University, Palisades, NY, USA

[b]Department of Earth and Environmental Sciences, Columbia University, New York, NY, USA

[c]DFG-Leibniz Center for Surface Process and Climate Studies, Institute of Earth and Environmental Science, University of Potsdam, Potsdam-Golm, Germany

[d]Alfred Wegener Institute for Polar and Marine Research, Bremerhaven, Germany

In press at Earth and Planetary Science Letters (2013)

Abstract

Dissolved ^{232}Th is added to the ocean though the partial dissolution of lithogenic materials such as aerosol dust in the same way as other lithogenically sourced and more biologically important trace metals such as Fe. Oceanic ^{230}Th, on the other hand, is sourced primarily from the highly predictable decay of dissolved ^{234}U. The rate at which dissolved ^{232}Th is released by mineral dissolution can be constrained by a Th removal rate derived from ^{230}Th:^{234}U disequilibria, assuming steady-state. Calculated fluxes of dissolved ^{232}Th can in turn be used to estimate fluxes of other lithogenically sourced dissolved metals as well as the original lithogenic supplies, such as aerosol dust deposition, given the concentration and fractional solubility of Th (or other metals) in the lithogenic material. This method is applied to 7 water column profiles from the Innovative North Pacific Experiment (INOPEX) cruise of 2009 and 2 sites from the subtropical North Pacific. The structure of shallow depth profiles suggests rapid scavenging at the surface and at least partial regeneration of dissolved ^{232}Th at 100-200 m depth. This rapid cycling could involve colloidal Th generated during mineral dissolution, which may not be subject to the same removal rates as the more truly dissolved ^{230}Th. An additional deep source of ^{232}Th was revealed in deep waters, most likely dissolution of seafloor sediments, and offers a constraint on dissolved trace element supply due to boundary exchange.

1. Introduction

The ocean is the ultimate receptor of eroded material from the continents. In the remote surface ocean, this process occurs only through deposition of eolian mineral dust (referred to also as aerosol dust or simply as dust) (Rea, 1994) and in some cases dust is a dominant source of soluble micronutrients necessary for biological productivity (Martin and Gordon, 1988). Quantification of aerosol dust input to the surface ocean has progressed in recent years using a combination of remote sensing and modeling techniques (Mahowald et al., 2005), but these models nonetheless are better constrained with observational tracer-based approaches using, for instance, dissolved Al (Measures and Brown, 1996) and more recently dissolved Th (Hsieh et al., 2011). The partial dissolution of hemipelagic sediments, or more generally, margin sediment exchange processes, may also contribute to the ocean budget of dissolved trace metals of paleoceanographic interest such as Nd (Lacan and Jeandel, 2005), Hf (van de Flierdt et al., 2004), as well as ^{232}Th (Roy-Barman, 2009). The importance of boundary exchange processes has been difficult to assess because knowledge of the rates involved in the biogeochemical cycle of these elements is lacking.

The long-lived thorium isotopes (^{232}Th and ^{230}Th: half-lives, 14.01 Ga (Holden, 1990) and 75.69 ka (Cheng et al., 2000), respectively) offer a way to determine rates of lithogenic element cycling in seawater. The shorter-lived, ^{230}Th, is radiogenic, with a well-quantified source from ^{234}U dissolved in seawater. To determine ^{230}Th production, ^{234}U concentrations are estimated using measured salinity and published estimates of the salinity-U relationship in North Pacific seawater (Chen et al., 1986) and the seawater ^{234}U/^{238}U ratio (Andersen et al., 2010). More than 99.8% of Th in seawater, however, is ^{232}Th, a primordial isotope added to seawater in the dissolved pool through the partial dissolution of lithogenic materials (Santschi et al., 2006).

Thorium (and therefore all Th isotopes) is highly insoluble in seawater and is rapidly removed from solution by scavenging onto particulate matter (Moore and Sackett, 1964).

The rate of Th removal by scavenging, equivalent to the inverse of the Th residence time, τ_{Th}, can be quantified using measurements of dissolved ^{230}Th, assuming steady-state against production by uranium decay. Production of ^{230}Th is given by the activity of ^{234}U (in units concordant with the ^{230}Th units) multiplied by the radioactive decay rate of ^{230}Th, λ_{230}. We take inventories of both ^{230}Th and its production due to ^{234}U decay to calculate residence time as a function of integrated depth (Eq. 1a). This residence time is applied to the integrated inventory of dissolved ^{232}Th to estimate the cumulative flux of ^{232}Th due to mineral dissolution (Hirose and Sugimura, 1987), from the surface to depth, z. A concentration, $[^{232}Th]_{litho}$, and fractional solubility, S_{Th}, of Th in the lithogenic material can then be used to estimate the flux of lithogenic material which produced the observed dissolved inventory (Eq. 1b), as described by Hsieh et al. (2011). In the surface of the open ocean, this lithogenic flux is generally assumed to be dissolution of aerosol dust, but near ocean margins, including the seafloor, an apparent lithogenic flux could arise from the partial dissolution of hemipelagic or resuspended pelagic sediments.

$$\tau_{Th}(z) = \frac{\int_0^z dissolved^{230}Th\, dz}{\int_0^z activity^{234}U * \lambda_{230}\, dz} \qquad \text{Eq. 1a}$$

$$Lithogenic\ flux(z) = \frac{\int_0^z dissolved\ ^{232}Th\, dz}{\tau_{Th}(z) \times [^{232}Th]_{litho} \times S_{Th}} = \frac{Dissolved\ \ ^{232}Th\ flux(z)}{[^{232}Th]_{litho} \times S_{Th}} \qquad \text{Eq. 1b}$$

Using depth profiles of dissolved ^{230}Th and ^{232}Th from the North Pacific, this study aims to: (1) quantify dust deposition at sites under the influence of the Asian dust plume, (2) critically evaluate the paired-Th isotope method for lithogenic fluxes in seawater, and (3) use deepwater ^{232}Th fluxes to demonstrate a deep source of dissolved ^{232}Th, with implications for boundary exchange.

2. Materials and Methods

Sampling for dissolved (<0.45 µm) ^{232}Th and ^{230}Th took place at seven locations (Fig. 1) during the SO202-INOPEX cruise of July-August 2009 (Gersonde, 2012). In this manuscript, Th, ^{232}Th and ^{230}Th refer to the dissolved phase unless otherwise noted. Sampling and analysis of thorium isotopes were carried out by GEOTRACES-compliant (intercalibrated) methods (www.geotraces.org), described fully by Anderson et al. (2012).

Four-to-five liter water samples were analyzed in batches of 10-12. Procedural blanks were determined by processing 4-5 L of Milli-Q water in an acid-cleaned cubitainer acidified to pH ~2 with 6 M HCl as a sample in each batch. For a measure of reproducibility, an aliquot of an intercalibrated working standard solution of dissolved ^{232}Th and ^{230}Th, SW-STD 2010-1 referred to by Anderson et al. (2012), was added to a separate cubitainer with 5 L of Milli-Q water (acidified to pH 2) and also processed like a sample in each batch. Total procedural blanks were 7.1-24.3 pg ^{232}Th and 0.8-1.6 fg ^{230}Th. These blanks are equivalent to 3-30% and 1-20% of the measured seawater ^{232}Th and ^{230}Th signals. Reproducibility of the ^{232}Th (~990 pg/g) and ^{230}Th (~250 fg/g) concentrations in SW-STD 2010-1 over several years has been 4.7% and 1.3%, respectively.

Concentrations of ^{230}Th were corrected for in-growth due to uranium decay during sample storage (1-2 years). In order to use ^{230}Th:^{234}U disequilibrium to derive a Th residence time, ^{230}Th concentrations must also be corrected for a proportion of ^{230}Th released by the dissolution of lithogenic materials. This is based on concurrent measurements of ^{232}Th, assuming a lithogenic ratio ^{230}Th/^{232}Th = 4.0×10^{-6} mol/mol (Roy-Barman et al., 2009). INOPEX results and complete method descriptions are available at PANGAEA and BCO-DMO.

3. Results and Discussion

3.1 Shallow dissolved ^{230}Th-^{232}Th profiles

The INOPEX depth profiles of ^{230}Th are discussed in detail elsewhere (Hayes et al., 2013). The observed near-linear increases in concentration with depth (Fig. 2) reflect the effects of reversible scavenging (Bacon and Anderson, 1982) whereby ^{230}Th, produced uniformly in the water column, is concentrated at depth through cycles of adsorption and desorption with sinking particles. This behavior, especially in the upper 1000 m, has been observed in almost all other ^{230}Th profiles from the region (Nozaki et al., 1981; Nozaki and Nakanishi, 1985; Nozaki et al., 1987; Roy-Barman et al., 1996).

Our results for ^{232}Th are more novel. At each of the seven INOPEX sites, most noticeably at the 4 stations near 40°N, where we expect the highest dust input (Fig. 1) (Mahowald et al., 2005), ^{232}Th increases in concentration with depth from 10 m (within the mixed layer) to a local subsurface maximum between 100-200 m depth (Fig. 2). These well-defined subsurface maxima in ^{232}Th lead us to discuss three possible explanations which are important in evaluating the paired-Th isotope method for lithogenic supplies: (1) lateral advection or eddy-diffusion of ^{232}Th at the subsurface maxima, (2) seasonality of eolian ^{232}Th deposition, and (3) non-steady-state Th scavenging and regeneration dynamics.

3.1.1 Hydrographic Influences

The subsurface ^{232}Th maxima could in principle reflect an advective/diffusive input, for instance, of water recently in contact with detrital sediment. This influence is addressed in two ways: hydrographic context (Fig. 3) and advective-diffusive scaling arguments in comparison to Th residence times. Each station was observed with a warm, fresh and shallow (17-35 m, Table 1) mixed layer, typical of summertime in the subarctic Pacific (Ohno et al., 2009). The mixed

layer depth criterion is a 0.125 kg m^{-3} change in potential density with respect to the surface (Levitus, 1982; Suga et al., 2004). The North Pacific mixed layer has great seasonal variability, however, with much deeper mixed layers in winter. In particular, in the western North Pacific between 30-45°N, mixed layer depths can often exceed 200 m (Ohno et al., 2009; Oka et al., 2007).

These deep mixed layers lead to the formation of various mode waters. North Pacific Subtropical Mode Water (STMW, σ_θ = 25.0-25.7 kg m^{-3}) (Bingham, 1992; Hanawa and Suga, 1995), known to be enriched in Al (Measures et al., 2005), outcrops or forms south of the Kuroshio Extension (generally south of 36°N, Fig. 1) (Chen, 2008; Oka et al., 2007). STMW is therefore not likely to influence the INOPEX sites (north of 38°N), although there is the possibility for cross frontal mixing in this region of high eddy kinetic energy (Ducet et al., 2000).

North Pacific Central Mode Water (CMW, σ_θ = 25.9-26.5 kg m^{-3}) and Transition Region Mode Water (TRMW, σ_θ = 26.4-26.6 kg m^{-3}) form from the deep winter mixed layers north of the Kuroshio Extension and south of the Subarctic Front (Hanawa and Talley, 2001; Oka et al., 2011), encompassing the region of stations SO202-36 through -44 (Fig. 1). The subsurface ^{232}Th maxima (at SO202-36 through -44) occur in the potential density layers, σ_θ = 25.7-26.5 kg m^{-3} (Fig. 2), overlapping with CMW and TRMW. These mode waters could receive detrital trace metal inputs from the Kuril-Kamchatka margin and/or the Okhotsk Sea via the Oyashio Current (Morton, 2010).

In the case of SO202-44, the subsurface ^{232}Th maximum coincides with a slight intrusion of higher O_2 waters (Fig. 3), indicative of a recently ventilated mode water (Measures et al., 2006) and suggestive that this station may be partially influenced by detritally enriched CMW. North Pacific Intermediate Water (NPIW), which also forms near the subarctic boundary is

notable in our profiles as a salinity minimum at 250-500 m depth, σ_θ = 26.8 kg m^{-3} (Talley, 1993). NPIW, however, is below the subsurface peaks in ^{232}Th. While we cannot rule out lateral transport processes based on hydrography alone, we now consider the timescales necessary for lateral transport.

Ocean dispersion transports non-conservative elements if the transport processes occur on a timescale shorter than the residence time of the element. The Th residence time in the upper 500 m (Table 1) at the INOPEX sites is 3-5 years. We expect horizontal eddy diffusivity, $K_{H,}$ at a typical rate of 10^3 m^2 s^{-1} (Kawabe, 2008), to reach roughly 500 km lateral extent within that timescale ($\Delta x = \sqrt{2K_H\tau_{Th}}$, parameterizing eddy diffusivity as a random-walk process). Station SO202-5 is 312 km from the Kamchatka margin and SO202-24 is 310 km from the nearest Aleutian coast, and therefore these stations will be influenced by any strong Th sources at those coasts by eddy-diffusion alone. Station SO202-44 is 850 km from the Japanese margin. This is longer than our estimated diffusion length but does not necessarily imply the station is isolated from coastal input. Rather the diffusion length is an e-folding length, meaning any coastal to open concentration difference in ^{232}Th will be reduced by 2.71 over that distance. Additionally, advective processes will occur on even faster timescales and over longer distances.

Drifter floats suggest eastward ocean velocities at ~500 m depth in the region of SO202-44 on the order of 1 cm/s (Iwao et al., 2003). Thus advection could carry a Th signal from the Japanese margin to SO202-44 in as little as 2.7 yrs, less than the 500-m Th residence time. Nonetheless, the similarity of the ^{232}Th profiles at SO202-36 through -44 argues against this possibility as one would expect attenuation of an advective signal with distance from the source. Stations SO202-32, -36, -39 and -41 are >1100 km (>3.5 yrs travel time for a 1 cm/s current) from any coast and are much less likely to be influenced by coastal sources of Th.

We cannot rule out the influence of coastal input, or lateral sources in general, from observations of $^{232}Th/^{230}Th$ alone. In future studies we suggest combined measurements of Th isotopes and ^{228}Ra. This isotope builds up in coastal water in contact with sediments, which contain its parent, ^{232}Th (Moore, 2000). The half-life of ^{228}Ra (5.75 yr) is similar to the residence time of Th in surface waters. Thus it is well suited to trace offshore transport on relevant timescales. The rapid attenuation of the ratio of ^{228}Ra to the long-lived ^{226}Ra (half-life of 1600 yrs) within ~300 km of the coast of Fukushima, Japan (Charette et al., 2013) suggests, therefore, that a significant fraction of coastal Th will not be transported offshore much further than this. Nevertheless, paired measurement of offshore gradients in ^{228}Ra and ^{232}Th are recommended for future studies to better constrain potential sedimentary sources of ^{232}Th.

3.1.2 Seasonality

The deposition of Asian dust over the North Pacific occurs seasonally, the strongest events happening in spring (Duce et al., 1980). This phenomenon has been documented through decadal time-series measurements of aerosol-Al (Parrington et al., 1983) and Fe (Johnson et al., 2003) in Hawaii, and aerosol-^{232}Th in Japan (Hirose et al., 2012). Variability in dissolved Fe in surface waters at ALOHA station (Fig. 1) has also been attributed to spring dust events (Boyle et al., 2005). Since the INOPEX samples were collected in July-August 2009, a time of low aerosol index (http://toms.gsfc.nasa.gov/) in the North Pacific, typical of the summer season, we need to account for how the seasonality of aerosol-^{232}Th input affects our observations. This is done in light of our ^{230}Th-based Th residence times.

The Th residence times calculated for the mixed layer at the INOPEX stations are all roughly 1 yr (Table 1). This reflects an apparent uniformity in scavenging removal of Th in the subarctic Pacific (Hayes et al., 2013). To contrast the subarctic Pacific with an environment of

much lower scavenging intensity, we calculate Th residence times in surface waters using the ^{230}Th-^{232}Th data available from the subtropical North Pacific (Anderson et al., 2012; Roy-Barman et al., 1996). The SAFe station was occupied in May 2009 and ALOHA was occupied in September 1994 for the data used here (see Fig. 1 for locations) which have been corrected for storage in-growth and lithogenic inputs. CTD data was not available from the Sept. 1994-ALOHA cruise, so we have assumed a 50 m mixed layer based on climatology (Church et al., 2013). The subtropical sites have a mixed layer Th residence time of ~2 yrs (Table 1).

In both the subarctic and subtropical North Pacific regions, where mixed layer Th residence times are 1-2 years, seasonal ^{232}Th inputs can be expected to result in muted seasonal changes in ^{232}Th concentrations. Additionally, we would also expect changes in surface ^{230}Th concentration due to short-term (weeks-months) scavenging events to be muted by the filter of a 1-2 year running average. However, Th residence times based on mixed layer ^{230}Th can be overestimated because of upwelling and vertical mixing of higher ^{230}Th-water from below (Luo et al., 1995). Strong seasonal variations in the surface water ^{234}Th from time-series studies in the northwestern North Pacific (Kawakami and Honda, 2007) and at ALOHA (Benitez-Nelson et al., 2001) also argue that a year-long mixed layer Th residence time is an overestimate. In fact, a disconcerting result of applying ^{230}Th-based residence times to ^{232}Th inventories in the mixed layer is an anomalously low ^{232}Th flux at SO202-39 because of an anomalously low ^{232}Th concentration in the mixed layer there (Table 1, Fig. 2), while one would expect consistent flux results for the proximal INOPEX stations in an annually-smoothed average. Based on the available data, it is not clear whether mixed layer ^{230}Th-^{232}Th will be sensitive to seasonality or if this is a limitation of using the longer-lived ^{230}Th to document intra-annual changes. Future time-series measurements should seek to elucidate this point.

3.1.3 Thorium cycling

Given the uncertainties in interpreting the mixed layer ^{230}Th-^{232}Th results, we investigate how ^{232}Th fluxes change as one integrates deeper into the water column, and therefore over a longer timescale. As described in Sec. 1, ^{230}Th production due to ^{234}U decay, ^{230}Th and ^{232}Th inventories are all integrated with depth to produce a residence time and flux that is representative of the water column between the surface and the chosen depth of integration. To fully capture the subsurface ^{232}Th maxima, we choose to integrate to 500 m depth. While by integrating deeper into the water column we lose information about shorter timescales which may be of interest, it reduces the potential uncertainty in Th residence times due to vertical redistribution of ^{230}Th, accounts for seasonal variations in mixed layer depth and particle cycling, and produces more geographically-consistent ^{232}Th fluxes (Table 1). Compared to the mixed layer calculations, Th residence times over 500 m depth increase by a factor of 2-7 (implying slower Th removal), while ^{232}Th fluxes increase by a factor of 3-20. In other words, ^{232}Th inventories increase with depth by more than is expected by the decrease in removal rate associated with a larger integrated water column.

Increased flux with integration depth could be an artifact of vertical mixing, which by causing an overestimation of the mixed layer ^{230}Th residence time could cause the mixed layer ^{232}Th flux to be underestimated (Eq. 1b). To estimate upward flux of ^{230}Th by mixing, we calculate the vertical ^{230}Th concentration gradient across the mixed layer (between 10 and 100 m) and multiply by a vertical mixing coefficient (K_v). For surface waters in this region, we use $K_v = 10^{-5}$ m^2s^{-1}, as determined by Charette et al. (2013). The resultant upward flux of ^{230}Th by vertical mixing (K_v*d^{230}Th/dz) for the INOPEX stations is 5-60% of in-situ production of ^{230}Th in the mixed layer. Thus, our Th residence times may be overestimated by a factor of 1.05-2.5,

and consequently the mixed layer ^{232}Th fluxes may be underestimated by the same factor. While the true K_v at these sites may have been $>10^{-5}$ m^2s^{-1}, this effect is most likely not a large enough to explain the relative increase in observed ^{232}Th fluxes when integrating to 500 m.

Similarly, vertical mixing can represent a supply or removal term for ^{232}Th in the mixed layer. Following an approach like that described above for ^{230}Th, for each station we calculate a flux of ^{232}Th due to vertical mixing and compare it to the magnitude of our original estimate of mixed layer dissolved ^{232}Th flux (Table 1). Results suggest that vertical mixing can range from a net source of ^{232}Th to the mixed layer, contributing a maximum of 50% to the calculated ^{232}Th flux at SO202-39, to a small net loss (only at SO202-32, where the concentration of ^{232}Th decreases below the mixed layer and the loss by vertical mixing represents 5% of the mixed layer ^{232}Th flux). When ^{232}Th is added to the mixed layer by vertical mixing, the calculated flux of dissolved ^{232}Th will overestimate the supply due to dust dissolution. This counteracts to some degree the underestimation of dust supply introduced by vertical mixing of ^{230}Th (see above). Therefore, we do not consider vertical mixing a significant factor in our observation of increased ^{232}Th flux with integration depth.

Lastly, we explore the possibility that the increase with integration depth of the calculated dissolved ^{232}Th flux results from the generation of operationally defined dissolved ^{232}Th (<0.45 μm) from particulate ^{232}Th by a process that does not significantly affect the dissolved ^{230}Th distribution involving colloidal particles (0.02–0.45 μm). Truly dissolved, or soluble, species are also operationally defined (<0.02 μm). It has been shown in seawater leaching experiments that Fe dissolved from aerosols is dominated by the colloidal fraction (Aguilar-Islas et al., 2010) so it is reasonable to hypothesize that Th dissolves from dust as colloids as well. Each ^{230}Th atom in the ocean however is produced from a single decay event that releases it into solution. The

average dissolved speciation of two Th isotopes may therefore be different, ^{230}Th more soluble, ^{232}Th more colloidal, because of their differing sources, with implications for their cycling in the water column. For instance, when colloidal ^{232}Th is converted into truly dissolved ^{232}Th, this represents a net addition of dissolved ^{232}Th unaccounted for by the adsorption/desorption (reversible scavenging) reactions of ^{230}Th.

Few data on marine colloidal ^{232}Th/^{230}Th exist. In two out of three samples from the Gulf of Mexico, it was found that a larger proportion of dissolved ^{232}Th existed in the colloidal phase than did the radiogenic ^{234}Th (Baskaran et al., 1992). However, it is worth noting that Baskaran et al. (1992) could not confidently exclude ^{232}Th contamination. In contrast, Roy-Barman et al. (2002) found that the ^{232}Th/^{230}Th ratio did not change between dissolved (<0.2 µm) and ultra-filtered (<1 kDa) seawater from the Mediterranean Sea, suggesting similar speciation of the 2 isotopes in both colloidal and truly dissolved size-classes.

Apparently low ^{232}Th concentrations in the mixed layer (most dramatically for example at SO202-39) could be the result of rapid removal by colloidal aggregation and/or biologically-mediated particle packaging followed by the sinking of these particles with which ^{230}Th does not equilibrate. Colloidal material has a very rapid turnover time (days to weeks) in the upper ocean (Moran and Buesseler, 1992) and laboratory experiments have shown that Th can be effectively regenerated from particles through protistan grazing (Barbeau et al., 2001). Therefore, apparently high ^{232}Th concentrations at depth (the subsurface maxima) could represent the disaggregation of those sinking particles into colloids or fully regenerated as truly dissolved Th.

Regeneration of Th at 100-200 m depth has also been documented for the shorter-lived Th isotopes, as excess activities of ^{234}Th (Buesseler et al., 2009; Maiti et al., 2010) and ^{228}Th (Li et al., 1980; Luo et al., 1995) over their soluble parent nuclides (^{238}U and ^{228}Ra, respectively).

While these isotopes are also products of in-situ decay (not dust dissolution), because of their much shorter half-lives (24.1 days and 1.9 yrs, respectively), their excess activities below the euphotic zone require rapid regeneration of particulate Th.

Perhaps the shorter-lived Th isotopes can capture rapid scavenging dynamics while ^{230}Th does not. For instance, we do not observe strong evidence for regeneration at depth in the ^{230}Th profiles, considering the near-linear depth profiles of dissolved ^{230}Th (Fig. 2). Alternatively, ^{230}Th concentration anomalies in profile may be smoothed by vertical mixing, as ^{230}Th displays larger depth gradients in concentration than the other Th isotopes. Future size-fractionated Th isotope studies in seawater will inform us about differing removal rates among the thorium isotopes (Marchal and Lam, 2012). For instance, the high depth-resolution ^{234}Th-^{232}Th-^{230}Th-^{228}Th data being collected by the GEOTRACES program will help test the hypothesis that each dissolved Th isotope is subject to similar removal rates. Identifying the chemical composition of the colloids important for cycling Th (e.g., lithogenic versus organic) would also be of great interest.

3.2 Full water column ^{232}Th profiles

Before applying the ^{232}Th data to estimate lithogenic fluxes, it is useful to consider the full-depth distribution of ^{232}Th measured in the INOPEX region (Fig. 4). Among stations SO202-36 through -44, the ^{232}Th profiles show concentration maxima above 500 m depth, minimum concentrations at ~1-3 km depth, and generally increasing concentrations within about 1 km of the seafloor. The only previously reported full-depth profile of dissolved ^{232}Th from the subarctic Pacific (north of 38° N), station AN-4 (39.6°N, 145.5°E) (Nozaki et al., 1987), did not sample above 1 km depth, and showed Th concentrations 2-5 times greater (100-240 pg/kg) than those observed at SO202-44 at similar depths. This may reflect higher Th input near the Japanese

coast but also could be related to differences in sampling and methodology as seawater Th analysis has progressed (Huh et al., 1989). Increasing Th concentration near the seafloor has also been found in the subtropical Pacific (Nozaki and Horibe, 1983; Okubo et al., 2012; Roy-Barman et al., 1996). The average dissolved ^{232}Th concentration for all the INOPEX samples is 33 pg/kg, higher than the average (~15 pg/kg) observed in the subtropical Pacific (Okubo et al., 2012; Roy-Barman et al., 1996) and tropical Pacific (Singh et al., 2013).

The "mid-depth-minimum" profile shape of the ^{232}Th profiles of SO202-32 through -44 is similar to that of Al in the North Pacific (Measures et al., 2005; Orians and Bruland, 1986). As Orians and Bruland (1986) pointed out for Al, we conclude that there are two sources of Th to the ocean: one shallow due to dust dissolution and one deep associated with sediment dissolution/resuspension; and one removal mechanism, scavenging throughout the water column. At SO202-5 and SO202-24, ^{232}Th appears to increase in concentration continuously with depth, implicating a full-depth sediment source from the nearby continental margin. Resuspension of sediments by deep currents along the Aleutian and Kurile margins (Owens and Warren, 2001) may enhance the release of dissolved ^{232}Th near the seafloor.

At all sites, the near-bottom source of dissolved ^{232}Th is most likely introduced by lateral mixing or advection along isopycnals that impinge on the seafloor where sediment resuspension/dissolution occurs. Upward mixing of dissolved ^{232}Th from the seafloor directly underlying the sampling sites is most likely too slow in comparison to lateral transport (Roy-Barman, 2009). We cannot at this time, however, directly trace the source of this deep ^{232}Th input, as sediment resuspension appears to be spatially inhomogeneous (Hayes et al., 2013; Okubo et al., 2012) and high quality data on dissolved ^{232}Th from the North Pacific margins do not yet exist.

To further dissect the Th cycle in the North Pacific, we calculate the depth-integrated dissolved ^{232}Th flux at all depths in the INOPEX, ALOHA and SAFe profiles (Fig. 5). The ^{232}Th flux always increases rapidly with integrated depth to at least 500 m. Excluding SO202-5 and SO202-24, which appear to receive ^{232}Th from the continental margin at all depths, the ^{232}Th flux does not increase greatly between 1 km and 3.5 km depth. We interpret this regular pattern to indicate that after the dissolved Th flux is generated due to dust dissolution above 1 km depth, little new Th is added in the deeper water column, until within about 1 km of the seafloor where the flux begins to increase again due to the bottom sediment source.

The full-depth dissolved ^{232}Th flux at the subtropical sites is 3-4 times smaller than the INOPEX sites. This likely reflects the greater aerosol-^{232}Th input in the subarctic; however, the subarctic Pacific may also be influenced by a greater sedimentary ^{232}Th source (boundary exchange).

3.3 Dissolved ^{232}Th-based dust fluxes

Because ^{232}Th fluxes change dramatically with integration depth, it is necessary to justify the depth at which depth-integrated dissolved ^{232}Th fluxes best represent input from dust. Originally we chose 500 m to integrate through features of the ^{232}Th concentration profile that suggest rapid Th cycling in the upper water column. In general, the integrated ^{232}Th fluxes reach an asymptote with integration depth around 1 km. Importantly, between 100 m and 1000 m integration depth, the relative variation between the station fluxes remains similar (Fig. 5). Therefore the exact integration depth within the zone of increasing ^{232}Th flux may be less important than choosing a standard depth, although this will influence the apparent fractional solubility (see below). We propose to continue using 500 m integration as a baseline for estimating open ocean dust fluxes from dissolved ^{232}Th-^{230}Th data. This may need to be revised

depending on the Th regeneration signals observed, seasonality in mixed layer depth, or proximity to advective/diffusive Th sources.

In order to estimate dust flux from dissolved ^{232}Th flux, estimates of the ^{232}Th concentration in dust and the fractional solubility of Th are necessary (Eq. 1b). Dust sources have ^{232}Th concentrations in a narrow range of the average for the upper continental crust (McGee et al., 2007). A recent study determined an end-member concentration for Th in East Asian aerosol dust of 14.6±0.2 ppm (Serno et al., in revision), making it simple to apply a $[Th]_{litho}$ with confidence for estimating dust fluxes (Eq. 1b). It is possible that volcanic ash presents another eolian source of dissolved ^{232}Th to the water column. Although Th solubility of volcanic ash is not known, the Th concentration of volcanic material in marine sediments from this region is 2.2 ppm (Serno et al., in revision), much lower than that of aerosol dust, and the contribution of volcanic material to the lithogenic flux (as determined in the sediments) becomes small with distance >500 km from the coast (Serno et al., in revision). Contribution from volcanic ash could therefore cause a small overestimate of dust deposition at stations SO202-5 and -24, but it is expected to be negligible at other stations.

The fractional solubility, S_{Th}, is much more difficult to estimate with available data. Previous studies have estimated this factor in the range 1-20% (Arraes-Mescoff et al., 2001; Hsieh et al., 2011; Roy-Barman et al., 2002). Following the approach of Hsieh et al. (2011), by fixing a $[Th]_{litho}$, and assuming the model-derived dust deposition estimates of Mahowald et al. (2005) are correct (within 20% uncertainty), one can use Eq. 1b and the calculated dissolved ^{232}Th fluxes to estimate the fractional solubility. Using our mixed layer fluxes, this technique implies S_{Th} = 2-10% for the INOPEX, ALOHA and SAFe sites, similar to that found by Hsieh et al., while using the 500-m fluxes we infer S_{Th}=15-40% (Table 2, Fig. 6). Increases in apparent

solubility may be due to dissolution or regeneration processes occurring at depth. For instance, lithogenic particles may continue to be leached at subsurface depths by the low pH microenvironments associated with microbial colonies or zooplankton. However, given the refractory nature of Th, it seems unlikely that S_{Th} can be as high as 40% under any oceanic conditions. We suggest that such high apparent fractional solubility indicates that the model-derived results underestimate the true dust deposition in this region, although lateral supply of sedimentary ^{232}Th cannot be excluded entirely (Sec. 3.1.1).

An independent estimate of Th solubility can be derived by comparing the measured upper water column ^{232}Th flux to an annually resolved measurement of aerosol ^{232}Th flux on land, Mt. Haruna, Japan (Hirose et al., 2010). After correction for local sources, in 2007, the annual total ^{232}Th flux was 27.6 μg $m^{-2}yr^{-1}$. The nearest dissolved ^{232}Th flux (SO202-44) is 4.7 μg $m^{-2}yr^{-1}$, implying 17% Th-solubility. We also compare our dissolved ^{232}Th fluxes to the total ^{232}Th fluxes determined in the underlying surface sediments at the INOPEX sites. The Holocene, eolian component of sediment flux was determined with geochemical end-members (terrigenous ^{4}He, ^{232}Th, and rare earth elements) and ^{230}Th-normalized burial fluxes (Serno et al., in revision). The eolian-^{232}Th sediment fluxes compared with the 500-m dissolved ^{232}Th fluxes indicate S_{Th} = 22±6%. Based on these two comparisons, we assume a fractional Th solubility of 20±5%.

Our estimates of dust deposition to the North Pacific (Table 2), derived by integrating ^{232}Th inventories to 500 m, agree with the model results (Mahowald et al. 2005) reasonably well for the subtropical sites (~0.4 g $m^{-2}yr^{-1}$), while in the subarctic our estimates are 1.3-2 times higher than predicted in the model (~1.6 g $m^{-2}yr^{-1}$ for SO202-36- through -44). We can also compare our 500-m dissolved ^{232}Th-based dust estimates with the Holocene dust deposition estimates from the underlying sediment-^{232}Th fluxes (Serno et al., in revision), while we

acknowledge that both of these techniques are subject to the uncertainty of lateral ^{232}Th transport in the water column. At 4 of the 6 INOPEX sites where both water column and sediment measurements were made, dissolved ^{232}Th- and sediment ^{232}Th-based dust fluxes agree within error. This is encouraging since the two techniques average over very different timescales (3-5 years in 500 m water depth versus thousands of years in the sediments).

Dissolved Al has also been used to estimate dust deposition in the North Pacific (Measures et al., 2005) in a similar way to that described for Th, although for Al, a residence time, in addition to a fractional solubility, must be assumed. These Al results from the subarctic suggest very low dust fluxes (< 0.3 g m^{-2} yr^{-1}), even lower than model-derived estimates. We hypothesize that the assumed Al residence time in surface waters (5 yrs) is overestimated, especially in the more productive subarctic Pacific (Shiller and Bairamadgi, 2006).

3.4 Dissolved metal fluxes based on dissolved ^{232}Th fluxes

If ^{232}Th sources can be used as a model for other lithogenic trace metals (Me), one can estimate the flux of metals derived from the same lithogenic source. This requires knowledge of the metal to ^{232}Th ratio of the source and the relative fractional solubility (Eq. 2):

$$Dissolved\ Me\ flux = \left(\frac{Me}{^{232}Th}\right)_{litho} \times \left(\frac{S_{Me}}{S_{Th}}\right) \times Dissolved\ ^{232}Th\ flux \qquad \text{(Eq. 2)}$$

The relative solubility of aerosol dust is also largely unconstrained, but it is currently being pursued in the GEOTRACES program through leaching experiments (Morton et al., 2013). Relative solubilities may have an advantage over separately-determined metal solubility during leaches in that they may be less sensitive to artifacts relating to, e.g., the length of leaching, the type of leach solution or adsorption to container walls. Relative solubility may also be less sensitive to the source of dust. For instance, while fractional Fe solubility estimates range by

orders of magnitude (Sholkovitz et al., 2012), the relative Fe/Th solubility may be more consistent among dust with differing source regions or atmospheric histories.

Increases in the apparent solubility when considering the longer-term processing of lithogenic particles, similar to that for Th, have been reported for Fe (Boyd et al., 2010; Frew et al., 2006; Hansard et al., 2009). On this basis, we infer a general similarity in the dissolution of relatively insoluble lithogenic elements such as Fe, Nd, etc. Assuming an Fe/Th ratio of the average continental crust, 3262 g g^{-1} (Taylor and McLennan, 1985), and congruent dissolution ($S_{Fe}/S_{Th} = 1$), the ^{232}Th flux data from the INOPEX sites around 40°N translates into a dissolved Fe flux due to dust dissolution of about 15 mg Fe $m^{-2}yr^{-1}$. Applying our assumed S_{Fe}=20% to model estimates of natural mineral Fe deposition (Mahowald et al., 2009) gives 5-10 mg Fe $m^{-2}yr^{-1}$. This suggests, similar to what was concluded for dust fluxes in Sec. 3.3, that models currently underestimate the flux of soluble aerosol Fe, at least in the INOPEX region.

Note that the dissolved ^{232}Th flux and the ^{232}Th-based dissolved Fe flux reflect the input of natural mineral aerosols. Total dissolved Fe fluxes, on the other hand, especially in a region downwind of industrial nations such as Japan and China, will likely have a significant anthropogenic component (Gao et al., 2007; Luo et al., 2008). Furthermore, volcanic ash contains little Th, but may be an important source of Fe (Duggen et al., 2010).

3.5 Bottom water ^{232}Th fluxes as a constraint on boundary exchange

While depth-integrated dissolved ^{232}Th fluxes arise primarily from the input of aerosol dust in shallow waters, additional fluxes near the seafloor appear to arise from the dissolution of post-depositional sediments (Figure 5). This may represent the boundary exchange source of trace elements suspected to play a role for elements of paleoceanographic interest such as Nd and Hf (Lacan and Jeandel, 2005; van de Flierdt et al., 2004). As an attempt to quantify this source,

we take the difference in integrated ^{232}Th flux between the bottom of each profile and 1 km depth (below which input from dust dissolution/regeneration processes attenuates). These results range from 1-5 µg ^{232}Th $m^{-2}yr^{-1}$ (Fig. 5), representing ~30% of the full-depth dissolved ^{232}Th flux. This probably underestimates the boundary exchange flux at SO202-5 and SO202-24 which may receive a sediment dissolution flux at all depths.

Here we also assume crustal Nd/Th and Hf/Th ratios of 2.4 and 0.54, in g g^{-1} respectively (Taylor and McLennan, 1985), and congruent dissolution. Of course, few data exist on S_{Nd} or S_{Hf} to test these assumptions. A field study in the North Atlantic estimated S_{Nd} =20% (Tachikawa et al., 1999), consistent with our assumption, while experimental leaches suggest smaller values S_{Nd} =1-2% (Greaves et al., 1994) and 5-12% (Arraes-Mescoff et al., 2001). Under our assumptions, the bottom water dissolved Th fluxes from the North Pacific sites imply bottom fluxes of 2.4-12 µg $m^{-2}yr^{-1}$ dissolved Nd and 0.5-2.7 µg $m^{-2}yr^{-1}$ dissolved Hf (Eq. 2). For scale, the water column inventories (~5 km depth) of dissolved Nd and Hf in the North Pacific are 26,000 µg m^{-2} (Amakawa et al., 2009) and 2100 µg m^{-2} (Firdaus et al., 2011), respectively. The residence time of these elements is also still under investigation, but for purposes of illustration, let us assume 500 yrs for both, within the range of estimated values (van de Flierdt et al., 2004). Under steady state, supply and removal fluxes for the full water column cycles of Nd and Hf would then be 52 and 7.1 µg $m^{-2}yr^{-1}$, respectively. Therefore the boundary exchange fluxes calculated are potentially significant (10's of percent, similar to Th).

4. Conclusions and Further Work

The long-lived Th isotopes offer a unique and powerful tool to evaluate the supply of trace elements from lithogenic sources. We have identified, however, a number of sources of uncertainty that must be addressed in future studies to further refine our estimates of lithogenic

fluxes. These include the lateral transport of ^{232}Th in the water column, seasonal effects of Th input and removal, the chemical speciation and size-partitioning of ^{232}Th and ^{230}Th in seawater, and fractional metal solubility.

Dissolved ^{232}Th and ^{230}Th distributions in the North Pacific demonstrate that the oceanic Th cycle is relatively simple, with two sources, including aerosol dust dissolution in shallow waters and sediment dissolution/resuspension in bottom water, and one removal mechanism, involving scavenging throughout the water column. The delivery mechanism of dissolved Th from dust dissolution, however, is relatively complex, possibly involving rapid export of colloidal Th and its subsequent regeneration or disaggregation within 500-1000 m below the sea surface. This mechanism, as well as the mechanism describing how Th is released from sediment dissolution/resuspension at the seafloor, deserves further investigation. Dissolved ^{232}Th fluxes, nonetheless, can be applied to estimate fluxes of other lithogenically-sourced dissolved trace metals (such as aerosol-derived Fe or boundary exchange-derived Nd or Hf), or fluxes of the parent lithogenic material (such as aerosol dust) with reasonable accuracy.

Acknowledgements

We acknowledge the German Ministry of Education and Research (BmBF) for financially supporting SO-202-INOPEX, the U. S. National Science Foundation for funding the work at L-DEO (award 1029211), and the crew of the R/V *Sonne*. Natalie Mahowald is thanked for providing the model estimates of dust deposition. Comments made by Jerry McManus, Samar Khatiwala, Leo Peña, Mathieu Roy-Barman, 3 anonymous reviewers, and Gideon Henderson were helpful during the writing of the manuscript. Figure 1 was produced using Ocean Data View (Schlitzer, 2011).

References

Aguilar-Islas, A.M., Wu, J., Rember, R., Johansen, A.M., Shank, L.M., 2010. Dissolution of aerosol-derived iron in seawater: Leach solution chemistry, aerosol type, and colloidal iron fraction. Mar. Chem. 120, 25-33.

Amakawa, H., Sasaki, K., Ebihara, M., 2009. Nd isotopic composition in the central North Pacific. Geochim. Cosmochim. Acta 73, 4705-4719.

Andersen, M.B., Stirling, C.H., Zimmermann, B., Halliday, A.N., 2010. Precise determination of the open ocean $^{234}U/^{238}U$ composition. Geochem. Geophys. Geosyst. 11, Q12003.

Anderson, R.F., Fleisher, M.Q., Robinson, L.F., Edwards, R.L., Hoff, J., Moran, S.B., Rutgers van der Loeff, M.M., Thomas, A.L., Roy-Barman, M., François, R., 2012. GEOTRACES intercalibration of ^{230}Th, ^{232}Th, ^{231}Pa, and prospects for ^{10}Be. Limnol. Oceanogr. Methods 10, 179-213.

Arraes-Mescoff, R., Roy-Barman, M., Coppola, L., Souhaut, M., Tachikawa, K., Jeandel, C., Sempéré, R., Yoro, C., 2001. The behavior of Al, Mn, Ba, Sr, REE and Th isotopes during in vitro degradation of large marine particles. Mar. Chem. 73, 1-19.

Bacon, M.P., Anderson, R.F., 1982. Distribution of thorium isotopes between dissolved and particulate forms in the deep sea. J. Geophys. Res. 87, 2045-2056.

Barbeau, K., Kujawinski, E.B., Moffett, J.W., 2001. Remineralization and recycling of iron, thorium and organic carbon by heterotrophic marine protists in culture. Aquat. Microb. Ecol. 24, 69-81.

Baskaran, M., Santschi, P.H., Benoit, G., Honeyman, B.D., 1992. Scavenging of thorium isotopes by colloids in seawater of the Gulf of Mexico. Geochim. Cosmochim. Acta 56, 3375-3388.

Benitez-Nelson, C., Buesseler, K.O., Karl, D.M., Andrews, J., 2001. A time-series study of particulate matter export in the North Pacific Subtropical Gyre based on ^{234}Th:^{238}U disequilibrium. Deep Sea Res. Pt. I 48, 2595-2611.

Bingham, F.M., 1992. Formation and Spreading of Subtropical Mode Water in the North Pacific. J. Geophys. Res. 97, 11177-11189.

Boyd, P.W., Mackie, D.S., Hunter, K.A., 2010. Aerosol iron deposition to the surface ocean — Modes of iron supply and biological responses. Mar. Chem. 120, 128-143.

Boyle, E.A., Bergquist, B.A., Kayser, R.A., Mahowald, N., 2005. Iron, manganese, and lead at Hawaii Ocean Time-series station ALOHA: Temporal variability and an intermediate water hydrothermal plume. Geochim. Cosmochim. Acta 69, 933-952.

Buesseler, K.O., Pike, S., Maiti, K., Lamborg, C.H., Siegel, D.A., Trull, T.W., 2009. Thorium-234 as a tracer of spatial, temporal and vertical variability in particle flux in the North Pacific. Deep-Sea Res. Pt. I 56, 1143-1167.

Charette, M.A., Breier, C.F., Henderson, P.B., Pike, S.M., Rypina, I.I., Jayne, S.R., Buesseler, K.O., 2013. Radium-based estimates of cesium isotope transport and total direct ocean discharges from the Fukushima Nuclear Power Plant accident. Biogeosciences 10, 2159-2167.

Chen, J.H., Lawrence Edwards, R., Wasserburg, G.J., 1986. ^{238}U, ^{234}U and ^{232}Th in seawater. Earth Planet. Sci. Lett. 80, 241-251.

Chen, S., 2008. The Kuroshio Extension front from satellite sea surface temperature measurements. J. Oceanogr. 64, 891-897.

Cheng, H., Edwards, R.L., Hoff, J., Gallup, C.D., Richards, D.A., Asmerom, Y., 2000. The half-lives of uranium-234 and thorium-230. Chem. Geol. 169, 17-33.

Church, M.J., Lomas, M.W., Muller-Karger, F., 2013. Sea change: Charting the course for biogeochemical ocean time-series research in a new millennium. Deep Sea Res. Pt. II 93, 2-15.

Duce, R., Unni, C., Ray, B., Prospero, J., Merrill, J., 1980. Long-range atmospheric transport of soil dust from Asia to the tropical North Pacific: Temporal variability. Science 209, 1522-1524.

Ducet, N., Le Traon, P.Y., Reverdin, G., 2000. Global high-resolution mapping of ocean circulation from TOPEX/Poseidon and ERS-1 and -2. J. Geophys. Res.: Oceans 105, 19477-19498.

Duggen, S., Olgun, N., Croot, P., Hoffmann, L., Dietze, H., Delmelle, P., Teschner, C., 2010. The role of airborne volcanic ash for the surface ocean biogeochemical iron-cycle: a review. Biogeosciences 7, 827-844.

Firdaus, M.L., Minami, T., Norisuye, K., Sohrin, Y., 2011. Strong elemental fractionation of Zr-Hf and Nb-Ta across the Pacific Ocean. Nat. Geosci. 4, 227-230.

Frew, R., Hutchins, D., Nodder, S., Sanudo-Wilhelmy, S., Tovar-Sanchez, A., Leblanc, K., Hare, C., Boyd, P., 2006. Particulate iron dynamics during FeCycle in subantarctic waters southeast of New Zealand. Global Biogeochem. Cycles 20, GB1S93.

Gao, Y., Anderson, J.R., Hua, X., 2007. Dust characteristics over the North Pacific observed through shipboard measurements during the ACE-Asia experiment. Atmos. Environ. 41, 7907-7922.

Gersonde, R., 2012. The expedition of the research vessel "Sonne" to the subpolar North Pacific and the Bering Sea in 2009 (SO202-INOPEX). Rep. Polar Mar. Res. 643, 1-323.

Greaves, M.J., Statham, P.J., Elderfield, H., 1994. Rare earth element mobilization from marine atmospheric dust into seawater. Mar. Chem. 46, 255-260.

Hanawa, K., Suga, T., 1995. A review on the subtropical mode water in the North Pacific (NPSTMW). Terra Scientific Publishing Company, Tokyo, Japan.

Hanawa, K., Talley, L.D., 2001. Mode waters, in: Siedler, G., Church, J., Gould, J. (Eds.), Ocean Circulation and Climate: International Geophysics Series. Academic Press, pp. 373-386.

Hansard, S.P., Landing, W.M., Measures, C.I., Voelker, B.M., 2009. Dissolved iron(II) in the Pacific Ocean: Measurements from the PO2 and P16N CLIVAR/CO2 repeat hydrography expeditions. Deep-Sea Res. Pt. I 56, 1117-1129.

Hayes, C.T., Anderson, R.F., Jaccard, S.L., François, R., Fleisher, M.Q., Soon, M., Gersonde, R., 2013. A new perspective on boundary scavenging in the North Pacific Ocean. Earth Planet. Sci. Lett. 369-370, 86-97.

Hirose, K., Igarashi, Y., Aoyama, M., Inomata, Y., 2010. Depositional behaviors of plutonium and thorium isotopes at Tsukuba and Mt. Haruna in Japan indicate the sources of atmospheric dust. J. Environ. Radioactiv. 101, 106-112.

Hirose, K., Kikawada, Y., Igarashi, Y., 2012. Temporal variation and provenance of thorium deposition observed at Tsukuba, Japan. J. Environ. Radioactiv. 108, 24-28.

Hirose, K., Sugimura, Y., 1987. Thorium isotopes in the surface air of the Western North Pacific Ocean. J. Environ. Radioactiv. 5, 459-475.

Holden, N.E., 1990. Total half-lives for selected nuclides. Pure & Appl. Chem. 62, 941-958.

Hsieh, Y.-T., Henderson, G.M., Thomas, A.L., 2011. Combining seawater ^{232}Th and ^{230}Th concentrations to determine dust fluxes to the surface ocean. Earth Planet. Sci. Lett. 312, 280-290.

Huh, C.-A., Moore, W.S., David C, K., 1989. Oceanic ^{232}Th: A reconnaissance and implications of global distribution from manganese nodules. Geochim. Cosmochim. Acta 53, 1357-1366.

Iwao, T., Endoh, M., Shikama, N., Nakano, T., 2003. Intermediate circulation in the northwestern North Pacific derived from subsurface floats. J. Oceanogr. 59, 893-904.

Johnson, K.S., Elrod, V.A., Fitzwater, S.E., Plant, J.N., Chavez, F.P., Tanner, S.J., Gordon, R.M., Westphal, D.L., Perry, K.D., Wu, J., Karl, D.M., 2003. Surface ocean-lower atmosphere interactions in the Northeast Pacific Ocean Gyre: Aerosols, iron, and the ecosystem response. Global Biogeochem. Cycles 17, 1063.

Kawabe, M., 2008. Vertical and horizontal eddy diffusivities and oxygen dissipation rate in the subtropical Northwest Pacific. Deep-Sea Res. Pt. I 55, 247-260.

Kawakami, H., Honda, M.C., 2007. Time-series observation of POC fluxes estimated from ^{234}Th in the northwestern North Pacific. Deep-Sea Res. Pt. I 54, 1070-1090.

Lacan, F., Jeandel, C., 2005. Neodymium isotopes as a new tool for quantifying exchange fluxes at the continent–ocean interface. Earth Planet. Sci. Lett. 232, 245-257.

Levitus, S., 1982. Climatological Atlas of the World Ocean, NOAA Prof. Paper. U.S. Govt. Print. Off., Washington, D.C., p. 173.

Li, Y.-H., Feely, H.W., Toggweiler, J.R., 1980. ^{228}Ra and ^{228}Th concentrations in GEOSECS Atlantic surface waters. Deep-Sea Res. Pt. A 27, 545-555.

Luo, C., Mahowald, N., Bond, T., Chuang, P.Y., Artaxo, P., Siefert, R., Chen, Y., Schauer, J., 2008. Combustion iron distribution and deposition. Global Biogeochem. Cycles 22, GB1012.

Luo, S., Ku, T.-L., Kusakabe, M., Bishop, J.K.B., Yang, Y.-L., 1995. Tracing particle cycling in the upper ocean with ^{230}Th and ^{228}Th: An investigation in the equatorial Pacific along 140°W. Deep-Sea Res. Pt. II 42, 805-829.

Mahowald, N.M., Baker, A.R., Bergametti, G., Brooks, N., Duce, R.A., Jickells, T.D., Kubilay, N., Prospero, J.M., Tegen, I., 2005. Atmospheric global dust cycle and iron inputs to the ocean. Global Biogeochem. Cycles 19, GB4025.

Mahowald, N.M., Engelstaedter, S., Luo, C., Sealy, A., Artaxo, P., Benitez-Nelson, C., Bonnet, S., Chen, Y., Chuang, P.Y., Cohen, D.D., 2009. Atmospheric Iron Deposition: Global Distribution, Variability, and Human Perturbations. Ann. Rev. Mar. Sci. 1, 245-278.

Maiti, K., Benitez-Nelson, C.R., Buesseler, K.O., 2010. Insights into particle formation and remineralization using the short-lived radionuclide, Thoruim-234. Geophys. Res. Lett. 37, L15608.

Marchal, O., Lam, P.J., 2012. What can paired measurements of Th isotope activity and particle concentration tell us about particle cycling in the ocean? Geochim. Cosmochim. Acta 90, 126-148.

Martin, J.H., Gordon, M.R., 1988. Northeast Pacific iron distributions in relation to phytoplankton productivity. Deep-Sea Res. Pt. A 35, 177-196.

McGee, D., Marcantonio, F., Lynch-Stieglitz, J., 2007. Deglacial changes in dust flux in the eastern equatorial Pacific. Earth Planet. Sci. Lett. 257, 215-230.

Measures, C.I., Brown, E.T., 1996. Estimating dust input to the Atlantic Ocean using surface water Al concentrations, in: Guerezoni, S., Chester, R. (Eds.), The impact of desert dust across the Mediterranean. Kluwer, Boston, pp. 305-315.

Measures, C.I., Brown, M.T., Vink, S., 2005. Dust deposition to the surface waters of the western and central North Pacific inferred from surface water dissolved aluminum concentrations. Geochem. Geophys. Geosyst. 6, Q09M03.

Measures, C.I., Cutter, G.A., Landing, W.M., Powell, R.T., 2006. Hydrographic observations during the 2002 IOC Contaminant Baseline Survey in the western Pacific Ocean. Geochem. Geophys. Geosyst. 7, Q03M06.

Moore, W.S., 2000. Determining coastal mixing rates using radium isotopes. Cont. Shelf Res. 20, 1993-2007.

Moore, W.S., Sackett, W.M., 1964. Uranium and thorium series inequilibrium in sea water. J. Geophys. Res. 69, 5401-5405.

Moran, S.B., Buesseler, K.O., 1992. Short residence time of colloids in the upper ocean estimated from ^{238}U-^{234}Th disequilibria. Nature 359, 221-223.

Morton, P.L., 2010. Trace metal biogeochemistry in the western North Pacific, PhD Dissert. Old Dominion University, Norfolk, VA.

Morton, P.L., Landing, W.M., Hsu, S.-C., Milne, A., Aguilar-Islas, A.M., Baker, A.R., Bowie, A.R., Buck, C.S., Gao, Y., Gichuki, S., Hastings, M.G., Hatta, M., Johansen, A.M., Losno, R., Mead, C., Patay, M.D., Swarr, G., Vendermark, A., Zamora, L.M., 2013. Methods for sampling and analysis of marine aerosols: results from the 2008 GEOTRACES aerosol intercalibration experiment. Limnol. Oceanogr.: Methods 11, 62-78.

Nozaki, Y., Horibe, Y., 1983. Alpha-emitting thorium isotopes in northwest Pacific deep waters. Earth Planet. Sci. Lett. 65, 39-50.

Nozaki, Y., Horibe, Y., Tsubota, H., 1981. The water column distributions of thorium isotopes in the western North Pacific. Earth Planet. Sci. Lett. 54, 203-216.

Nozaki, Y., Nakanishi, T., 1985. ^{231}Pa and ^{230}Th profiles in the open ocean water column. Deep-Sea Res. Pt. A 32, 1209-1220.

Nozaki, Y., Yang, H.-S., Yamada, M., 1987. Scavenging of Thorium in the Ocean. J. Geophys. Res. 92, 772-778.

Ohno, Y., Iwasaka, N., Kobashi, F., Sato, Y., 2009. Mixed layer depth climatology of the North Pacific based on Argo observations. J. Oceanogr. 65, 1-16.

Oka, E., Kouketsu, S., Toyama, K., Uehara, K., Kobayashi, T., Hosoda, S., Suga, T., 2011. Formation and Subduction of Central Mode Water Based on Profiling Float Data, 2003-08. J. Phys. Oceanogr. 41, 113-129.

Oka, E., Talley, L.D., Suga, T., 2007. Temporal variability of winter mixed layer in the mid-to high-latitude North Pacific. J. Oceanogr. 63, 293-307.

Okubo, A., Obata, H., Gamo, T., Yamada, M., 2012. ^{230}Th and ^{232}Th distributions in mid-latitudes of the North Pacific Ocean: Effect of bottom scavenging. Earth Planet. Sci. Lett. 339–340, 139-150.

Orians, K.J., Bruland, K.W., 1986. The biogeochemistry of aluminum in the Pacific Ocean. Earth Planet. Sci. Lett. 78, 397-410.

Owens, W.B., Warren, B.A., 2001. Deep circulation in the northwest corner of the Pacific Ocean. Deep Sea Res. Pt. I 48, 959-993.

Parrington, J.R., Zoller, W.H., Aras, N.K., 1983. Asian dust: Seasonal transport to the Hawaiian Islands. Science 220, 195-197.

Rea, D.K., 1994. The paleoclimatic record provided by eolian deposition in the deep sea: The geologic history of wind. Rev. Geophys. 32, 159-195.

Roy-Barman, M., 2009. Modelling the effect of boundary scavenging on thorium and protactinium profiles in the ocean. Biogeosciences 6, 3091-3197.

Roy-Barman, M., Chen, J.H., Wasserburg, G.J., 1996. ^{230}Th-^{232}Th systematics in the central Pacific Ocean: The sources and the fates of thorium. Earth Planet. Sci. Lett. 139, 351-363.

Roy-Barman, M., Coppola, L., Souhaut, M., 2002. Thorium isotopes in the western Mediterranean Sea: an insight into the marine particle dynamics. Earth Planet. Sci. Lett. 196, 161-174.

Roy-Barman, M., Lemaître, C., Ayrault, S., Jeandel, C., Souhaut, M., Miquel, J.C., 2009. The influence of particle composition on Thorium scavenging in the Mediterranean Sea. Earth and Planetary Science Letters 286, 526-534.

Santschi, P.H., Murray, J.W., Baskaran, M., Benitez-Nelson, C.R., Guo, L.D., Hung, C.C., Lamborg, C., Moran, S.B., Passow, U., Roy-Barman, M., 2006. Thorium speciation in seawater. Mar. Chem. 100, 250-268.

Schlitzer, R., 2011. http://odv.awi.de.

Serno, S., Winckler, G., Anderson, R.F., Hayes, C.T., McGee, D., Machalett, B., Ren, H., Straub, S.M., Gersonde, R., Haug, G.H., in revision. Eolian dust input to the Subarctic North Pacific. Earth Planet. Sci. Lett.

Shiller, A.M., Bairamadgi, G.R., 2006. Dissolved gallium in the northwest Pacific and the south and central Atlantic Oceans: Implications for aeolian Fe input and a reconsideration of profiles. Geochem. Geophys. Geosyst. 7, Q08M09.

Sholkovitz, E.R., Sedwick, P.N., Church, T.M., Baker, A.R., Powell, C.F., 2012. Fractional solubility of aerosol iron: Synthesis of a global-scale data set. Geochim. Cosmochim. Acta 89, 173-189.

Singh, A.K., Marcantonio, F., Lyle, M., 2013. Water column ^{230}Th systematics in the eastern equatorial Pacific Ocean and implications for sediment focusing. Earth Planet. Sci. Lett. 362, 294-304.

Suga, T., Motoki, K., Aoki, Y., Macdonald, A.M., 2004. The North Pacific climatology of winter mixed layer and mode waters. J. Phys. Oceanogr. 34, 3-22.

Tachikawa, K., Jeandel, C., Roy-Barman, M., 1999. A new approach to the Nd residence time in the ocean: the role of atmospheric inputs. Earth Planet. Sci. Lett. 170, 433-446.

Talley, L.D., 1993. Distribution and Formation of North Pacific Intermediate Water. J. Phys. Oceanogr. 23, 517-537.

Taylor, S.R., McLennan, S.M., 1985. The Continental Crust: Its Composition and Evolution. Blackwell, Oxford.

van de Flierdt, T., Frank, M., Lee, D.-C., Halliday, A.N., Reynolds, B.C., Hein, J.R., 2004. New constraints on the sources and behavior of neodymium and hafnium in seawater from Pacific Ocean ferromanganese crusts. Geochim. Cosmochim. Acta 68, 3827-3843.

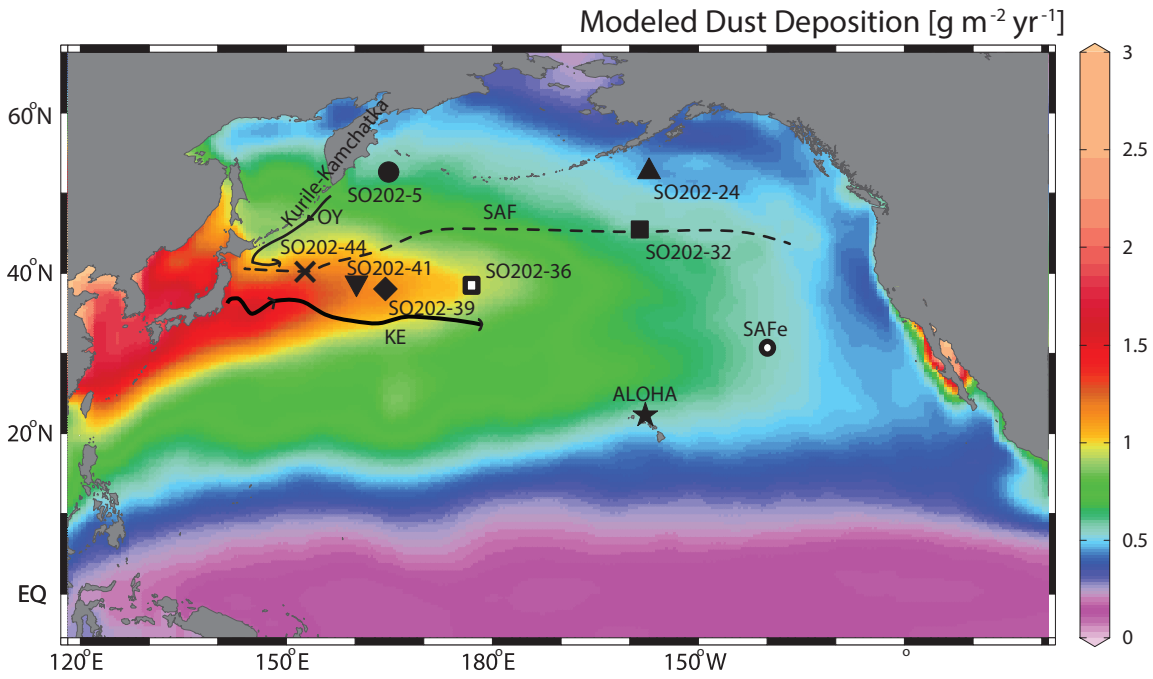

Figure 1. Map of the locations from which dissolved Th data is presented in the paper overlain with the model-derived atmospheric dust deposition estimates of Mahowald et al. (2005). Schematic representations of the Subarctic Front (SAF), the Kuroshio Extension (KE) and Oyashio Current (OY) are included as drawn by Harrison et al. (2004) and Chen (2008).

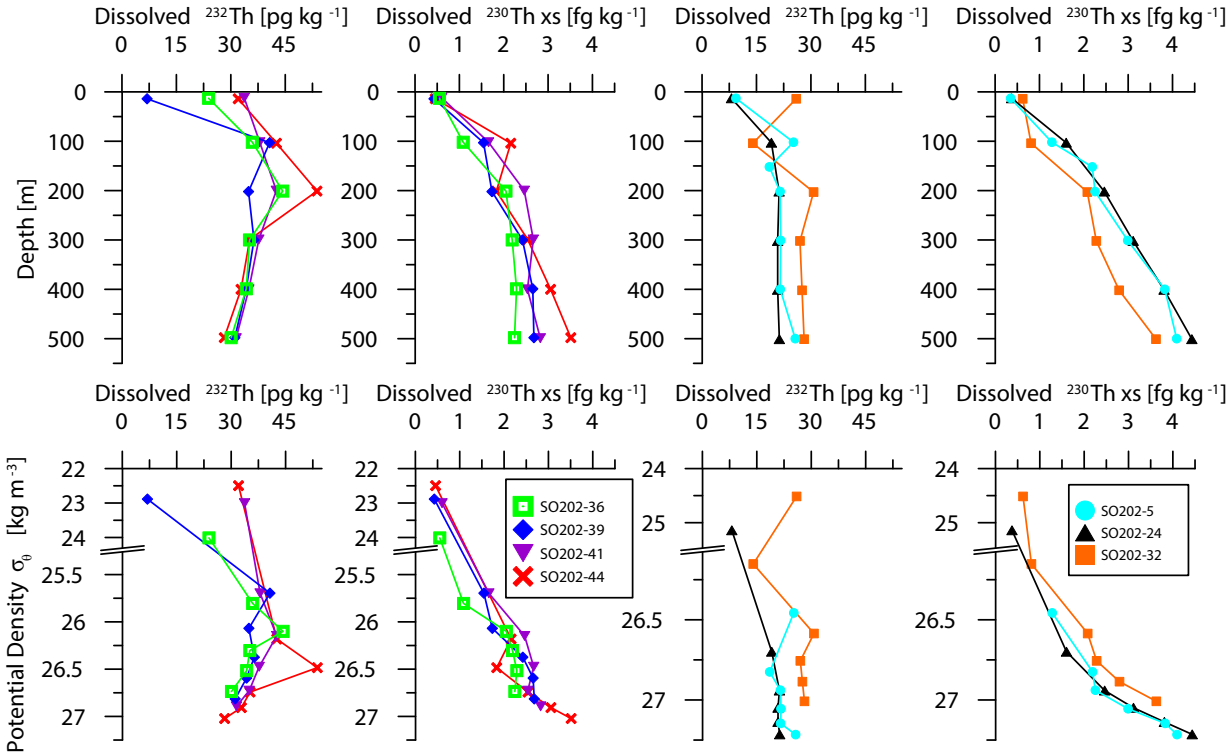

Figure 2. Shallow depth profiles of dissolved ^{232}Th and ^{230}Th from the INOPEX stations along coordinates of water depth (top) and potential density (bottom). The profiles in the left four panels are located along 40°N (Fig. 1) and are expected to receive higher dust input than the stations whose profiles are plotted in the right four panels, according to the Mahowald et al. (2005) model.

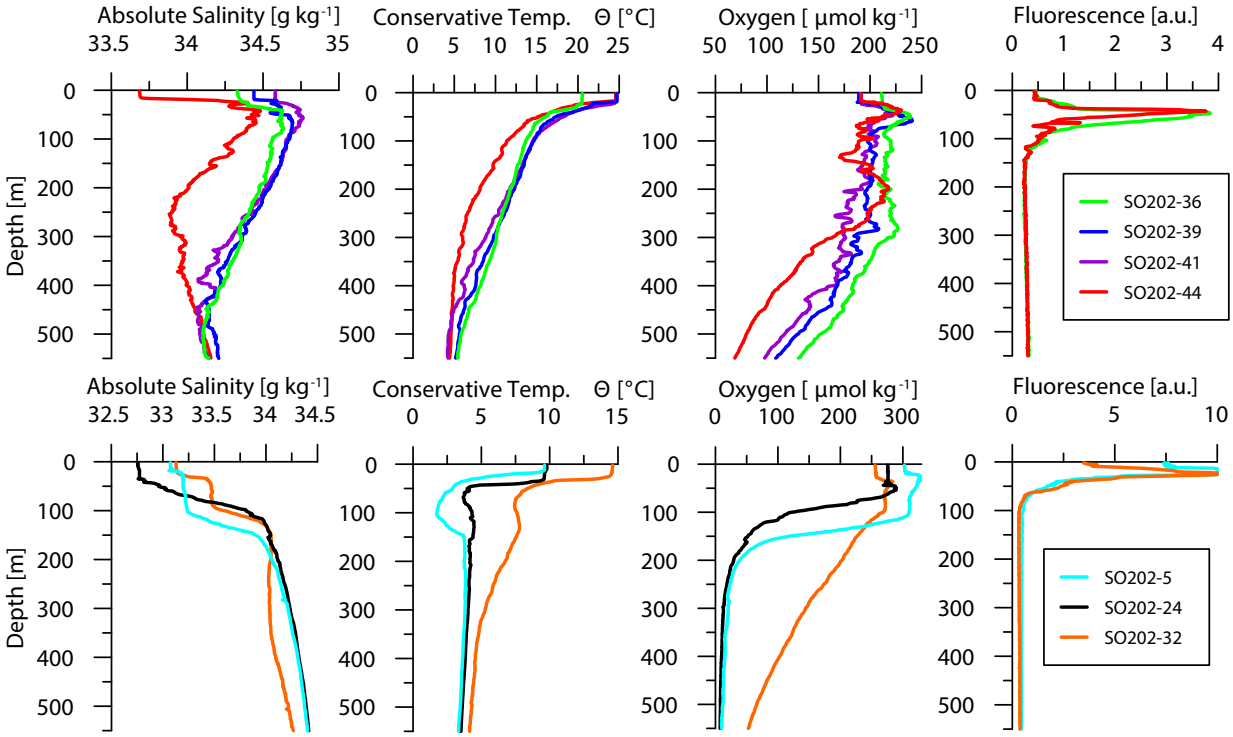

Figure 3. Hydrographic parameters calculated from CTD measurements for the INOPEX stations. Fluorometer measurements (arbitrary units) were only available from some stations.

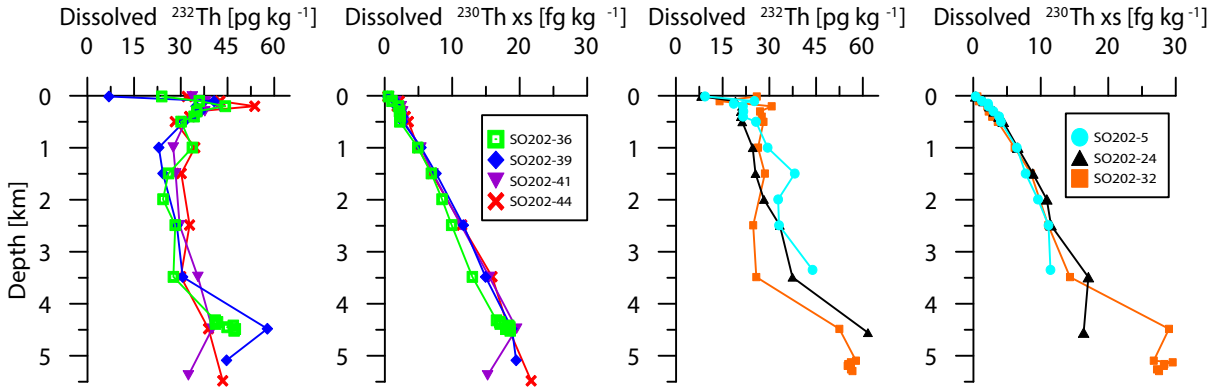

Figure 4. Full depth profiles of dissolved ^{232}Th and ^{230}Th from the INOPEX sites. Measurement errors are smaller than or equal to the symbol size.

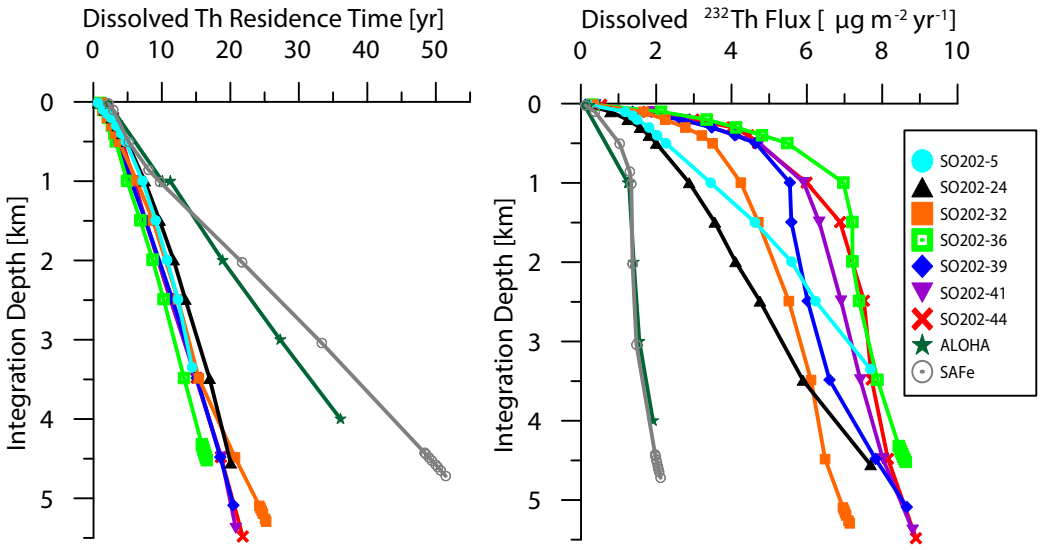

Figure 5. Depth profiles of depth-integrated dissolved Th residence times (left) and ^{232}Th fluxes (right) for the locations in Fig. 1. Error bars on the x-axes are 3-5% in both cases and are omitted for clarity. Disssolved ^{232}Th-^{230}Th from ALOHA and SAFe were reported by Roy-Barman et al. (1996) and Anderson et al. (2012), respectively.

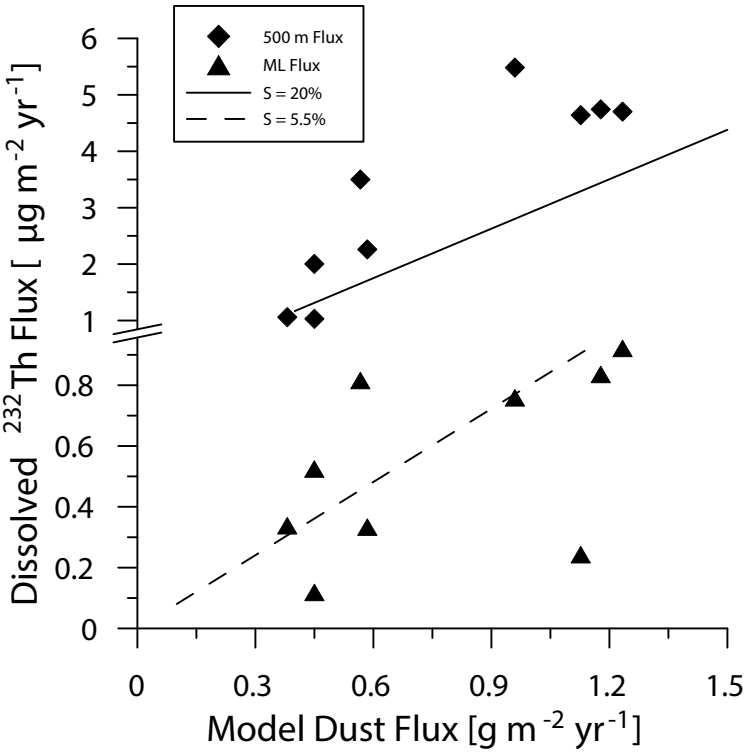

Figure 6. Dissolved ^{232}Th fluxes as calculated for the mixed layer (triangles) and by integrating Th inventories from the surface to 500 m depth (diamonds) from the locations in Fig. 1 against model-derived estimates of dust deposition for the same locations (Mahowald et al., 2005). The dotted and solid lines represent a constant fractional Th solubility of 5.5 and 20%, respectively, both assuming a Th concentration in East Asian dust of 14.6 ppm (Serno et al., in revision). Note break in y-axis.

Table 1. Dissolved Th residence times and fluxes (steady state rates of supply and removal) calculated for the mixed layer (ML), and by integrating from the sea surface to 500 m water depth. Mixed layer depths (MLD) were determined as the depth at which potential denisty became 0.125 kg m^{-3} greater than at the surface from CTD (Fig. 3) at the time of sampling.

Station	MLD [a] (m)	τ_{Th} (ML, yrs)	τ_{Th} (500 m, yrs)	^{232}Th flux (ML, µg m^{-2} yr^{-1})	^{232}Th flux (500 m, µg m^{-2} yr^{-1})
SO202-5	18	0.7 ± 0.3	4.7 ± 0.1	0.33 ± 0.07	2.26 ± 0.07
SO202-24	35	0.7 ± 0.2	4.9 ± 0.1	0.52 ± 0.04	2.00 ± 0.05
SO202-32	26	1.2 ± 0.2	3.7 ± 0.1	0.82 ± 0.05	3.50 ± 0.10
SO202-36	24	1.0 ± 0.3	3.3 ± 0.1	0.76 ± 0.10	5.48 ± 0.23
SO202-39	19	0.8 ± 0.3	3.6 ± 0.1	0.24 ± 0.05	4.64 ± 0.16
SO202-41	22	1.1 ± 0.3	4.0 ± 0.1	0.84 ± 0.10	4.74 ± 0.15
SO202-44	17	0.8 ± 0.3	4.2 ± 0.1	0.92 ± 0.16	4.70 ± 0.14
ALOHA	50[b]	2.2 ± 1.3	6.4 ± 1.2	0.34 ± 0.06	1.06 ± 0.26
SAFe	15	2.2 ± 0.5	5.2 ± 0.4	0.12 ± 0.03	1.03 ± 0.09

[a]MLD in the region of SO202 stations is highly seasonal. Data here was collected in late summer while winter mixed layers can exceed 200 m (see section 3.1.2).

[b]CTD data was not available from the 1994 cruise from which this data was collected by Roy-Barman et al. (1996). Surface samples were taken from 25 m depth and noted to be within the mixed layer. We chose 50 m mixed layer based on climatology (Church et al. 2013).

Table 2. Apparent fractional Th solubilities derived by comparing model-derived dust deposition

Station	Model-Dust Deposition ($g\ m^{-2}\ yr^{-1}$)	S_{Th} (ML, %) [b]	S_{Th} (500 m, %) [c]	Dissolved Th-derived dust deposition [d] (500 m, S_{Th} = 20%, $g\ m^{-2}\ yr^{-1}$)
SO202-5	0.58 ± 0.12	3.9 ± 1.8	26.5 ± 6.7	0.77 ± 0.20
SO202-24	0.45 ± 0.09	8.0 ± 2.8	30.5 ± 7.7	0.69 ± 0.17
SO202-32	0.57 ± 0.11	9.9 ± 2.6	42.3 ± 10.7	1.20 ± 0.30
SO202-36	0.96 ± 0.19	5.4 ± 2.1	39.1 ± 10.0	1.88 ± 0.48
SO202-39	1.13 ± 0.23	1.5 ± 0.6	28.2 ± 7.1	1.59 ± 0.40
SO202-41	1.18 ± 0.24	4.9 ± 1.6	27.6 ± 7.0	1.62 ± 0.41
SO202-44	1.23 ± 0.25	5.1 ± 1.8	26.1 ± 6.6	1.61 ± 0.41
ALOHA	0.38 ± 0.08	6.1 ± 3.7	19.1 ± 7.6	0.36 ± 0.13
SAFe	0.45 ± 0.09	1.8 ± 0.5	15.7 ± 4.2	0.35 ± 0.09

[a]Dust deposition estimates extracted from the model results of Mahowald et al. (2005), assuming 20% uncertainty

[b]Fractional solubility of Th using ML dissolved ^{232}Th fluxes, assuming model dust deposition is correct and the concentration of Th in East Asian dust is 14.6 ±0.2 ppm (Serno et al., in revision)

[c]Fractional solubility of Th using dissolved ^{232}Th fluxes integrated from the sea surface to 500 m depth, assuming model dust deposition is correct and the concentration of Th in East Asian dust is 14.6±0.2 ppm (Serno et al., in revision)

[d]Dust deposition estimates based on ^{232}Th fluxes integrated from the sea surface to 500 m depth, assuming a fractional Th solubility of 20±5% (see section 3.3), and a Th concentration in East Asian dust of 14.6±0.2 ppm (Serno et al., in revision)

Chapter 3. Chemical fractionation of $^{231}Pa/^{230}Th$ in the Pacific Ocean: paleoceanographic implications

Christopher T. Hayes[a,b], Robert F. Anderson[a,b], Martin Q. Fleisher[a], Sascha Serno[a,c], Gisela Winckler[a,b], Rainer Gersonde[d]

[a]Lamont-Doherty Earth Observatory of Columbia University, Palisades, NY, USA

[b]Department of Earth and Environmental Sciences, Columbia University, New York, NY, USA

[c]DFG-Leibniz Center for Surface Process and Climate Studies, Institute of Earth and Environmental Science, University of Potsdam, Potsdam-Golm, Germany

[d]Alfred Wegener Institute for Polar and Marine Research, Bremerhaven, Germany

In preparation for Earth and Planetary Science Letters

Abstract

The ratio of unsupported protactinium-231 to thorium-230 in marine sediments, $(Pa/Th)_{xs}$, is potentially sensitive to several processes of oceanographic and climatological interest: deep ocean circulation, marine biological productivity (as it relates to total particle flux) and particle composition (specifically biogenic opal and authigenic Mn). In order to attribute variations in $(Pa/Th)_{xs}$ observed in sediment records to changes in specific processes through time, a better understanding of the chemical cycling of these elements in the modern ocean is necessary. To this end, a survey was undertaken of $(Pa/Th)_{xs}$ in surface sediments from the subarctic Pacific (SO202-INOPEX expedition) in combination with a Pacific-wide compilation of published data. Throughout the Pacific, $(Pa/Th)_{xs}$ is robustly correlated with the opal content of sediments. In the North and equatorial Pacific, simultaneous positive correlations with productivity indicators suggest that boundary scavenging and opal scavenging combine to enhance the removal of Pa in the eastern equatorial Pacific and subarctic Pacific. Deep ocean water mass ageing (>3.5 km) associated with the Pacific overturning appears to play a secondary role in determining the basin scale distribution of $(Pa/Th)_{xs}$. We hypothesize that through time $(Pa/Th)_{xs}$ distributions in the Pacific could define the evolving boundaries of contrasting biogeographic provinces in the North Pacific, while the influence of hydrothermal scavenging of Pa potentially confounds this approach in the South Pacific.

1. Introduction

Chemical proxies of past ocean change are built upon knowledge of an association between certain elements or isotopes and a controlling ocean property or process. The ratio of the radionuclides ^{231}Pa to ^{230}Th, in excess of that supported by the *in-situ* decay of their respective parents, $(Pa/Th)_{xs}$, in ocean sediments has multiple potential controls: biological productivity, total particle flux, advective overturning circulation or particle composition (Chase et al., 2002; Kumar et al., 1993; Walter et al., 1999; Yu et al., 1996). To determine how variations in $(Pa/Th)_{xs}$ in sediment records can be interpreted as a proxy for a process of interest, observations of $(Pa/Th)_{xs}$ in oceanic environments that differ in the potentially controlling parameters are necessary.

Here we report new $(Pa/Th)_{xs}$ data from the SO202-INOPEX expedition to the subarctic Pacific (Gersonde, 2012), which sampled environments of relatively high rates of biological productivity and burial of biogenic opal. To assess the influence of the Pacific overturning circulation and a larger range of oceanic particle composition and flux, we combine the INOPEX data with published surface sediment data throughout the Pacific basin. Enhanced removal of Pa due to opal scavenging is found to be the most robust influence on $(Pa/Th)_{xs}$ in modern Pacific sediments. We briefly discuss how this proxy might be used in determining how the geographic distribution of particle composition, which is ultimately related to biogeographic community structure, has evolved over glacial-interglacial cycles.

2. Background and approach: potentially controlling processes

Dissolved uranium is homogeneously distributed throughout the ocean with a uniform isotopic composition (Andersen et al., 2010; Chen et al., 1986; Weyer et al., 2008). This leads to

a constant and well-known production of the daughter products ^{231}Pa (from ^{235}U) and ^{230}Th (from ^{234}U) throughout the water column at a constant initial activity ratio of 0.093. Because of their particle-reactive, insoluble nature, Pa and Th are removed to the seafloor by scavenging onto particles on timescales of 50-200 yrs and 10-40 yrs (Henderson and Anderson, 2003), respectively, i.e., rapidly compared to their respective half-lives: 32,760 yrs for ^{231}Pa (Robert et al., 1969) and 75,690 yrs for ^{230}Th (Cheng et al., 2000). It is their uniform source and differential timescales of removal by scavenging which make them potentially sensitive to several processes: particle flux, overturning circulation and particle composition. We elaborate on each process below and describe how we assess the associated influence on $(Pa/Th)_{xs}$ distributions. Section 2.4 describes the new surface sediment data presented here and the published results used in our analysis.

2.1 Biological productivity, total particle flux and boundary scavenging

Regional variations in biological productivity are closely related, though not equivalent, to regional variations in total particle flux, as sinking particles are dominated by biogenic components, at least in most of the open ocean (François et al., 2002; Honjo et al., 2008). When lateral gradients in particle flux exist, scavenged elements are potentially removed preferentially in areas of high particle flux often associated with ocean margins, a concept termed boundary scavenging (Bacon et al., 1976; Spencer et al., 1981). More intense scavenging reduces ^{231}Pa and ^{230}Th concentrations in margin seawater to a greater degree than in the open ocean. This situation creates lateral gradients in concentration which should cause dispersive fluxes of both nuclides from low to high flux sites. More ^{231}Pa, relative to ^{230}Th, can be transported laterally because of its longer residence time (Bacon, 1988). This interpretation is consistent with the finding of

many studies in the Pacific (Anderson et al., 1983a; Anderson et al., 1983b; Lao et al., 1993; Lao et al., 1992b; Mohamed and Tsunogai, 1998; Shimmield et al., 1986; Yang et al., 1986) that the $(Pa/Th)_{xs}$ of particulate matter and sediments from the continental margin are generally much higher than those of open-ocean sites. A recent investigation of boundary scavenging in the water column found that Pa is more efficiently scavenged throughout the entire subarctic Pacific gyre, not only at continental margins (Hayes et al., 2013).

To assess the influence of boundary scavenging on sedimentary $(Pa/Th)_{xs}$, we use satellite-derived estimates of net primary productivity (NPP) and export productivity (EP, the fraction of primary productivity which is exported below the euphotic zone). These parameters are not equivalent to particle flux, which is more relevant to scavenging, but more biological production of organic carbon at the surface (NPP) and its export to depth (EP) are both likely related to scavenging intensity (Coale and Bruland, 1987). The excellent geographic coverage of satellite records allows us to estimate these parameters for any given location. Long term annual averages of NPP were calculated using monthly SeaWiFS-data (1997-2009, 1/6°-resolution) and the standard VGPM algorithm (http://www.science.oregonstate.edu/ocean.productivity) (Behrenfeld and Falkowski, 1997). Average EP values were calculated according to Laws et al. (2000) as a function of the aforementioned NPP and the World Ocean Atlas 2009 sea-surface temperature (Locarnini et al., 2010) at 1°-resolution.

One could in principle also compare sedimentary $(Pa/Th)_{xs}$ with burial fluxes calculated by ^{230}Th-normalization (François et al., 2004) to assess the influence of boundary scavenging since both these parameters are based on the same measured quantities. Th-normalization calculates a sediment flux assuming ^{230}Th is being buried at its production rate in the overlying

water column. The burial or preserved sediment flux is to first order related to particle flux or scavenging intensity in the overlying water column; however spatial variations in burial fluxes become decoupled with spatial variations in particle rain because of the differential preservation of oceanic particles. For instance, biogenic $CaCO_3$ particles contribute to scavenging throughout the water column, but will only contribute to the total burial flux if the core site is above the calcite compensation depth (~4.5 km over most of the Pacific (Berger and Winterer, 1974)). Additionally, burial fluxes of biogenic opal (Nelson et al., 1995) and organic matter (Emerson and Hedges, 1988) are highly attenuated signals of their particle rain to the seafloor and the degree of attenuation is spatially variable. Therefore, we appeal to the satellite-derived productivity indicators in the absence of a better available metric of scavenging intensity.

2.2 Overturning circulation

The differential removal rates of Pa and Th by scavenging is also the basis for a potential sensitivity of sedimentary $(Pa/Th)_{xs}$ to lateral advection by deep ocean circulation (Marchal et al., 2000; Yu et al., 1996). Scavenging is a reversible process, i.e. the average Th and Pa atom experiences several cycles of adsorption and desorption as they are removed to the seafloor by sinking particles (Bacon and Anderson, 1982; Nozaki et al., 1981). This causes the scavenged radionuclides to become concentrated with depth in the water column. In fact, a linear increase in concentration with depth is expected for a steady-state balance between radionuclide production and removal by scavenging in the absence of lateral circulation.

Where deep ocean ventilation occurs, surface waters with low ^{231}Pa and ^{230}Th concentrations are injected to depth. In these regions, such as the North Atlantic, observed ^{231}Pa and ^{230}Th concentrations in deep water are less than predicted by reversible scavenging (Cochran

et al., 1987; Moran et al., 1997; Moran et al., 1995; Moran et al., 2002; Vogler et al., 1998). As a deep water mass ages and spreads laterally, particles sinking into it from above will experience enhanced desorption of ^{231}Pa and ^{230}Th until the higher steady-state radionuclide concentration is reached (François, 2007; Thomas et al., 2006). Because of its shorter residence time (faster response time, 10-40 yrs), ^{230}Th returns to a steady-state with respect to scavenging faster than ^{231}Pa (50-200 yrs). Consequently, dissolved ^{231}Pa/^{230}Th in deep waters are expected to increase with water mass age since ventilation.

The meridional overturning circulation of the Atlantic is believed to result in a large southward transport of ^{231}Pa relative to ^{230}Th because the ventilation timescale of that basin is on the order of the Pa residence time (<200 yrs) (Yu et al., 1996). The Pacific meridional overturning circulation (PMOC), however, occurs over longer timescales (>500 yrs) (Matsumoto, 2007) and at more zonally disperse spatial scales. The schematic overturning, a northward inflow at high southern latitudes of Lower Circumpolar Deep Water (LCDW) and subsequent upwelling in northern mid-latitudes to form a southward return flow of North Pacific Deep Water (NPDW) (Kawabe and Fujio, 2010; Macdonald et al., 2009) clearly influences the distribution of long-lived circulation tracers such as natural radiocarbon (Schlosser et al., 2001) or dissolved silicon (Talley et al., 2003), but it is unclear whether Pa will be redistributed by PMOC (Hayes et al., 2013; Luo et al., 2012).

A complete treatment of the influence of deep circulation in the Pacific is beyond the scope of this paper and may require a 3-dimensional circulation modeling approach with imposed particle fields and scavenging dynamics that are becoming more realistic (Dutay et al., 2009; Siddall et al., 2005). As a simplified and expedient approach, we will compare

sedimentary $(Pa/Th)_{xs}$ with bottom water (>3.5 km) mean age (Khatiwala et al., 2012), defined as the mean of the distribution of transit times between a location and the sea surface, estimated at 1°-resolution.

2.3 Particle composition

All marine particle types do not scavenge Pa and Th with equal intensity based on experimental and observational work (Chase et al., 2002; Geibert and Usbeck, 2004; Guo et al., 2002; Kretschmer et al., 2011; Scholten et al., 2005; Yu et al., 2001). In general, it has been recognized that Pa has a higher affinity for biogenic opal (Chase, 2008; Chase et al., 2002; DeMaster, 1979; Taguchi et al., 1989) and authigenic manganese oxides (Anderson et al., 1983a; Kadko, 1980) compared with the other major sedimentary components (e.g., calcium carbonate or clay/lithogenic material), while Th is scavenged more equally among different particle types. Thus, it is possible that the $^{231}Pa/^{230}Th$ ratio in sediments represents the relative contribution of biogenic opal and/or manganese oxides to scavenging.

The fractionation factor (Th/Pa), F, is a measure of the intensity with which Th is scavenged relative to Pa. It is defined (Anderson et al., 1983a) as the ratio of the distribution coefficient (atoms radionuclide per gram particulate matter over atoms radionuclide per gram seawater) of Th over that of Pa. Equivalently, F equals the $^{231}Pa/^{230}Th$ in seawater over $(Pa/Th)_{xs}$ in sediments or particulate matter. In particulate material dominated by biogenic opal (Chase et al., 2002; Venchiarutti et al., 2011a; Venchiarutti et al., 2011b; Walter et al., 2001; Walter et al., 1997) or when authigenic Mn oxides (MnO_2, for simplicity) are present (Anderson et al., 1983a), measured F values are close to 1. When other phases (calcium carbonate and clay) dominate, F is generally much larger, 10 to 20 (Chase et al., 2002; Luo and Ku, 1999; Moran et al., 2001). One

expects, therefore, that in areas where particles contain little opal or MnO_2, particulate $^{231}Pa/^{230}Th$ will be low due to the preference for Th during scavenging. As opal or MnO_2 content increase, relatively more Pa will be scavenged, increasing the Pa/Th ratio.

We will compare $(Pa/Th)_{xs}$ observations to the concentration of opal in the sediments (opal%). The preserved $(Pa/Th)_{xs}$ is thought to represent equilibration with respect to scavenging onto the particles within about 1 km of the seafloor (Thomas et al., 2006), and the deep particulate $^{231}Pa/^{230}Th$ is generally unaffected during burial (Anderson et al., 1983b; Chase et al., 2003b; Scholten et al., 2005; Taguchi et al., 1989). Unfortunately, particulate opal concentration changes during burial because of sediment diagenesis at the seafloor. Deep particulate rain of opal is nonetheless positively related to opal% in surface sediments in the equatorial Pacific and Southern Ocean (Pacific sector) (Sayles et al., 2001). Therefore, without attempting to correct burial fluxes for sediment diagenesis, we use measured opal% as a qualitative indicator of the importance of opal during scavenging in the water column. Concurrent measurements of MnO_2 and $(Pa/Th)_{xs}$ are limited but we signify examples in the literature where this particle composition effect can be important.

Because concurrent measurements of radionuclides and particle composition in the water column are sparse, we will eventually make an assumption that geographic variation in particle composition is largely produced by contrast in biological community structure. For instance, eutrophic conditions favor large phytoplankton such as diatoms (opal producers) while oligotrophic conditions favor small phytoplankton such as coccolithophores ($CaCO_3$ producers) (Alvain et al., 2008; Eppley and Peterson, 1979; Falkowski et al., 1998; Kostadinov et al., 2010; Ryther, 1969). The ratio opal:$CaCO_3$ of sinking particles, which is positively correlated with

particulate $(Pa/Th)_{xs}$ globally (Chase et al., 2002), exhibits strong contrast across biogeographic boundaries in the Pacific (Honjo et al., 2008). Additionally, distributions of dissolved ^{231}Pa and ^{230}Th in the North Pacific water column indicate a threshold of scavenging intensity for both nuclides between the subtropical and subarctic gyres (Hayes et al., 2013). Oceanic conditions which favor certain phytoplankton and/or particle compositions arise due to inter-related environmental factors such as atmospheric circulation, light availability, and nutrient availability. Furthermore, distinct oceanic regions are physically bound by continents or ocean fronts and pycnoclines (Longhurst, 2006). To extend our understanding of the Pa/Th cycle in the modern ocean we will spatially extrapolate within defined biogeographic provinces (Longhurst, 2006).

2.4 Materials and Methods

The new data presented here comprise a surface sediment $(Pa/Th)_{xs}$ survey of the INOPEX cruise of July-August 2009 in the subarctic Pacific and selected samples for which $(Pa/Th)_{xs}$ has been previously reported (Lao et al., 1992b) and new opal% data are available (Fig. 1). We assume modern age for INOPEX samples since the sediment-water interface was successfully collected, although independent age constraints have not been made. Sediments were analyzed by published methods for thorium, protactinium and uranium isotopes (Fleisher and Anderson, 2003) and opal (Mortlock and Froelich, 1989). U, Th and opal data from the INOPEX multicores have been previously reported (Serno et al., in revision). INOPEX water samples were collected and analyzed by intercalibrated methods developed for the GEOTRACES program (Anderson et al., 2012) and have been previously described (Hayes et al., 2013).

To investigate the distribution of $(Pa/Th)_{xs}$ in a wider range of oceanographic conditions we compiled available modern surface sediment data. In general we report $(Pa/Th)_{xs}$ as corrected for detrital-supported fractions and age-decay by the original authors but in some cases this has been recalculated and some cores have only limited age constraints. For INOPEX cores, a detrital U/Th activity ratio of 0.5 was applied based on detrital sediments near Japan (Taguchi and Narita, 1995). If not corrected for by the original authors for other sites, we assumed detrital U/Th = 0.7, the basin-wide average (Henderson and Anderson, 2003). For locations with multiple data of Holocene age, the younger datum is used. A subgroup of sites has opal% data. We assign to each site NPP, EP and bottom water age estimates only if the site is within a half-grid-node radius of the nearest gridded datum. In the case of bottom water age (mean age below 3.5 km), only sites deeper than 3.5 km are assigned an age. Bibliographic information for the database is found in the Supplemental Material (Table S1, Appendix 1). INOPEX surface sediment data is archived at PANGAEA (pangaea.de) and the U.S. National Climate Data Center.

3. **Results and discussion**

3.1 INOPEX surface sediment $(Pa/Th)_{xs}$ survey

The subarctic Pacific has long been known as a preferential sink for ^{231}Pa (Yang et al., 1986). High particulate fluxes and high opal contents of sinking particles (Taguchi et al., 1989) have been invoked to explain the enhanced removal of ^{231}Pa over ^{230}Th in this region, through the boundary scavenging (Sec. 2.1) and particle composition (Sec. 2.3) mechanisms, respectively. The INOPEX surface sediment survey allows us to revisit these hypotheses with

greater geographic resolution, higher precision (ICP-MS) measurements and more knowledge of sediment composition (opal% in particular).

Results are presented in Figure 2 of $(Pa/Th)_{xs}$, opal%, NPP and EP for the INOPEX and northwestern Pacific sites (Lao et al., 1992b). We do not expect oceanic Pa/Th fractionation to apply to the semi-isolated basin of the Bering Sea (sites SO202-10 through -22), and sediment from the shallow site SO202-26 (742 m water depth) was characterized by heavily winnowed sand (Gersonde, 2012) and thus not representative of the fine fraction of settling particles assumed to carry the scavenged ^{231}Pa and ^{230}Th. These sites are excluded in analyses of linear dependence. We report the Pearson correlation coefficient, r, which denotes the direction and strength of the linear correlation between two variables. The strength of correlation is associated with the (somewhat arbitrary) categories: none, small, medium and strong for absolute r values between 0-0.09, 0.1-0.3, 0.3-0.5 and 0.5-1, respectively.

Throughout the subarctic Pacific, $(Pa/Th)_{xs}$ is strongly correlated ($r = 0.67$) with opal% (Fig. 2D), consistent with opal being a major carrier phase for the removal of ^{231}Pa from the water column. Nearly all of the $(Pa/Th)_{xs}$ values are above the production ratio of 0.093. Clearly, we confirm previous findings that the subarctic Pacific is a large scale sink for ^{231}Pa (Lao et al., 1992b; Yang et al., 1986). Nonetheless, there is considerable scatter in the $(Pa/Th)_{xs}$ vs. opal% relationship which we cannot specifically attribute to variations in sediment diagenesis without intimate knowledge of the sedimentary environments (sedimentation rate, bioturbation mixing depth, etc.) (Sayles et al., 2001). Sedimentary opal concentrations are not well correlated with total burial flux (Fig. 2C), indicating at least that opal% is driven not only by preservation but also influenced by variation in opal rain to the sediments.

In contrast, $(Pa/Th)_{xs}$ has a small negative correlation with NPP (Fig. 2A, r = -0.24) in the INOPEX survey. This suggests that total particle flux and the associated boundary scavenging mechanism are not as important as opal% for the enhanced removal of ^{231}Pa in the subarctic Pacific. A better positive correlation is found between $(Pa/Th)_{xs}$ and EP (Fig. 2B, r = 0.60). Thus the flux of organic carbon exported to depth (EP) may more accurately represent scavenging intensity throughout the water column than does its net production at the surface (NPP). The better correlation with EP may also be found because higher EP is often associated with diatom productivity (Buesseler, 1998) and mineral ballasting by biogenic opal enhances the downward flux of organic carbon (François et al., 2002; Honda and Watanabe, 2010).

This survey confirms that the subarctic Pacific is a basin-wide sink for ^{231}Pa. A strong association with opal concentration suggests that particle composition is largely responsible for this chemical fractionation. Assuming a long-term steady-state, $(Pa/Th)_{xs}$ ratios elevated above the production ratio require a lateral transport of ^{231}Pa to the subarctic by ocean circulation, if we further assume that ^{230}Th is laterally transported to a lesser extent than ^{231}Pa. The transport of ^{231}Pa to sites of its highest removal by opal occurs by eddy diffusion generally, but deep advection also may contribute. As the overturning circulation in the Pacific encompasses both the northern and southern hemispheres, it is difficult to assess the influence of PMOC on the fate of ^{231}Pa removal in the subarctic in isolation. We now turn to the Pacific-wide survey to address the influence of PMOC while testing the other potential controlling parameters (particle flux and particle composition) under a larger range of oceanic conditions.

3.2 Pacific $(Pa/Th)_{xs}$ and statistical analysis of basin-wide influences

Confirming previous mapping exercises (Walter et al., 1999; Yang et al., 1986), our compilation of $(Pa/Th)_{xs}$ in Pacific surface sediments (Fig. 3) shows three regions of enhanced ^{231}Pa removal in the Pacific at large: the subarctic Pacific, the eastern equatorial Pacific and the Pacific sector of the Southern Ocean, indicated by ratios well above production (0.093). As well, the subtropical gyres show a deficit of ^{231}Pa with ratios well below the production ratio. This new compilation affords an investigation of the reasons behind this large-scale chemical fractionation of Pa/Th in greater geographical detail than has been possible before. In Fig. 4, we present basin wide maps of the potential forcings against each of which we test for correlations with the observed $(Pa/Th)_{xs}$ in Fig. 5.

We divide the analysis into a series of zonal regions for the following reasons. A distinct response is expected for $(Pa/Th)_{xs}$ of the Pacific sector of the Southern Ocean (>60°S). It is obviously connected to the other ocean basins through the Antarctic Circumpolar Current and it has very high opal fluxes in the water column (Honjo et al., 2000). Additionally, the Laws et al. (2000) algorithm for EP may not be optimal for the Southern Ocean, where the relationship between export efficiency and net production differs from the rest of the ocean (Maiti et al., 2013). The equatorial region (5°N-10°S) is considered separately as it has the largest East-West gradients in productivity, opal%, and in bottom water age (Fig. 4). The northern (55°N-5°N) and southern (10°S-60°S) hemisphere regions both contain a strong subtropical to subpolar contrast in productivity but differ significantly in mean bottom water age (>500 yrs). We plot samples from the Bering Sea in Fig. 5 for completeness but will not interpret them for reasons mentioned (Sec. 3.1). Finally, we exclude from the correlation analysis any sites shallower than 2 km water

depth (see Fig. S1), sites with analytical uncertainty in $(Pa/Th)_{xs}$ >20%, and sites that are influenced by hydrothermal scavenging (Sec. 3.3).

In Table 1, we show the correlation coefficients between $(Pa/Th)_{xs}$ and NPP, EP, opal%, and bottom water age. We consider first the indices of total particle flux (NPP and EP) and opal scavenging (opal%) for each region and then consider bottom water age in terms of the whole basin.

South of 60°S, correlation between $(Pa/Th)_{xs}$ and NPP or EP is weak to none ($r < 0.15$). Similar results are found using the Maiti et al. (2013) algorithm for EP, developed for the Southern Ocean. The better positive correlation ($r = 0.55$) between $(Pa/Th)_{xs}$ and opal% suggests that opal scavenging is the dominating influence here. In fact total particle flux has been found to be less important than the opal content of particles in determining $(Pa/Th)_{xs}$ in all sectors of the Southern Ocean (Dezileau et al., 2003; Walter et al., 1999; Walter et al., 1997)

Within 10°S-60°S, no correlation is found between EP and $(Pa/Th)_{xs}$ and, surprisingly, with NPP, a medium negative correlation ($r = -0.4$) is found. This is due to the fact that high NPP and EP values are estimated along the subtropical frontal zone (~40-50°S) whereas the observed $(Pa/Th)_{xs}$ along this latitude band is consistently low. This region of the southwest Pacific has very low sedimentation rates (<2 mm kyr^{-1}) (Schmitz et al., 1986). Therefore, it is possible that the surface sediments here are not modern and the reported $(Pa/Th)_{xs}$ values are too low because of uncorrected age decay. If initial $(Pa/Th)_{xs}$ at these high productivity (NPP > 150 gC m^{-2} yr^{-1}, EP > 75 gC m^{-2} yr^{-1}) sites from 40-50°S is assumed to be similar to sites with comparable productivity estimates in the North Pacific (ratios of 0.15-0.2, see Fig. 4B), an age correction of 100-120 kyr is necessary. On the other hand, one could argue that the medium correlation (r =

0.41) between $(Pa/Th)_{xs}$ and opal% within 10°S-60°S suggests a similar decoupling between total particle flux and opal scavenging as was found in the Southern Ocean. Nonetheless, this region has few opal% data (Fig. 4C). This is true generally in the South Pacific subtropical gyre, even in global sediment databases (Seiter et al., 2004). Future sediment surveys in the South Pacific are required to better understand the $(Pa/Th)_{xs}$ distribution there.

In the equatorial (5°N-10°S) Pacific, $(Pa/Th)_{xs}$ ratios are increasingly correlated with NPP ($r = 0.26$), EP ($r = 0.44$) and opal% ($r = 0.64$). This situation may be analogous to that seen in the INOPEX survey (Sec. 3.1) in which opal% shows the highest linear correlation to $(Pa/Th)_{xs}$, and the increase in correlation from NPP to EP is related to the export efficiency of diatoms and/or the mineral ballasting effect of opal found at higher EP. Pichat et al. (2004) found that $(Pa/Th)_{xs}$ was strongly correlated with EP in the eastern equatorial Pacific, interpreted as a clear expression of boundary scavenging. Many cores from the western equatorial Pacific, however, have higher $(Pa/Th)_{xs}$ ratios than would be predicted by the trend with EP found in the east. Authors reporting these results invoked particle composition effects (either opal or MnO_2 scavenging) to explain the western equatorial results.

In the North (55°N-5°N) Pacific, $(Pa/Th)_{xs}$ has a strong correlation with NPP, EP and opal% ($r > 0.65$, Table 1). This makes it difficult to separate the total particle flux and particle composition effects in the North Pacific. In the North Pacific especially, the two mechanisms of enhanced Pa removal (total particle flux and opal scavenging) may combine.

At first glance, it might appear water mass ageing is also hopelessly convolved in the North (and equatorial) Pacific $(Pa/Th)_{xs}$ distribution (Fig. 5C), given the positive correlations between bottom water age north of 10°S (Table 1). However there are two arguments supporting

the view that these correlations are spurious due to the covariance of bottom water age and opal% and to a lesser extent, particle flux.

The youngest bottom water ages in the Pacific are 300-400 years. This indicates the basin is not ventilated entirely from the proximal LCDW source in Southern Ocean but more extended circulation pathways from other sources of deep water such as the North Atlantic contribute to the ventilation (Broecker et al., 1998; Khatiwala et al., 2012). After deep water formation and subsequent large-scale flow, one expects ^{231}Pa to tend toward higher "equilibrium" values most quickly within the first 200-300 years (1-2 residence times) of isolation from ventilation (Gherardi et al., 2010; Rutgers v. d. Loeff and Berger, 1993). Even if the "starting age" of ventilation (northward flow of LCDW) is taken to be ~400 years, the apparent positive relationship between $(Pa/Th)_{xs}$ and water mass age only begins 600 years later (Fig. 5C), in the Northern Hemisphere. There is a lack of sensitivity to water mass age in the first few hundred years since perturbation by ventilation, precisely when the greatest effect is expected.

Second, south of 10°S, $(Pa/Th)_{xs}$ ratios are anti-correlated ($r = -0.46$) with bottom water age, opposing the expected influence of water mass ageing. In addition to ventilation, some authors have argued that deep water ^{231}Pa/^{230}Th ratios are perturbed (made lower) across the Southern Ocean because of intense Pa-scavenging by opal. Dissolved ^{231}Pa/^{230}Th is then expected to increase with subsequent ageing of northward flowing water masses (Negre et al., 2010; Thomas et al., 2006). While our mapping efforts (Fig. 3) clearly indicate the Southern Ocean as a large-scale sink of Pa, most likely due to opal scavenging, no measurable depletion of seawater ^{231}Pa has been found along isopycnals across the Antarctic Polar Front in the Pacific (Chase et al., 2003b). The enhanced uptake of Pa in the Southern Ocean must be balanced by Pa

supply by eddy diffusion with the South Pacific gyre and/or the southward advection of NPDW. Therefore deep water $^{231}Pa/^{230}Th$ in the Southern Ocean does not appear to be "re-set" by opal scavenging.

The positive correlations with water mass age most likely results from covariance of water mass age with opal% and particle flux in the east-west sense in the equatorial Pacific and in the subtropical-subarctic sense in the North Pacific. One exception in that covariance is with total particle flux indices (NPP and EP) in the northwest subarctic Pacific where NPP and EP decline in the northward direction from local maxima along ~40°N while $(Pa/Th)_{xs}$ and opal% remain high or continue to increase toward the continental margin in the north.

3.2.1 Geographic variation in seawater $^{231}Pa/^{230}Th$ and fractionation factors

When assuming a steady-state removal of Pa and Th to the sediments on the basin scale, one loses some detail in how the two elements become spatially fractionated in the water column. Water column Pa/Th distributions will be of great use in distinguishing the removal mechanisms discussed above. For instance, boundary scavenging and water mass ageing influence both the dissolved and particulate radionuclide phases whereas particle composition effects can cause a change in particle/sediment $(Pa/Th)_{xs}$ without a change in the dissolved phase. Unfortunately at present the available data on water column $^{231}Pa/^{230}Th$ in the Pacific is sparse.

We have compiled the available data on bottom water (within 500 m of the seafloor) $^{231}Pa/^{230}Th$ ratio (dissolved or total, dissolved plus particulate) from the Pacific (Fig. 6A), a subset of which can be used in conjunction with the surface sediment database to calculate fractionation factors (Fig. 6B). This includes the INOPEX sites for which fractionation factors are reported for the first time. Where total ^{231}Pa and ^{230}Th concentrations were used to estimate

F, minor corrections for the particulate phase (18% of total for Th (Roy-Barman et al., 1996) and 4% for Pa (Nozaki et al., 1998)) were made following the method described by Hayes et al. (2013). The range in observed seawater $^{231}Pa/^{230}Th$ activity ratio is between 0.2 and 0.6, with some tendency for the higher ratios to be associated with the areas of higher productivity and/or opal flux along the equator, the northwestern North Pacific and the Antarctic polar front. The range in observed fractionation factors is roughly 1 to 10. Higher values are associated with the opal-poor regions of the (sub)tropical Pacific and low values are associated with the opal-rich (sub)polar regions. At least in this sparse survey, the relative range in $(Pa/Th)_{xs}$ is larger than that of the dissolved ratio. Therefore, variable fractionation during scavenging must play a significant role in determining the sedimentary $(Pa/Th)_{xs}$ across the Pacific.

3.3 $(Pa/Th)_{xs}$ across biogeochemical provinces and hydrothermal scavenging of Pa

In a basin-wide sense, while our correlation analysis indicates opal scavenging as the most robust influence on surface sediment $(Pa/Th)_{xs}$ ratios, this analysis has excluded the findings in the Pacific of enhanced ^{231}Pa scavenging by MnO_2 associated with hydrothermal activity (Frank et al., 1994; Kadko, 1980; Lao et al., 1992b; Shimmield and Price, 1988; Walter et al., 1999). This effect is expressed in $(Pa/Th)_{xs}$ ratios above 0.093 along or near the East Pacific Rise (EPR), markedly between 10-20°S where one expects a deficit of Pa, as observed in the rest of the South Pacific subtropical gyre, due to very low productivity (and opal%, assumedly, Fig. 4, (Seiter et al., 2004)). One might expect similar scavenging of Pa along the length of the EPR, the Pacific-Antarctic Ridge, the Chile Rise, the Galapagos Rift, and the Juan de Fuca Ridge (all roughly indicated by the 3.5 km isobar in Fig. 3). Additionally, particles in neutrally buoyant plumes originating from vent sites may reach up to 100 km off-axis away from

the vent sites (German et al., 2002). Therefore hydrothermal scavenging is potentially a wide-spread sink for Pa throughout the deep Pacific (Hayes et al., 2013). Indeed, new observations from the Atlantic (Chapter 4) indicate that hydrothermal scavenging and near-bottom scavenging processes in general can have "downstream" impacts on dissolved $^{231}Pa/^{230}Th$ distributions up to 100's of km away the site of local scavenging.

Since hydrothermal formation of authigenic MnO_2 is unrelated to the overlaying biological productivity, hydrothermal Pa scavenging confounds the linkage between ^{231}Pa removal and biogeographic contrast. Studies also report enhanced scavenging of ^{231}Pa due to diagenetic MnO_2 formed in the sediments near the North American continental margin due to high organic matter inputs and redox cycling (Anderson et al., 1983a; Lao et al., 1993; Lao et al., 1992b; Shimmield et al., 1986); in this case, however, the total particle flux and particle composition removal mechanisms combine to enhance Pa scavenging as was found with the covariation of opal% and productivity indices in the North Pacific.

To quantify the redistribution of ^{231}Pa throughout the Pacific, we extrapolate the observed $(Pa/Th)_{xs}$ survey within 16 defined biogeographic provinces (Fig. 7, Table 2) (Longhurst, 2006). We make the assumption that the strongest contrasts in total particle flux, opal scavenging, and diagenetic MnO_2 (and therefore the contrasts in Pa removal) occur across these province boundaries. Each province was assigned the mean and standard deviation of the average $(Pa/Th)_{xs}$ for all sites within the province boundaries (Table 2). We do not extrapolate to the Archipelagic Deep Basins, the Tasman Sea, or the New Zealand Coastal provinces (ARCH, TASM, and NEWZ in Fig. 3, 7) because these provinces are very shallow and/or not represented by any $(Pa/Th)_{xs}$ data. We altered the Kuroshio Current province (KURO) to only include area

east of Japan. The Austral Polar, Antarctic, and Subantarctic provinces (APLR, ANTA, SANT) are artificially confined between 70°W in the east and 120°E in the west (for which the South Subtropical Convergence, SSTC is also artificially confined) in our calculations.

By assuming the flux of ^{230}Th to the sediments is everywhere equal, the extrapolated map can be interpreted as displaying variation in ^{231}Pa flux, or removal, to the sediments (see also Fig S3). Using the related assumption of each province having a similar mean depth (roughly true since only deep provinces are used in this analysis), the sum of each province's $(Pa/Th)_{xs}$ ratio, $(Pa/Th)_{xs,i}$, weighted by each its fractional contribution to the total surface area, $f(SA)_i$ should equal the production ratio, 0.093, assuming steady-state for the Pacific radionuclide budget (Eq. 1).

$$Production\ ratio\ (0.093) = \sum_i \left(\frac{Pa}{Th}\right)_{xs,i} * f(SA)_i \qquad \text{Eq. 1}$$

The total surface area-weighted $(Pa/Th)_{xs}$ ratio in Pacific sediments by this analysis is 0.087 ± 0.003, slightly below the production ratio. In Table 2, we also calculate the percentage of Pa removed in each province relative to the total Pa produced in the Pacific, f(Pa removed), again assuming a basin-wide (Pa/Th) production ratio of 0.093. This parameter allows us to quantify relative enhancement of Pa removal for various provinces. For instance, the combined provinces PSAW, PSAE, CCAL, KURO, CHIL, PEQD, APLR and ANTA represent 23% of the surface area of the Pacific considered but they are responsible for 32% of the Pa removal (see Table 2 for province names). The remaining Pacific: NPSW, NPTG, PNEC, WARM, SPSG, SSTC, and NPPF, thus represents 77% of the surface area but only 62% of the Pa removal. While we have assumed a uniform removal flux of ^{230}Th, modeling efforts (Henderson et al., 1999) and sediment trap studies (Yu et al., 2001) estimate that up to 30% of the production of

^{230}Th is redistributed into the same high productivity areas that serve as preferentials sinks for ^{231}Pa. This implies that the contrast in Pa removal is most likely greater than calculated above. Nonetheless, in our calculated budget, roughly 6% of the Pacific's Pa production is left unaccounted for.

Perhaps the large areas of the EPR which have yet to be mapped in terms of $(Pa/Th)_{xs}$, in particular in the SPSG (see Fig. 3), could make up for this difference via hydrothermal scavenging of Pa. Two alternative scenarios for the apparent imbalance of Pa budget are (1) the result of undersampling the continental margins, particularly of Antarctica, where very high $(Pa/Th)_{xs}$ ratios may be found or (2) the subtropical provinces underestimate the true modern $(Pa/Th)_{xs}$ because of unaccounted-for age-decay. With regard to (1), the coastal provinces represent small fractional surface areas (and shallower water depths, representing a very small fractional Pacific volume), making it difficult to change the basin-wide average by this explanation. The subtropical provinces, however, represent large fractional surface areas and the Pa budget is much more sensitive to the average ratios used there. Similarly, the contribution of hydrothermal scavenging, if it exists, is most likely in the South Pacific where the largest area of hydrothermal ridge systems are found (see Fig. 3). In the North Pacific therefore, we are most confident in attributing the redistribution of Pa to biogeographic constrast.

3.4 Paleo-mapping of biogeographic province contrast

Given these findings, how should variation in past Pacific $(Pa/Th)_{xs}$ ratios be interpreted? In a record from a single site, independent evidence of variation in total particle flux, changes in particle composition, or changes in deep water ventillation must be sought in order to ascribe changes in $(Pa/Th)_{xs}$ to a specific process. Alternatively, mapping the spatial distribution of

$(Pa/Th)_{xs}$ ratios in the past provides the context to interpret the large-scale redistribution of Pa. In the modern Pacific, the influence of deep water circulation was generally found to be overridden by scavenging effects, and the deep Pacific is believed to have remained weakly ventilated since at least the last glacial maximum (Bradtmiller et al., 2010; Jaccard and Galbraith, 2013; Jaccard et al., 2009; Keigwin, 1987; Lund et al., 2011). The mid-ocean ridge system may have remained a large-scale sink for Pa throughout the Pleistocene in the South Pacific (e.g., Frank et al., 1994). By contrast in the North Pacific we can attribute past redistribution of Pa as primarily due to provincial contrast in diatom productivity (opal scavenging), and to a lesser extent total particle flux and diagenetic MnO_2 scavenging (which coincide with regions of high opal scavenging in the North Pacific).

In particular, paleo-mapping across the North Pacific subtropics (NPSW and NPTG) and in the high productivity and upwelling provinces in the subarctic (KURO, PSAW, PSAE, and CCAL) would be of interest to monitor any change in the intensity of biogeographic contrast between the provinces or in the location of the province boundaries themselves. This knowledge can be further related to the physical forcings (atmospheric circulation, oceanic fronts and nutrient supply to surface waters) which define the provinces and is therefore valuable information for paleoclimate studies. Despite the confounding influence of hydrothermal scavenging, the modern South Pacific and Pacific sector of the Southern Ocean displayed the most robust sensitvity to opal% in our analysis. Therefore, the $(Pa/Th)_{xs}$ contrast between the equatorial provinces (PNEC and PEQD) and the surrounding subtropical provinces, between the South Pacific Subtropical Gyre and the Peru-Chile upwelling province, and between the Subantarctic and Antarctic provinces may be very sensitive to regional changes in diatom

productivity in the past. Unfortunately, in all of these potential applications the subtropical regions will be more difficult to characterize on millenial-scale time slices as their slow sedimentation rates limit temporal resolution.

To illustrate the potential of this technique, we compiled the available data for $(Pa/Th)_{xs}$ from cores, including SO202-07-6 (51°16'N, 167°42'E, Serno et al., unpublished), that have dated sections of the last glacial maximum (19-24 ka) (Fig. 8) (Berelson et al., 1997; Bradtmiller et al., 2006; Bradtmiller et al., 2009; Chase et al., 2003a; Frank et al., 1994; Lao et al., 1992a; Pichat et al., 2004; Shimmield et al., 1986; Yang et al., 1995). For cores with multiple data in this age range, an average $(Pa/Th)_{xs}$ was taken.

This follows the work of Lao et al. (1992a) who invoked reduced boundary scavenging in glacial times, largely based on lower $(Pa/Th)_{xs}$ ratios (with respect to modern) in cores off the coast of Oregon and Peru and slightly higher than modern $(Pa/Th)_{xs}$ ratios in some interior Pacific sites. Lao et al. (1992a) suggested that higher fluxes of lithogenic particles throughout the glacial Pacific reduced the ocean residence time of Pa enough that its lateral redistribution by dispersion was reduced. Glacial $(Pa/Th)_{xs}$ ratios well above the production ratio published subsequently from large regions of the Southern Ocean (Bradtmiller et al., 2009; Chase et al., 2003a), the equatorial Pacific (Bradtmiller et al., 2006; Yang et al., 1995), the EPR (Frank et al., 1994), and one new core from the subarctic (Serno et al, unpublished) suggest that Pa was redistributed laterally across the basin in a similar sense to today, although perhaps to a lesser extent than in the modern ocean as Lao et al. (1992a) concluded. Future mapping of the poorly represented glacial subarctic Pacific could evaluate the hypothesis that the three modern regions of enhanced Pa removal persisted in the glacial ocean. This in turn could support the hypothesis

that a similar biogeographic contrast in diatom productivity and particle flux existed and that the locations of the associated major ocean fronts were similar to today.

4. Conclusions

New surface sediment $(Pa/Th)_{xs}$ data from the subarctic Pacific display a clear sensitivity to opal scavenging. A Pacific-wide compilation of sedimentary $(Pa/Th)_{xs}$ data is also consistent with enhanced removal of Pa due to opal scavenging. Scavenging of ^{231}Pa is additionally sensitive to the total particle flux and the abundance of particulate MnO_2. The influence of deep water ventillation associated with the Pacific overturning circulation appears to be outweighed by opal scavenging and boundary scavenging effects. We offer the concept of biogeography to estimate a Pa removal budget for the Pacific, but note that hydrothermal scavenging may be accounted for insufficiently in this approach. Past changes in the position of the oceanic fronts separating biogeographic provinces may be reconstructed through regional or basin-wide paleo-mapping of $(Pa/Th)_{xs}$ distributions.

Acknowledgements

We acknowledge the German Ministry of Education and Research (BmBF) and the U. S. National Science Foundation (award 1029211) for funding. Thanks go to the crew of the R/V *Sonne*, the INOPEX participants, Samar Khatiwala for providing the estimates of mean age and to Jerry McManus and Leo Peña for comments.

References

Alvain, S., Moulin, C., Dandonneau, Y., Loisel, H., 2008. Seasonal distribution and succession of dominant phytoplankton groups in the global ocean: A satellite view. Global Biogeochem. Cycles 22, GB3001.

Andersen, M.B., Stirling, C.H., Zimmermann, B., Halliday, A.N., 2010. Precise determination of the open ocean $^{234}U/^{238}U$ composition. Geochem. Geophys. Geosyst. 11, Q12003.

Anderson, R.F., 2002. Radionuclides from GoFlo water bottle samples. Woods Hole Oceanographic Institution: United States JGOFS Data Server http://usjgofs.whoi.edu/jg/serv/jgofs/eqpac/tt013/rad_GoFlo.html0.

Anderson, R.F., Bacon, M.P., Brewer, P.G., 1983a. Removal of ^{230}Th and ^{231}Pa at ocean margins. Earth Planet. Sci. Lett. 66, 73-90.

Anderson, R.F., Bacon, M.P., Brewer, P.G., 1983b. Removal of ^{230}Th and ^{231}Pa from the open ocean. Earth Planet. Sci. Lett. 62, 7-23.

Anderson, R.F., Fleisher, M.Q., Robinson, L.F., Edwards, R.L., Hoff, J., Moran, S.B., Rutgers van der Loeff, M.M., Thomas, A.L., Roy-Barman, M., François, R., 2012. GEOTRACES intercalibration of ^{230}Th, ^{232}Th, ^{231}Pa, and prospects for ^{10}Be. Limnol. Oceanogr. Methods 10, 179-213.

Anderson, R.F., Lao, Y., Broecker, W.S., Trumbore, S.E., Hofmann, H.J., Wolfli, W., 1990. Boundary scavenging in the Pacific Ocean: a comparison of ^{10}Be and ^{231}Pa. Earth Planet. Sci. Lett. 96, 287-304.

Bacon, M.P., 1988. Tracers of chemical scavenging in the ocean: boundary effects and large-scale chemical fractionation. Philos. Trans. R. Soc. London, Ser. A 325, 147-160.

Bacon, M.P., Anderson, R.F., 1982. Distribution of thorium isotopes between dissolved and particulate forms in the deep sea. J. Geophys. Res. 87, 2045-2056.

Bacon, M.P., Spencer, D.W., Brewer, P.G., 1976. ^{210}Pb/^{226}Ra and ^{210}Po/^{210}Pb disequilibria in seawater and suspended particulate matter. Earth Planet. Sci. Lett. 32, 277-296.

Behrenfeld, M.J., Falkowski, P.G., 1997. Photosynthetic rates derived from satellite-based chlorophyll concentration. Limnol. Oceanogr. 42, 1-20.

Berelson, W.M., Anderson, R.F., Dymond, J., Demaster, D., Hammond, D.E., Collier, R., Honjo, S., Leinen, M., McManus, J., Pope, R., Smith, C., Stephens, M., 1997. Biogenic budgets of particle rain, benthic remineralization and sediment accumulation in the equatorial Pacific. Deep Sea Res. Pt. II 44, 2251-2282.

Berger, W.H., Winterer, E.L., 1974. Plate stratigraphy and the fluctuating carbonate line, in: Hsu, K.J., Jenkins, H.C. (Eds.), Pelagic Sediments: On Land and under the Sea. Int. Assoc. Sedim., Spec. Publ., pp. 11-48.

Bernat, M., Goldberg, E.D., 1968. Thorium isotopes in the marine environment. Earth Planet. Sci. Lett. 5, 308-312.

Bradtmiller, L.I., Anderson, R.F., Fleisher, M.Q., Burckle, L.H., 2006. Diatom productivity in the equatorial Pacific Ocean from the last glacial period to the present: A test of the silicic acid leakage hypothesis. Paleoceanography 21, PA4201.

Bradtmiller, L.I., Anderson, R.F., Fleisher, M.Q., Burckle, L.H., 2009. Comparing glacial and Holocene opal fluxes in the Pacific sector of the Southern Ocean. Paleoceanography 24, PA2214.

Bradtmiller, L.I., Anderson, R.F., Sachs, J.P., Fleisher, M.Q., 2010. A deeper respired carbon pool in the glacial equatorial Pacific Ocean. Earth Planet. Sci. Lett. 299, 417-425.

Broecker, W.S., Peacock, S.L., Walker, S., Weiss, R., Fahrbach, E., Schroeder, M., Mikolajewicz, U., Heinze, C., Key, R., Peng, T.H., Rubin, S., 1998. How much deep water is formed in the Southern Ocean? J. Geophys. Res. 103, 15833-15843.

Buesseler, K.O., 1998. The decoupling of production and particulate export in the surface ocean. Global Biogeochem. Cycles 12, 297-310.

Chase, Z., 2008. Chapter 11 Sediment Signatures of U- and Th-Series Nuclides and their Application as Paleoceanographic Tracers, in: Krishnaswami, S., Cochran, J.K. (Eds.), Radioactivity in the Environment. Elsevier, pp. 383-416.

Chase, Z., Anderson, R.F., Fleisher, M.Q., Kubik, P.W., 2002. The influence of particle composition and particle flux on scavenging of Th, Pa and Be in the ocean. Earth Planet. Sci. Lett. 204, 215-229.

Chase, Z., Anderson, R.F., Fleisher, M.Q., Kubik, P.W., 2003a. Accumulation of biogenic and lithogenic material in the Pacific sector of the Southern Ocean during the past 40,000 years. Deep Sea Res. Pt. II 50, 799-832.

Chase, Z., Anderson, R.F., Fleisher, M.Q., Kubik, P.W., 2003b. Scavenging of ^{230}Th, ^{231}Pa and ^{10}Be in the Southern Ocean (SW Pacific sector): the importance of particle flux, particle composition and advection. Deep Sea Res. Pt. II 50, 739-768.

Chen, J.H., Lawrence Edwards, R., Wasserburg, G.J., 1986. ^{238}U, ^{234}U and ^{232}Th in seawater. Earth Planet. Sci. Lett. 80, 241-251.

Cheng, H., Edwards, R.L., Hoff, J., Gallup, C.D., Richards, D.A., Asmerom, Y., 2000. The half-lives of uranium-234 and thorium-230. Chem. Geol. 169, 17-33.

Coale, K.H., Bruland, K.W., 1987. Oceanic stratified euphotic zone as elucidated by ^{234}Th:^{238}U disequilibria. Limnol. Oceanogr. 32, 189-200.

Cochran, J.K., Krishnaswami, S., 1980. Radium, thorium, uranium, and ^{210}Pb in deep-sea sediments and sediment pore waters from the North Equatorial Pacific. Am. J. Sci. 280, 849-889.

Cochran, J.K., Livingston, H.D., Hirschberg, D.J., Surprenant, L.D., 1987. Natural and anthropogenic radionuclide distributions in the northwest Atlantic Ocean. Earth Planet. Sci. Lett. 84, 135-152.

DeMaster, D.J., 1979. The marine budgets of silica and ^{32}Si, PhD Dissert. Yale University, New Haven, CT.

Dezileau, L., Bareille, G., Reyss, J.L., 2003. The ^{231}Pa/^{230}Th ratio as a proxy for past changes in opal fluxes in the Indian sector of the Southern Ocean. Mar. Chem. 81, 105-117.

Dutay, J.C., Lacan, F., Roy-Barman, M., Bopp, L., 2009. Influence of particle size and type on ^{231}Pa and ^{230}Th simulation with a global coupled biogeochemical-ocean general circulation model: A first approach. Geochem. Geophys. Geosyst. 10, Q01011.

Emerson, S., Hedges, J.I., 1988. Processes controlling the organic carbon content of open ocean sediments. Paleoceanography 3, 621-634.

Eppley, R.W., Peterson, B.J., 1979. Particulate organic matter flux and planktonic new production in the deep ocean. Nature 282, 677.

Falkowski, P.G., Barber, R.T., Smetacek, V., 1998. Biogeochemical controls and feedbacks on ocean primary production. Science 281, 200-206.

Fleisher, M.Q., Anderson, R.F., 2003. Assessing the collection efficiency of Ross Sea sediment traps using ^{230}Th and ^{231}Pa. Deep Sea Res. Pt. II 50, 693-712.

François, R., 2007. Paleoflux and Paleocirculation from Sediment ^{230}Th and ^{231}Pa/^{230}Th, in: Hillaire-Marcel, C., de Vernal, A. (Eds.), Developments in Marine Geology. Elsevier, pp. 681-716.

François, R., Frank, M., Rutgers van der Loeff, M.M., Bacon, M.P., 2004. ^{230}Th normalization: An essential tool for interpreting sedimentary fluxes during the late Quaternary. Paleoceanography 19, PA1018.

François, R., Honjo, S., Krishfield, R., Manganini, S., 2002. Factors controlling the flux of organic carbon to the bathypelagic zone of the ocean. Global Biogeochem. Cycles 16, 1087.

Frank, M., Eckhardt, J.-D., Eisenhauer, A., Kubik, P.W., Dittrich-Hannen, B., Segl, M., Mangini, A., 1994. Beryllium-10, thorium-230, and protactinium-231 in Galapagos microplate sediments: Implications of hydrothermal activity and paleoproductivity changes during the last 100,000 years. Paleoceanography 9, 559-578.

Geibert, W., Usbeck, R., 2004. Adsorption of thorium and protactinium onto different particle types: experimental findings. Geochim. Cosmochim. Acta 68, 1489-1501.

German, C.R., Colley, S., Palmer, M.R., Khripounoff, A., Klinkhammer, G.P., 2002. Hydrothermal plume-particle fluxes at 13°N on the East Pacific Rise. Deep Sea Res. Pt. I 49, 1921-1940.

Gersonde, R., 2012. The expedition of the research vessel "Sonne" to the subpolar North Pacific and the Bering Sea in 2009 (SO202-INOPEX). Rep. Polar Mar. Res. 643, 1-323.

Gherardi, J.M., Luo, Y., Francois, R., McManus, J.F., Allen, S.E., Labeyrie, L., 2010. Reply to comment by S. Peacock on "Glacial-interglacial circulation changes inferred from $^{231}Pa/^{230}Th$ sedimentary record in the North Atlantic region". Paleoceanography 25, PA2207.

Guo, L., Chen, M., Gueguen, C., 2002. Control of Pa/Th ratio by particulate chemical composition in the ocean. Geophys. Res. Lett. 29, 1961.

Hayes, C.T., Anderson, R.F., Jaccard, S.L., François, R., Fleisher, M.Q., Soon, M., Gersonde, R., 2013. A new perspective on boundary scavenging in the North Pacific Ocean. Earth Planet. Sci. Lett. 369-370, 86-97.

Henderson, G.M., Anderson, R.F., 2003. The U-series Toolbox for Paleoceanography. Rev. Mineral. Geochem. 52, 493-531.

Henderson, G.M., Heinze, C., Anderson, R.F., Winguth, A.M.E., 1999. Global distribution of the ^{230}Th flux to ocean sediments constrained by GCM modelling. Deep Sea Res. Pt. I 46, 1861-1893.

Honda, M.C., Watanabe, S., 2010. Importance of biogenic opal as ballast of particulate organic carbon (POC) transport and existence of mineral ballast-associated and residual POC in the Western Pacific Subarctic Gyre. Geophys. Res. Lett. 37, L02605.

Honjo, S., Francois, R., Manganini, S., Dymond, J., Collier, R., 2000. Particle fluxes to the interior of the Southern Ocean in the Western Pacific sector along 170°W. Deep Sea Res. Pt. II 47, 3521-3548.

Honjo, S., Manganini, S.J., Krishfield, R.A., Francois, R., 2008. Particulate organic carbon fluxes to the ocean interior and factors controlling the biological pump: A synthesis of global sediment trap programs since 1983. Prog. Oceanogr. 76, 217-285.

Huh, C.-A., Zahnle, D.L., Small, L.F., Noshkin, V.E., 1987. Budgets and behaviors of uranium and thorium series isotopes in Santa Monica Basin sediments. Geochim. Cosmochim. Acta 51, 1743-1754.

Jaccard, S.L., Galbraith, E.D., 2013. Direct ventilation of the North Pacific did not reach the deep ocean during the last deglaciation. Geophys. Res. Lett. 40, 199-203.

Jaccard, S.L., Galbraith, E.D., Sigman, D.M., Haug, G.H., Francois, R., Pedersen, T.F., Dulski, P., Thierstein, H.R., 2009. Subarctic Pacific evidence for a glacial deepening of the oceanic respired carbon pool. Earth Planet. Sci. Lett. 277, 156-165.

Kadko, D., 1980. A detailed study of some uranium series nuclides at an abyssal hill area near the east Pacific Rise at 8°45′N. Earth Planet. Sci. Lett. 51, 115-131.

Kadko, D., 1983. A multitracer approach to the study of erosion in the northeast equatorial Pacific. Earth Planet. Sci. Lett. 63, 13-33.

Kawabe, M., Fujio, S., 2010. Pacific ocean circulation based on observation. J. Oceanogr. 66, 389-403.

Keigwin, L.D., 1987. North Pacific deep water formation during the latest glaciation. Nature 330, 362-364.

Khatiwala, S., Primeau, F., Holzer, M., 2012. Ventilation of the deep ocean constrained with tracer observations and implications for radiocarbon estimates of ideal mean age. Earth Planet. Sci. Lett. 325–326, 116-125.

Kostadinov, T.S., Siegel, D.A., Maritorena, S., 2010. Global variability of phytoplankton functional types from space: assessment via the particle size distribution. Biogeosciences 7, 3239-3257.

Kretschmer, S., Geibert, W., Rutgers v. d, L., Michiel M., Schnabel, C., Xu, S., Mollenhauer, G., 2011. Fractionation of ^{230}Th, ^{231}Pa, and ^{10}Be induced by particle size and composition within an opal-rich sediment of the Atlantic Southern Ocean. Geochim. Cosmochim. Acta 75, 6971-6987.

Ku, T.-L., 1966. Uranium series disequilibrium in deep sea sediments, PhD Dissert. Columbia University, New York, NY.

Kumar, N., Gwiazda, R., Anderson, R.F., Froelich, P.N., 1993. ^{231}Pa/^{230}Th ratios in sediments as a proxy for past changes in Southern Ocean productivity. Nature 362, 45-48.

Lam, P.J., Robinson, L.F., Blusztajn, J., Li, C., Cook, M.S., McManus, J.F., Keigwin, L.D., 2013. Transient stratification as the cause of the North Pacific productivity spike during deglaciation. Nat. Geosci. 6, 622-626.

Lao, Y., Anderson, R.F., Broecker, W.S., 1992a. Boundary scavenging and deep-sea sediment dating: constraints from excess ^{230}Th and ^{231}Pa. Paleoceanography 7, 783-798.

Lao, Y., Anderson, R.F., Broecker, W.S., Hofmann, H.J., Wolfli, W., 1993. Particulate fluxes of ^{230}Th, ^{231}Pa, and ^{10}Be in the northeastern Pacific Ocean. Geochim. Cosmochim. Acta 57, 205-217.

Lao, Y., Anderson, R.F., Broecker, W.S., Trumbore, S.E., Hofmann, H.J., Wolfli, W., 1992b. Transport and burial rates of ^{10}Be and ^{231}Pa in the Pacific Ocean during the Holocene period. Earth Planet. Sci. Lett. 113, 173-189.

Laws, E.A., Falkowski, P.G., Smith, W.O., Jr., Ducklow, H., McCarthy, J.J., 2000. Temperature effects on export production in the open ocean. Global Biogeochem. Cycles 14, 1231-1246.

Locarnini, R.A., Mishonov, A.V., Antonov, J.I., Boyer, T.P., Garcia, H.E., Baranova, O.K., Zweng, M.M., Johnson, D.R., 2010. World Ocean Atlas 2009, Volume 1: Temperature. U. S. Government Printing Office, Washington, D. C.

Longhurst, A., 2006. Ecological Geography of the Sea, 2nd ed. Academic Press, San Diego.

Lund, D.C., Mix, A.C., Southon, J., 2011. Increased ventilation age of the deep northeast Pacific Ocean during the last deglaciation. Nature Geosci. 4, 771-774.

Luo, S., Ku, T.-L., 1999. Oceanic $^{231}Pa/^{230}Th$ ratio influenced by particle composition and remineralization. Earth Planet. Sci. Lett. 167, 183-195.

Luo, Y., Francois, R., Allen, S.E., 2012. The influence of deep water circulation on the distribution of ^{231}Pa and ^{230}Th in the water column and sediments of the Pacific Ocean. Mineral. Mag. 75, 2042.

Macdonald, A.M., Mecking, S., Robbins, P.E., Toole, J.M., Johnson, G.C., Talley, L., Cook, M., Wijffels, S.E., 2009. The WOCE-era 3-D Pacific Ocean circulation and heat budget. Prog. Oceanogr. 82, 281-325.

Maiti, K., Charette, M.A., Buesseler, K.O., Kahru, M., 2013. An inverse relationship between production and export efficiency in the Southern Ocean. Geophys. Res. Lett. 40, 1557-1561.

Mangini, A., Kühnel, U., 1987. Depositional history in the Clarion-Clipperton zone during the last 250,000 years–^{230}Th and ^{231}Pa methods. Geol. Jahrb. D 87, 105-121.

Marchal, O., François, R., Stocker, T.F., Joos, F., 2000. Ocean thermohaline circulation and sedimentary $^{231}Pa/^{230}Th$ ratio. Paleoceanography 15, 625-641.

Matsumoto, K., 2007. Radiocarbon-based circulation age of the world oceans. J. Geophys. Res. 112, C09004.

Mohamed, C.A.R., Narita, H., Harada, K., Tsunogai, S., 1996. Sedimentation of natural radionuclides on the seabed across the northern Japan Trench. Geochem. J. 30, 217-229.

Mohamed, C.A.R., Tsunogai, S., 1998. ^{231}Pa in hemipelagic sediments: Is it affected by boundary scavenging? Geochem. J. 32, 11-20.

Moran, S.B., Charette, M.A., Hoff, J.A., Edwards, R.L., Landing, W.M., 1997. Distribution of ^{230}Th in the Labrador Sea and its relation to ventilation. Earth Planet. Sci. Lett. 150, 151-160.

Moran, S.B., Hoff, J.A., Buesseler, K.O., Edwards, R.L., 1995. High precision ^{230}Th and ^{232}Th in the Norwegian Sea and Denmark by thermal ionization mass spectrometry. Geophys. Res. Lett. 22, 2589-2592.

Moran, S.B., Shen, C., C, Weinstein, S.E., Hettinger, L.H., Hoff, J.H., Edmonds, H.N., Edwards, R.L., 2001. Constraints on deep water age and particle flux in the equatorial and South Atlantic Ocean based on seawater ^{231}Pa and ^{230}Th data. Geophys. Res. Lett. 28, 3437-3440.

Moran, S.B., Shen, C.C., Edmonds, H.N., Weinstein, S.E., Smith, J.N., Edwards, R.L., 2002. Dissolved and particulate ^{231}Pa and ^{230}Th in the Atlantic Ocean: constraints on intermediate/deep water age, boundary scavenging, and ^{231}Pa/^{230}Th fractionation. Earth Planet. Sci. Lett. 203, 999-1014.

Mortlock, R.A., Froelich, P.N., 1989. A simple method for the rapid determination of biogenic opal in pelagic marine sediments. Deep Sea Res. Pt. A 36, 1415-1426.

Müller, P.J., Mangini, A., 1980. Organic carbon decomposition rates in sediments of the pacific manganese nodule belt dated by ^{230}Th and ^{231}Pa. Earth Planet. Sci. Lett. 51, 94-114.

Narita, H., Abe, R., Tate, K., Kim, Y.-I., Harada, K., Tsunogai, S., 2003. Anomalous Large Scavenging of ^{230}Th and ^{231}Pa Controlled by Particle Composition in the Northwestern North Pacific. J. Oceanogr. 59, 739-750.

Negre, C., Zahn, R., Thomas, A.L., Masqué, P., Henderson, G., Martinez-Mendez, G., Hall, I.R., Mas, J.L., 2010. Reversed flow of Atlantic deep water during the Last Glacial Maximum. Nature 468, 84-88.

Nelson, D.M., Tréguer, P., Brzezinski, M.A., Leynaert, A., Quéguiner, B., 1995. Production and dissolution of biogenic silica in the ocean: Revised global estimates, comparison with regional data and relationship to biogenic sedimentation. Global Biogeochem. Cycles 9, 359-372.

Nozaki, Y., Horibe, Y., Tsubota, H., 1981. The water column distributions of thorium isotopes in the western North Pacific. Earth Planet. Sci. Lett. 54, 203-216.

Nozaki, Y., Nakanishi, T., 1985. ^{231}Pa and ^{230}Th profiles in the open ocean water column. Deep-Sea Res. Pt. A 32, 1209-1220.

Nozaki, Y., Yamada, M., Nakanishi, T., Nagaya, Y., Nakamura, K., Shitashima, K., Tsubota, H., 1998. The distribution of radionuclides and some trace metals in the water columns of the Japan and Bonin trenches. Oceanol. Acta 21, 469-484.

Nozaki, Y., Yang, H.-S., 1987. Th and Pa isotopes in the waters of the western margin of the pacific near Japan: Evidence for release of ^{228}Ra and ^{227}Ac from slope sediments. J. Oceanogr. 43, 217-227.

Pichat, S., Sims, K.W.W., François, R., McManus, J.F., Brown Leger, S., Albarède, F., 2004. Lower export production during glacial periods in the equatorial Pacific derived from $(^{231}Pa/^{230}Th)_{xs,0}$ measurements in deep-sea sediments. Paleoceanography 19, PA4023.

Robert, J., Miranda, C.F., Muxart, R., 1969. Mesure de la periode du protactinium-231 par microcalorimetrie. Radiochim. Acta 11, 104-108.

Roy-Barman, M., Chen, J.H., Wasserburg, G.J., 1996. ^{230}Th-^{232}Th systematics in the central Pacific Ocean: The sources and the fates of thorium. Earth Planet. Sci. Lett. 139, 351-363.

Rutgers v. d. Loeff, M., Berger, G.W., 1993. Scavenging of ^{230}Th and ^{231}Pa near the Antarctic polar front in the South Atlantic. Deep Sea Res. Pt. I 40, 339-357.

Ryther, J.H., 1969. Photosynthesis and Fish Production in the Sea. Science 166, 72-76.

Sayles, F.L., Martin, W.R., Chase, Z., Anderson, R.F., 2001. Benthic remineralization and burial of biogenic SiO2, CaCO3, organic carbon, and detrital material in the Southern Ocean along a transect at 170° West. Deep Sea Res. Pt. II 48, 4323-4383.

Schlosser, P., Bullister, J.L., Fine, R., Jenkins, W.J., Key, R., Roether, W., Smethie, W.M., 2001. Transformation and age of water masses, in: Siedler, G., Church, J., Gould, J.J. (Eds.), Ocean circulation & climate observation and modeling of the global ocean. Academic Press, San Diego, pp. 428-452.

Schmitz, W., Mangini, A., Stoffers, P., Glasby, G.P., Plüger, W.L., 1986. Sediment accumulation rates in the southwestern Pacific Basin and Aitutaki Passage. Mar. Geol. 73, 181-190.

Scholten, J.C., Fietzke, J., Mangini, A., Stoffers, P., Rixen, T., Gaye-Haake, B., Blanz, T., Ramaswamy, V., Sirocko, F., Schulz, H., Ittekkot, V., 2005. Radionuclide fluxes in the Arabian Sea: the role of particle composition. Earth Planet. Sci. Lett. 230, 319-337.

Seiter, K., Hensen, C., Schröter, J., Zabel, M., 2004. Organic carbon content in surface sediments—defining regional provinces. Deep Sea Res. Pt. I 51, 2001-2026.

Serno, S., Winckler, G., Anderson, R.F., Hayes, C.T., McGee, D., Machalett, B., Ren, H., Straub, S.M., Gersonde, R., Haug, G.H., in revision. Eolian dust input to the Subarctic North Pacific. Earth Planet. Sci. Lett.

Shimmield, G.B., Murray, J.W., Thomson, J., Bacon, M.P., Anderson, R.F., Price, N.B., 1986. The distribution and behaviour of ^{230}Th and ^{231}Pa at an ocean margin, Baja California, Mexico. Geochim. Cosmochim. Acta 50, 2499-2507.

Shimmield, G.B., Price, N.B., 1988. The scavenging of U, ^{230}Th and ^{231}Pa during pulsed hydrothermal activity at 20°S, East Pacific Rise. Geochim. Cosmochim. Acta 52, 669-677.

Siddall, M., Henderson, G.M., Edwards, N.R., Frank, M., Müller, S.A., Stocker, T.F., Joos, F., 2005. ^{231}Pa/^{230}Th fractionation by ocean transport, biogenic particle flux and particle type. Earth and Planet. Sci. Lett. 237, 135-155.

Spencer, D.W., Bacon, M.P., Brewer, P.G., 1981. Models of the distribution of ^{210}Pb in a section across the North Equatorial Atlantic Ocean. J. Mar. Res. 39, 119-138.

Taguchi, K., Harada, K., Tsunogai, S., 1989. Particulate removal of ^{230}Th and ^{231}Pa in the biologically productive northern North Pacific. Earth Planet. Sci. Lett. 93, 223-232.

Taguchi, K., Narita, H., 1995. ^{230}Th and ^{231}Pa distributions in surface sediments off Enshunada, Japan, in: Sakai, H., Nozaki, Y. (Eds.), Biogeochemical Processes and Ocean Flux in the Western Pacific. TERRAPUB, Tokyo, pp. 375-382.

Talley, L.D., Reid, J.L., Robbins, P.E., 2003. Data-Based Meridional Overturning Streamfunctions for the Global Ocean. J. Clim. 16, 3213-3226.

Thomas, A.L., Henderson, G.M., Robinson, L.F., 2006. Interpretation of the ^{231}Pa/^{230}Th paleocirculation proxy: New water-column measurements from the southwest Indian Ocean. Earth Planet. Sci. Lett. 241, 493-504.

Venchiarutti, C., Roy-Barman, M., Freydier, R., van Beek, P., Souhaut, M., Jeandel, C., 2011a. Influence of intense scavenging on Pa-Th fractionation in the wake of Kerguelen Island (Southern Ocean). Biogeosciences 8, 3187-3201.

Venchiarutti, C., van der Loeff, M.R., Stimac, I., 2011b. Scavenging of ^{231}Pa and thorium isotopes based on dissolved and size-fractionated particulate distributions at Drake Passage (ANTXXIV-3). Deep Sea Res. Pt. II 58, 2767-2784.

Vogler, S., Scholten, J., Rutgers van der Loeff, M., Mangini, A., 1998. ^{230}Th in the eastern North Atlantic: the importance of water mass ventilation in the balance of ^{230}Th. Earth Planet. Sci. Letters 156, 61-74.

Walter, H.-J., Rutgers v. d. Loeff, M.M., Francois, R., 1999. Reliability of the ^{231}Pa/^{230}Th Activity Ratio as a Tracer for Bioproductivity of the Ocean, in: Fischer, W., Wefer, G. (Eds.), Use of Proxies in Paleoceanography: Examples for the South Atlantic. Springer-Verlag, Berlin, pp. 393-408.

Walter, H.J., Geibert, W., Rutgers van der Loeff, M.M., Fischer, G., Bathmann, U., 2001. Shallow vs. deep-water scavenging of ^{231}Pa and ^{230}Th in radionuclide enriched waters of the Atlantic sector of the Southern Ocean. Deep Sea Res. Pt. I 48, 471-493.

Walter, H.J., Rutgers van der Loeff, M.M., Hoeltzen, H., 1997. Enhanced scavenging of ^{231}Pa relative to ^{230}Th in the South Atlantic south of the Polar Front: Implications for the use of the ^{231}Pa/^{230}Th ratio as a paleoproductivity proxy. Earth Planet. Sci. Lett. 149, 85-100.

Weyer, S., Anbar, A.D., Gerdes, A., Gordon, G.W., Algeo, T.J., Boyle, E.A., 2008. Natural fractionation of ^{238}U/^{235}U. Geochim. Cosmochim. Acta 72, 345-359.

Yang, H.-S., Nozaki, Y., Sakai, H., Masuda, A., 1986. The distribution of ^{230}Th and ^{231}Pa in the deep-sea surface sediments of the Pacific Ocean. Geochim. Cosmochim. Acta 50, 81-89.

Yang, Y.-L., Elderfield, H., Pedersen, T.F., Ivanovich, M., 1995. Geochemical record of the Panama basin during the last glacial maximum carbon event shows that the glacial ocean was not suboxic. Geology 23, 1115-1118.

Yu, E.-F., Francois, R., Bacon, M.P., 1996. Similar rates of modern and last-glacial ocean thermohaline circulation inferred from radiochemical data. Nature 379, 689-694.

Yu, E.-F., Francois, R., Bacon, M.P., Fleer, A.P., 2001. Fluxes of ^{230}Th and ^{231}Pa to the deep sea: implications for the interpretation of excess ^{230}Th and ^{231}Pa/^{230}Th profiles in sediments. Earth Planet. Sci. Lett. 191, 219-230.

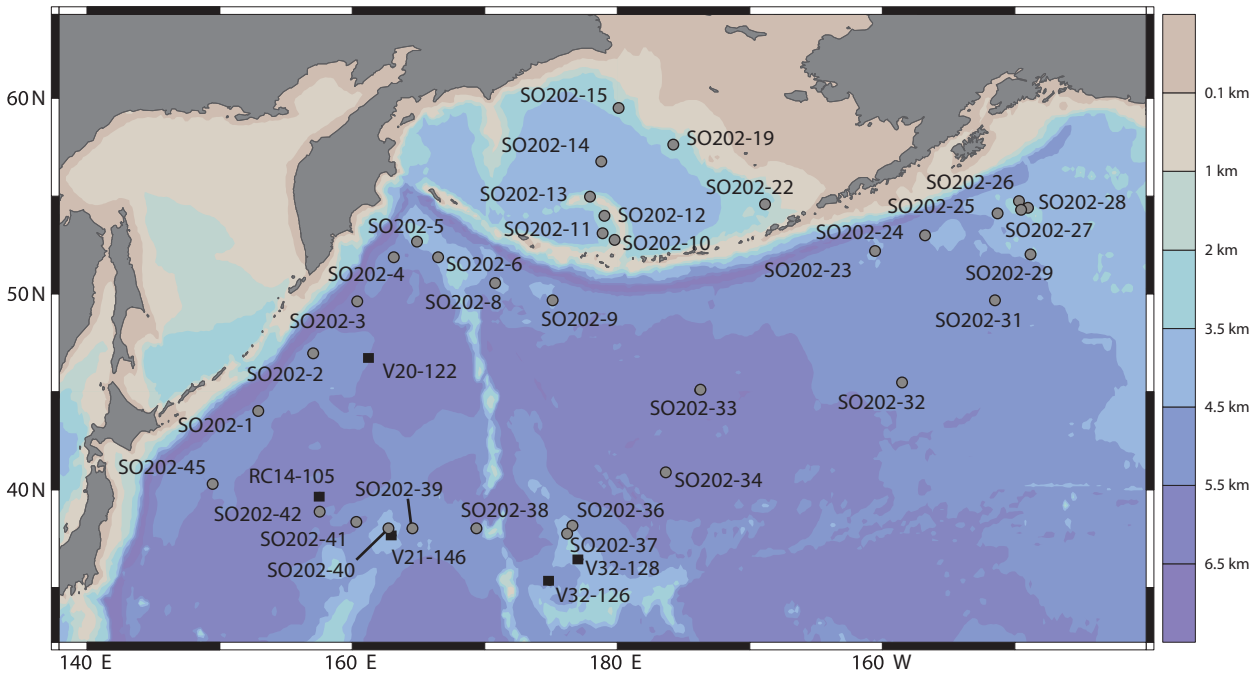

Figure 1. Map of coring sites for which new $(Pa/Th)_{xs}$ and/or opal% data are presented here. SO202 cores (gray circles) are from the INOPEX cruise (Gersonde, 2012). Radionuclide data for Vema (V) and Conrad (RC) cores (black squares) have been previously published (Lao et al., 1992b). The scheme of bathymetric shading is displayed on the right.

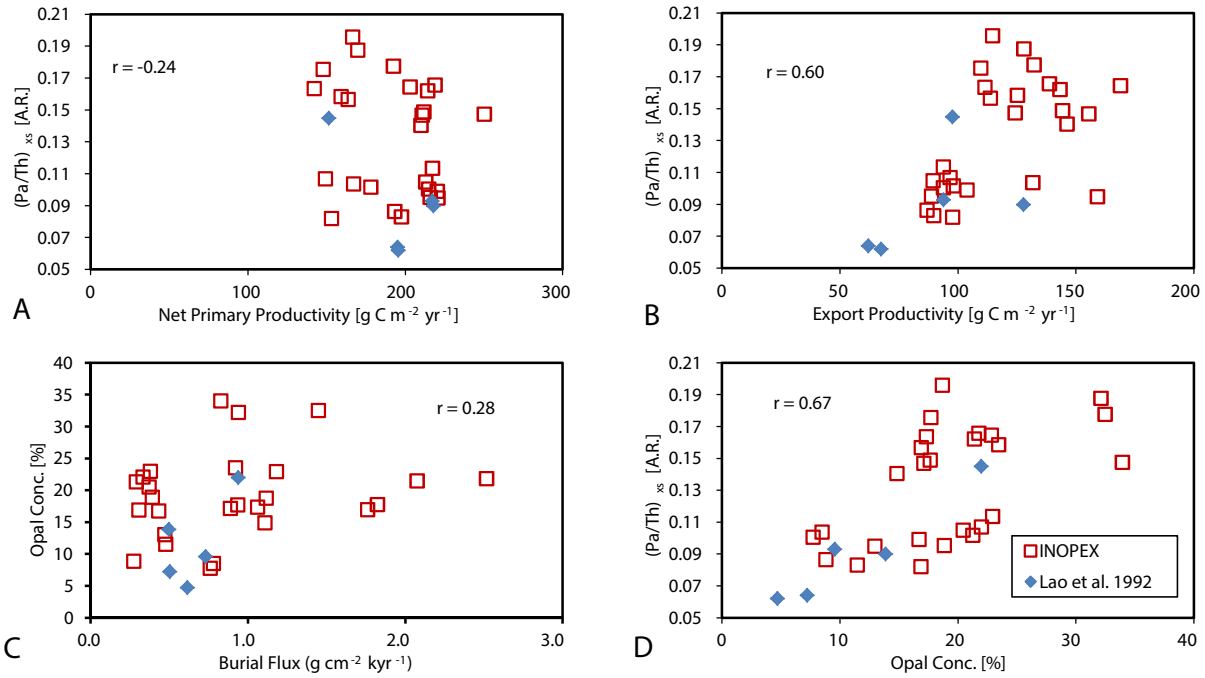

Figure 2. $(Pa/Th)_{xs}$ results from 31 coretops from the subarctic Pacific (see Fig. 1), excluding sites from the Bering Sea and SO202-26, versus (A) net primary productivity, (B) export productivity and (D) opal concentration. (C) shows the relationship between opal% and ^{230}Th-normalized total mass burial flux. Error bars are equal to or smaller than the symbol size. Reported in the insets is the Pearson linear correlation coefficient, r.

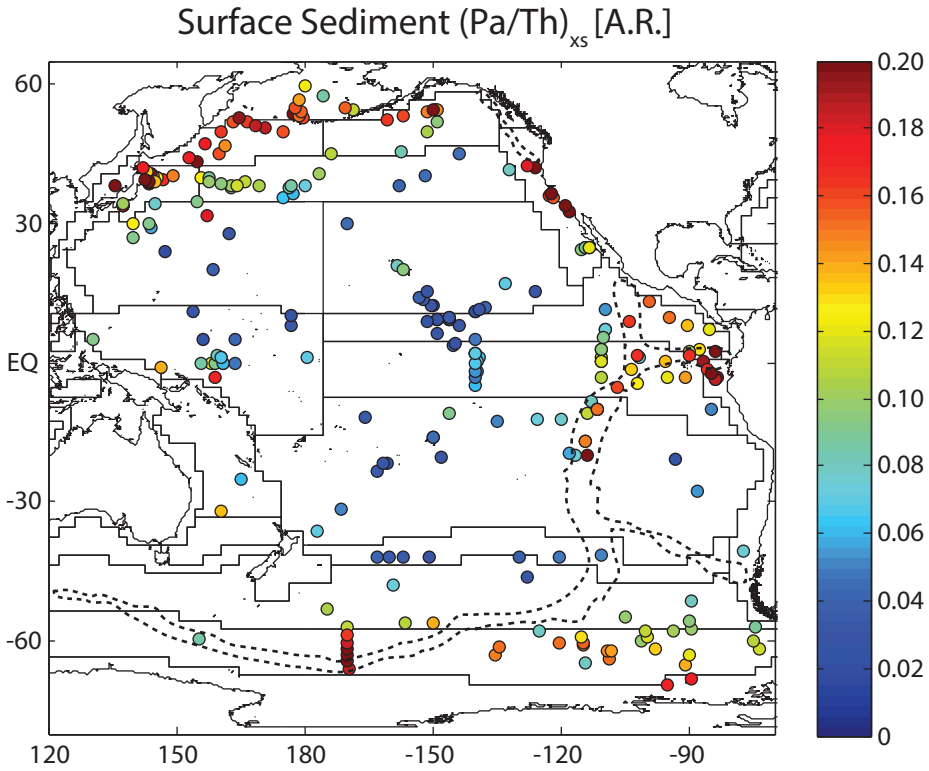

Figure 3. Map of surface sediment $(Pa/Th)_{xs}$ activity ratio [A.R.] of data from this study compiled with published results (see Table S1 for references).Thin lines demarcate the biogeographic provinces as defined by Longhurst (2006) (See Fig. 7 and Table 2 for province names). The heavy dashed lines approximate the 3.5 km isobar which also roughly trace the mid-ocean ridge system in the Pacific.

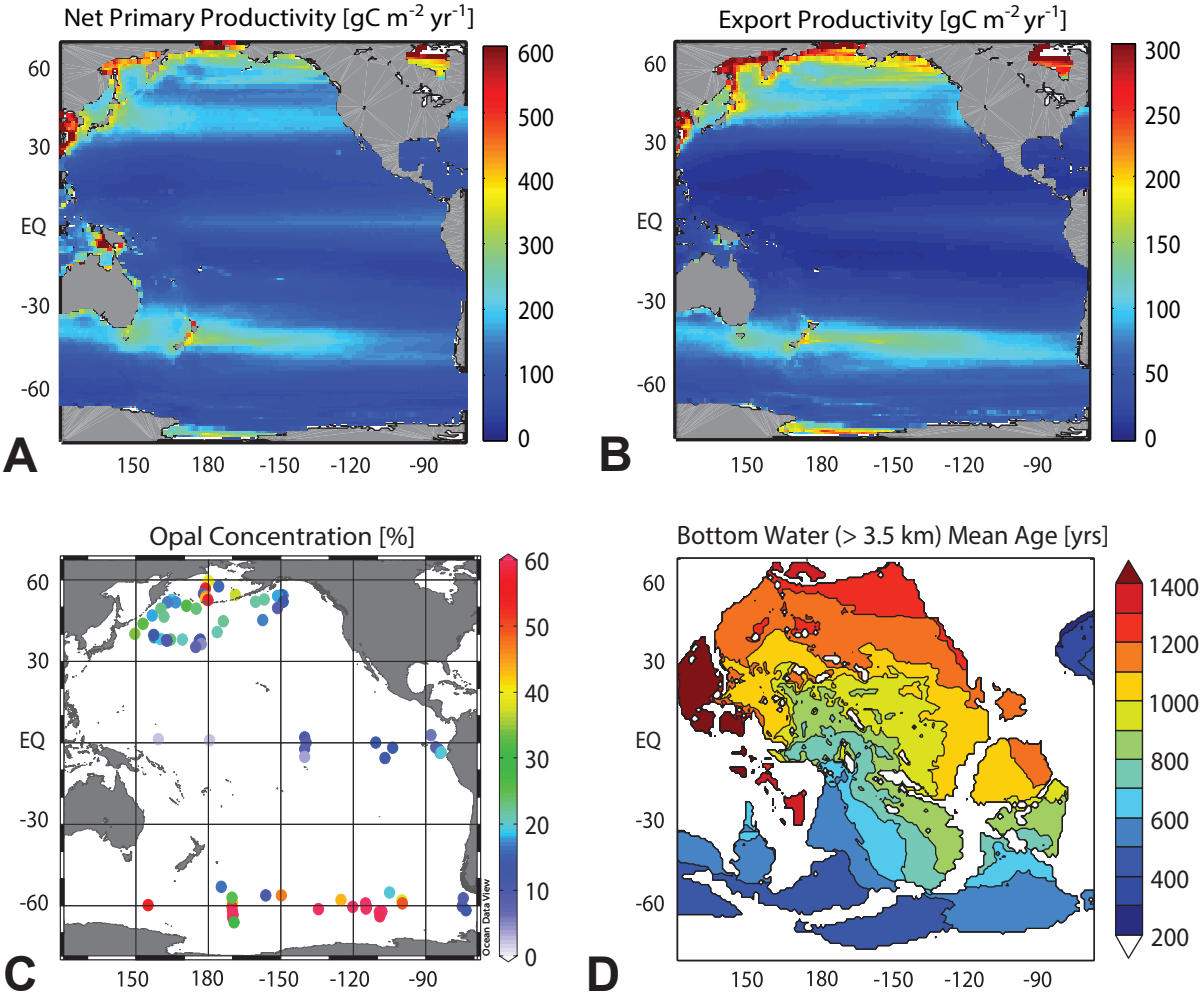

Figure 4. (A) Map of net primary productivity and (B) export productivity as estimated from satellite data (Sec. 2.1). (C) Map of opal concentration in sediments for which $(Pa/Th)_{xs}$ has also been measured. (D) Map of bottom water (>3.5 km) age as estimated by Khatiwala et al. (2012).

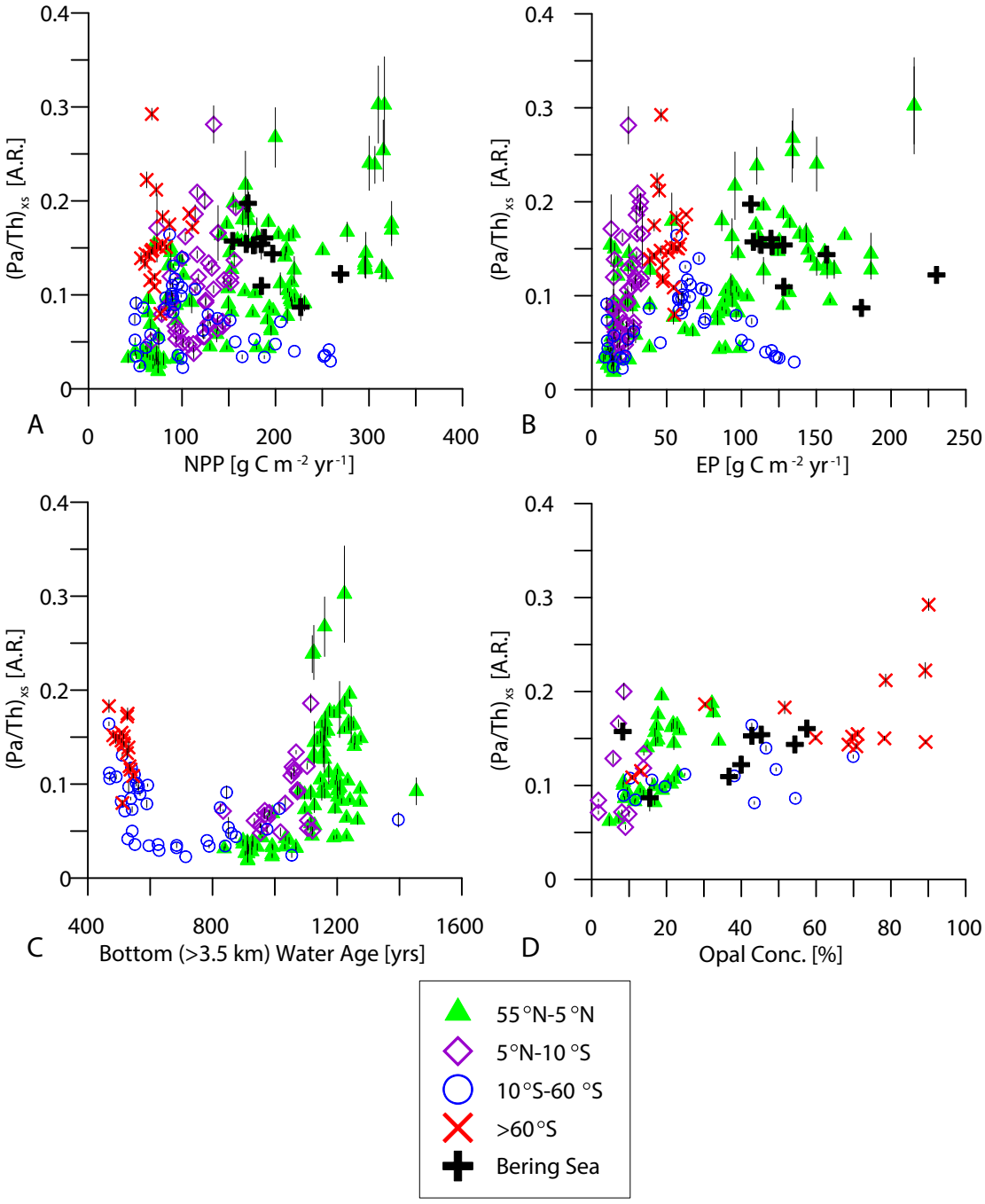

Figure 5. Cross plots of observed (Pa/Th)xs activity ratios in the Pacific versus (A) net primary productivity (NPP), (B) export productivity (EP), (C) bottom water (>3.5 km) age and (D) opal concentration. These sites are all deeper than 2 km water depth, have analytical uncertainties in (Pa/Th)xs < 20%, and have not been designated in the literature to be affected by hydrothermal scavenging.

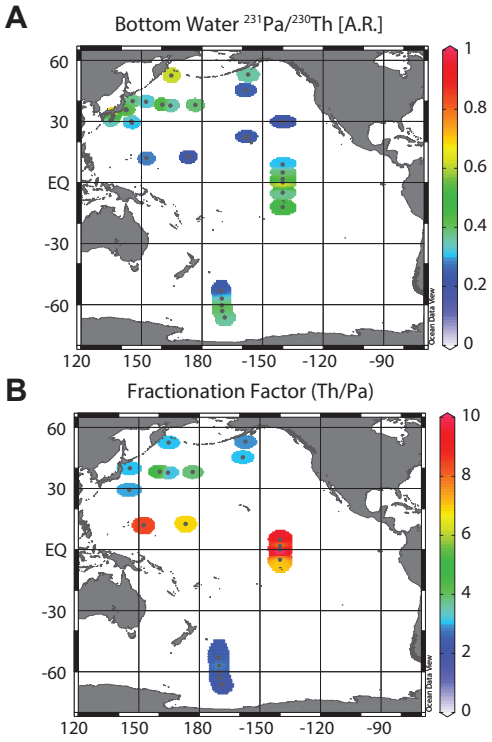

Figure 6. Available (A) bottom water $^{231}Pa/^{230}Th$ activity ratios [A.R.] and (B) fractionation factors calculated between bottom water and the underlying sediment from this study and the literature (Anderson, 2002; Anderson et al., 2012; Berelson et al., 1997; Chase et al., 2003b; François, 2007; Hayes et al., 2013; Nozaki and Nakanishi, 1985; Nozaki and Yang, 1987; Yang et al., 1986).

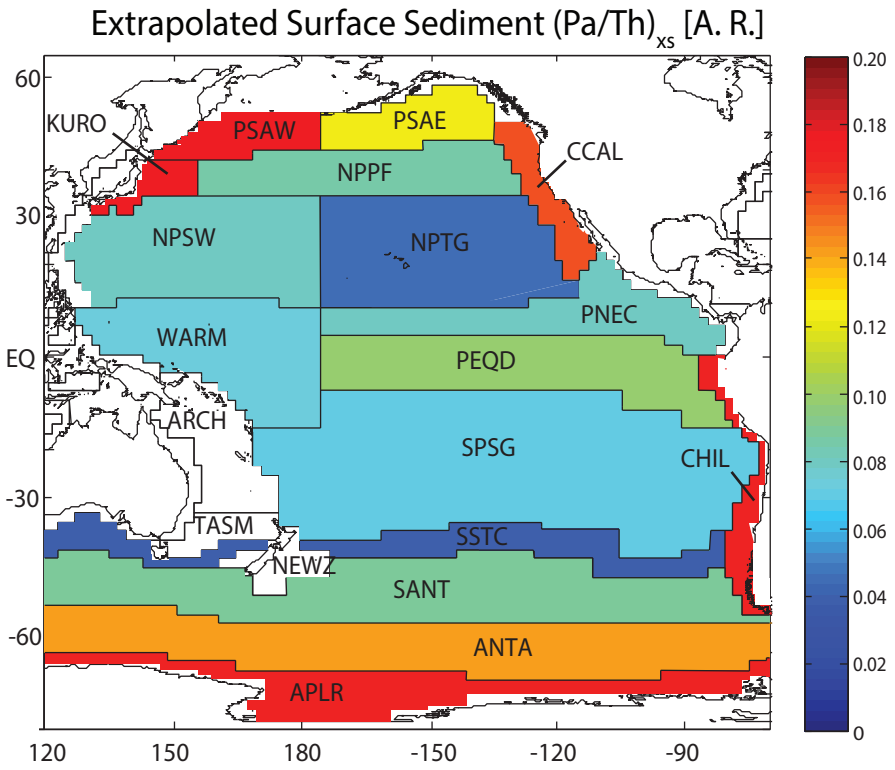

Figure 7. Interpolated map of $(Pa/Th)_{xs}$ activity ratios [A.R.] in Pacific surface sediments generated by representing each of 16 defined biogeographic provinces (Longhurst, 2006) by the average $(Pa/Th)_{xs}$ ratio observed in that province. See Table 2 for the full names of biogeographic provinces.

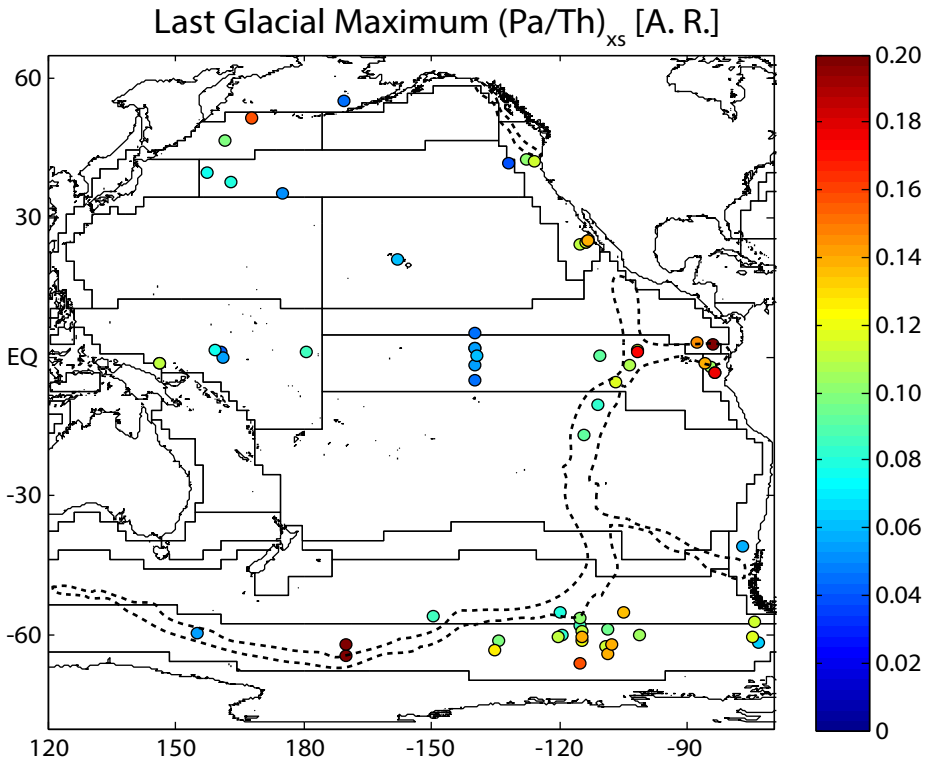

Figure 8. Map of $(Pa/Th)_{xs}$ activity ratios [A.R.] in sediments from the last glacial maximum (19-24 ka) according to published data (see Sec. 3.4 for references). Thin lines demarcate the modern biogeographic provinces as defined by Longhurst (2006) (See Fig. 7 and Table 2 for province names). The heavy dashed lines approximate the 3.5 km isobar which also roughly trace the mid-ocean ridge system in the Pacific.

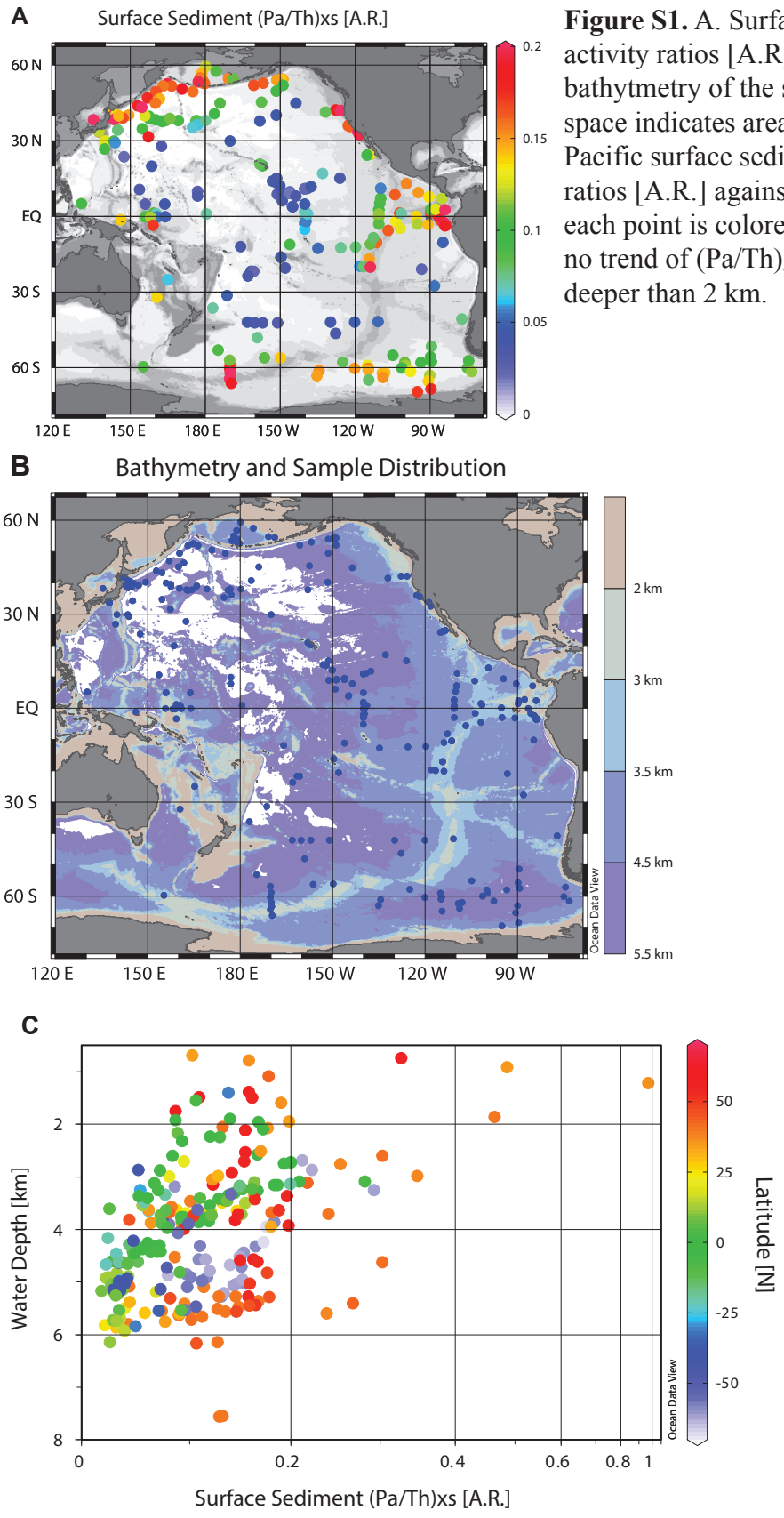

Figure S1. A. Surface sediment $(Pa/Th)_{xs}$ activity ratios [A.R] replotted. B. Detailed bathytmetry of the sample distribution. White space indicates areas deeper than 5.5 km. C. Pacific surface sediment $(Pa/Th)_{xs}$ activity ratios [A.R.] against water depth [km] in which each point is colored by latitude [°N]. There is no trend of $(Pa/Th)_{xs}$ with depth for sites deeper than 2 km.

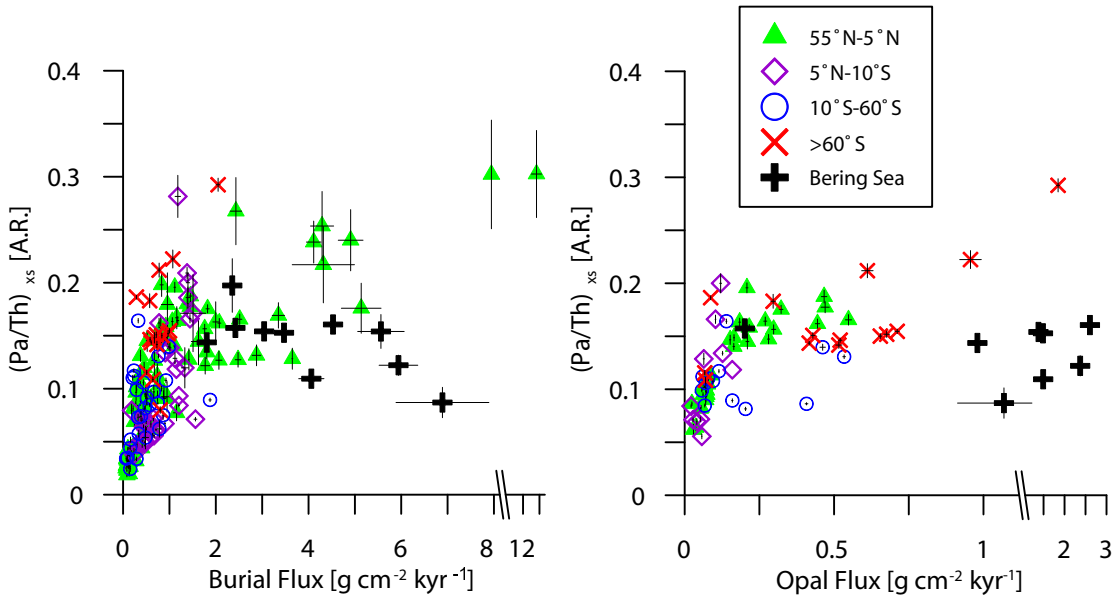

Figure S2. (Pa/Th)xs versus 230Th-normalized total mass burial flux (left) and opal flux (right). These sites are all deeper than 2 km water depth, have analytical uncertainties in (Pa/Th)xs <20%, and have not been designated in the literature to be affected by hydrothermal scavenging.

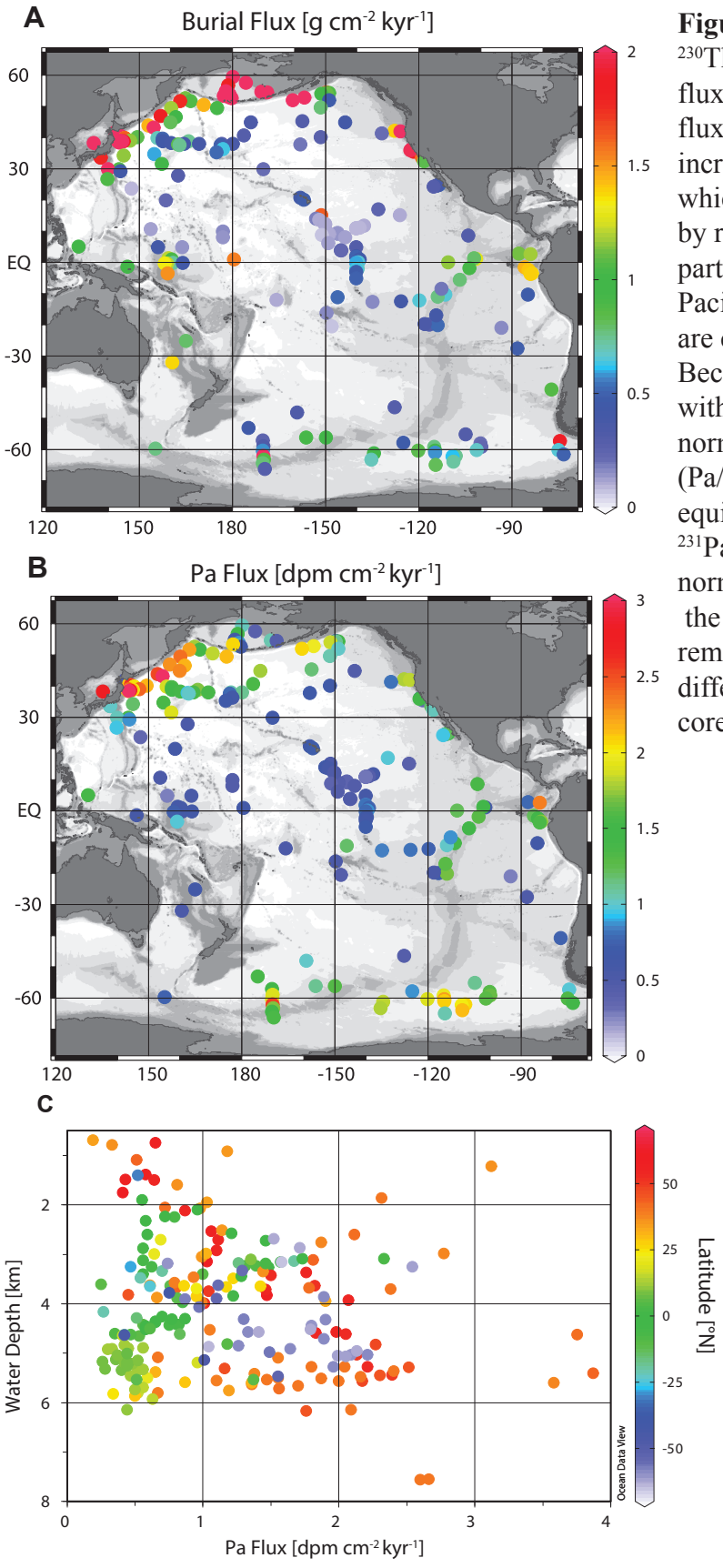

Figure S3. Spatial distribution of ^{230}Th-normalized total mass burial flux (A) and ^{230}Th-normalized ^{231}Pa flux (B). There is some trend of increasing Pa flux with depth (C), which is expected if Pa is removed by reversible scavenging, in particular for sites in the North Pacific and Southern Ocean (points are colored by latitude [°N]). Because ^{230}Th fluxes also increase with depth (assumed in the normalization technique), $(Pa/Th)_{xs}$ ratios are essentially equivalent to ^{230}Th-normalized ^{231}Pa fluxes which have been normalized by water depth. Thus the $(Pa/Th)_{xs}$ ratio is a proxy for Pa removal and is not majorly biased by differening water depth among the core sites.

Table 1. Correlation coefficients between Pacific surface sediment $(Pa/Th)_{xs}$ and: Net Primary Productivity (NPP), Export Productivity (EP), sediment opal concentration (opal%), and bottom water (>3.5km) age among different latitude bands

Correlation Coefficients (r-values)

	55°N-5°N	5°N-10°S	10°S-60°S	>60°S
NPP	0.66	0.26	-0.40	0.14
EP	0.73	0.44	0.00	0.10
opal%	0.67	0.64	0.41	0.55
Age	0.60	0.53	-0.46	-0.46

Number of sites in analysis

	55°N-5°N	5°N-10°S	10°S-60°S	>60°S
NPP	111	44	43	21
EP	106	44	43	21
opal%	31	15	13	14
Age	111	25	40	17

Table 2. Budget of Pa removal in the Pacific. The biogeographic provinces (Longhurst 2006) are considered to have the average $(Pa/Th)_{xs}$ activity ratio [A.R.] of the sites included within each province. The fractional surface areas, f(SA), of the provinces are then used to calculate a weighted average $(Pa/Th)_{xs}$ for the whole basin (box below). Further assuming as basin wide removal ratio equal to the production ratio (0.093), the surface-area weighted $(Pa/Th)_{xs}$ can be used to estimate the fraction of total Pa produced in the Pacific removed in each province, f(Pa removed).

Province	Code	No. of Sites	Avg. $(Pa/Th)_{xs}$ [A.R.]	±	SA [10^6 km^2]	f(SA) [%]	f(Pa removed) [%]
Antarctic	ANTA	28	0.141	0.047	2.8	2.1	3.1
Austral Polar	APLR	2	0.174	0.002	3.0	2.2	4.1
California Upwelling Coastal	CCAL	15	0.158	0.012	1.0	0.7	1 .2
Chile-Peru Coastal	CHIL	6	0.172	0.020	2.6	2.0	3.6
Kuroshio Current	KURO	18	0.177	0.015	1.4	1.1	2.0
North Pacific Polar Frontal	NPPF	19	0.085	0.006	7.2	5.4	4. 9
North Pacific Subtropical Gyre (West)	NPSW	8	0.087	0.01 7	10.5	7.9	7.4
North Pacific Tropical Gyre	NPTG	13	0.045	0.006	14.7	11.1	5.4
Pacific Equatorial Divergence	PEQD	24	0.098	0.008	13.7	10.3	10.8
North Pacific Equatorial Counter Current	PNEC	19	0.076	0.012	9.3	7.0	5.7
Pacific subarctic gyre (East)	PSAE	9	0.128	0.010	3.2	2.4	3 .3
Pacific subarctic gyre (West)	PSAW	10	0.177	0.011	2.9	2.1	4.1
Subantarctic	SANT	12	0.089	0.009	21.5	16.1	15.5
South Pacific Subtropical Gyre	SPSG	22	0.076	0.010	29.0	21.8	17.9
South Subtropical Convergence	SSTC	6	0.040	0.004	5.9	4.4	1.9
West Pacific Warm Pool	WARM	17	0.073	0.010	4.6	3.5	2.7
		Total SA-weighted $(Pa/Th)_{xs}$	0.087	0.003	Total 133.2		Total 93.8

Table S1. References cited for Pacific $(Pa/Th)_{xs}$ survey and the biogeographic provinces represented by those references.

Reference (in alphabetical order)	Biogeographic province(s) represented See Fig. 6 for province locations
Anderson et al., 1983b	NPTG
Anderson et al., 1990	PNEC, SPSG, WARM, CHIL
Berelson et al., 1997	PEQD, PNEC
Bernat and Goldberg, 1968	NPTG
Bradtmiller et al., 2006	CHIL, PEQD, PNEC
Bradtmiller et al., 2009	ANTA, SANT
Chase et al., 2003a	ANTA, SANT
Cochran and Krishnaswami, 1980	NPTG, PNEC
DeMaster, 1979	PEQD
Frank et al., 1994	PEQD
Hayes et al. (this study)	PSAE, PSAW, NPPF, KURO, Bering Sea
Huh et al., 1987	CCAL
Kadko, 1980	PNEC
Kadko, 1983	NPTG
Ku, 1966	ANTA, NPSW, SPSG
Lam et al., 2013	PSAW
Lao et al., 1992b	ANTA, SANT, CHIL, NPPF, NPTG, PEQD, PSAW, Bering Sea
Mangini and Kühnel, 1987	PNEC
Mohamed et al., 1996; Mohamed and Tsunogai, 1998	KURO
Müller and Mangini, 1980	PEQD, NPTG, PNEC
Narita et al., 2003	KURO
Pichat et al., 2004	PEQD, WARM
Schmitz et al., 1986	SANT, SPSG, SSTC
Shimmield and Price, 1988	SPSG
Shimmield et al., 1986	CCAL
Taguchi and Narita, 1995	KURO, NPSW
Walter et al., 1999	APLR, ANTA, CHIL, PEQD, PNEC, SANT, WARM
Yang et al., 1986	NPSW, KURO, ARCH, NPPF, NPTG, PSAW, SANT, SPSG, WARM, PNEC, Bering Sea
Yang et al., 1995	PNEC

Chapter 4. ^{230}Th and ^{231}Pa on the US GEOTRACES North Atlantic section and implications for modern and paleoceanographic chemical fluxes

Christopher T. Hayes[a,b], Robert F. Anderson[a,b], Martin Q. Fleisher[a], Kuo-Fang Huang[c], Laura F. Robinson[d,e], Yanbin Lu[f], Hai Cheng[f,g], R. Lawrence Edwards[f], S. Bradley Moran[h]

[a]Lamont-Doherty Earth Observatory of Columbia University, Palisades, NY, USA

[b]Department of Earth & Environmental Sciences, Columbia University, New York, NY, USA

[c]Department of Geology & Geophysics, Woods Hole Oceanographic Institution, Woods Hole, MA, USA

[d]Department of Marine Chemistry & Geochemistry, Woods Hole Oceanographic Institution, Woods Hole, MA, USA

[e]School of Earth Sciences, University of Bristol, Bristol, United Kingdom

[f]Department of Earth Sciences, University of Minnesota, Minneapolis, MN, USA

[g]Institute of Global Environmental Change, Xi'an Jiaotong University, Xi'an, China

[h]Graduate School of Oceanography, University of Rhode Island, Narragansett, RI, USA

In preparation for Deep Sea Research, Part II

Abstract

The long-lived uranium decay products ^{230}Th and ^{231}Pa are widely used as quantitative tracers of adsorption to sinking particles (scavenging) in the ocean by exploiting the principles of radioactive disequilibria. Because of their preservation in the Pleistocene sediment record and through largely untested assumptions about their chemical behavior in the water column, the two radionuclides have also been used as proxies for a variety of chemical fluxes in the past ocean. This includes the vertical flux of particulate matter to the seafloor, the lateral flux of insoluble elements to continental margins (boundary scavenging), and the southward flux of water out of the deep North Atlantic. In a section of unprecedented vertical and zonal resolution, the distributions of ^{230}Th and ^{231}Pa across the North Atlantic shed light on the marine cycling of these radionuclides which further informs their use as tracers of chemical flux. Enhanced scavenging intensities are observed in benthic layers of resuspended sediments on the eastern and western margins and in a hydrothermal plume emanating from the Mid-Atlantic Ridge. Boundary scavenging is clearly expressed in the water column along a transect between Mauritania and Cape Verde which is used to quantify a bias in sediment fluxes calculated using ^{230}Th-normalization and to demonstrate enhanced ^{231}Pa removal from the deep North Atlantic by this mechanism. The influence of deep ocean ventilation that leads to the southward export of ^{231}Pa is apparent but convolved with spatial variability in scavenging intensity. The observations presented here are of use in constraining biogeochemical cycles of trace metals in the modern ocean and in ground-truthing paleo-proxy applications which should be ultimately confirmed in ocean circulation models.

1. Introduction

The motivations to quantify chemical fluxes in the ocean are manifold. For instance, marine biological productivity is set by the balance between nutrient sources and sinks in surface waters and global climate is influenced by the redistribution of heat and salt associated with the ocean's overturning circulation. The well-known rates of radioactive production and decay of ^{230}Th and ^{231}Pa (half-lives 75.69 kyr (Cheng et al., 2000) and 32.76 kyr (Robert et al., 1969), respectively), in addition to their insoluble nature, make them attractive tools to quantify the rates of the marine processes in which they are involved. These include removal from the water column by adsorption to particles (scavenging), redistribution by ocean circulation, and sedimentation to the seafloor. Unfortunately, the influences of these processes on radionuclide distributions are potentially convolved. This study aims to utilize the spatial distribution of ^{230}Th and ^{231}Pa across the U.S. GEOTRACES North Atlantic transect (Fig. 1) to characterize the modern cycling of these isotopes in effort to more completely calibrate their use as flux tracers in the modern and past ocean.

Because their production (^{234}U and ^{235}U decay, respectively) is uniform throughout the ocean (Andersen et al., 2010; Delanghe et al., 2002; Robinson et al., 2004; Weyer et al., 2008), the key question in ^{230}Th and ^{231}Pa cycling in the water column is the balance between removal mechanisms. These are primarily (1) the downward flux by scavenging onto sinking particles and (2) lateral fluxes by advection and eddy diffusion. If lateral fluxes can be neglected, the concentration of the scavenged nuclide is expected to increase linearly with depth, representing an "equilibrium" between adsorption onto, and desorption from, vertically homogeneous sinking particles, a concept known as reversible scavenging (Bacon and Anderson, 1982; Krishnaswami et al., 1976; Nozaki et al., 1981).

Deviations from linearity in the radionuclide profiles therefore signal where this vertical equilibrium is perturbed by lateral fluxes or where the scavenging intensity has changed. This is admittedly a simple approach, as relatively linear depth profiles are not inconsistent with some lateral flux by dispersion (Roy-Barman, 2009; Venchiarutti et al., 2008). In a basin-scale view, nonetheless, characterizing anomalies to the predictions of reversible scavenging is our first step in deconvolving the oceanic ^{230}Th and ^{231}Pa cycles. Three such anomalies, boundary scavenging, the effects of recently ventilated deep water, and bottom scavenging, appear in unprecedented detail in our North Atlantic section (Fig. 1). We now provide a context for these findings.

1.1 Boundary scavenging of ^{230}Th and ^{231}Pa

Boundary scavenging (Bacon, 1988; Bacon et al., 1976; Spencer et al., 1981) is the enhanced removal of scavenged-type elements (Bruland and Lohan, 2003) at ocean margins. When lateral gradients in particle flux exist, as between biologically productive ocean margin regions and oligotrophic ocean interior regions, insoluble elements are removed from the water column by scavenging to a greater extent at the margin versus the interior. The resulting gradient in radionuclide concentration produces a dispersive flux toward the margin from the interior. Lateral transport in the water column toward ocean margins is more significant for ^{231}Pa than for ^{230}Th because it is removed vertically by scavenging more slowly. The residence time with respect to scavenging of ^{231}Pa is 50-200 yrs while that for ^{230}Th is 10-40 yrs (Henderson and Anderson, 2003). On the basis of the boundary scavenging concept alone, elevated ^{231}Pa/^{230}Th ratios in both the dissolved and particulate phase at ocean margins are expected. Prior to this study, the lateral gradients in the dissolved ^{231}Pa/^{230}Th ratio or in dissolved ^{230}Th (^{231}Pa) concentrations, predicted by the boundary scavenging concept, have not been definitively observed in the North Atlantic.

Modeling efforts have concluded that in ~70% of the ocean, ^{230}Th is redistributed laterally by no more than 30% of its in situ production in the water column (Henderson et al., 1999), consistent with available observations from sediment traps (Yu et al., 2001). However, on the basis of sedimentary records some authors have argued that water column ^{230}Th redistribution could be much greater than 30% due to boundary scavenging-type mechanisms, specifically along the equator in the Pacific (Broecker, 2008; Lyle et al., 2005; Lyle et al., 2007). This claim derives from a concern regarding ^{230}Th-normalization, a method for calculating sediment accumulation rates on the basis of sedimentary ^{230}Th concentrations (Bacon, 1984; François et al., 2004). This method assumes that the burial flux of ^{230}Th is equal to its rate of production by ^{234}U decay in the overlying water column, which allows one to correct for the lateral redistribution of sediments at the seafloor (sediment focusing). Because glacial-interglacial changes in sediment focusing have enhanced or diminished apparent accumulation rates by more than a factor of 2 (Francois et al., 1990; Suman and Bacon, 1989), the approach has been defended on the basis that neglecting a relatively small bias in the assumption that ^{230}Th burial is equivalent to its production in the overlying water column is justified (François et al., 2007; Siddall et al., 2008). One aim of this study is to quantitatively estimate the magnitude of ^{230}Th redistribution due to boundary scavenging.

While the effect of boundary scavenging of ^{231}Pa is well-expressed in the Pacific (Anderson et al., 1983; Anderson et al., 1990; Walter et al., 1999; Yang et al., 1986), it is considered to be suppressed in the Atlantic. This is because this basin is ventilated by southward flowing North Atlantic Deep Water (NADW) on timescales (<100-200 yrs) (Broecker et al., 1991) shorter than the Pa residence time with respect to scavenging (Walter et al., 1999; Yu et al., 1996; Yu et al., 2001). This means Pa can be transported south by deep water flow before it

can be dispersed to North Atlantic margins. Although some studies have found evidence, in the form of sedimentary $^{231}Pa/^{230}Th$ activity ratios above that produced in seawater by uranium decay of 0.093, for the enhanced removal of ^{231}Pa in the upwelling area off Northwest Africa (Legeleux et al., 1995; Lippold et al., 2012b; Mangini and Diester-Haas, 1983), studies of the North American (Anderson et al., 1994; Lippold et al., 2012a) and the northern Brazil (Lippold et al., 2011) margins do not support boundary scavenging of Pa. The dissolved $^{231}Pa/^{230}Th$ distribution toward the margins of our transect (Fig. 1) will be used to determine the significance of boundary scavenging in the North Atlantic in light of its recent ventilation.

1.2 The impact of Atlantic circulation

The possibility of boundary scavenging notwithstanding, previous studies have demonstrated that deepwater distributions of ^{230}Th and ^{231}Pa are significantly perturbed by the influence of the recent ventilation of NADW (Luo et al., 2010; Moran et al., 1997; Moran et al., 1995; Moran et al., 2002; Scholten et al., 2001; Vogler et al., 1998). Deep convection at sites of deep water formation results in the injection to depth and propagation along deepwater flow paths of ^{231}Pa and ^{230}Th concentrations which are lower than predicted by reversible scavenging (Moran et al., 1997; Moran et al., 1995; Moran et al., 2002). As the water mass ages, isolated from further perturbations to scavenging equilibrium, dissolved ^{230}Th concentrations increase due to exchange with sinking particles, reaching a steady-state distribution relatively rapidly (determined by the residence time of 10-40 yrs), while ^{231}Pa responds more slowly (residence time of 50-200 yrs) because of the differing scavenging rates of the two elements (Moran et al., 2001; Rutgers v. d. Loeff and Berger, 1993). The longer residence time of ^{231}Pa allows for its southward export with NADW, leaving a ^{231}Pa deficit in deep North Atlantic sediments (Yu et al., 1996). This is the basis for using the sedimentary $^{231}Pa/^{230}Th$ ratio as an indicator of the

strength of the Atlantic meridional overturning circulation (McManus et al., 2004). The present water column transect is also intended to document the impact of ventilation on ^{231}Pa and the ^{231}Pa/^{230}Th ratio.

In the absence of variations in scavenging intensity, one expects ^{230}Th and ^{231}Pa concentrations and the ^{231}Pa/^{230}Th ratio to increase with water mass age. The strongest response to ageing occurs within 1 to 2 water column residence times after deep-water formation. Our section is appropriate to test this prediction because deep water age, or the time since deep-water (as averaged below 2 km) has been isolated from the atmosphere, ranges from <50 yrs in the west to >250 yrs in the east (Broecker et al., 1991). We have extracted an estimate of mean age for our North Atlantic transect from a recent inversion of ventilation tracer observations (^{14}C, CFCs, PO_4^*, temperature and salinity) by Khatiwala et al. (2012). These ages, which represent that time since a water parcel was last at the surface, taking into account contributions from multiple pathways and source regions, are referred to in the text as either mean ages or ventilation ages.

In addition to consideration of water mass ageing, we put our transect into hydrographic context with the salinity and neutral density (γ_n) section in Fig. 1. The dome of salty subtropical mode water, also known as Eighteen Degree Water, is apparent in the upper 500-800 m and is roughly bound at depth by γ_n = 26.65 kg m^{-3} (LeBel et al., 2008). The remaining density surfaces in Fig. 1 demarcate the boundaries between the various sources of NADW, which are defined most clearly in the Northwest section between Bermuda and Woods Hole, Mass., known as Line W (Toole et al., 2011). These are, in order of increasing density, Upper and Classic Labrador Sea Water, Iceland-Scotland Overflow Water, and Denmark-Strait Overflow Water, which is underlain by Antarctic Bottom Water (AABW, γ_n > 28.125). While we name the densest layer of

water in the western basin AABW, this far from its source the water mass must have gone through significant mixing with the overlaying NADW.

The deep waters of the Northeastern Atlantic (>3 km depth) are not as clearly defined by the contributions to NADW and are characterized by a relatively homogeneous water mass called Northeast Atlantic Deep Water (NEADW). NEADW is sourced by a mixture of NADW and AABW which enters the Northeast basin largely through the Romanche Trench near the equator and a smaller proportion through the Vema Fracture Zone at 11°N (Broecker et al., 1980; Schlitzer, 1987; Schlitzer et al., 1985). The intermediate water in the southeastern portion of the cruise track intersects the northern extent of the salinity minimum (and silicic acid maximum) originating from Antarctic Intermediate Water (AAIW) (Talley, 1999; Tsuchiya, 1989), outlined in Fig. 1. Lastly, the high salinity intrusion of Mediterranean Outflow Water (MOW) at ~1 km depth is well represented on the largely south-north part of the transect approaching Portugal.

1.3 Bottom scavenging

Deep water ^{231}Pa and ^{230}Th concentrations can also be perturbed by changes in scavenging intensity near the seafloor (bottom scavenging) associated with a change in particle concentration or particle composition. Nepheloid layers (Biscaye and Eittreim, 1977; McCave, 1986), or zones up to 100's of meters above the seafloor of increased particle concentration caused by the resuspension of sediments, have been known to enhance the scavenging of the shorter-lived ^{234}Th (half-life 24.1 days) in the northwest (Bacon and Rutgers v. d. Loeff, 1989; DeMaster et al., 1991) and northeast (Schmidt, 2006; Turnewitsch et al., 2008; Turnewitsch and Springer, 2001) Atlantic. Previous studies in the North Atlantic have suggested that bottom scavenging could reduce the ^{230}Th concentration in deep water, but since the same effect can be achieved via recent water mass ventilation without invoking a change in scavenging intensity,

ventilation was the preferred explanation (Moran et al., 1997; Moran et al., 1995; Vogler et al., 1998). However, recent results from the Pacific, where the ventilation effect is not large enough to produce observed radionuclide depletions in deepwater, have confirmed early observations (Bacon and Anderson, 1982; Nozaki and Nakanishi, 1985) that significant bottom scavenging indeed occurs for ^{230}Th (Hayes et al., 2013; Okubo et al., 2012; Singh et al., 2013) and ^{231}Pa (Hayes et al., 2013).

Based on extensive observations in the northwest Atlantic of thick nepheloid layers (Biscaye and Eittreim, 1977; Brewer et al., 1976), our transect is well-situated to determine the effect of sediment resuspension on ^{230}Th and ^{231}Pa. In addition to increased particle loading, bottom scavenging may also be affected by a change in particle composition. This section is also well-suited to test the hypotheses that ^{230}Th and ^{231}Pa are scavenged especially efficiently by authigenic iron and manganese oxide phases associated with hydrothermal activity at the mid-Atlantic ridge (German et al., 1991; German et al., 1993) or by (oxy)hydroxide coatings of particles formed in regions of organic-rich sediment diagenesis at ocean margins (Anderson et al., 1983; Bacon et al., 1976; Shimmield et al., 1986). To infer likely changes in scavenging intensity in our transect, we utilize the distribution of the particle beam attenuation coefficient, C_p, as measured by transmissometer from CTD casts, which is, to first order, linearly related to particle concentration (Bishop, 1986; Gardner et al., 1985), although the sensitivity of C_p to particle concentration is known to vary with particle size and composition (Baker and Lavelle, 1984; Richardson, 1987).

2. Methods

The U.S. Geotraces North Atlantic transect (Fig. 1) consisted of two legs. KN199-4 (referred to as GT10) from Lisbon, Portugal to Mindelo, Cape Verde was completed in Oct-Nov

2010. KN204-1 (referred to as GT11) from Woods Hole, Massachusetts to Praia, Cape Verde via St. Georges, Bermuda was completed in Nov-Dec 2011. Radionuclide data were produced by three collaborating laboratories which were intercalibrated (Anderson et al., 2012) to analyze dissolved (<0.45 μm) and particulate (0.45-51 μm) ^{232}Th, ^{230}Th, and ^{231}Pa in seawater: the Lamont-Doherty Earth Observatory of Columbia University (L-DEO), the Woods Hole Oceanographic Institution (WHOI) and the University of Minnesota (UMN). Five liter water samples were collected using conventional Niskin bottles, filtered with 0.45 μm Acropak^{TM}-500 filter capsules, and acidified to pH = 1.8 at sea for storage according GEOTRACES protocols. Particulate samples representing 55-350 L of seawater were collected by McLane Research in situ pumps (Lam and Morris, Patent Pending) using paired 0.8 μm Pall Supor800 polyethersulfone filters (Bishop et al., 2012).

Th and Pa isotopes (including the added tracers ^{229}Th and ^{233}Pa) were co-precipitated with Fe (oxy)hydroxide for pre-concentration and purification using acid digestions (HNO_3/HF/$HClO_4$, depending on the laboratory) and ion exchange chromatography. Filter samples were co-precipitated with Fe after complete dissolution (HNO_3/$HClO_4$/HF). Radionuclide concentrations (reported as fg, 10^{-15} g, radionuclide per kg seawater) were determined by isotope dilution inductively-coupled plasma mass spectrometry. The analytical procedures used at L-DEO, WHOI, and UMN have been fully described by Anderson et al. (2012), Auro et al. (2012), and Shen et al. (Shen et al., 2003; Shen et al., 2002; Shen et al., 2012), respectively.

We correct measured dissolved radionuclide concentrations for in-growth due to uranium decay during sample storage. In-growth during sample storage from particulate U concentrations is negligible (Ohnemus, pers. comm.). In order to isolate the signature of scavenging in the

dissolved phase we also correct ^{230}Th and ^{231}Pa concentrations for a contribution produced by the partial dissolution of U-containing lithogenic material based on dissolved ^{232}Th as described by Hayes et al. (2013), assuming a crustal ^{238}U/^{232}Th ratio and congruent dissolution of ^{232}Th, ^{230}Th and ^{231}Pa. Similarly, in the particulate phase we correct measured ^{230}Th and ^{231}Pa for a lithogenic component based on particulate ^{232}Th. All radionuclide concentrations discussed in the text are corrected for lithogenic sources and are denoted as "xs". For more information on data analysis see the metadata associated with these datasets at BCO-DMO (bco-dmo.org). Forthcoming studies will present and interpret the distribution of ^{232}Th and particulate radionuclides in their own right. These results are used here only for the interpretation of the dissolved (or total) ^{230}Th and ^{231}Pa distributions.

3.1 Results and Discussion

3.1 Sections of dissolved ^{230}Th xs and ^{231}Pa xs

Deviations from linear concentration-depth profiles as predicted by the model of reversible scavenging are immediately apparent in the North Atlantic sections (Fig. 2). Both radionuclides display substantial lateral concentration gradients, some of which are clearly related to recent ventilation. Generally, lower concentrations of both radionuclides are found in the western and northern parts of the transect, coincident with younger mean ages (Fig 2E). Additionally low concentrations of ^{231}Pa xs in shallow water (Fig. 2D) take on a dome structure, coinciding with EDW, and are presumably reflective of the rapid (<10 yrs) ventilation of this subtropical mode water (Jenkins, 1988).

Notably unrelated to any change in mean age (Fig. 2E), ^{230}Th xs also has reduced concentrations throughout the water column in the section between Cape Verde and Mauritania (Cape Verde transect, Fig. 2B) coincident with increasing particle concentrations (Fig 2A, 5000-

6500 km section distance). The plunging isolines of ^{230}Th xs concentration toward the continental margin on this transect are strong evidence for the process of boundary scavenging occurring. We quantify the lateral transport of ^{230}Th xs and ^{231}Pa xs associated with this boundary scavenging in section 3.2.

Both radionuclides show vertical concentration anomalies as well. Concentrations generally increase linearly from the surface to depth but nearly always begin to decrease toward the seafloor. These negative deviations with respect to reversible scavenging generally start higher in the water column for dissolved ^{231}Pa xs (2-3 km depth) than for dissolved ^{230}Th xs (4-5 km). This is a pervasive feature in the Atlantic (Luo et al., 2010; Moran et al., 2002; Scholten et al., 2008; Scholten et al., 2001; Vogler et al., 1998) which has been largely attributed to the advection of NADW in previous work.

At stations GT-10-01, GT11-04, GT11-06, GT11-08, and GT11-10, however, the dissolved radionuclide depletions can be clearly associated with a large increase in beam attenuation related to higher particle concentration (Fig. 2A) and presumably bottom scavenging. Additionally, the near-bottom waters at GT11-16 (mid-Atlantic ridge) and GT10-09 (African margin) have a more modest increase in C_p, but very large dissolved phase depletions. The near-bottom particles at these two sites showed a clear enrichment in metal oxides (Lam et al., in prep.), the former being up to 40% authigenic Fe oxides from a hydrothermal plume at the mid-Atlantic ridge, the latter being enrichment of authigenic Fe and Mn oxides (each 2-3% of the particle mass) related to reducing conditions in the surface sediments created by organic matter diagenesis. It thus seems likely that bottom scavenging due to increased particle abundance and/or unique particulate chemistry is at least as significant as ventilation in regulating the distributions of dissolved ^{230}Th xs and ^{231}Pa xs across the North Atlantic. In section 3.3, we give

a few examples of how ventilation and bottom scavenging may be convolved in determining ^{230}Th xs and ^{231}Pa xs distributions. The de-convolution of these effects requires sensitivity testing in 3-dimensional ocean models which is beyond the scope of this study.

3.2 Quantification of boundary scavenging

Enhanced removal of trace elements at ocean margins is supported by advective and diffusive fluxes that arise due to the lateral concentration gradients imposed by lateral gradients in scavenging intensity (Bacon, 1988). To quantify the magnitude of this flux, one can calculate the lateral concentration gradients from concentration profiles. Since radionuclides are exchanged between dissolved and adsorbed forms faster than they are removed to the seafloor (Bacon and Anderson, 1982), for mass continuity, one must consider the total radionuclide concentration (dissolved plus particulate). In Figure 3, we plot particulate and total ^{230}Th xs and ^{231}Pa xs for the stations between Mauritania and GT11-22. Total ^{230}Th xs concentrations (Fig. 3C) are consistently lower at stations closer to the African margin, at nearly all depths. Total ^{231}Pa xs (Fig. 3D), on the other hand, is largely uniform among these stations. These observations are consistent with the boundary scavenging concept. Th-230, being more sensitive to the lateral gradient in scavenging intensity approaching the margin, is drawn down more efficiently than ^{231}Pa, which, because of its longer residence time, can support higher concentration at the margin supplied by lateral dispersion. Consequently, both dissolved and particulate ^{231}Pa/^{230}Th xs ratios are higher at the margin versus the interior (Fig. 3E-F), as predicted by Bacon (1988).

In one dimension (x, an isopycnal surface, since circulation occurs preferentially along lines of constant seawater density), for total ^{230}Th xs (Th), the steady-state mass balance is:

$$\frac{dTh}{dt} = P - S\frac{dTh_p}{dz} - u\frac{dTh}{dx} + K_H\frac{d^2Th}{dx^2} \qquad \text{Eq. 1}$$

P is production due to ^{234}U decay. S is the particle sinking rate which, when multiplied by the vertical gradient of particulate ^{230}Th concentration (second term on right-hand side of Eq. 1), represents the downward flux by scavenging. The third and fourth terms on the right-hand side of Eq. 1 represents lateral fluxes due to advection (isopycnal velocity, u, multiplied by the first isopyncal concentration gradient) and eddy diffusion (isopycnal eddy diffusion coefficient, K_H, multiplied by the second isopycnal concentration gradient), respectively.

In order to affect the steady-state mass balance, the advective and diffusive terms must occur on a timescale appropriate to the residence time, τ, of the tracer. The residence times, as defined by the water column inventory of radionuclide divided by its integrated production in the water column, between GT10-09 and GT11-22 for ^{230}Th and ^{231}Pa, respectively, are 10-28 yrs and 120-150 yrs. The corresponding length scales over which lateral eddy diffusivity should be considered are ~800-1300 km for ^{230}Th and 2750-3080 km for ^{231}Pa ($\Delta x = \sqrt{2K_H\tau}$, parameterizing eddy diffusivity as a random walk process), using $K_H = 10^3$ m^2 s^{-1}, as determined in the Northeast Atlantic (Ledwell et al., 1998). The advective length scale ($\Delta x = u\tau$) depends linearly on the current speed and will be >1500 km for both radionuclides if u is greater than a typical deep current speed of 2 mm/s. However, because east-west velocities cyclically change direction in this region (Zenk et al., 1991) and their magnitude is difficult to estimate for the deep ocean, we do not attempt to quantify the advective flux.

The isopycnal gradients in ^{230}Th are discretely estimated using the observations from GT10-09, GT10-10, GT10-11 and GT10-12 (Fig. 3C). We do not include GT11-22 in the analysis because it makes the transect larger than the ^{230}Th-mixing length scale (~1400 km). Within the analytical uncertainties we cannot derive isopycnal ^{231}Pa gradients that are significantly different than zero. Th-230 concentrations were interpolated onto a common set of

isopycnals (Fig. 4A), and because GT10-11 and GT10-12 are nearly indistinguishable we average these two profiles and consider the average profile representative of the region at the mid-point between the two stations. Uncertainties were accounted for and propagated in the calculations by assuming a conservative analytical uncertainty for total ^{230}Th xs of 1.5%. Two isopycnal gradients (Fig. 4B) were calculated by differencing the concentration profiles, between GT10-09 and GT10-10 and between GT10-10 and GT10-11/12, and dividing by the lateral distance between the stations. A positive gradient is defined as lower concentration in the east (leading to lateral fluxes toward Mauritania). Then the second isopycnal gradient (Fig. 4C) was calculated by differencing the two isopycnal gradient profiles and dividing by the distance between the mid-points of the stations used to calculate the first gradient (Fig. 4D).

The second isopycnal gradient is variable above γ_n = 27.8 (1.2 km depth), but below this density surface, in the bulk of the water column, the gradient is consistently positive (down gradient toward Mauritania). By multiplying the d^2Th/dx^2 profile by K_H (10^3 m^2 s^{-1}), and integrating with depth (~0-3 km), we estimate the lateral convergence of ^{230}Th xs to the margin (technically between two boxes, encompassing stations GT10-10/11/12 and GT10-09/10, respectively) as 670 ± 225 pg m^{-2} yr^{-1}. In 3 km of seawater, ^{230}Th production due to U decay is 1630 pg m^{-2} yr^{-1} and thus the diffusive flux adds 41 ± 14% to the water column production in the margin box (and removes the equivalent from production in the open-ocean box). This is consistent with the upper limit for the model-derived redistribution of water column ^{230}Th (Henderson et al., 1999).

Th-230 normalized sediment fluxes will therefore be biased (underestimated) by up to 30-50% for core sites at high productivity continental margins such as offshore Mauritania. The magnitude of the complementary bias (overestimation) in ^{230}Th-normalized fluxes in the interior

ocean is likely to be smaller than 30-50%. This is because the ^{230}Th added to the relatively small zone of high productivity at the margin is drawn from a much larger pool of the subtropical North Atlantic gyre. The subtropical gyre ^{230}Th budget, however, cannot be fully constrained here because there are likely additional lateral removal fluxes of ^{230}Th to other more expansive high productivity regions such as the equatorial or subpolar North Atlantic (Henderson et al., 1999).

Interestingly, the degree of boundary scavenging (and its impact on lateral ^{230}Th redistribution) may have changed through time (Lao et al., 1992). Nonetheless, the 40% redistribution estimate can be seen as close to a global maximum (in the modern ocean at least) since the Canary Current upwelling regime in which our observations are made produces one of the largest lateral gradients in productivity (and in turn particle flux) in the world (Behrenfeld and Falkowski, 1997). Thus our finding supports the use of ^{230}Th-normalization to reconstruct sediment fluxes within cited uncertainties (François et al., 2004).

Although we cannot directly estimate the magnitude of boundary scavenging for ^{231}Pa because the lateral water column ^{231}Pa gradients are not discernible, we can use the ^{230}Th results in conjunction with the particulate ^{231}Pa/^{230}Th xs data (Fig. 3F) to estimate the redistribution of ^{231}Pa. The near-bottom ^{231}Pa/^{230}Th xs ratio of particulate material, $(Pa/Th)_{bottom}$, should represent the ratio of sinking flux for the two elements. If both elements were being buried at their production rate by U decay, we would expect this ratio to be 0.093 (activity units, see dotted line, Fig. 3F). Therefore the actual ratio of sinking flux to overlaying production for ^{231}Pa, $(F/P)_{Pa}$, is proportional to that of ^{230}Th, weighted by the deviation of the near-bottom particulate material from the production ratio:

$$(F/P)_{Pa} = (F/P)_{Th} * (Pa/Th)_{bottom} / 0.093 \qquad \text{(Eq. 2)}$$

The average particulate $^{231}Pa/^{230}Th$ ratio at GT10-09, 1 km above the seafloor (~2-3 km depth), is 0.15 (Fig. 3F). Using $(F/P)_{Th} = 1.4$ as calculated above, we estimate that ^{231}Pa is being buried at 2.3 times its production in the overlaying water column at this site. While clearly a region of enhanced ^{231}Pa removal, this region will likely not account for observed depletion of ^{231}Pa in deep North Atlantic sediment. High productivity areas such as GT10-09, where boundary scavenging of ^{231}Pa is occurring, are likely only a small volumetric percentage of the basin (Lippold et al., 2012b). This is indicated by the sharp decrease in particulate $^{231}Pa/^{230}Th$ xs ratio between stations GT10-09 and GT10-10 (Fig. 3F). Nonetheless, more detailed mapping of the extent of this type of enhanced ^{231}Pa burial on the North African margin is required before its impact on the basin-wide Pa budget can be quantified (Marchal et al., 2000).

3.3 Bottom scavenging and ventilation: convoluted influences across the North Atlantic

Both ^{231}Pa xs and ^{230}Th xs (Fig. 2) have negative concentration anomalies associated with the high salinity waters of the Mediterranean Outflow Water (MOW, ~1 km depth at station GT10-01, Fig. 1). This is expected due to the high particle load of MOW, a result of the interaction of the flow of Mediterranean Water over the Gibralter Strait and the Iberian margin (McCave and Hall, 2002; Thorpe, 1972), which is known to enhance scavenging of ^{234}Th and ^{228}Th (half-life 1.8 yrs, parent ^{228}Ra) (Schmidt, 2006). Unexpectedly, the low radionuclide concentrations (causing negative deviations to a linear profile) appear to be advected along with the flow of MOW to station GT10-03 and even to GT10-05 for ^{231}Pa xs, while the high particle concentrations (on the basis of C_p, Fig. 2A) are not, i.e. the downstream effects are not necessarily due to in-situ scavenging. There is a strong boundary in ^{231}Pa xs concentrations and water mass age between GT10-05 and GT10-07 at 2 km depth (Fig. 2), indicating more recently ventilated water to the north, making it difficult to separate the downstream effects of

specifically MOW from a large-scale influence of other NADW components. This is the first of several examples of how ventilation and bottom scavenging combine to produce low concentration anomalies in the water column radionuclide distributions.

Second, we look in more detail at the impact of the enhanced scavenging observed at station GT11-16, also known as the TAG hydrothermal site (Rona, 1980; Rona et al., 1984). Clearly, dissolved ^{230}Th xs and ^{231}Pa xs are removed from solution in the observed hydrothermal plume around 3.3 km depth (Figs. 2B, 2D). But it also appears that the low concentration anomaly in the plume is dispersed by circulation to shallower depths in the water column. The TAG concentration profile departs negatively for dissolved ^{230}Th xs at 2.1 km, and for dissolved ^{231}Pa xs at 1.5 km. Furthermore, the low radionuclide concentrations appear to be advected to sites west of the ridge. For both radionuclides at 2.5 km depth, concentrations at GT11-14 are lower than they are to the west at GT11-12, opposite the expected trend due to water mass ageing.

Westward and shoaling propagation of the hydrothermal scavenging anomaly is consistent with theory, i.e. buoyant plume water rising and heading west due to geostrophic considerations (Speer, 1989). We note that these "downstream" hydrothermal effects (both vertical and lateral) are not caused only by the observed venting at the TAG site but are more likely the integrated result of vent sites all along the ridge (German et al., 2010). This is support for the hypothesis that hydrothermal vents are a basin-scale sink of Pa in the deep ocean (Hayes et al., 2013). However, because the observed hydrothermal anomaly and its far-field effect occur in a region with strong zonal and meridional gradients in water mass age, it is difficult to remove the influence of ventilation and isolate the hydrothermal scavenging magnitude. For instance, one could estimate the removal flux of ^{231}Pa (or ^{230}Th) by using the deficit of the observed

concentration profile compared to a linear profile (expected due to reversible scavenging). The expected profile however cannot be chosen *a priori*, because in a region of recent deep water ventilation one does not expect a linear profile.

Similarly, along Line W (GT11-01 thru GT11-10), dissolved ^{230}Th xs and ^{231}Pa xs concentrations are clearly depleted near the bottom (Figs. 2B, 2D) due to increased particle concentrations in nepheloid layers (Fig. 2A). Depletion of ^{230}Th and ^{231}Pa below 3.5 km depth cannot be attributed to ventilation, the conventional explanation (e.g., Luo et al., 2010), because ventilation time scales increase with depth below 3.5 km (Fig. 3E). Nonetheless, the fact that ^{230}Th and ^{231}Pa concentrations at mid-depth (1-3km) along Line W, the depth range of maximum southward NADW transport (Cunningham et al., 2007; Kanzow et al., 2010; Talley et al., 2003), are much lower than at the corresponding depths in the eastern basin at GT11-20 and GT11-22 (Fig. 2D, D), where particle concentrations (C_p values) are similar to those along Line W (Fig. 2A), seems clearly related to the east-west gradient in ventilation age. Radionuclide depletions due to bottom scavenging and recent ventilation again here seems convolved in a way that is difficult to untangle with static tracer observations.

In yet another combination of influences, dissolved ^{230}Th xs and ^{231}Pa xs concentrations both decrease toward the bottom at GT11-20 and GT11-22 at ~4 km and 2.5 km depth respectively where there is no evidence for increased particle concentrations or recent ventilation. While the deep water in the Northeast Atlantic has been long isolated from the atmosphere (>500 yrs), it may not have been this long since a significant scavenging event occurred. The northward inflow of NEADW from the Romanche Trench occurs on a timescale of 30 years based on radiocarbon distributions (Schlitzer et al., 1985). The mid-Atlantic ridge is associated with enhanced turbulent mixing because of its complex topography (Polzin et al.,

1996) and with metalliferous sediments from hydrothermal activity. Both of these factors could cause bottom scavenging of ^{230}Th and ^{231}Pa from water flowing through the gaps in the ridge, the former via resuspension of sediments and the latter by the increased scavenging efficiency of Fe-Mn oxides. A radionuclide depleted signal could then be advected northward, carrying with it its scavenging history. While this scenario is highly speculative, such are the possible interactions between deep water flow and bottom scavenging that need to be accounted for in a fuller understanding of the marine cycling of ^{230}Th and ^{231}Pa.

3.4 Apparent controls on the ^{231}Pa/^{230}Th ratio

Sensitivity tests in a scavenging-circulation ocean model, which can vary bottom scavenging intensity and ventilation ages independently, may be able to resolve the significance of each process in determining radionuclide distributions in the North Atlantic. This uncertainty notwithstanding, it is informative to inspect the section of the dissolved ^{231}Pa/^{230}Th xs ratio (Fig. 2C) with a motivation to examine its proxy applications. High ratios along the Cape Verde transect are consistent with the boundary scavenging discussed in section 3.2. In the areas of clear bottom scavenging along Line W and at the TAG hydrothermal site, the ratio is also elevated above the corresponding mid-depth values. This is because the ^{230}Th is scavenged more intensely (larger depletion from the dissolved phase) relative to ^{231}Pa at these locations. In analogy to the boundary scavenging due to lateral gradients in scavenging intensity, the bottom scavenging sites may act as small sinks for Pa, in that the imposed enhanced removal of Pa is partially compensated by greater dispersive fluxes because of its longer residence time.

The impact of ventilation on the dissolved ^{231}Pa/^{230}Th xs distribution (Fig. 2C), however, is not obvious. For instance, between 2-3 km depth (excluding GT11-16) the ^{231}Pa/^{230}Th ratio changes very little between 500 and 4200 km section distance (Fig. 2C), along which the

ventilation age has a strong lateral gradient between roughly 80 yrs in the west and 400 yrs in the east. This range in age is the exact time period in which one expects the strongest return to a steady-state of ^{231}Pa concentrations after ventilation (Gherardi et al., 2010), according to a 1-dimensional mixing-scavenging model (Moran et al., 2001; Rutgers v. d. Loeff and Berger, 1993). The dissolved ^{231}Pa/^{230}Th xs ratio of course increases further toward the African margin as ventilation age also increases, but this is primarily due to the stronger removal of dissolved ^{230}Th xs (boundary scavenging, sec. 3.2) at the eastern margin. The observed zonal gradient in dissolved ^{231}Pa/^{230}Th xs is not consistent with removal of ^{231}Pa by southward flow between 2-3 km depth, which one expects to be strongest in the west (Wunsch and Heimbach, 2006). Whether the ^{231}Pa/^{230}Th distribution is rather responding to the zonally integrated southward flow of NADW remains to be demonstrated in a 3-D dimensional circulation-scavenging model.

In the deep basins (4-6 km depth), however, likely not influenced by the African margin processes, the dissolved ^{231}Pa/^{230}Th xs ratio is clearly higher on the eastern side of the mid-Atlantic ridge, as expected from the trend in mean age (Fig. 2D), perhaps reflecting the integrated removal of ^{231}Pa (relative to ^{230}Th) by southward flow throughout the water column. Additionally, the ratio decreases with depth (below 1 km and away from bottom scavenging sites), most significantly at the deep central basin stations GT11-12 and GT11-20. The decrease with depth of the ^{231}Pa/^{230}Th ratio in the Atlantic has been suggested to reflect the southward export of ^{231}Pa by deep water circulation (Lippold et al., 2011; Luo et al., 2010). Whether this effect could also be contributed to by a change in elemental fractionation during scavenging with depth due to changing particle compositions (Moran et al., 2002) remains to be clearly demonstrated. We will address this possibility in a forthcoming study of the particulate and dissolved ^{230}Th and ^{231}Pa in comparison to the measured mass and major chemical composition

($CaCO_3$, opal, organic matter, lithogenic material and authigenic metal oxides) of the particles along this transect.

A curious, yet robust feature in the dissolved $^{231}Pa/^{230}Th$ xs transect is the structure seen in the upper 1-1.2 km. High ratios near the surface are consistent with ^{230}Th being more intensely scavenged out of the mixed layer, but a secondary subsurface maximum in dissolved $^{231}Pa/^{230}Th$ xs ratio around 1 km depth is observed at nearly every station. In the section between the mid-ocean ridge and Mauritania, the secondary dissolved $^{231}Pa/^{230}Th$ xs maximum overlaps with AAIW (cf. Fig. 1). Yet, the persistence of the $^{231}Pa/^{230}Th$ maximum in the more northern parts of the transect do not support an association with AAIW. An alternative scenario is that a high $^{231}Pa/^{230}Th$ ratios throughout shallow water (0-1200 m), related to more intense scavenging of ^{230}Th, is overprinted with the strong minimum around 500 m depth which could be related to the low ^{231}Pa content and rapid ventilation of EDW. Yet another possible scenario is that the subsurface dissolved $^{231}Pa/^{230}Th$ xs maximum is related to the preferential regeneration of dissolved ^{231}Pa released during diatom dissolution (since biogenic opal is a strong scavenger of ^{231}Pa (Chase et al., 2002)). This is not supported, however, by either the silicic acid distribution (except within AAIW, Fig. 5B) or the particulate opal distribution (Lam et al., pers. comm.). In any case, the possibility of ^{231}Pa (and perhaps $^{231}Pa/^{230}Th$) tracing shallow or intermediate water circulation is worth further attention since its longer-lived removal timescale and uniform production offers a complement to the traditional transient tracers of shallow circulation (^{3}H-^{3}He, CFC's).

As a way of summarizing these observations we cross-plot the dissolved $^{231}Pa/^{230}Th$ xs data with another potential circulation tracer measured on the same water samples, silicic acid. The silicic acid distribution along our transect (Fig. 5B) has a strong resemblance to the inverse

estimates of mean age (Fig. 2E). Silicic acid is added to deep water through the dissolution of diatom opal exported from surface water and accumulates with deep water age (Broecker and Peng, 1982). Furthermore, its distribution is sensitive to the overturning circulation since NADW has very low (preformed) silicic acid and southern-sourced waters (AABW and AAIW) have much higher end-member concentrations (Sarmiento et al., 2007). There is a wide scatter in the relationship between dissolved $^{231}Pa/^{230}Th$ xs and silicic acid (Fig. 5A) and the overall negative trend reflects that fact the $^{231}Pa/^{230}Th$ ratio generally decreases with depth while silicic acid (and ventilation age) increase with depth. At some given depths (color scheme of points in Fig. 5A), however, $^{231}Pa/^{230}Th$ may be positively related with silicic acid. For instance, around 1 km depth a positive trend possibly related to the influence of AAIW can be seen. Some of the high $^{231}Pa/^{230}Th$ values at 3-4 km depth, however, are related to locations of bottom scavenging (marked in Fig. 5A) and therefore cannot be ascribed to water mass ageing.

While a basin-sale, integrated influence of the southward export of NADW cannot be ruled out, the distribution of dissolved $^{231}Pa/^{230}Th$ appears to be insensitive to water mass age across the North Atlantic. In order to validate the use of the $^{231}Pa/^{230}Th$ ratio as a paleo-indicator of the AMOC, a more complex conceptual model needs to be developed, including the influences of boundary scavenging and bottom scavenging demonstrated here. We note that a possibly more informative investigation of the evolution the $^{231}Pa/^{230}Th$ ratio along the path of NADW circulation is currently being completed by European groups working on a meridional GEOTRACES section along the western basin of the entire Atlantic (GA02, see geotraces.org).

4. Summary

The cycling of ^{230}Th and ^{231}Pa in the ocean is complex. Deviations from the behavior expected from a simple model of reversible scavenging are apparent across the North Atlantic

and improved spatial resolution allows us to study them in greater detail than has been done before. Boundary scavenging of ^{230}Th in an exceptionally productive region off Northwest Africa was constrained to 40 ± 10 % of its water column production, helping to quantify the uncertainties associated with ^{230}Th-normalized sediment fluxes. Enhanced removal of ^{231}Pa occurs on the Africa margin as well but quantitative conclusions about the significance of this sink in the basin-scale Pa budget cannot be made without more detailed mapping of the region. Both recent ventilation and bottom scavenging cause deep-water depletions of ^{230}Th and ^{231}Pa. The dissolved ^{231}Pa/^{230}Th ratio traces locations of intense scavenging intensity while its distribution in the transect is not consistent with a simple relationship to water-mass age. We observe several examples where the effects of scavenging and ventilation are convolved which provide excellent test cases for sensitivity studies of removal mechanisms in future ocean modeling of these isotopes. Circulation and scavenging affect many trace metals of biogeochemical and paleoceanographic interest (e.g. Fe, Co, Al), and thus further constraining the cycling of ^{230}Th and ^{231}Pa will be of broad appeal in the oceanographic community.

Acknowledgements

Funding for ship time, sampling operations, and hydrographic data was provided by the U. S. National Science Foundation to the US GEOTRACES North Atlantic Transect Management team of W. Jenkins (OCE-0926423), E. Boyle (OCE-0926204), and G. Cutter (OCE-0926092). Radionuclide studies were supported by NSF (OCE-0927064 to L-DEO, OCE-0926860 to WHOI, OCE-0927757 to URI, and OCE-0927754 to UMN). The crew of the R/V *Knorr*, the Ocean Data Facility team (Mary Johnson, Rob Palomares, Susan Becker, and Courtney Schatzman), and the science team samplers for Niskin bottles and in situ pumps (Katharina Pahnke, Brett Longworth, Paul Morris, Daniel Ohnemus, Kuanbo Zhou, Sylvain

Rigaud and Stephanie Owens) are all acknowledged for their critical roles in the success of these cruises. On-shore analysis efforts of Maureen Auro, Joanne Boudreau, and the WHOI Plasma Facility are greatly appreciated. Figures 1, 2 and 5 were created using Ocean Data View (Schlitzer, 2011).

References

Andersen, M.B., Stirling, C.H., Zimmermann, B., Halliday, A.N., 2010. Precise determination of the open ocean $^{234}U/^{238}U$ composition. Geochem. Geophys. Geosyst. 11, Q12003.

Anderson, R.F., Bacon, M.P., Brewer, P.G., 1983. Removal of ^{230}Th and ^{231}Pa at ocean margins. Earth Planet. Sci. Lett. 66, 73-90.

Anderson, R.F., Fleisher, M.Q., Biscaye, P.E., Kumar, N., Dittrich, B., Kubik, P., Suter, M., 1994. Anomalous boundary scavenging in the Middle Atlantic Bight: evidence from ^{230}Th, ^{231}Pa, ^{10}Be and ^{210}Pb. Deep Sea Res. Pt. II 41, 537-561.

Anderson, R.F., Fleisher, M.Q., Robinson, L.F., Edwards, R.L., Hoff, J., Moran, S.B., Rutgers van der Loeff, M.M., Thomas, A.L., Roy-Barman, M., François, R., 2012. GEOTRACES intercalibration of ^{230}Th, ^{232}Th, ^{231}Pa, and prospects for ^{10}Be. Limnol. Oceanogr. Methods 10, 179-213.

Anderson, R.F., Lao, Y., Broecker, W.S., Trumbore, S.E., Hofmann, H.J., Wolfli, W., 1990. Boundary scavenging in the Pacific Ocean: a comparison of ^{10}Be and ^{231}Pa. Earth Planet. Sci. Lett. 96, 287-304.

Auro, M.E., Robinson, L.F., Burke, A., Bradtmiller, L.I., Fleisher, M.Q., Anderson, R.F., 2012. Improvements to 232-thorium, 230-thorium, and 231-protactinium analysis in seawater arising from GEOTRACES intercalibration. Limnol. Oceanogr.: Methods 10, 464-474.

Bacon, M.P., 1984. Glacial to interglacial changes in carbonate and clay sedimentation in the Atlantic Ocean estimated from ^{230}Th measurements. Chem. Geol. 46, 97-111.

Bacon, M.P., 1988. Tracers of chemical scavenging in the ocean: boundary effects and large-scale chemical fractionation. Philos. Trans. R. Soc. London, Ser. A 325, 147-160.

Bacon, M.P., Anderson, R.F., 1982. Distribution of thorium isotopes between dissolved and particulate forms in the deep sea. J. Geophys. Res. 87, 2045-2056.

Bacon, M.P., Rutgers v. d. Loeff, M.M., 1989. Removal of thorium-234 by scavenging in the bottom nepheloid layer of the ocean. Earth Planet. Sci. Lett. 92, 157-164.

Bacon, M.P., Spencer, D.W., Brewer, P.G., 1976. $^{210}Pb/^{226}Ra$ and $^{210}Po/^{210}Pb$ disequilibria in seawater and suspended particulate matter. Earth Planet. Sci. Lett. 32, 277-296.

Baker, E.T., Lavelle, J.W., 1984. The effect of particle size on the light attenuation coefficient of natural suspensions. J. Geophys. Res.: Oceans 89, 8197-8203.

Behrenfeld, M.J., Falkowski, P.G., 1997. Photosynthetic rates derived from satellite-based chlorophyll concentration. Limnol. Oceanogr. 42, 1-20.

Biscaye, P.E., Eittreim, S.L., 1977. Suspended particulate loads and transports in the nepheloid layer of the abyssal Atlantic Ocean. Mar. Geol. 23, 155-172.

Bishop, J.K., Lam, P.J., Wood, T.J., 2012. Getting good particles: Accurate sampling of particles by large volume in-situ filtration. Limnol. Oceanogr.: Methods 10, 681-710.

Bishop, J.K.B., 1986. The correction and suspended particulate matter calibration of Sea Tech transmissometer data. Deep Sea Res. Pt. A 33, 121-134.

Brewer, P.G., Spencer, D.W., Biscaye, P.E., Hanley, A., Sachs, P.L., Smith, C.L., Kadar, S., Fredericks, J., 1976. The distribution of particulate matter in the Atlantic Ocean. Earth Planet. Sci. Lett. 32, 393-402.

Broecker, W., 2008. Excess sediment ^{230}Th: Transport along the sea floor or enhanced water column scavenging? Global Biogeochem. Cycles 22, GB1006.

Broecker, W.S., Blanton, S., Smethie, W.M., Ostlund, G., 1991. Radiocarbon decay and oxygen utilization in the Deep Atlantic Ocean. Global Biogeochem.Cycles 5, 87-117.

Broecker, W.S., Peng, T.-H., 1982. Tracers in the Sea. Lamont-Doherty Geol. Obs., Palisades, NY.

Broecker, W.S., Takahashi, T., Stuiver, M., 1980. Hydrography of the central Atlantic—II waters beneath the Two-Degree Discontinuity. Deep Sea Res. Pt. A 27, 397-419.

Bruland, K., Lohan, M., 2003. Controls of Trace Metals in Seawater. Treatise on Geochemistry 6, 23-47.

Chase, Z., Anderson, R.F., Fleisher, M.Q., Kubik, P.W., 2002. The influence of particle composition and particle flux on scavenging of Th, Pa and Be in the ocean. Earth Planet. Sci. Lett. 204, 215-229.

Cheng, H., Edwards, R.L., Hoff, J., Gallup, C.D., Richards, D.A., Asmerom, Y., 2000. The half-lives of uranium-234 and thorium-230. Chem. Geol. 169, 17-33.

Cunningham, S.A., Kanzow, T., Rayner, D., Baringer, M.O., Johns, W.E., Marotzke, J., Longworth, H.R., Grant, E.M., Hirschi, J.J.-M., Beal, L.M., Meinen, C.S., Bryden, H.L., 2007. Temporal Variability of the Atlantic Meridional Overturning Circulation at 26.5°N. Science 317, 935-938.

Delanghe, D., Bard, E., Hamelin, B., 2002. New TIMS constraints on the uranium-238 and uranium-234 in seawaters from the main ocean basins and the Mediterranean Sea. Mar. Chem. 80, 79-93.

DeMaster, D.J., Brewster, D.C., McKee, B.A., Nittrouer, C.A., 1991. Rates of particle scavenging, sediment reworking, and longitudinal ripple formation at the HEBBLE site based on measurements of ^{234}Th and ^{210}Pb. Mar. Geol. 99, 423-444.

Francois, R., Bacon, M.P., Suman, D.O., 1990. Thorium-230 profiling in deep-sea sediments: High-resolution records of flux and dissolution of carbonate in the equatorial Atlantic during the last 24,000 years. Paleoceanography 5, 761-787.

François, R., Frank, M., Rutgers van der Loeff, M., Bacon, M.P., Geibert, W., Kienast, S., Anderson, R.F., Bradtmiller, L., Chase, Z., Henderson, G., 2007. Comment on" Do geochemical estimates of sediment focusing pass the sediment test in the equatorial Pacific?" by M. Lyle et al.

François, R., Frank, M., Rutgers van der Loeff, M.M., Bacon, M.P., 2004. ^{230}Th normalization: An essential tool for interpreting sedimentary fluxes during the late Quaternary. Paleoceanography 19, PA1018.

Gardner, W.D., Biscaye, P.E., Zaneveld, J.R.V., Richardson, M.J., 1985. Calibration and comparison of the LDGO nephelometer and the OSU transmissometer on the Nova Scotian rise. Mar. Geol. 66, 323-344.

German, C.R., Fleer, A.P., Bacon, M.P., Edmond, J.M., 1991. Hydrothermal scavenging at the Mid-Atlantic Ridge: radionuclide distributions. Earth Planet. Sci. Lett. 105, 170-181.

German, C.R., Higgs, N.C., Thomson, J., Mills, R., Elderfield, H., Blusztajn, J., Fleer, A.P., Bacon, M.P., 1993. A geochemical study of metalliferous sediment from the TAG Hydrothermal Mound, 26°08′N, Mid-Atlantic Ridge. J. Geophys. Res.: Solid Earth 98, 9683-9692.

German, C.R., Thurnherr, A.M., Knoery, J., Charlou, J.L., Jean-Baptiste, P., Edmonds, H.N., 2010. Heat, volume and chemical fluxes from submarine venting: A synthesis of results from the Rainbow hydrothermal field, 36°N MAR. Deep Sea Res. Pt. I 57, 518-527.

Gherardi, J.M., Luo, Y., Francois, R., McManus, J.F., Allen, S.E., Labeyrie, L., 2010. Reply to comment by S. Peacock on "Glacial-interglacial circulation changes inferred from ^{231}Pa/^{230}Th sedimentary record in the North Atlantic region". Paleoceanography 25, PA2207.

Hayes, C.T., Anderson, R.F., Jaccard, S.L., François, R., Fleisher, M.Q., Soon, M., Gersonde, R., 2013. A new perspective on boundary scavenging in the North Pacific Ocean. Earth Planet. Sci. Lett. 369-370, 86-97.

Henderson, G.M., Anderson, R.F., 2003. The U-series Toolbox for Paleoceanography. Rev. Mineral. Geochem. 52, 493-531.

Henderson, G.M., Heinze, C., Anderson, R.F., Winguth, A.M.E., 1999. Global distribution of the ^{230}Th flux to ocean sediments constrained by GCM modelling. Deep Sea Res. Pt. I 46, 1861-1893.

Jenkins, W.J., 1988. The Use of Anthropogenic Tritium and Helium-3 to Study Subtropical Gyre Ventilation and Circulation. Phil. Trans. R. Soc. London, Ser. A 325, 43-61.

Kanzow, T., Cunningham, S.A., Johns, W.E., Hirschi, J.J.M., Marotzke, J., Baringer, M.O., Meinen, C.S., Chidichimo, M.P., Atkinson, C., Beal, L.M., Bryden, H.L., Collins, J., 2010. Seasonal Variability of the Atlantic Meridional Overturning Circulation at 26.5°N. J. Clim. 23, 5678-5698.

Khatiwala, S., Primeau, F., Holzer, M., 2012. Ventilation of the deep ocean constrained with tracer observations and implications for radiocarbon estimates of ideal mean age. Earth Planet. Sci. Lett. 325–326, 116-125.

Krishnaswami, S., Lal, D., Somayajulu, B.L.K., Weiss, R.F., Craig, H., 1976. Large-volume in-situ filtration of deep Pacific waters: Mineralogical and radioisotope studies. Earth Planet. Sci. Lett. 32, 420-429.

Lam, P.J., Morris, P.J., Patent Pending. In situ marine sample collection system and methods, Goodwin Docket No. WHOI-005PR.

Lao, Y., Anderson, R.F., Broecker, W.S., 1992. Boundary scavenging and deep-sea sediment dating: constraints from excess ^{230}Th and ^{231}Pa. Paleoceanography 7, 783-798.

LeBel, D.A., Smethie Jr, W.M., Rhein, M., Kieke, D., Fine, R.A., Bullister, J.L., Min, D.-H., Roether, W., Weiss, R.F., Andrié, C., Smythe-Wright, D., Peter Jones, E., 2008. The formation rate of North Atlantic Deep Water and Eighteen Degree Water calculated from CFC-11 inventories observed during WOCE. Deep Sea Res. Pt. I 55, 891-910.

Ledwell, J.R., Watson, A.J., Law, C.S., 1998. Mixing of a tracer in the pycnocline. J. Geophys. Res.: Oceans 103, 21499-21529.

Legeleux, F., Reyss, J.-L., Floris, S., 1995. Entrainement des metaux vers les sediments sur les marges continentales de l'Atlantic Est. C. R. Acad. Sci. Paris 320 (serie IIa), 1195-1202.

Lippold, J., Gherardi, J.-M., Luo, Y., 2011. Testing the ^{231}Pa/^{230}Th paleocirculation proxy: A data versus 2D model comparison. Geophys. Res. Lett. 38, L20603.

Lippold, J., Luo, Y., Francois, R., Allen, S.E., Gherardi, J., Pichat, S., Hickey, B., Schulz, H., 2012a. Strength and geometry of the glacial Atlantic Meridional Overturning Circulation. Nature Geosci. 5, 813-816.

Lippold, J., Mulitza, S., Mollenhauer, G., Weyer, S., Heslop, D., Christl, M., 2012b. Boundary scavenging at the East Atlantic margin does not negate use of ^{231}Pa/^{230}Th to trace Atlantic overturning. Earth Planet. Sci. Lett. 333–334, 317-331.

Luo, Y., Francois, R., Allen, S.E., 2010. Sediment $^{231}Pa/^{230}Th$ as a recorder of the rate of the Atlantic meridional overturning circulation: insights from a 2-D model. Ocean Sciences 6, 381-400.

Lyle, M., Mitchell, N., Pisias, N., Mix, A., Martinez, J.I., Paytan, A., 2005. Do geochemical estimates of sediment focusing pass the sediment test in the equatorial Pacific? Paleoceanography 20, PA1005.

Lyle, M., Pisias, N., Paytan, A., Martinez, J.I., Mix, A., 2007. Reply to comment by R. Francois et al. on "Do geochemical estimates of sediment focusing pass the sediment test in the equatorial Pacific?": Further explorations of ^{230}Th normalization. Paleoceanography 22, PA1217.

Mangini, A., Diester-Haas, L., 1983. Excesss Th-230 in sediments off NW Africa traces upwelling in the past, in: Thiede, J., Suess, E. (Eds.), Coastal upwelling: Its Sediment Record (Part A). Plenum Press, New York, pp. 455-470.

Marchal, O., François, R., Stocker, T.F., Joos, F., 2000. Ocean thermohaline circulation and sedimentary $^{231}Pa/^{230}Th$ ratio. Paleoceanography 15, 625-641.

McCave, I.N., 1986. Local and global aspects of the bottom nepheloid layers in the world ocean. Neth. J. Sea Res. 20, 167-181.

McCave, I.N., Hall, I.R., 2002. Turbidity of waters over the Northwest Iberian continental margin. Prog. Oceanogr. 52, 299-313.

McManus, J.F., Francois, R., Gherardi, J.M., Keigwin, L.D., Brown-Leger, S., 2004. Collapse and rapid resumption of Atlantic meridional circulation linked to deglacial climate changes. Nature 428, 834-837.

Moran, S.B., Charette, M.A., Hoff, J.A., Edwards, R.L., Landing, W.M., 1997. Distribution of ^{230}Th in the Labrador Sea and its relation to ventilation. Earth Planet. Sci. Lett. 150, 151-160.

Moran, S.B., Hoff, J.A., Buesseler, K.O., Edwards, R.L., 1995. High precision ^{230}Th and ^{232}Th in the Norwegian Sea and Denmark by thermal ionization mass spectrometry. Geophys. Res. Lett. 22, 2589-2592.

Moran, S.B., Shen, C., C, Weinstein, S.E., Hettinger, L.H., Hoff, J.H., Edmonds, H.N., Edwards, R.L., 2001. Constraints on deep water age and particle flux in the equatorial and South Atlantic Ocean based on seawater ^{231}Pa and ^{230}Th data. Geophys. Res. Lett. 28, 3437-3440.

Moran, S.B., Shen, C.C., Edmonds, H.N., Weinstein, S.E., Smith, J.N., Edwards, R.L., 2002. Dissolved and particulate ^{231}Pa and ^{230}Th in the Atlantic Ocean: constraints on intermediate/deep water age, boundary scavenging, and $^{231}Pa/^{230}Th$ fractionation. Earth Planet. Sci. Lett. 203, 999-1014.

Nozaki, Y., Horibe, Y., Tsubota, H., 1981. The water column distributions of thorium isotopes in the western North Pacific. Earth Planet. Sci. Lett. 54, 203-216.

Nozaki, Y., Nakanishi, T., 1985. ^{231}Pa and ^{230}Th profiles in the open ocean water column. Deep-Sea Res. Pt. A 32, 1209-1220.

Okubo, A., Obata, H., Gamo, T., Yamada, M., 2012. ^{230}Th and ^{232}Th distributions in mid-latitudes of the North Pacific Ocean: Effect of bottom scavenging. Earth Planet. Sci. Lett. 339–340, 139-150.

Polzin, K.L., Speer, K.G., Toole, J.M., Schmitt, R.W., 1996. Intense mixing of Antarctic Bottom Water in the equatorial Atlantic Ocean. Nature 380, 54-57.

Richardson, M.J., 1987. Particle size, light scattering and composition of suspended particulate matter in the North Atlantic. Deep Sea Res. Pt. A 34, 1301-1329.

Robert, J., Miranda, C.F., Muxart, R., 1969. Mesure de la periode du protactinium-231 par microcalorimetrie. Radiochim. Acta 11, 104-108.

Robinson, L.F., Belshaw, N.S., Henderson, G.M., 2004. U and Th concentrations and isotope ratios in modern carbonates and waters from the Bahamas. Geochim. Cosmochim. Acta 68, 1777-1789.

Rona, P.A., 1980. TAG Hydrothermal Field: Mid-Atlantic Ridge crest at latitude 26°N. J. Geol. Soc. London 137, 385-402.

Rona, P.A., Thompson, G., Mottl, M.J., Karson, J.A., Jenkins, W.J., Graham, D., Mallette, M., Von Damm, K., Edmond, J.M., 1984. Hydrothermal activity at the Trans-Atlantic Geotraverse Hydrothermal Field, Mid-Atlantic Ridge crest at 26°N. J.f Geophys. Res.: Solid Earth 89, 11365-11377.

Roy-Barman, M., 2009. Modelling the effect of boundary scavenging on thorium and protactinium profiles in the ocean. Biogeosciences 6, 3091-3197.

Rutgers v. d. Loeff, M., Berger, G.W., 1993. Scavenging of ^{230}Th and ^{231}Pa near the Antarctic polar front in the South Atlantic. Deep Sea Res. Pt. I 40, 339-357.

Sarmiento, J.L., Simeon, J., Gnanadesikan, A., Gruber, N., Key, R.M., Schlitzer, R., 2007. Deep ocean biogeochemistry of silicic acid and nitrate. Global Biogeochem. Cycles 21, GB1S90.

Schlitzer, R., 1987. Renewal rates of East Atlantic deep water estimated by inversion of ^{14}C data. J. Geophys. Res.: Oceans 92, 2953-2969.

Schlitzer, R., 2011. http://odv.awi.de.

Schlitzer, R., Roether, W., Weidmann, U., Kalt, P., Loosli, H.H., 1985. A meridional ^{14}C and ^{39}Ar section in northeast Atlantic deep water. J. Geophys. Res.: Oceans 90, 6945-6952.

Schmidt, S., 2006. Impact of the Mediterranean Outflow Water on particle dynamics in intermediate waters of the Northeast Atlantic, as revealed by ^{234}Th and ^{228}Th. Mar. Chem. 100, 289-298.

Scholten, J.C., Fietzke, J., Mangini, A., Garbe-Schönberg, C.D., Eisenhauer, A., Schneider, R., Stoffers, P., 2008. Advection and scavenging: Effects on ^{230}Th and ^{231}Pa distribution off Southwest Africa. Earth Planet. Sci. Lett. 271, 159-169.

Scholten, J.C., Fietzke, J., Vogler, S., Rutgers van der Loeff, M.M., Mangini, A., Koeve, W., Waniek, J., Stoffers, P., Antia, A., Kuss, J., 2001. Trapping efficiencies of sediment traps from the deep Eastern North Atlantic: the ^{230}Th calibration. Deep Sea Res. Pt. II 48, 2383-2408.

Shen, C.-C., Cheng, H., Edwards, R.L., Moran, S.B., Edmonds, H.N., Hoff, J.A., Thomas, R.B., 2003. Measurement of Attogram Quantities of ^{231}Pa in Dissolved and Particulate Fractions of Seawater by Isotope Dilution Thermal Ionization Mass Spectroscopy. Anal. Chem. 75, 1075-1079.

Shen, C.-C., Lawrence Edwards, R., Cheng, H., Dorale, J.A., Thomas, R.B., Bradley Moran, S., Weinstein, S.E., Edmonds, H.N., 2002. Uranium and thorium isotopic and concentration measurements by magnetic sector inductively coupled plasma mass spectrometry. Chem. Geol. 185, 165-178.

Shen, C.-C., Wu, C.-C., Cheng, H., Lawrence Edwards, R., Hsieh, Y.-T., Gallet, S., Chang, C.-C., Li, T.-Y., Lam, D.D., Kano, A., Hori, M., Spötl, C., 2012. High-precision and high-resolution carbonate ^{230}Th dating by MC-ICP-MS with SEM protocols. Geochim. Cosmochim. Acta 99, 71-86.

Shimmield, G.B., Murray, J.W., Thomson, J., Bacon, M.P., Anderson, R.F., Price, N.B., 1986. The distribution and behaviour of ^{230}Th and ^{231}Pa at an ocean margin, Baja California, Mexico. Geochim. Cosmochim. Acta 50, 2499-2507.

Siddall, M., Anderson, R.F., Winckler, G., Henderson, G.M., Bradtmiller, L.I., McGee, D., Franzese, A., Stocker, T.F., Müller, S.A., 2008. Modeling the particle flux effect on distribution of ^{230}Th in the equatorial Pacific. Paleoceanography 23, PA2208.

Singh, A.K., Marcantonio, F., Lyle, M., 2013. Water column ^{230}Th systematics in the eastern equatorial Pacific Ocean and implications for sediment focusing. Earth Planet. Sci. Lett. 362, 294-304.

Speer, K.G., 1989. a forced baroclinic vortex around a hydrothermal plume. Geophysical Research Letters 16, 461-464.

Spencer, D.W., Bacon, M.P., Brewer, P.G., 1981. Models of the distribution of ^{210}Pb in a section across the North Equatorial Atlantic Ocean. J. Mar. Res. 39, 119-138.

Suman, D.O., Bacon, M.P., 1989. Variations in Holocene sedimentation in the North American Basin determined from ^{230}Th measurements. Deep Sea Res. Pt. A 36, 869-878.

Talley, L.D., 1999. Some aspects of ocean heat transport by the shallow, intermediate and deep overturning circulations, Mechanisms of Global Climate Change at Millenial Time Scales, Geophys. Monogr. Amer. Geophy. Union, pp. 1-22.

Talley, L.D., Reid, J.L., Robbins, P.E., 2003. Data-Based Meridional Overturning Streamfunctions for the Global Ocean. J. Clim. 16, 3213-3226.

Thorpe, S., 1972. A sediment cloud below the Mediterranean outflow. Nature 239, 326-327.

Toole, J.M., Curry, R.G., Joyce, T.M., McCartney, M., Peña-Molino, B., 2011. Transport of the North Atlantic Deep Western Boundary Current about 39°N, 70°W: 2004–2008. Deep Sea Res. Pt. II 58, 1768-1780.

Tsuchiya, M., 1989. Circulation of the Antarctic Intermediate Water in the North Atlantic Ocean. J. Mar. Res. 47, 747-755.

Turnewitsch, R., Reyss, J.-L., Nycander, J., Waniek, J.J., Lampitt, R.S., 2008. Internal tides and sediment dynamics in the deep sea—Evidence from radioactive $^{234}Th/^{238}U$ disequilibria. Deep Sea Res. Pt. I 55, 1727-1747.

Turnewitsch, R., Springer, B.M., 2001. Do bottom mixed layers influence 234Th dynamics in the abyssal near-bottom water column? Deep Sea Res. Pt. I 48, 1279-1307.

Venchiarutti, C., Jeandel, C., Roy-Barman, M., 2008. Particle dynamics study in the wake of Kerguelen Island using thorium isotopes. Deep Sea Research Part I: Oceanographic Research Papers 55, 1343-1363.

Vogler, S., Scholten, J., Rutgers van der Loeff, M., Mangini, A., 1998. ^{230}Th in the eastern North Atlantic: the importance of water mass ventilation in the balance of ^{230}Th. Earth Planet. Sci. Letters 156, 61-74.

Walter, H.-J., Rutgers v. d. Loeff, M.M., Francois, R., 1999. Reliability of the $^{231}Pa/^{230}Th$ Activity Ratio as a Tracer for Bioproductivity of the Ocean, in: Fischer, W., Wefer, G. (Eds.), Use of Proxies in Paleoceanography: Examples for the South Atlantic. Springer-Verlag, Berlin, pp. 393-408.

Weyer, S., Anbar, A.D., Gerdes, A., Gordon, G.W., Algeo, T.J., Boyle, E.A., 2008. Natural fractionation of $^{238}U/^{235}U$. Geochim. Cosmochim. Acta 72, 345-359.

Wunsch, C., Heimbach, P., 2006. Estimated Decadal Changes in the North Atlantic Meridional Overturning Circulation and Heat Flux 1993–2004. J. Phys. Oceanogr. 36, 2012-2024.

Yang, H.-S., Nozaki, Y., Sakai, H., Masuda, A., 1986. The distribution of ^{230}Th and ^{231}Pa in the deep-sea surface sediments of the Pacific Ocean. Geochim. Cosmochim. Acta 50, 81-89.

Yu, E.-F., Francois, R., Bacon, M.P., 1996. Similar rates of modern and last-glacial ocean thermohaline circulation inferred from radiochemical data. Nature 379, 689-694.

Yu, E.-F., Francois, R., Bacon, M.P., Fleer, A.P., 2001. Fluxes of ^{230}Th and ^{231}Pa to the deep sea: implications for the interpretation of excess ^{230}Th and $^{231}Pa/^{230}Th$ profiles in sediments. Earth Planet. Sci. Lett. 191, 219-230.

Zenk, W., Klein, B., Schroder, M., 1991. Cape Verde Frontal Zone. Deep Sea Res. Pt. A 38, Supplement 1, S505-S530.

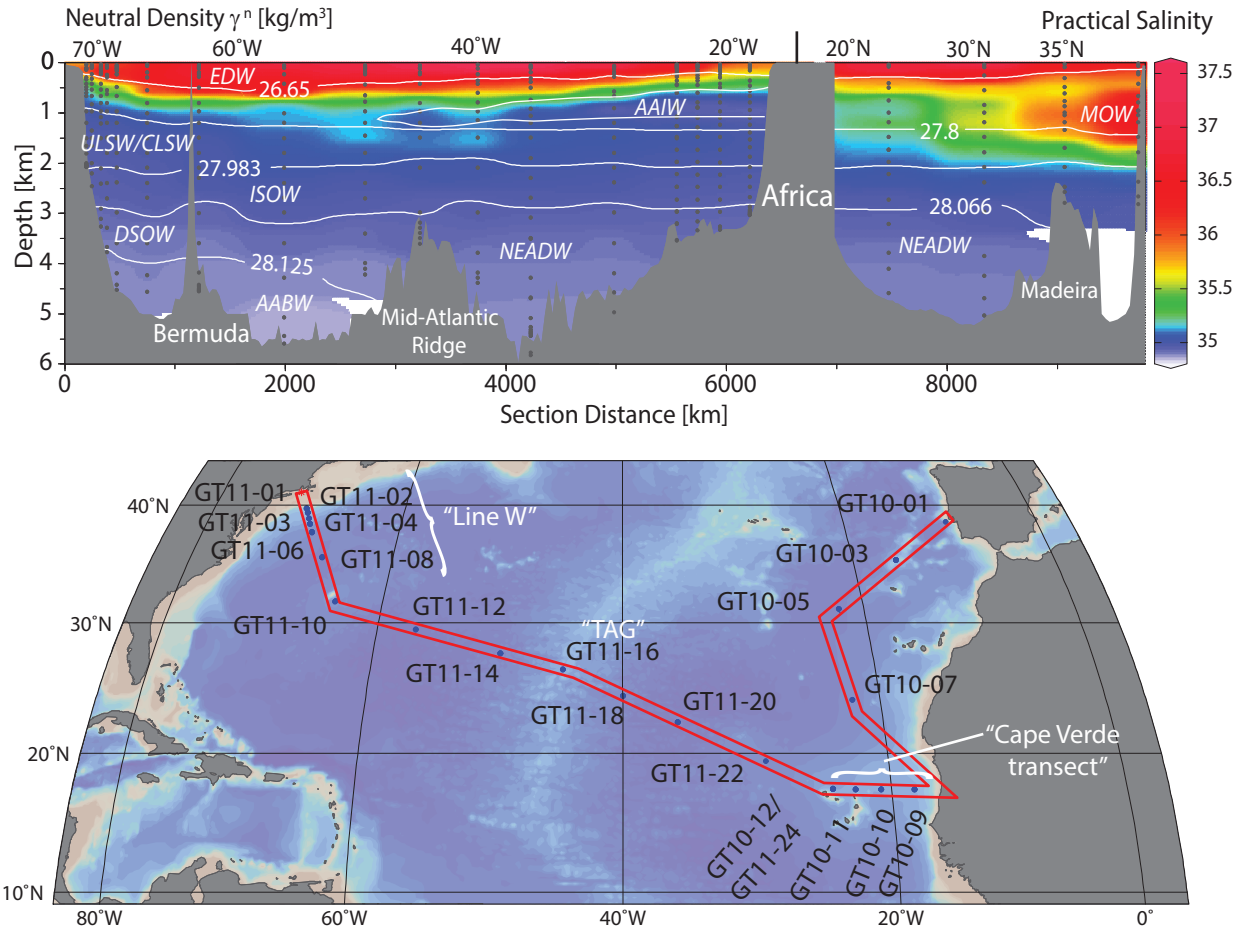

Figure 1. Map of the US GEOTRACES North Atlantic transect and section of salinity as measured in the Niskin bottle rosette casts. Neutral density overlays define, in order of increasing density, the bottom of Eighteen Degree Water (EDW), Upper and Classic Labrador Sea Water (ULSW/CLSW), Iceland-Scotland Overflow Water (ISOW), Denmark-Strait Overflow Water (DSOW) and Antarctic Bottom Water (AABW), defined largely for the western basin by Toole et al. (2010) and LeBel et al. (2008). The deep (>3 km) eastern basin is filled with a more homogeneous water mass named Northeast Atlantic Deep Water (NEADW) (Schlitzer et al., 1985). The southeastern section is influenced by Antarctic Intermediate Water (AAIW) at about ~1 km depth and the northeastern margin is clearly influenced by the high salinity Mediterranean Outflow Water (MOW). Station names are referred to in the text as labeled here.

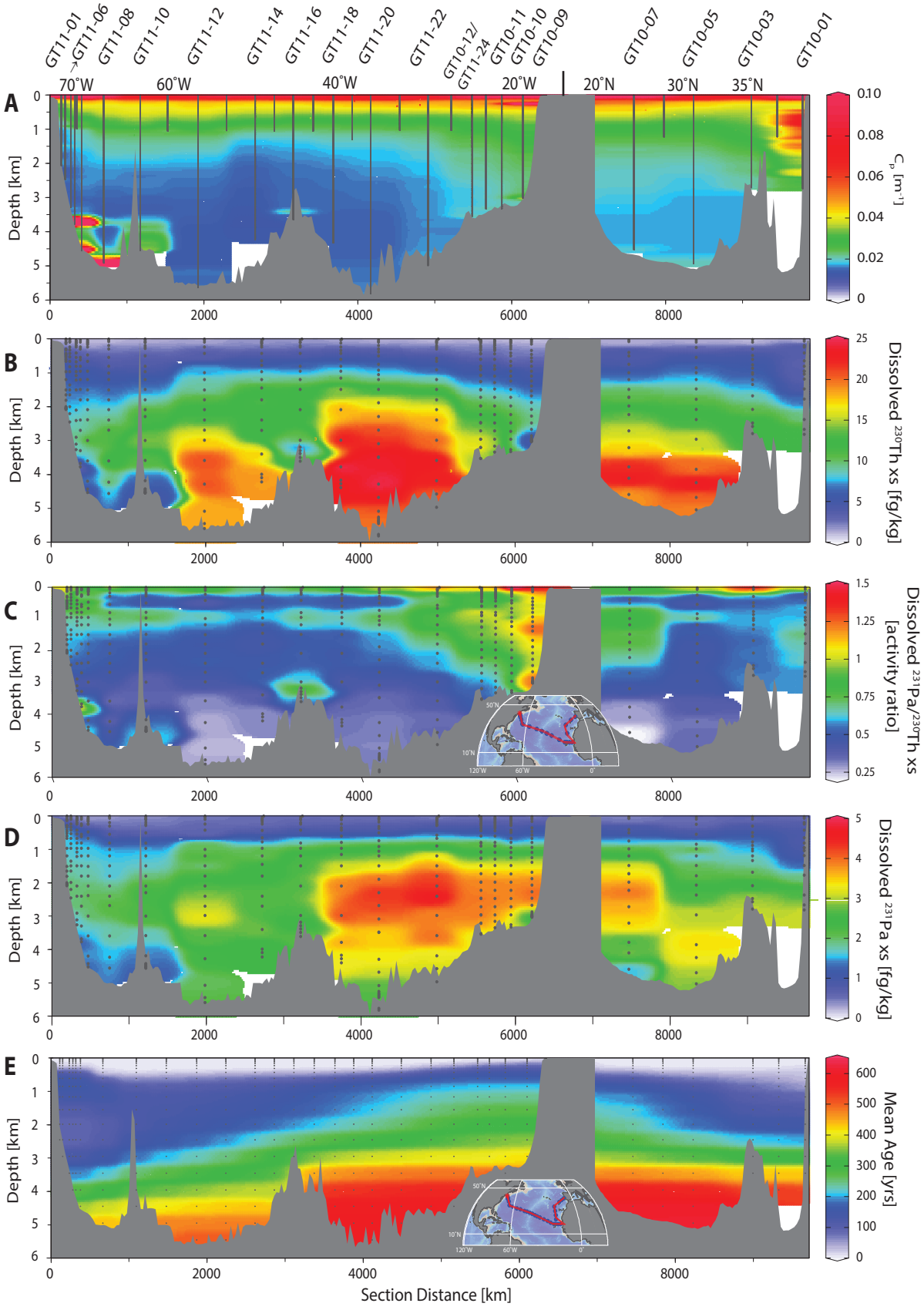
GT11-01
GT11-06
GT11-08
GT11-10
GT11-12
GT11-14
GT11-16
GT11-18
GT11-20
GT11-22
GT10-12/
GT11-24
GT10-11
GT10-10
GT10-09
GT10-07
GT10-05
GT10-03
GT10-01
70°W
60°W
40°W
20°W
20°N
30°N
35°N
A
B
C
D
E
Depth [km]
Section Distance [km]
0
2000
4000
6000
8000
C_p [m^{-1}]
0.10
0.08
0.06
0.04
0.02
Dissolved ^{230}Th xs [fg/kg]
25
20
15
10
5
Dissolved ^{231}Pa/^{230}Th xs [activity ratio]
1.5
1.25
1
0.75
0.5
0.25
Dissolved ^{231}Pa xs [fg/kg]
Mean Age [yrs]
600
500
400
300
200
100

Figure 2. (previous page) Property sections of the US GEOTRACES North Atlantic transect. (A) Particle beam attenuation coefficient, C_p, determined by transmissometer. CTD casts are marked in black. (B) Dissolved (<0.45 μm) ^{230}Th, (C) ^{231}Pa/^{230}Th activity ratio, and (D) ^{231}Pa. Black dots indicate discrete measurements. (E) Mean age of seawater since being at the surface as estimated by Khatiwala et al. (2012) Station locations for radioncuclide data are as labeled in the map of Figure 1. Panels A and E, in addition, have data from shallow "demi" stations occupied in between full depth stations, as plotted in the inset map of panel E. See Fig. 1 for neutral density surfaces not included here for clarity.

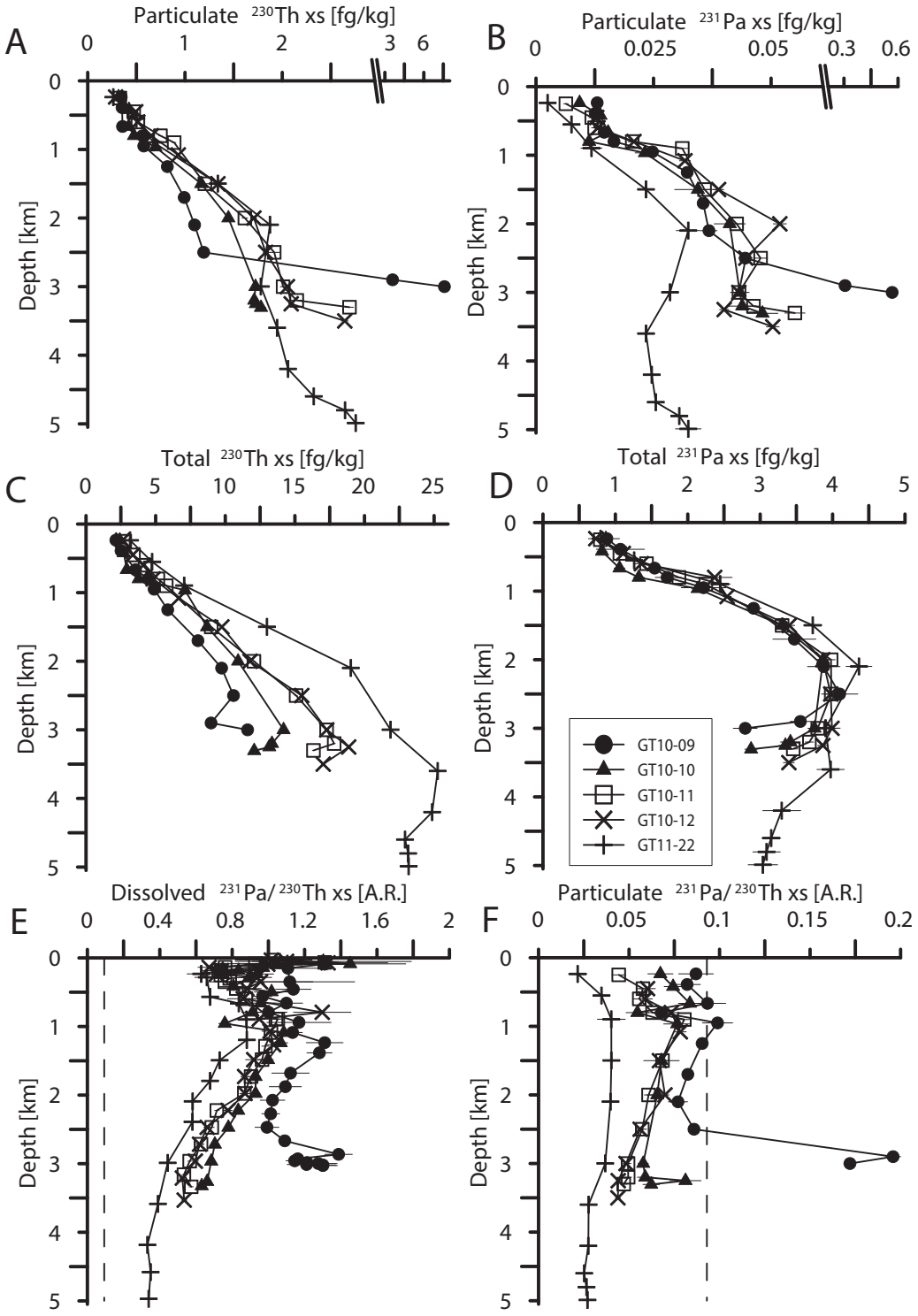

Figure 3. Depth profiles of particulate (0.45-51 μm) (A, B) and total (C, D) ^{230}Th xs and ^{231}Pa xs and the dissolved (<0.45 μm) (E) and particulate (F) ^{231}Pa/^{230}Th xs ratio from stations along a zonal transect between Mauritania and west of Cape Verde. The dashed lines in (E) and (F) represent the activity ratio of ^{231}Pa/^{230}Th produced by uranium decay (0.093). Legend relates station names as located in Figure 1.

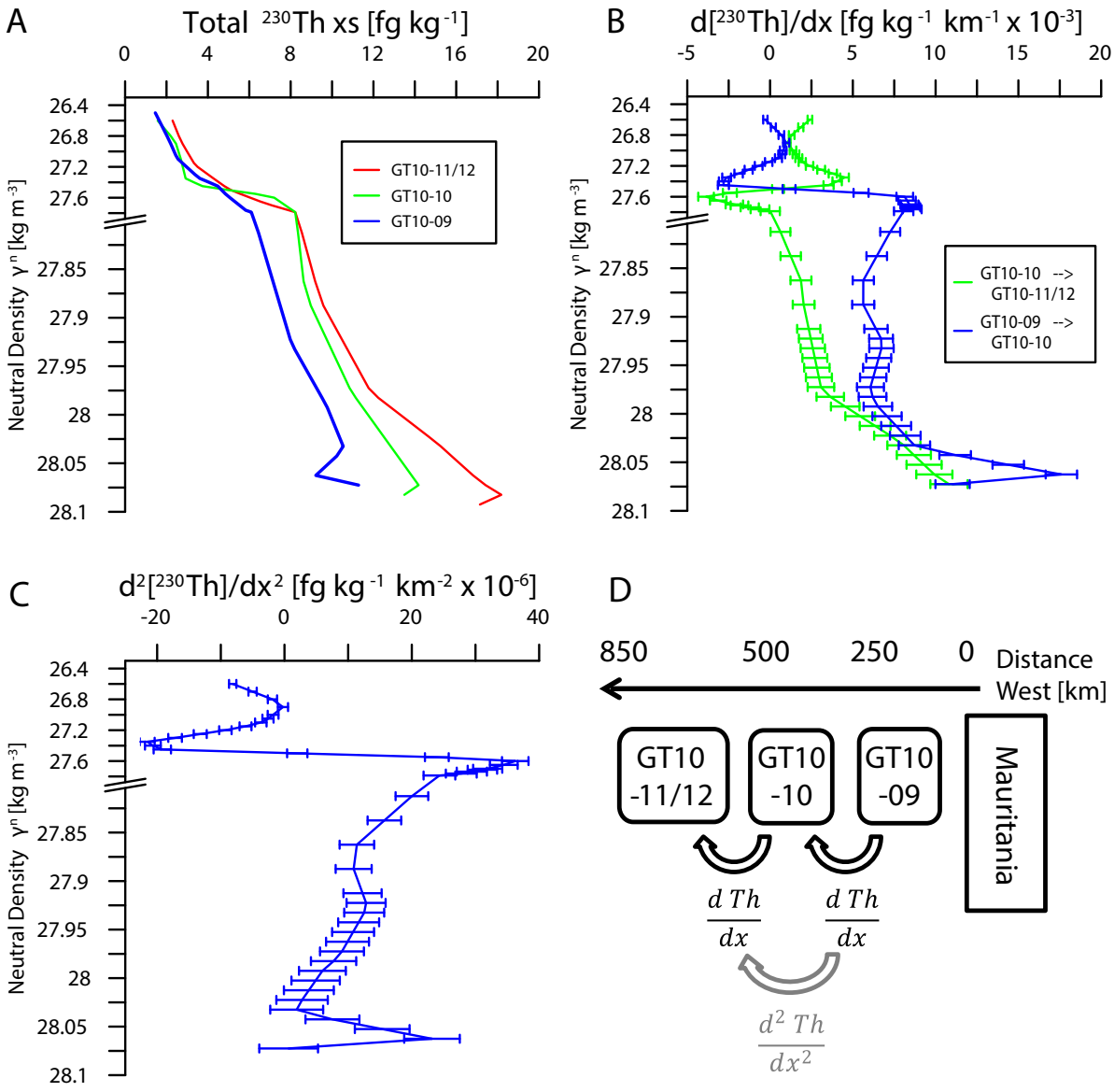

Figure 4. (A) Depth profiles of total ^{230}Th interpolated onto a common set of isopycnal surfaces. (B) Discretely calculated lateral concentration gradients in total ^{230}Th. Units are fg x 10^{-3} radionuclide per kilogram seawater per kilometer distance (C) Discretely calculated second lateral concentration gradient in total ^{230}Th. Units are fg x 10^{-6} radionuclide per kilogram seawater per square kilometer (D) Schematic demonstrating the concept of calculating lateral gradients using the concentration difference between depth profiles and the distance separating the profile locations along the Cape Verde transect.

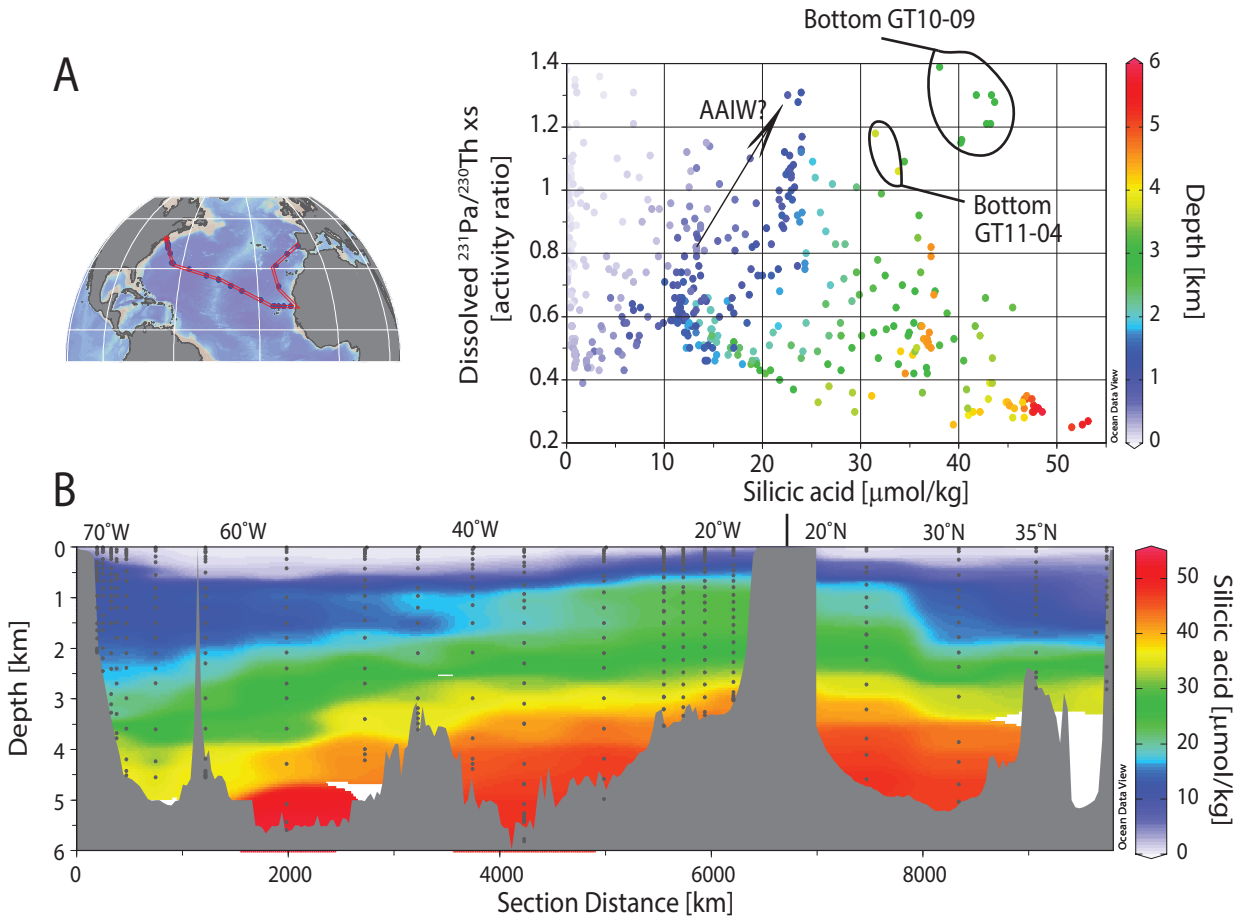

Figure 5. (A) Dissolved ^{231}Pa/^{230}Th xs ratios versus silicic acid measured in the same samples. The arrow indicates a possible positive trend between ^{231}Pa/^{230}Th xs ratios and silicic acid carried by Antarctic Intermediate Water (AAIW). The circled points represent locations of bottom scavenging which causes elevated ^{231}Pa/^{230}Th xs ratios which are unrelated to the circulation patterns traced by silicic acid (B) Silicic acid distribution along the North Atlantic transect.

Chapter 5. Scavenging intensity and fractionation of ^{230}Th and ^{231}Pa in the North Atlantic Ocean: results from the GEOTRACES transect

Christopher T. Hayes[a,b,] Robert F. Anderson[a,b], Martin Q. Fleisher[a], Phoebe J. Lam[c], Daniel C. Ohnemus[c], Kuo-Fang Huang[d], Laura F. Robinson[c,e], Yanbin Lu[f], Hai Cheng[f,g], R. Lawrence Edwards[f], S. Bradley Moran[h]

[a]Lamont-Doherty Earth Observatory of Columbia University, Palisades, NY, USA
[b]Department of Earth & Environmental Sciences, Columbia University, New York, NY, USA
[c]Department of Marine Chemistry & Geochemistry, Woods Hole Oceanographic Institution, Woods Hole, MA, USA
[d]Department of Geology & Geophysics, Woods Hole Oceanographic Institution, Woods Hole, MA, USA
[e]School of Earth Sciences, University of Bristol, Bristol, United Kingdom
[f]Department of Earth Sciences, University of Minnesota, Minneapolis, MN, USA
[g]Institute of Global Environmental Change, Xi'an Jiaotong University, Xi'an, China
[h]Graduate School of Oceanography, University of Rhode Island, Narragansett, RI, USA

In preparation for Deep Sea Research, Part II

Abstract

There is a need for a better understanding of the scavenging behavior of the radiogenic isotopes ^{231}Pa and ^{230}Th in the ocean in order to fully validate their use as proxies in the sediment record and the water column. As one example, particulate ^{231}Pa/^{230}Th ratios are interpreted to reflect either ocean ventilation or changes in the composition of settling particles. We address the second of these possibilities through direct measurements of dissolved (<0.45 μm) and particulate (0.45-51 μm) ^{231}Pa/^{230}Th, along with major particle composition, from the U. S. GEOTRACES transect across the North Atlantic. These measurements allow calculation of distribution coefficients and fractionation factors which are independent of ocean circulation. We find elevated scavenging intensities of both Th and Pa in a hydrothermal plume at the Mid-Atlantic ridge and near the seafloor off the coast of West Africa, indicating a high scavenging efficiency for authigenic Fe/Mn oxides. Biogenic opal was not a significant scavenging phase for either element, essentially because of its low abundance in the water column, although this may be a result of synoptic sampling. Distribution coefficients in shallow (< 200 m) depths are anomalously low which suggests either the unexpected result of a low scavenging intensity for organic matter or that, in water masses containing abundant organic-rich particles, a greater percentage of scavenged radionuclides exist in the colloidal phase.

1. Introduction

The natural radionuclides ^{230}Th and ^{231}Pa are used for a variety of purposes in the ocean because of their uniform production due to U decay, their tendencies to rapidly adsorb to particles (scavenging), and their sensitivity to ocean ventilation (Henderson and Anderson, 2003). Although the chemical mechanism for this is not known, it is clear from radioactive disequilibria with their parent U isotopes that Pa is removed by scavenging more slowly than Th (Sackett, 1960). This overall differential in scavenging intensity is the key feature in their water column behavior which forms the basis of using the scavenged ^{231}Pa/^{230}Th ratio (written as Pa/Th in the text as shorthand) as a paleo-indicator of the strength of the Atlantic meridional overturning circulation (AMOC) (François, 2007; McManus et al., 2004; Yu et al., 1996).

However, it has also been shown that scavenging intensity for both elements can vary with particle type in the ocean (Anderson et al., 1983b; Chase et al., 2002; Walter et al., 1999) and in laboratory experiments (Geibert and Usbeck, 2004; Guo et al., 2002a; Luo and Ku, 1999). Changing proportions of different particle types over geologic time may overprint other influences on the Pa/Th sediment record such as the AMOC. While previous work has demonstrated a particle composition effect on Pa/Th scavenging, there is still debate about what are the major carrier phases (Chase and Anderson, 2004; Luo and Ku, 2004; Roy-Barman et al., 2009) and the importance of chemical fractionation during scavenging on basin-wide radionuclide budgets (Lippold et al., 2012; Luo et al., 2010; Siddall et al., 2007). Here we present measurements of dissolved and particulate (adsorbed) ^{230}Th and ^{231}Pa from the U. S. GEOTRACES North Atlantic transect in conjunction with measurements of the mass and major chemical composition of the suspended particles, to calculate scavenging intensities and the

degree to which Pa and Th are fractionated during scavenging in a basin-wide, analytically-consistent context.

2. Approach

The chemical composition of particles in the ocean has regional variations due to differential inputs (e.g., proximity to lithogenic sources, contrasting biological communities, etc.) and depth-dependent variations due to the dissolution or regeneration of particles due to thermodynamic and biological factors. Thus, we here utilize the U. S. North Atlantic GEOTRACES transect (Fig. 1) in an observational study of scavenging intensities across natural variations in particle compositions. Completed in two cruises, KN199-4 (GT10) and KN204-1 (GT11), the dissolved (<0.45 μm) radionuclide (^{230}Th, ^{231}Pa) data, produced by 3 collaborating labs, has been described previously in a basin-wide context (Chapter 4). The particulate (0.45-51 μm) radionuclide data presented here were produced solely at the Lamont-Doherty Earth Observatory of Columbia University. The dissolved samples were analyzed at 16-24 depths per station and the particulate samples at 12 depths per stations. If not within 10 m in the upper 1 km or within 50 m below 1 km, we linearly interpolated the particulate radionuclide profile onto the dissolved radionuclide depths for better comparison.

The composition (and mass) of particles collected in-situ on the cruise was analyzed by Phoebe Lam's group at the Woods Hole Oceanographic Institution. Briefly, separate analytical procedures were performed to measure the lithogenic material (lith), particulate organic matter (POM), calcium carbonate ($CaCO_3$), biogenic opal (opal), and authigenic $Fe(OH)_3$ and MnO_2. Lithogenic material was based on particulate Ti and a continental crustal Ti concentration, and the authigenic Fe and Mn phases were determined by the excess of particulate Fe and Mn over that expected from crustal Fe/Ti and Mn/Ti ratios. The chemical weights of each component

were then added to estimate the total suspended particulate matter (SPM) concentration for each filter sample.

The basic intensity parameter for scavenging is the distribution coefficient, K_d. This is defined (for Th in Eq. 1, but similarly for Pa), as the ratio of the adsorbed radionuclide to dissolved radionuclide per unit seawater (sometimes called K), normalized by the suspended matter concentration. K_d here is expressed as atoms radionuclide per gram of particulate matter over atoms radionuclide per gram of seawater (g/g). We emphasize that K_d is operationally defined in terms of its size partitioning. If the radionuclides are to any great extent adsorbed/complexed with a colloidal phase (smaller than 450 nm), the operationally defined "dissolved" concentration will be an overestimate of the truly dissolved or soluble radionuclide concentration and the particulate radionuclide may be underestimated. The apparent K_d will be biased low.

$$K_d(Th) = \frac{Th_{xs}^{p}}{Th^{d}} \times \frac{1}{SPM} = K(Th) \times \frac{1}{SPM} \qquad \left[Units: \frac{Th\ per\ g\ particles}{Th\ per\ g\ seawater}\right] \qquad \text{(Eq. 1)}$$

The adsorbed ^{230}Th is considered as the particulate ^{230}Th which is found in excess (xs) of that supported by U decay in the particulate lithogenic material. The measured particulate ^{230}Th is corrected for by a supported fraction based on measured particulate ^{232}Th (as a proxy for particulate U), and a ^{230}Th/^{232}Th ratio representative of lithogenic material. Using particulate ^{232}Th to correct for supported ^{230}Th has the advantage over using ^{234}U directly because water column particulate U contains an authigenic component (Anderson, 1982) which is difficult to independently estimate. However, not all of the measured particulate ^{232}Th is representative of lithogenic material either, as some of the ^{232}Th is in the adsorbed phase (Robinson et al., 2008). In the correction for supported ^{230}Th, one can take into account an adsorbed fraction of ^{232}Th, f(ads. ^{232}Th) (Eq. 2).

$$^{230}Th^{p}_{xs} = {}^{230}Th^{p}_{meas} - \left(\frac{^{230}Th}{^{232}Th}\right)_{litho} \times [1 - f(ads.\ {}^{232}Th)] \times {}^{232}Th^{p}_{meas} \qquad \text{(Eq. 2)}$$

The adsorbed fraction of ^{232}Th is estimated by making an assumption that the two Th isotopes, ^{230}Th and ^{232}Th, should be subject to the same scavenging intensity, as defined by K(Th) in Eq. 1. In this way, the adsorbed component of ^{232}Th is equal to the Th distribution coefficient multiplied by the measured dissolved ^{232}Th, which divided by the total particulate ^{232}Th, gives the adsorbed fraction of ^{232}Th (Eq. 3).

$$f(ads.\ {}^{232}Th) = \frac{K(Th) \times {}^{232}Th^{d}}{{}^{232}Th^{p}_{meas}} = \frac{{}^{230}Th^{p}_{xs}}{{}^{230}Th^{d}} \times \frac{{}^{232}Th^{d}}{{}^{232}Th^{p}_{meas}} \qquad \text{(Eq. 3)}$$

By substituting Eq. 3 into Eq. 2, the adsorbed ^{230}Th can be solved for explicitly (Eq. 4).

$$^{230}Th^{p}_{xs} = \frac{{}^{230}Th^{p}_{meas} - \left(\frac{^{230}Th}{^{232}Th}\right)_{litho} \times {}^{232}Th^{p}_{meas}}{1 - \left(\frac{^{230}Th}{^{232}Th}\right)_{litho} \times \frac{^{232}Th^{d}}{^{230}Th^{d}}} \qquad \text{(Eq. 4)}$$

To calculate the adsorbed ^{231}Pa (Eq. 5), we use a lithogenic ^{231}Pa/^{232}Th ratio, and the adsorbed fraction of ^{232}Th calculated from Eq. 3. The fractions of particulate ^{230}Th and ^{231}Pa supported by decay in lithogenic material ranged from 0-32% and 0-37% respectively depending on water depth (adsorbed concentrations generally increase with water depth) and lithogenic content. The fraction of particulate ^{232}Th in the adsorbed phase was 30-40% in most cases, consistent with previous estimates (Robinson et al. 2008).

$$^{231}Pa^{p}_{xs} = {}^{231}Pa^{p}_{meas} - \left(\frac{^{231}Pa}{^{232}Th}\right)_{litho} \times [1 - f(ads.\ {}^{232}Th)] \times {}^{232}Th^{p}_{meas} \qquad \text{(Eq. 5)}$$

In order to statistically interpret the variations in K_d values with respect to particle composition, we consider each measured K_d a linear sum of contributions from each major particle phase (lith, $CaCO_3$, opal, POM, $Fe(OH)_3$, MnO_2) (cf. Li, 2005). Each contribution is the

product of the K_d for a pure end-member phase (unknown), weighted by its fraction of the total mass of a particle sample (Eq. 6).

$$K_d = f(lith) * K_d^{lith} + f(CaCO_3) * K_d^{CaCO_3} + f(opal) * K_d^{opal} + f(POM) * K_d^{POM}$$
$$+ f(Fe(OH)_3) * K_d^{Fe(OH)_3} + f(MnO_2) * K_d^{MnO_2} \quad \text{(Eq. 6)}$$

This is done for each particle sample (e.g., sample 1, 2, 3, … in Eq. 7) and the pure end-member K_d's can be solved for using a non-negative least-squares regression (since a negative K_d is not physically meaningful).

$$\begin{bmatrix} K_d^1 \\ K_d^2 \\ K_d^3 \\ \dots \end{bmatrix} = \begin{bmatrix} K_d^{lith} \\ K_d^{CaCO_3} \\ K_d^{opal} \\ K_d^{POM} \\ K_d^{Fe(OH)_3} \\ K_d^{MnO_2} \end{bmatrix} \times \begin{bmatrix} f(lith)^1 & f(CaCO_3)^1 & f(opal)^1 & f(POM)^1 & f(Fe(OH)_3)^1 & f(MnO_2)^1 \\ f(lith)^2 & f(CaCO_3)^2 & f(opal)^2 & f(POM)^2 & f(Fe(OH)_3)^2 & f(MnO_2)^2 \\ f(lith)^3 & f(CaCO_3)^3 & f(opal)^3 & f(POM)^3 & f(Fe(OH)_3)^3 & f(MnO_2)^3 \\ & & & \dots & & \end{bmatrix} \quad \text{(Eq. 7)}$$

Finally, we estimate the degree to which Th and Pa are fractionated during scavenging using the fractionation factor, F(Th/Pa) (Anderson et al., 1983b), which is the intensity of Th scavenging relative to that of Pa (Eq. 8) or ratio of the corresponding K_d's. Note that in calculating F(Th/Pa) from the definition of K_d given in equation 1, the SPM term will cancel. Thus the fractionation factor is independent of particle concentration and should be a function only of particle composition. F may, however, be subject to a bias related to size-partitioning if Th and Pa exist in a colloidal phase at differing proportions.

$$F\left(\frac{Th}{Pa}\right) = \frac{K_d(Th)}{K_d(Pa)} = \frac{Th_{xs}^p}{Th^d} \div \frac{Pa_{xs}^p}{Pa^d} \quad \text{(Eq. 8)}$$

Fractionation factors for specific particle types have been determined using experimental techniques or in locations dominated by certain phases. There are large variations in the results (see compilation by Roberts et al. (2009)) but somewhat of a consensus view is that biogenic opal and Fe/Mn oxide phases scavenge Th and Pa with the same intensity, F(Th/Pa) ~ 1. Most

other phases such as clays or calcium carbonate are believed to greatly prefer scavenging of Th, F(Th/Pa) ~ 10-20. There has been no consensus on the fractionation associated with scavenging by organic matter. We attempt to estimate phase-specific fractionation factors in this study as well using the end-member K_d's from the described statistical regression.

3. Results

3.1 Distribution coefficient estimates

We first examine the depth distribution of the K_d measurements for the North Atlantic transect stations (Fig. 2). The K_d profile has logarithmic changes of a similar structure with depth for both elements. The lowest K_d's are found in the upper 400 m. Below 500 m depth, except for near bottom anomalies of elevated values at GT10-09 and GT11-16, the K_d is largely uniform with depth, ~2-3 x 10^7 g/g for Th and 1-2 x 10^6 g/g for Pa.

In Figure 3 we put the K_d observations into the context of particle concentration and composition before proceeding with the statistical analysis in Sec. 4.1. We have sorted the data by increasing K_d(Th) (Fig. 3A) and use this same order to show the percent-weight composition of the major particle components (Fig. 3B) and the SPM for each sample (Fig. 3C). With a few exceptions, the particle samples are primarily mixtures of lithogenic material, $CaCO_3$, and POM. Opal was consistently a relatively minor component (0-14% by weight). Generally, increasing K_d values are associated with increasing lithogenic content, decreasing POM content, and decreasing SPM. Whether these general trends are related to true differences in the scavenging characteristics of the different particle types or to biases in our K_d estimates due to an increased proportion of colloidal Th and Pa at higher POM and SPM contents will be addressed in Sec. 4.2.

The near-bottom elevated K_d values (~10^8 g/g for Th and 10^7 g/g for Pa, Fig. 2), on the other hand, can be immediately associated with unique particle chemistry (Fig. 3, sample

numbers 106-113). At GT11-16, also known as the TAG hydrothermal site, a hydrothermal plume was observed at ~3.3 km depth and the particulate material in and surrounding it were 9-51% authigenic Fe hydroxide by weight (but interestingly little Mn oxide enrichment was observed). At station GT10-09 near Mauritania, two near-bottom samples were taken within a layer of resuspended sediments containing 2-3% each of $Fe(OH)_3$ and MnO_2. Metal oxide enrichments clearly enhance the scavenging of both Th and Pa.

Another interesting anomaly in this dataset comes from the bottom 2 samples of GT11-04 where a relatively particle-laden nepheloid layer (SPM = 730-1200 µg/L) of resuspended sediments (70% lithogenics) was observed. Despite SPM values orders of magnitude above the oceanic background (5-10 µg/L), the measured K_d values for Th and Pa were still in the typical range observed in deep water (Fig. 2).

3.2 Fractionation factor F(Th/Pa) estimates

The fact that the relative changes in K_d(Th) and K_d(Pa) values track each other quite closely (Fig 2, Fig. 3A) is representative of a relatively uniform fractionation factor across the transect (10-20, mean ~15). There is nonetheless a significant trend of the fractionation factor with depth (Fig. 4). The highest F(Th/Pa) values are found shallower than 1 km depth, particularly for the more interior sites (GT10-07, GT11-12, GT11-16, and GT11-22). The shallow water (< 1 km), however, also has the greatest variability and analytical uncertainty (>50% in some cases) in fractionation factor. The analytical uncertainty is large in part because error propagation in calculating F(Th/Pa) results in the compounding of analytical error from 4 separate analyses (Eq. 8). The largest contributor to the error (in shallow waters especially) is from the particulate ^{231}Pa analysis for which the sample size (<2 fg ^{231}Pa) approaches our limit of detection as defined by 3 standard deviations of ^{231}Pa in filter blanks (0.25 fg ^{231}Pa).

The fractionation factor below 1 km depth, generally decreases with depth for nearly all stations (Fig. 4) as has been observed in the equatorial and south Atlantic (Moran et al., 2002). The lowest F(Th/Pa) values obtained are 6-7 in the Fe and Mn oxide enrichment at the bottom of GT10-09. Interestingly there is a sharp increase in F(Th/Pa) in the heavily particle-laden nepheloid layer at GT11-04, possibly indicating high fractionation associated with the predominantly lithogenic particles there. That the fractionation factor generally decreases with depth is a reflection of the character of the scavenging particles having an increasing affinity to scavenge Pa relative to Th. Although throughout the whole water column Th is clearly preferentially scavenged over Pa by a factor of more than 7 at these sites, the preferential scavenging of Th over Pa is reduced with depth. Either the deep particles have a smaller affinity to scavenge Th or a greater affinity to scavenge Pa, the latter appearing more consistent with the K_d data (Fig. 2). Whether this can be clearly related to a distinction in particle composition is most adequately determined with the described statistical regression of K_d values (Sec. 4).

We put our fractionation factor observations into a basin-wide context with previously published results in Figure 5. Plotting all the water column observations as a function of latitude, one can see that throughout the (sub)tropical Atlantic (40°N-40°S) the fractionation factor is nearly always above 5. The results from the equatorial and subtropical South Atlantic (Moran et al., 2002; Scholten et al., 2008) have a range in F(Th/Pa) which is consistent with that observed in the North Atlantic transect. It appears that only at high latitudes (Labrador Sea, Moran et al., 2002; and south of 50°S, Walter et al., 1997) does F(Th/Pa) become lower than 5. Lower fractionation factors at high latitudes have been attributed to increased contents of biogenic opal (Moran et al., 2002; Walter et al., 1999) presumably because diatoms are more prevalent in nutrient-rich, (sub)polar waters.

If the lower F(Th/Pa) values at high latitudes are assumed to result from increased K_d(Pa), one can infer a longer water column residence time for Pa throughout the (sub)tropical Atlantic (because it is removed less intensely there). This would mean that mid- and low-latitude Pa is more sensitive than high latitude Pa to redistribution by circulation, either by advection or eddy diffusion. However, decreased values of F(Th/Pa) at high latitude could also result because of lower K_d(Th) values (with no change in K_d(Pa)), as some studies have determined the K_d(Th) for opal is particularly low (Chase et al., 2002; Siddall et al., 2005). This caveat highlights the value of analyzing SPM in addition to dissolved and particulate radionuclides to be able to consider the geographic variation in K_d(Th) and K_d(Pa) separately. This presentation of the fractionation data (Fig. 5) is also somewhat incomplete since the plotted sites are largely from the interior ocean. If more sites were included from high productivity upwelling sites near the coast or along the equator where diatoms are more prevalent, lower fractionation factors may be observed at low latitudes as well.

4. Discussion

4.1 End-member distribution coefficient regressions

The results of the non-negative least squares regression between the measured K_d's for Th and Pa and the particle component concentrations are listed in Table 1. For visual inspection of the correlations, the K_d and particle composition data are cross-plotted for Th (Fig. 6) and Pa (Fig. 7). Significant end-member K_d values could not be derived for opal or POM for both Th and Pa. The end-member K_d values for lithogenic material and $CaCO_3$ imply strong fractionation associated with the adsorption of Th relative to Pa, consistent with previous work (Chase et al., 2002; Geibert and Usbeck, 2004).

The K_d values for Fe and Mn (hydr)oxides (10^8-10^9 g/g for Th, 10^7-10^8 g/g for Pa) are orders of magnitude above those for lithogenics and $CaCO_3$ (~10^7 g/g for Th, ~10^6 g/g for Pa), confirming the clear enhanced scavenging intensity inferred from depth profiles of K_d (Fig. 2). The MnO_2 K_d values reported here are much larger than what has been determined experimentally (Geibert and Usbeck, 2004; Guo et al., 2002a), but are consistent with measured K_d values from the Panama Basin where enrichment of MnO_2 in the surface sediments occurs (1-2% MnO_2; Anderson et al., 1983a), similar to that observed at GT10-09. Additionally, Roy-Barman et al. (2009) estimated an even higher K_d(Th) for MnO_2 of 60-110 x 10^8 g/g based on sediment traps from the Mediterranean Sea. These observations suggest that authigenic MnO_2 formed naturally is more reactive toward adsorption than when prepared in the laboratory. In oceanic settings, MnO_2 occurs as coatings, providing much higher reactive surface area than afforded by pure phases in the laboratory.

The enhanced intensity of scavenging by $Fe(OH)_3$ is not surprising given the known influence of intensified scavenging by hydrothermal plume particles (German et al., 1991). What is surprising are the fractionation factors estimated for MnO_2 (F = 5) and $Fe(OH)_3$ (F = 11) (Table 1), implying still a strong preference for scavenging Th. Previous work, on the other hand, has concluded that these phases do not fractionate the two elements during scavenging (F = 1) (Anderson et al., 1983b). Experimental studies have also found F close to 1 for manganese oxides, but for iron oxides F was determined as 4-5 (Geibert and Usbeck, 2004; Guo et al., 2002a). De-convolving the distributions coefficients using particle composition in terms of reactive surface area rather than weight percentage may help explain these discrepancies. The measurement of reactive surface area of undisturbed oceanic particles, however, presents a great

analytical challenge, and it may be that oceanic K_d and F values will always be to some extent operationally-defined.

The dynamic range in opal concentration in the dataset is small, <10, and opal did not have any apparent positive or negative relationship with either K_d(Th) or K_d(Pa) (Figs. 6B, 7B). This is unfortunate in that we cannot directly test the hypothesis that sedimentary Pa/Th ratios in the North Atlantic are controlled by the influence of opal scavenging (Keigwin and Boyle, 2008) with this dataset. We can conclude that it appears opal was not a major scavenging phase of Th or Pa along our transect. There is a possibility that our sampling suffers from a seasonal bias. In the Sargasso Sea diatoms are generally only a very small proportion of the phytoplankton community but their greatest abundances occur during winter/spring blooms (Nelson and Brzezinski, 1997), whereas our sampling took place in late fall (Oct-Dec). We would expect the variation in particle composition associated with diatom blooms to occur mostly in the upper water column (<1000 m), however, since deep sediment traps (3200 m) from near Bermuda have recorded very constant particle composition throughout the year for more than 10 yrs (Conte et al., 2001).

Despite low variation in opal concentrations, the opal/$CaCO_3$ ratio does vary by about 2 orders of magnitude. This ratio was suggested as the primary determinant of particulate Pa/Th ratios on the basis of a global compilation of sediment trap-seawater comparisons (Chase et al., 2002). Our data from the North Atlantic are largely consistent with the log-log correlation between the opal/$CaCO_3$ ratio and particulate Pa/Th ratio found by Chase et al. (Fig 8). A few of the outliers on this plot (results from this study with the highest Pa/Th ratio) are expected because these were the samples that had significant (2-3%) MnO_2-enrichment at GT10-09. What is immediately apparent from Fig. 8, though, is that the North Atlantic transect points fall only

on the low opal/$CaCO_3$-Pa/Th ratio side of the correlation. In fact, very few of the Pa/Th observations from this study fall above the activity ratio initially produced by U decay (0.093), which would be an indicator of preferential Pa scavenging. Furthermore, the consistency between the results of this study and the global compilation suggest that a cause for the low particulate Pa/Th ratios is the low opal/$CaCO_3$ ratios of North Atlantic particles (Honjo et al., 2008). This explanation, however, may only hold for the subtropical North Atlantic in which most of our observations are made and in which picoplankton and $CaCO_3$-producing coccolithophorids are favored in primary production over microplankton such as opal-producing diatoms. Further work in the subarctic and equatorial Atlantic may lend support to the hypothesis that large-scale regimes exist with distinct Pa/Th fractionation coinciding with biogeographic provinces (Chapter 3; Longhurst, 2006).

POM concentrations appeared to have an inverse relationship with K_d(Th) and K_d(Pa) (Figs. 6D, 7D). If using a standard least squares regression, K_d(Th) and K_d(Pa) for POM are negative. This finding is very much at odds with experimental and observational work that suggests very high sorption affinities, relative to inorganic subtrates, for Th and Pa of organic macromolecules such as polysaccharides containing extracelluar polymeric substances (EPS) (e.g., Guo et al., 2002b; Quigley et al., 2002; Roberts et al., 2009; Santschi et al., 2006). In the next section we explore the possibility that the finding of low K_d values for Th and Pa may actually be an artifact related to increased proportions of colloidal Th and Pa associated with high POM surface waters.

To summarize how changing particle composition affects the scavenging characteristics of Th and Pa, we calculate the contribution to the total observed scavenging intensity (K_d) of each individual particle phase (end-member K_d for phase x, multiplied by the concentration of

phase x in the particle sample). In this presentation of the data (Fig. 9), one can see that major carrier phases (largest contributions to the total K_d) of both Th and Pa in the North Atlantic are lithogenic material and $CaCO_3$. The high fractionation factors associated with these phases (Table 1, F = 10-20) explains the overall high fractionation factors observed throughout the transect (Figs. 2, 5). Interestingly, the K_d(Pa) for MnO_2 is so high (2.5×10^8 g/g) that even at the low MnO_2 concentrations of the typical particles (0.1-0.3%, perhaps related to oxide coatings on detrital clays), we estimate that this phase is contributing 10-20% of overall Pa scavenging. Finally, the Fe and Mn oxide phases for both elements are clearly the dominant scavenging phase in the hydothermal plume samples (Fig. 9, sample nos. 105-110) and to a lesser extent in the bottom-boundary layer GT10-09 samples (Fig. 9, sample nos. 102, 104).

4.2 The colloid conspiracy

In the vein of Turekian's "great particle conspiracy" (1977) in which sorption/scavenging processes were revealed to play a dominant role in the cycling of trace metals in the ocean, in this section we discuss the possibility that colloidal organic matter plays a dominant role in scavenging Th and Pa in shallow waters. While we have no measurements on colloidal organic matter or specific organic molecules/polymers known for radionuclide adsorption, we would expect these to roughly scale with POM content (Benner et al., 1992; Sugimura and Suzuki, 1988). Of course, POM content is largest in particle samples from the upper 200 m (POM = 60-80%), coincident with the lowest measured K_d values as well as relatively high SPM content (10-20 µg/L) (Figs. 2, 3, 6, 7).

An additional piece of evidence which implicates an increasing proportion of colloidal radionuclides at high SPM (and POM) contents is the relationship between the measured distribution coefficients and particle concentration (Fig. 10). Referred to as the particle

concentration effect (Honeyman et al., 1988), it has been shown that measured K_d values for Th are considerably lower in near-shore waters where particle concentrations (>10^3 µg/L) are much higher than in oceanic waters (SPM = 10^0-10^2 µg/L). This effect is attributed to a larger proportion of (adsorbed) colloidal Th, which passes through filters and thus appears as dissolved, at higher particle concentrations (Henderson et al., 1999; Moran and Buesseler, 1993). The particle concentration effect has been shown to affect the size-partitioning of many particle-reactive trace metals, such as Al, Pb, Hg, and Fe (Moran and Moore, 1989; Moran et al., 1996), so presumably it would also hold for Pa. It is significant in our study, however, that a trend of lower K_d's with high SPM (log-log scale) is seen even at the typical oceanic particle concentrations. The samples with the highest POM content (equivalent to those at <200 m depth) are consistently on the low-K_d end of the observed trends (Fig. 10) giving further support to the association of some type of organic matter with a greater proportion of colloidal radionuclides.

Apparently low K_d values could also be the result of low molecular weight organic molecules with high complexation capacities which essentially stabilize Th (or Pa) in solution (Barbeau et al., 2001). This would be consistent with the finding of elevated Th complexation capacity confined to the upper 200-300 m of the ocean (Hirose et al., 2011; Hirose and Tanoue, 1994; 1998) and is difficult to distinguish from the colloidal hypothesis with the available data.

If one assumes the low shallow water K_d's are artifacts and that the true K_d's in shallow water should be similar to the more uniform values found in mid- to deep water (1-3 km depth), one can estimate the fraction of "dissolved" radionuclide that would have to be found in the colloidal/complexed phase, f(colloid), by mass balance. Essentially, f(colloid) is directly proportional to the relative deviation of the measured K_d (Eq. 9). Assuming a true K_d(Th) = 1.5 x 10^7 g/g, the dissolved phase of ^{230}Th as measured is implied to be up to 80-90% colloidal (at a

maximum, most shallow samples are estimated between 30-60% colloidal). A similar result, f(colloid) = 20-90%, is obtained for ^{231}Pa (assuming true K_d(Pa) = 2 x 10^6 g/g).

$$f(colloid) = 1 - \frac{true\ K_d}{measured\ K_d} \qquad \text{Eq. 9}$$

Very little work on colloidal ^{230}Th (or ^{231}Pa) has been done, but colloidal ^{234}Th, reviewed by Guo and Santschi (1997), has received attention for its application in quantifying organic matter export. The colloidal fraction of dissolved ^{234}Th has been estimated over a large range (0-78%). This large range is in part because of the analytical and operational issues associated with ultrafiltration techniques (e.g. Dai et al., 1998; Dai and Benitez-Nelson, 2001), but generally, f(colloid) values for ^{234}Th greater than 50% are found only in near-shore waters with particle concentrations on the order of 10-100 mg/L. Thus, the estimated 80-90% colloidal fraction of ^{230}Th (^{231}Pa) reported here in for oceanic waters is a novel result worth attempting to replicate in other oceanic environments. Future work to determine the size partitioning of ^{230}Th would also be helpful in understanding the scavenging removal of Th in shallow waters, which is of particular relevance for the use of dissolved ^{232}Th fluxes as a tracer of lithogenic inputs based on ^{230}Th scavenging removal (Hsieh et al., 2011; Chapter 2).

Because of the possible bias in our K_d estimates imparted by a presence of an organic colloidal fraction of radionuclides, we must defend the statistical approach (Sec. 4.1) used to determine scavenging intensity of different particle types. As well, if Th and Pa have colloidal content of differing proportions (different magnitude of bias in K_d(Th) vs. K_d(Pa)), our estimates of fractionation factors (Eq. 8) could be subject to the same type of artifact. Obviously we have less confidence in our derived scavenging parameters where the presence of a significant colloidal radionuclide phase is most likely to occur (shallow water, high POM content). The content of the most reactive organic sorption/complexing agents is most likely to decrease depth

via respiration processes (Cho and Azam, 1988; Lee et al., 2004). Furthermore, given that the anomalous K_d values are confined to the upper 500 m, the mid- and deep water results (sample no. > 15 in Fig. 3) are most likely reliable and suitable for determining the relative scavenging intensity and fractionation factors associated with different phases. Nonetheless, the statistical approach employed here would be improved with further information on the size-partitioning of the radionuclides. Additionally, rather than simply POM, characterizing types of POM, and their size partitioning, which may differ in their scavenging tendencies (poly acid saccharides, proteins, lipids, etc.) will provide more information about the mechanism of scavenging by organic matter.

5. Summary

In this study, we confirm previous work that lithogenic material and $CaCO_3$ are major carrier phases of scavenged Th in the North Atlantic Ocean. Mn and Fe oxide phases have scavenging intensities orders of magnitude larger than the other major particle components for both elements. Metal oxides are most likely only major scavenging phases in a limited number of settings. These include sites of hydrothermal venting and near-shore environments where sediments undergo intense redox cycling due to high respiration rates of organic matter that creates Fe and/or Mn-oxide coatings on other particulate phases. Although, in our calculations scavenging intensity of MnO_2 for Pa is so high that even at very low concentration (such as the oxide coatings of clay), this phase contributes significantly to Pa scavenging (~10%).

In our sampling, opal was not a major phase of the particles (< 15%) and was not correlated with an increase in Pa scavenging intensity. We cannot therefore directly test the hypothesis that sedimentary Pa/Th ratios are controlled by opal scavenging rather than the intensity of overturning circulation in the North Atlantic. However, if the low concentration of

opal we observed across the transect is characteristic of the basin on a year-round basis, then it may be that the Pa cycle in the North Atlantic (in the modern case, at least) is not significantly perturbed by opal scavenging.

Despite a lack of statistical correlation between POM and scavenging intensities, anomalously low K_d values in shallow water intimate the possibility that organic colloids or complexing agents play a significant role in scavenging/complexing both radionuclides. Future work should pursue the seasonal variability of particle composition and scavenging intensities (as determined by in-situ pumps), size-fractionation of dissolved ^{230}Th and ^{231}Pa to determine the role of colloids, and further characterization of POM (and colloidal OM) to determine which organic compounds are associated with the strongest scavenging intensities and as well as their spatial extent.

Acknowledgements

Cruise management was funded by the U. S. National Science Foundation to the US GEOTRACES North Atlantic Transect Management team of W. Jenkins (OCE-0926423), E. Boyle (OCE-0926204), and G. Cutter (OCE-0926092). Radionuclide studies were supported by NSF (OCE-0927064 to LDEO, OCE-0926860 to WHOI, OCE-0927757 to URI, and OCE-0927754 to U MN). The crew of the R/V *Knorr*, the Ocean Data Facility team (Mary Johnson, Rob Palomares, Susan Becker, and Courtney Schatzman), and the science team samplers for Niskin bottles and in situ pumps (Katharina Pahnke, Brett Longworth, Paul Morris, Daniel Ohnemus, Kuanbo Zhou, Sylvain Rigaud and Stephanie Owens) are all acknowledged for their critical roles in the success of these cruises. Figure 1 was created using Ocean Data View (Schlitzer, 2011).

References

Anderson, R.F., 1982. Concentration, vertical flux, and remineralization of particulate uranium in seawater. Geochim. Cosmochim. Acta 46, 1293-1299.

Anderson, R.F., Bacon, M.P., Brewer, P.G., 1983a. Removal of ^{230}Th and ^{231}Pa at ocean margins. Earth Planet. Sci. Lett. 66, 73-90.

Anderson, R.F., Bacon, M.P., Brewer, P.G., 1983b. Removal of ^{230}Th and ^{231}Pa from the open ocean. Earth Planet. Sci. Lett. 62, 7-23.

Barbeau, K., Kujawinski, E.B., Moffett, J.W., 2001. Remineralization and recycling of iron, thorium and organic carbon by heterotrophic marine protists in culture. Aquat. Microb. Ecol. 24, 69-81.

Benner, R., PakulskiI, J.D., McCarthy, M., Hedges, J.I., Hatcher, P.G., 1992. Bulk chemical characteristics of dissolved organic matter in the ocean. Science 255, 1561-1564.

Chase, Z., Anderson, R.F., 2004. Comment on "On the importance of opal, carbonate, and lithogenic clays in scavenging and fractionating ^{230}Th, ^{231}Pa and ^{10}Be in the ocean" by S. Luo and T.-L. Ku. Earth Planet. Sci. Lett. 220, 213-222.

Chase, Z., Anderson, R.F., Fleisher, M.Q., Kubik, P.W., 2002. The influence of particle composition and particle flux on scavenging of Th, Pa and Be in the ocean. Earth Planet. Sci. Lett. 204, 215-229.

Cho, B.C., Azam, F., 1988. Major role of bacteria in biogeochemical fluxes in the ocean's interior. Nature 332, 441-443.

Conte, M.H., Ralph, N., Ross, E.H., 2001. Seasonal and interannual variability in deep ocean particle fluxes at the Oceanic Flux Program (OFP)/Bermuda Atlantic Time Series (BATS) site in the western Sargasso Sea near Bermuda. Deep Sea Res. Pt. II 48, 1471-1505.

Dai, M., Buesseler, K.O., Ripple, P., Andrews, J., Belastock, R.A., Gustafsson, Ö., Moran, S.B., 1998. Evaluation of two cross-flow ultrafiltration membranes for isolating marine organic colloids. Mar. Chem. 62, 117-136.

Dai, M.H., Benitez-Nelson, C.R., 2001. Colloidal organic carbon and ^{234}Th in the Gulf of Maine. Mar. Chem. 74, 181-196.

François, R., 2007. Paleoflux and Paleocirculation from Sediment ^{230}Th and ^{231}Pa/^{230}Th, in: Hillaire-Marcel, C., de Vernal, A. (Eds.), Developments in Marine Geology. Elsevier, pp. 681-716.

Geibert, W., Usbeck, R., 2004. Adsorption of thorium and protactinium onto different particle types: experimental findings. Geochim. Cosmochim. Acta 68, 1489-1501.

German, C.R., Fleer, A.P., Bacon, M.P., Edmond, J.M., 1991. Hydrothermal scavenging at the Mid-Atlantic Ridge: radionuclide distributions. Earth Planet. Sci. Lett. 105, 170-181.

Guo, L., Chen, M., Gueguen, C., 2002a. Control of Pa/Th ratio by particulate chemical composition in the ocean. Geophys. Res. Lett. 29, 1961.

Guo, L., Hung, C.-C., Santschi, P.H., Walsh, I.D., 2002b. ^{234}Th scavenging and its relationship to acid polysaccharide abundance in the Gulf of Mexico. Mar. Chem. 78, 103-119.

Guo, L., Santschi, P.H., 1997. Composition and cycling of colloids in marine environments. Rev. Geophys. 35, 17-40.

Henderson, G.M., Anderson, R.F., 2003. The U-series Toolbox for Paleoceanography. Rev. Mineral. Geochem. 52, 493-531.

Henderson, G.M., Heinze, C., Anderson, R.F., Winguth, A.M.E., 1999. Global distribution of the ^{230}Th flux to ocean sediments constrained by GCM modelling. Deep Sea Res. Pt. I 46, 1861-1893.

Hirose, K., Saito, T., Lee, S.H., Gastaud, J., 2011. Vertical distributions of the strong organic ligand in the twilight zone of Southern Hemisphere Ocean particulate matter. Prog. Oceanogr. 89, 108-119.

Hirose, K., Tanoue, E., 1994. Thorium-particulate matter interaction. Thorium complexing capacity of oceanic particulate matter: Theory. Geochim. Cosmochim. Acta 58, 1-7.

Hirose, K., Tanoue, E., 1998. The vertical distribution of the strong ligand in particulate organic matter in the North Pacific. Mar. Chem. 59, 235-252.

Honeyman, B.D., Balistrieri, L.S., Murray, J.W., 1988. Oceanic trace metal scavenging: the importance of particle concentration. Deep Sea Res. Pt. A 35, 227-246.

Honjo, S., Manganini, S.J., Krishfield, R.A., Francois, R., 2008. Particulate organic carbon fluxes to the ocean interior and factors controlling the biological pump: A synthesis of global sediment trap programs since 1983. Prog. Oceanogr. 76, 217-285.

Hsieh, Y.-T., Henderson, G.M., Thomas, A.L., 2011. Combining seawater ^{232}Th and ^{230}Th concentrations to determine dust fluxes to the surface ocean. Earth Planet. Sci. Lett. 312, 280-290.

Keigwin, L.D., Boyle, E.A., 2008. Did North Atlantic overturning halt 17,000 years ago? Paleoceanography 23, PA1101.

Lee, C., Wakeham, S., Arnosti, C., 2004. Particulate organic matter in the sea: The composition conundrum. AMBIO 33, 565-575.

Li, Y.-H., 2005. Controversy over the relationship between major components of sediment-trap materials and the bulk distribution coefficients of ^{230}Th, ^{231}Pa, and ^{10}Be. Earth Planet. Sci. Lett. 233, 1-7.

Lippold, J., Luo, Y., Francois, R., Allen, S.E., Gherardi, J., Pichat, S., Hickey, B., Schulz, H., 2012. Strength and geometry of the glacial Atlantic Meridional Overturning Circulation. Nature Geosci. 5, 813-816.

Longhurst, A., 2006. Ecological Geography of the Sea, 2nd ed. Academic Press, San Diego.

Luo, S., Ku, T.-L., 1999. Oceanic ^{231}Pa/^{230}Th ratio influenced by particle composition and remineralization. Earth Planet. Sci. Lett. 167, 183-195.

Luo, S., Ku, T.-L., 2004. On the importance of opal, carbonate, and lithogenic clays in scavenging and fractionating ^{230}Th, ^{231}Pa and ^{10}Be in the ocean. Earth Planet. Sci. Lett. 220, 201-211.

Luo, Y., Francois, R., Allen, S.E., 2010. Sediment ^{231}Pa/^{230}Th as a recorder of the rate of the Atlantic meridional overturning circulation: insights from a 2-D model. Ocean Sciences 6, 381-400.

McManus, J.F., Francois, R., Gherardi, J.M., Keigwin, L.D., Brown-Leger, S., 2004. Collapse and rapid resumption of Atlantic meridional circulation linked to deglacial climate changes. Nature 428, 834-837.

Moran, S.B., Buesseler, K.O., 1993. Size-fractionated ^{234}Th in continental shelf waters off New England: Implications for the role of colloids in oceanic trace metal scavenging. J. Mar. Res. 51, 893-922.

Moran, S.B., Moore, R.M., 1989. The distribution of colloidal aluminum and organic carbon in coastal and open ocean waters off Nova Scotia. Geochim. Cosmochim. Acta 53, 2519-2527.

Moran, S.B., Shen, C.C., Edmonds, H.N., Weinstein, S.E., Smith, J.N., Edwards, R.L., 2002. Dissolved and particulate ^{231}Pa and ^{230}Th in the Atlantic Ocean: constraints on intermediate/deep water age, boundary scavenging, and ^{231}Pa/^{230}Th fractionation. Earth Planet. Sci. Lett. 203, 999-1014.

Moran, S.B., Yeats, P.A., Balls, P.W., 1996. On the role of colloids in trace metal solid-solution partitioning in continental shelf waters: a comparison of model results and field data. Cont. Shelf Res. 16, 397-408.

Nelson, D.M., Brzezinski, M.A., 1997. Diatom growth and productivity in an oligotrophic midocean gyre: A 3-yr record from the Sargasso Sea near Bermuda. Limnol. Oceanogr. 42, 473-486.

Quigley, M.S., Santschi, P.H., Hung, C.-C., Guo, L., Honeyman, B.D., 2002. Importance of acid polysaccharides for ^{234}Th complexation to marine organic matter. Limnol. Oceanogr. 47, 367-377.

Roberts, K.A., Xu, C., Hung, C.-C., Conte, M.H., Santschi, P.H., 2009. Scavenging and fractionation of thorium vs. protactinium in the ocean, as determined from particle-water partitioning experiments with sediment trap material from the Gulf of Mexico and Sargasso Sea. Earth Planet. Sci. Lett. 286, 131-138.

Robinson, L.F., Noble, T.L., McManus, J.F., 2008. Measurement of adsorbed and total $^{232}Th/^{230}Th$ ratios from marine sediments. Chem. Geol. 252, 169-179.

Roy-Barman, M., Lemaître, C., Ayrault, S., Jeandel, C., Souhaut, M., Miquel, J.C., 2009. The influence of particle composition on thorium scavenging in the Mediterranean Sea. Earth Planet. Sci. Lett. 286, 526-534.

Sackett, W.M., 1960. Protactinium-231 content of ocean water and sediments. Science 132, 1761-1762.

Santschi, P.H., Murray, J.W., Baskaran, M., Benitez-Nelson, C.R., Guo, L.D., Hung, C.C., Lamborg, C., Moran, S.B., Passow, U., Roy-Barman, M., 2006. Thorium speciation in seawater. Mar. Chem. 100, 250-268.

Schlitzer, R., 2011. http://odv.awi.de.

Scholten, J.C., Fietzke, J., Mangini, A., Garbe-Schönberg, C.D., Eisenhauer, A., Schneider, R., Stoffers, P., 2008. Advection and scavenging: Effects on ^{230}Th and ^{231}Pa distribution off Southwest Africa. Earth Planet. Sci. Lett. 271, 159-169.

Siddall, M., Henderson, G.M., Edwards, N.R., Frank, M., Müller, S.A., Stocker, T.F., Joos, F., 2005. $^{231}Pa/^{230}Th$ fractionation by ocean transport, biogenic particle flux and particle type. Earth and Planet. Sci. Lett. 237, 135-155.

Siddall, M., Stocker, T.F., Henderson, G.M., Joos, F., Frank, M., Edwards, N.R., Ritz, S.P., Müller, S.A., 2007. Modeling the relationship between $^{231}Pa/^{230}Th$ distribution in North Atlantic sediment and Atlantic meridional overturning circulation. Paleoceanography 22, PA2214.

Sugimura, Y., Suzuki, Y., 1988. A high-temperature catalytic oxidation method for the determination of non-volatile dissolved organic carbon in seawater by direct injection of a liquid sample. Mar. Chem. 24, 105-131.

Turekian, K.K., 1977. The fate of metals in the oceans. Geochim. Cosmochim. Acta 41, 1139-1144.

Walter, H.-J., Rutgers v. d. Loeff, M.M., Francois, R., 1999. Reliability of the $^{231}Pa/^{230}Th$ Activity Ratio as a Tracer for Bioproductivity of the Ocean, in: Fischer, W., Wefer, G. (Eds.), Use of Proxies in Paleoceanography: Examples for the South Atlantic. Springer-Verlag, Berlin, pp. 393-408.

Walter, H.J., Rutgers van der Loeff, M.M., Hoeltzen, H., 1997. Enhanced scavenging of ^{231}Pa relative to ^{230}Th in the South Atlantic south of the Polar Front: Implications for the use of the $^{231}Pa/^{230}Th$ ratio as a paleoproductivity proxy. Earth Planet. Sci. Lett. 149, 85-100.

Yu, E.-F., Francois, R., Bacon, M.P., 1996. Similar rates of modern and last-glacial ocean thermohaline circulation inferred from radiochemical data. Nature 379, 689-694.

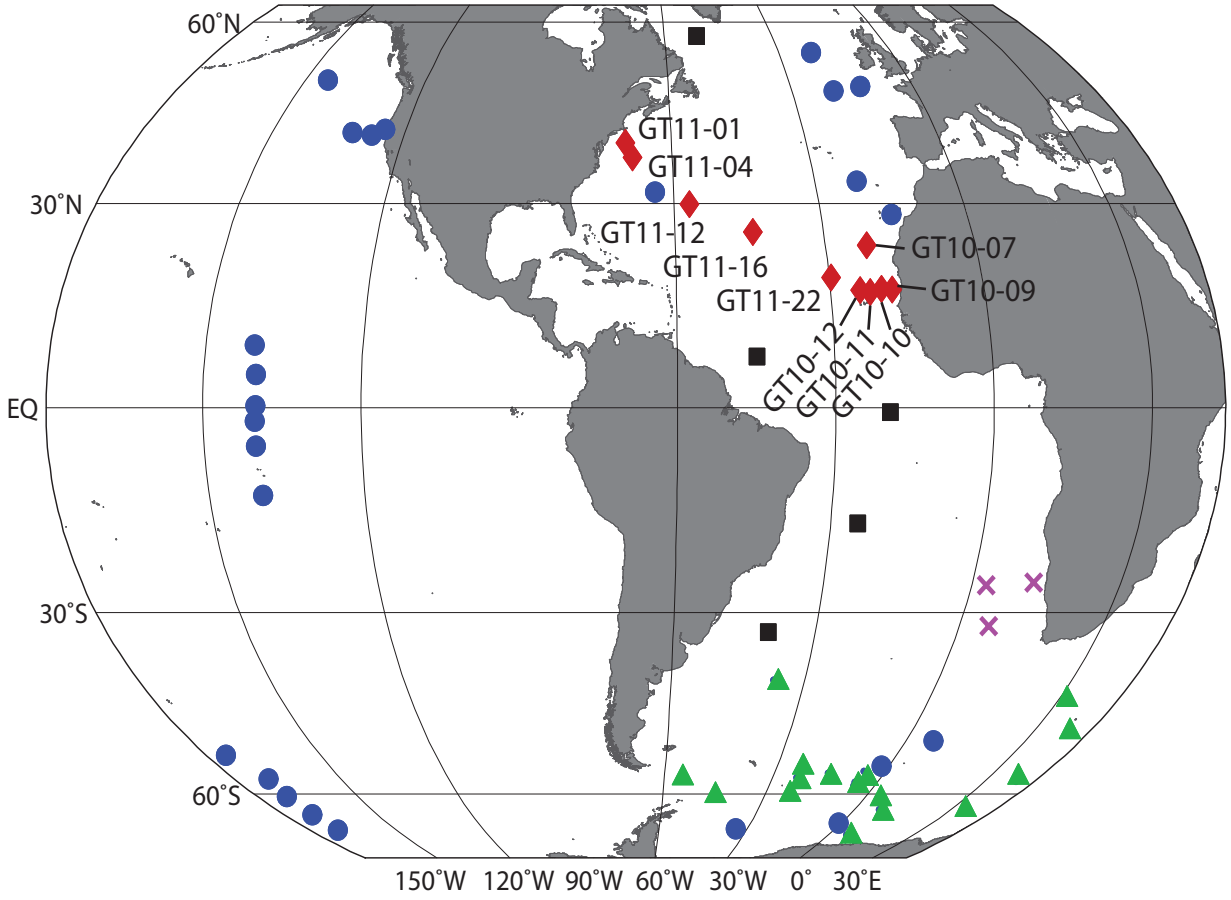

Figure 1. Map of the sites from the US North Atlantic GEOTRACES cruises (red diamonds) reported on in this study in comparison to sites for which water column fractionation factors, F(Th/Pa), have been reported by Moran et al. (2002) (black squares), Walter et al. (1997) (green triangles) and Scholten et al. (2008) (purple x's) and sites from a global compilation of sediment trap Pa/Th and particle composition reported by Chase et al (2002) (blue dots).

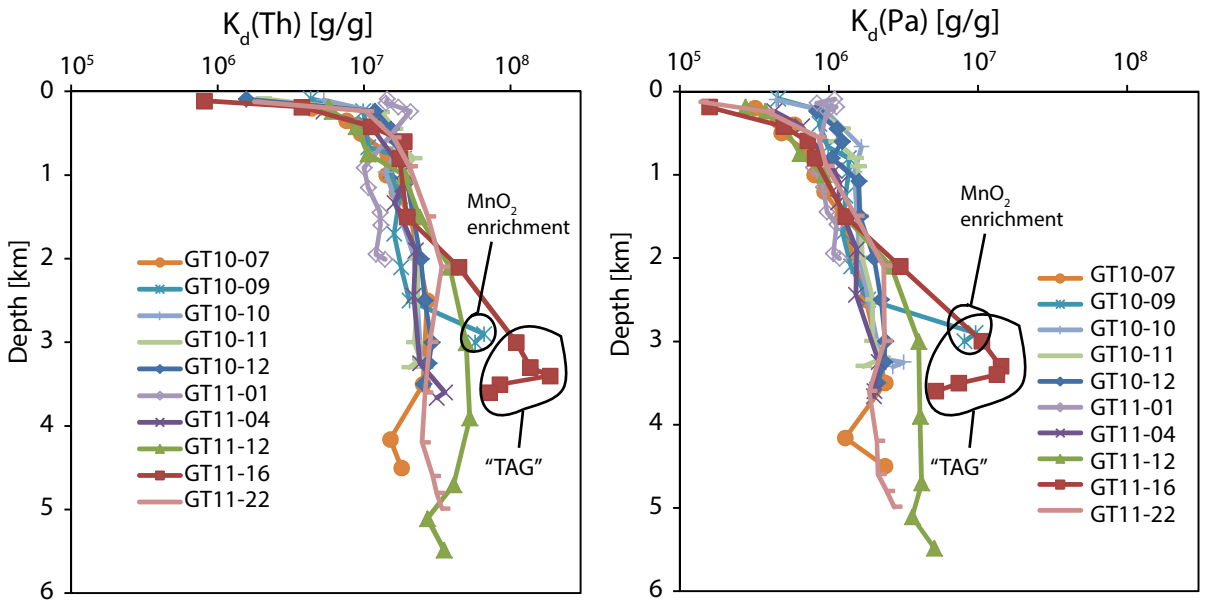

Figure 2. Depth profiles of the distribution coefficient (K_d) for ^{230}Th (A) and ^{231}Pa (B) from the US GEOTRACES locations mapped in Figure 1. Circled are the anomalous high K_d values associated with authigenic $Fe(OH)_3$ at the TAG hydrothermal site, GT11-16, and authigenic MnO_2 enrichment in a bottom nepheloid layer at GT10-09, an upwelling region off the coast of Mauritania.

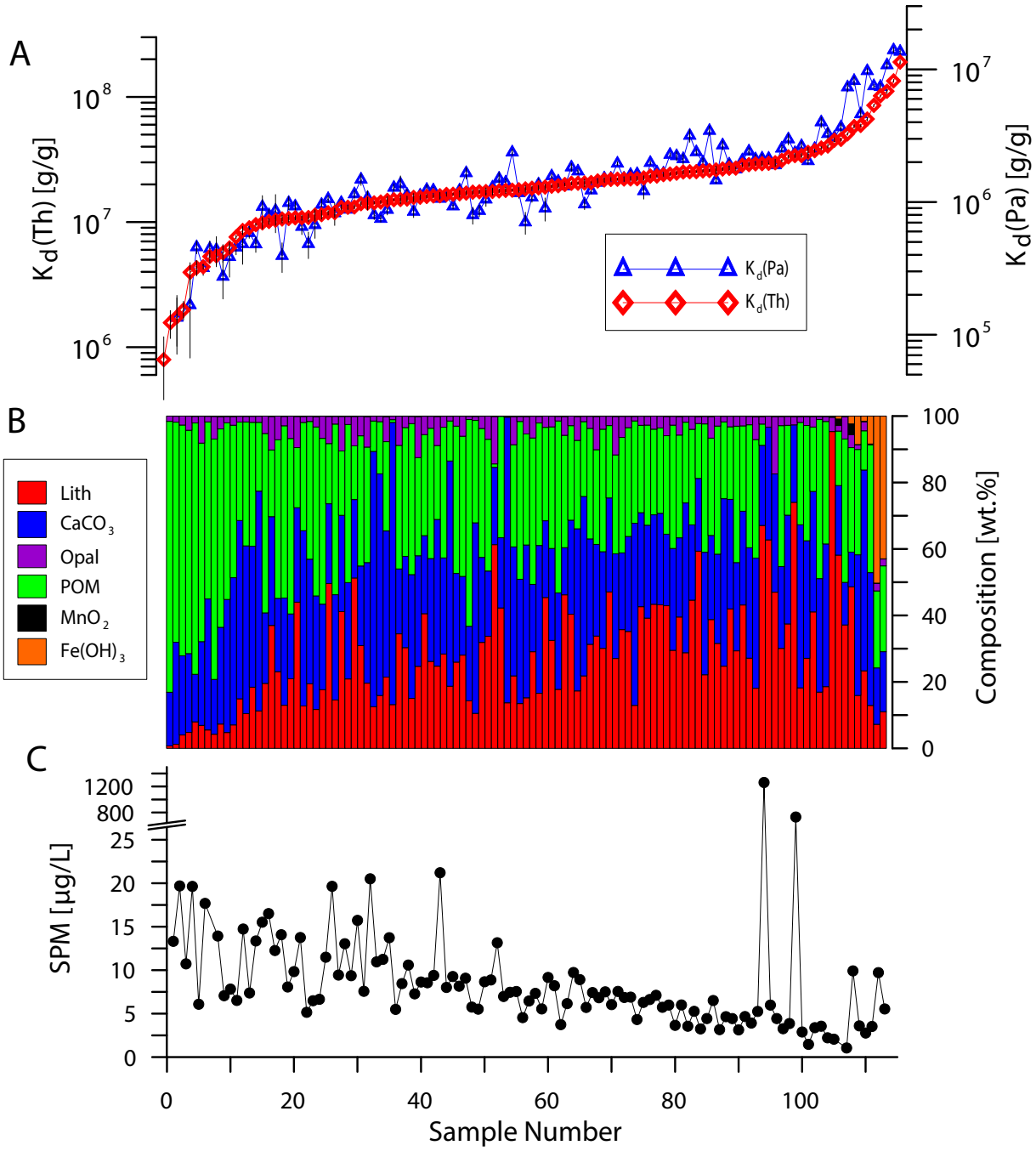

Figure 3. K_d results for all samples analyzed in this study sorted by increasing K_d(Th) (red diamonds) (A). Note the corresponding K_d(Pa) values (blue triangles) (A) are on their own, offset scale on the right. (B) Corresponding particle compositions (% weights of lithogenic material, $CaCO_3$, biogenic opal, particulate organic matter, MnO_2 and $Fe(OH)_3$) and (C) suspended particulate matter concentrations of the particle samples ordered in the same way as (A). The error bars shown in (A) represent the propagated errors associated with the analysis of particulate and dissolved radionuclides and suspended matter concentration.

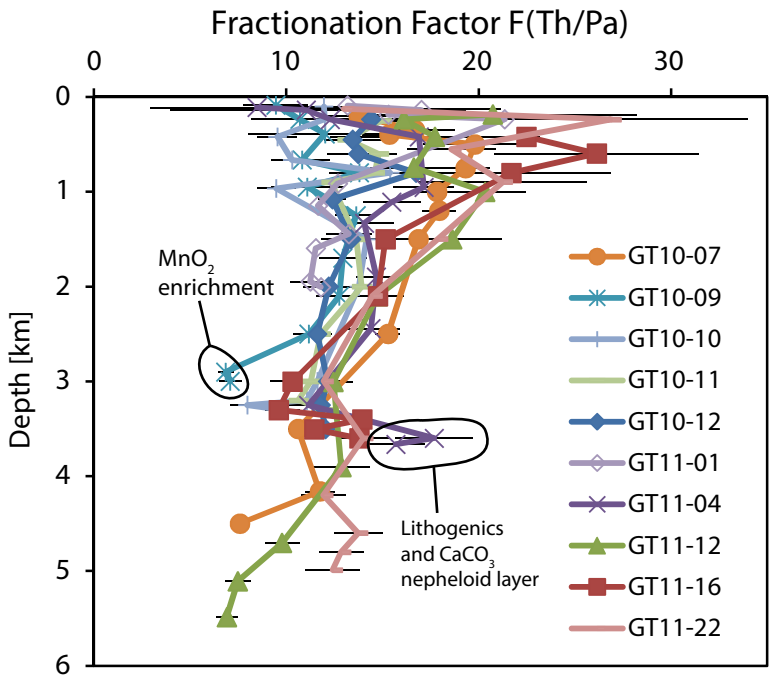

Figure 4. Depth profiles of the fractionation factor, F(Th/Pa), for the US GEOTRACES locations mapped in Figure 1. The error bars represent the propagated errors associated with the analyses of dissolved and particulate radionuclides. Circled are anomalous results associated with the manganese oxide enrichement in the nepheloid layer at GT10-09, the upwelling site near the coast of Mauritania and with the heavily particle-laden nepheloid (~1000 µg/L) layer observed at GT11-04, along Line W in the Northwest Atlantic, which was composed predominantly of lithogenic material and calcium carbonate.

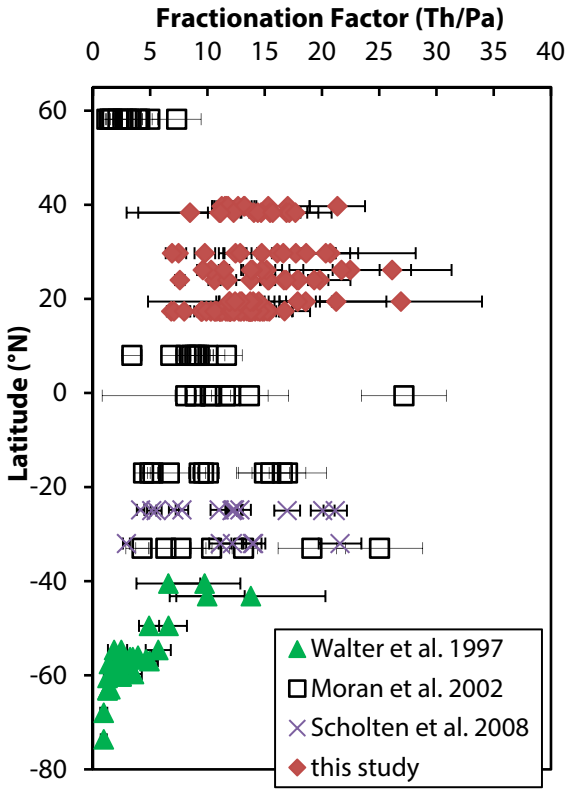

Figure 5. Fractionation factors, F(Th/Pa), calculated between seawater and suspended particles in the water column, determined from the US GEOTRACES transect (red diamonds) compared with published estimates reported by Moran et al. (2002), Walter et al. (1997), and Scholten et al. (2008) as a function of latitude in the Atlantic. See Figure 1 for station locations.

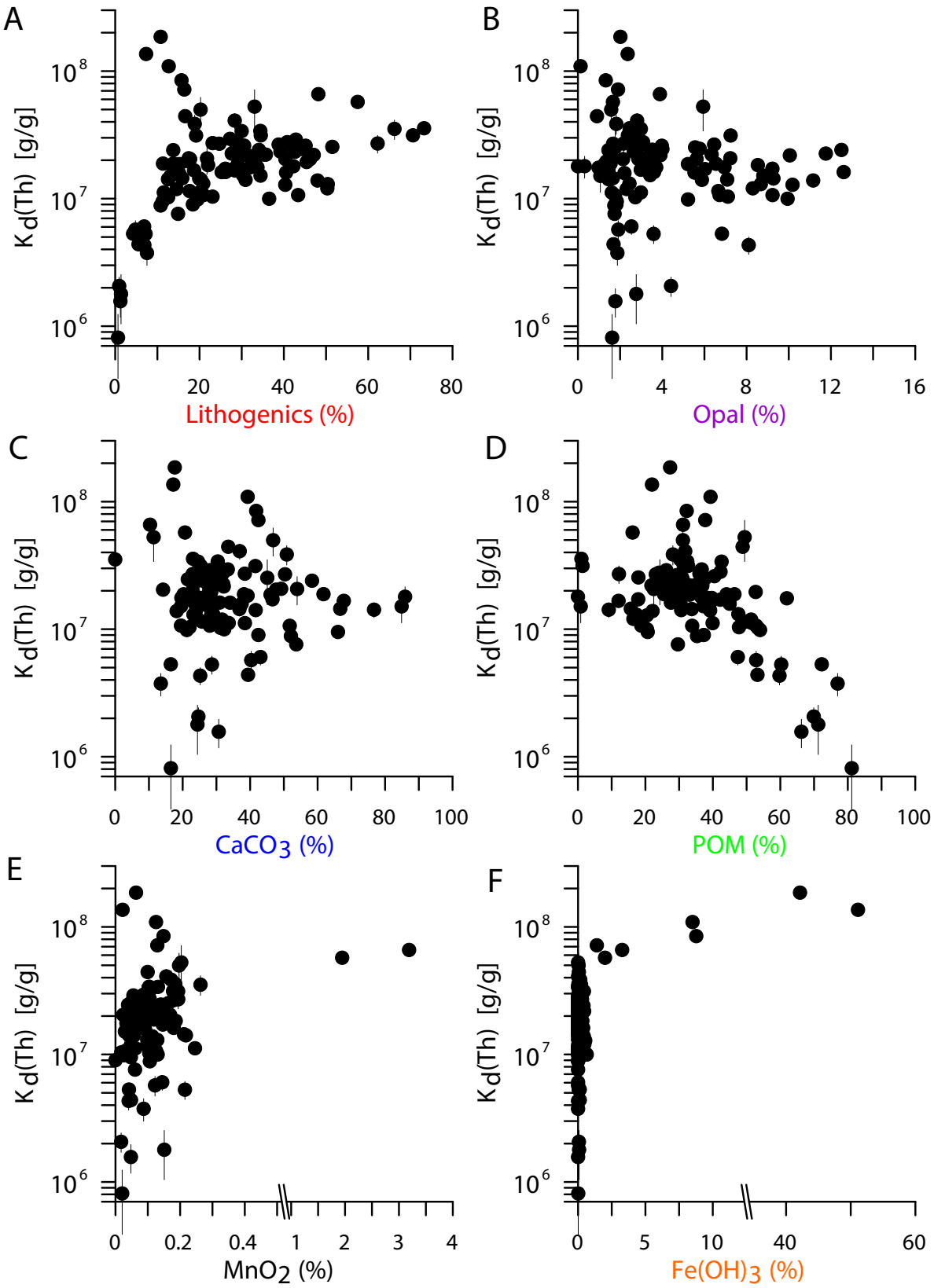

Figure 6. Cross-plots of K_d(Th) versus the particulate matter content of lithogenic material (A), opal (B), $CaCO_3$ (C), particulate organic matter (D), manganese oxides (E), and iron hydroxides (F).

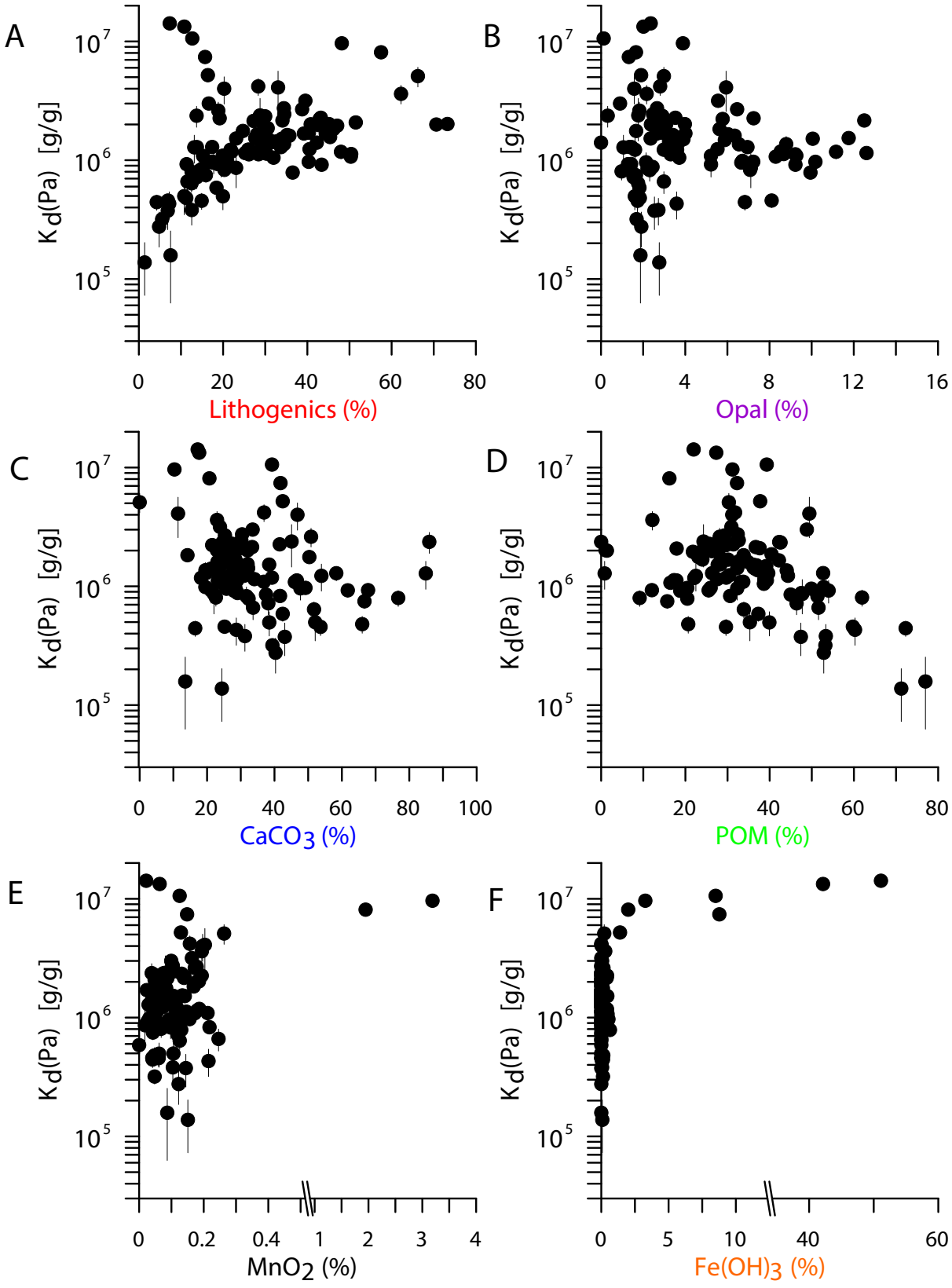

Figure 7. Cross-plots of K_d(Pa) versus the particulate matter content of lithogenic material (A), opal (B), $CaCO_3$ (C), particulate o rganic matter (D), manganese oxides (E), and iron hydroxides (F).

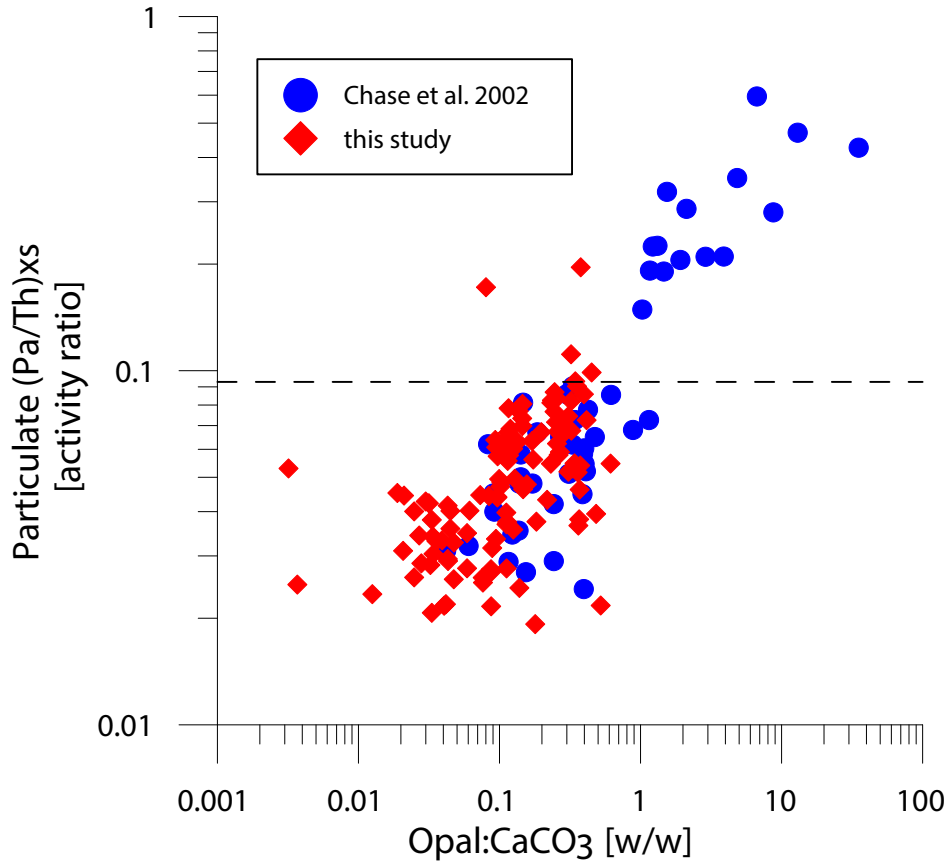

Figure 8. The ratio of adsorbed Pa/Th (particulate xs) on suspended particles from the US GEOTRACES transect versus the opal to $CaCO_3$ ratio of the particles compared with the xs Pa/Th ratio and opal/$CaCO_3$ of global sediments trap material (Chase et al. 2002, see Fig. 1 for station locations). Note that both axes are log-scale. The horizontal dotted line represents the Pa/Th activity produced initially by U decay in seawater (0.093).

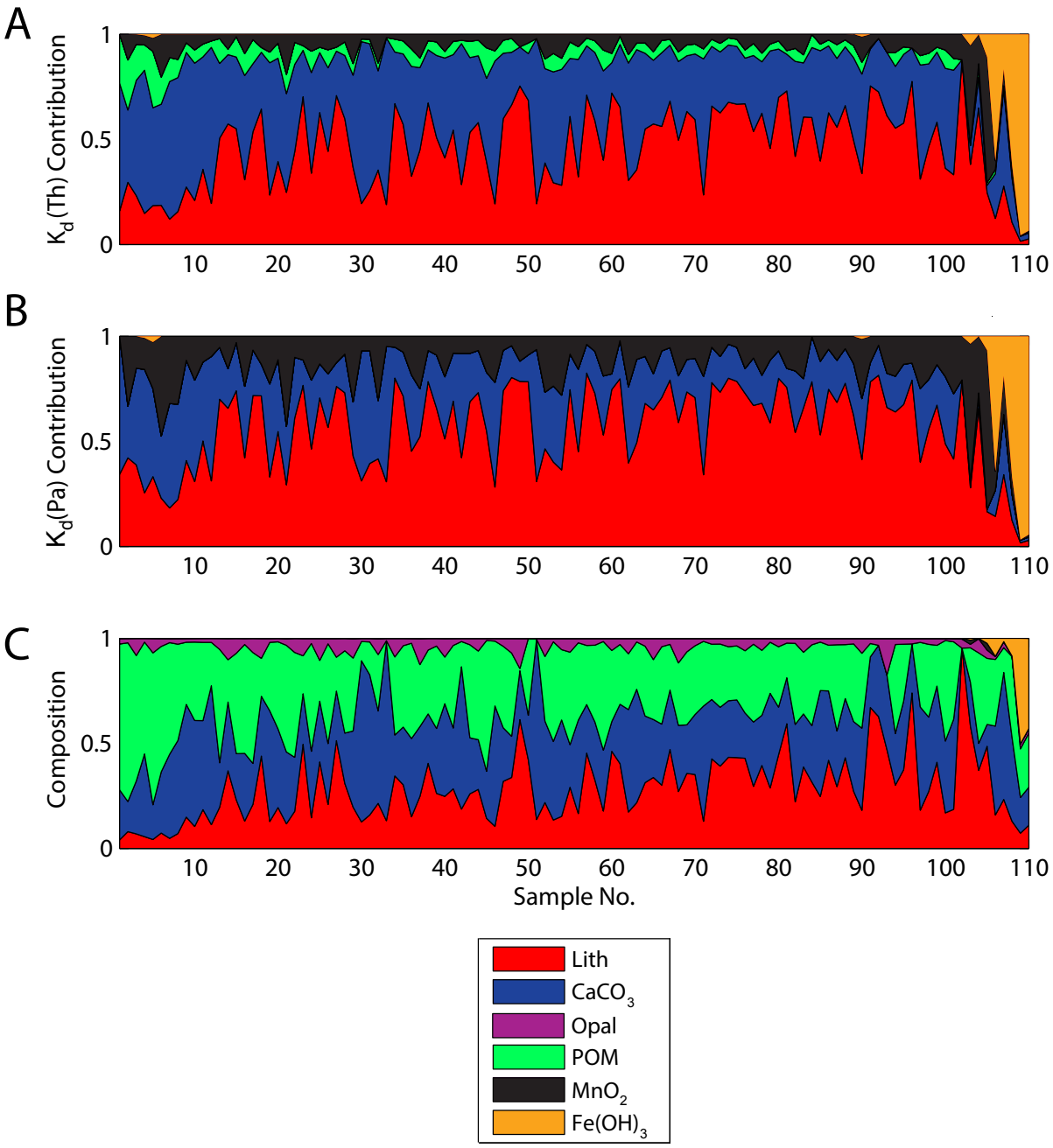

Figure 9. The fractional contribution of the major particle components to the total scavenging (measured K_d) of Th (A) and Pa (B) in comparison to the weight-composition (C) of the particles analyzed in this study on the same sample no. axis as in Figure 3 (ordered by increasing K_d(Th)).

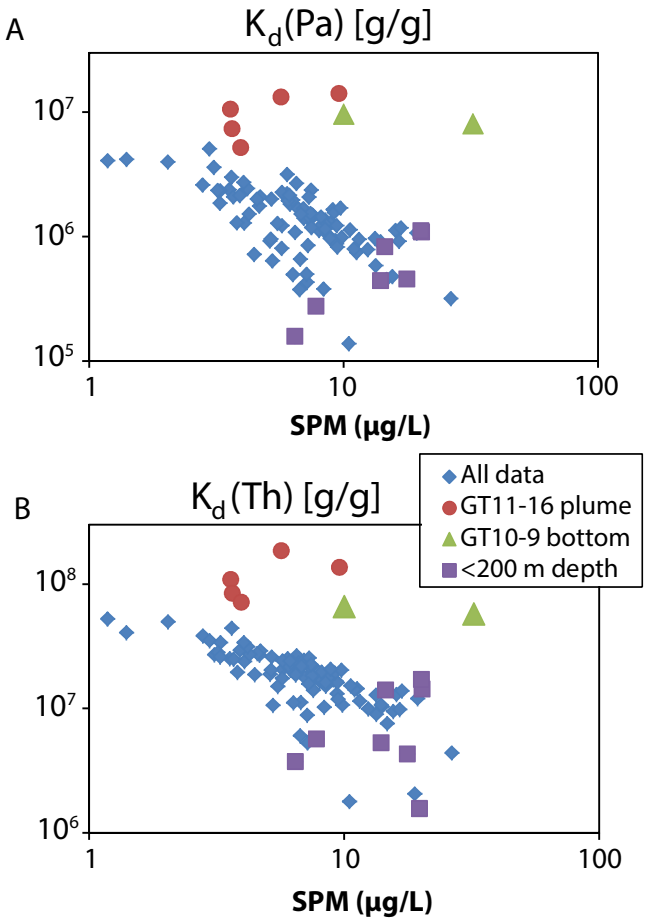

Figure 10. Log-log scatter plots of K_d(Pa) (A) and K_d(Th) (B) versus suspended particulate matter (SPM) concentration from our study sites. While there is a general trend for decreasing K_d values at higher SPM, and samples from shallower than 200 m water depth, especially, fall on the low-K_d-high-SPM end of the trend, we highlight that the stations for which metal oxide scavenging is significant (GT11-16 and GT10-09) do not fall on this trend.

Table 1. Results of a non-negative least squares regression between distribution coefficients (K_d) for Th and Pa and the major particle component concentrations (lithogenic material, calcium carbonate, biogenic opal, particulate organic matter, and authigenic Mn and Fe (hydr)oxide phases). Shown are the derived end-member distribution coefficients for pure phases and their associated fractionation factors ($F = K_d(Th) / K_d(Pa)$).

	K_d(Th) $x10^7$ (g/g)	± $x10^7$ (g/g)	K_d(Pa) $x10^6$ (g/g)	± $x10^6$ (g/g)	F(Th/Pa)	±
Lith	3.8	0.7	3.6	0.6	10	3
$CaCO_3$	2.5	0.6	1.2	0.5	21	11
Opal	0.0	4.3	0.0	3.6		
POM	0.3	0.6	0.0	0.5		
MnO_2	138	39	252	33	5	2
$Fe(OH)_3$	34	2	30	2	11	1